POLYMER ASSISTED NANOMATERIALS IMMOBILIZED BIOMOLECULES AND THEIR POTENTIAL APPLICATIONS

A thesis submitted in partial fulfillment of the requirements for the degree of
Doctor of Philosophy

Rocktotpal Konwarh

Registration Number 034 of 2010

School of Science

Department of Chemical Sciences

Tezpur University

January, 2013

.....Dedicated to my parents, teachers and friends!!...

Touch a Scientist and You Touch a Child!!

.....·Ray Douglas Bradbury

(American novelist, Playwright)

ABSTRACT

The 'contact sport' of material science and life science has led to a myriad of innovations of the present day. Amongst others, immobilized biomolecules onto various classes of novel materials have fetched applications across different realms. In this context, the thesis entitled, '*Polymer assisted nanomaterials immobilized biomolecules and their potential applications*' is focused on the development of a few hybrid bio-polymeric nanomaterials/ nanocomposites for prospective applications in the industrial and biomedical domains. As dealt with in the introductory chapter of the thesis, it is pertinent to mention that the recent years have witnessed a substantial progress in biomolecule immobilization studies including the hunt for appropriate immobilization platform, protocols for efficient and easy immobilization with emphasis on green approaches, advancements in characterization tools and strategies, ever widening spectrum of candidates for immobilization and so on. The basic idea of the studies reported in this thesis is to confine/anchor the biomolecules of interest onto the *avant-garde* polymer supported nanomaterials for their stability and functional reuse. These strategies are envisaged to make the bio-active molecules much more efficient and cost effective for their prospective applications. The thesis deals with the preparation of various immobilization platforms (like polymer supported magnetic and antimicrobial nanoparticles, conducting nanofibers and electrospun polymeric nanofibers), and optimization of their preparative protocols as well as immobilization strategy of different biomolecules of interest like biocatalysts, medically important phytocompounds and antibiotic for applications ranging from leather industry to detergent industry and drug delivery. Various tools like UV-visible spectroscopy, FTIR, XRD, VSM, SEM, TEM complemented by *in silico* analysis) and various investigations like alterations in enzyme activity, anti-lipid peroxidation and so on, were exploited to probe into the plausible modulations in the physico-chemical properties of the immobilized platform and the biomolecule of interest respectively. Furthermore, action at the bio-interface (across different levels ranging from a few selected microbes to eukaryotes like plant seeds and animal cell lines) of these materials was probed into as a function of their shape-size-concentration accord.

In this context, *Bacillus subtilis* keratinase was immobilized onto poly(ethylene glycol) supported iron oxide nanoparticles for prospective depilatory (hair-removal) applications in leather industry, while porcine pancreatic lipase (exhibiting synergy with detergents for oil de-staining) and *Aspergillus niger* amyloglucosidase (for starch saccharification and starch de-staining) were trapped on antibacterial and magnetically recyclable poly(ethylene glycol) supported silver-iron oxide exotic nanostructures, as characterized by various spectroscopic and analytical tools. These immobilization studies (reported in the second chapter) have relied on the use of the green chemistry tool of sonication in tuning the physico-chemical properties including the morphological modulations of the immobilization platform and thermostability, storage stability, reusability and kinetic parameters of the immobilized enzyme. The preparation of the silver nanoparticles of the immobilization platforms was based on use of various bio-resources (*Mesua ferrea* Linn. leaf extract and orange peel). However, the nanomaterials prepared through green routes may not be green per se as far as their interaction at the bio-interface is concerned. Thus, a few *in vitro* actions of starch (a biopolymer, instead of the afore-stated poly(ethylene glycol)) templated silver nanoparticles prepared using the same bio-resources were probed into as a function of their shape-size-surface chemistry accord (described in the third chapter). Starch supported silver nanoparticles (3-12 nm), prepared using the reductive potency of aqueous extract of orange peel exhibited anti-lipid peroxidation (of goat liver homogenate), DPPH scavenging, synergy with Rifampicin against *Bacillus subtilis* MTCC 736 and cytocompatibility with the human leukemic monocytic cell line, THP-1. On the other hand, evaluation of phytotoxicity on *Cucumis sativus,* compromise on amplification of a 263 base pair mammalian DNA sequence in PCR and anti-microbial potency vouched for the differential action of starch templated silver nanostructure with branched morphology (~440 nm, along the long axis with average branch diameter of 11.5 nm) (generated on aging) and sonicated spherical silver nanoparticles (average diameter, 5.4 nm), prepared using the reductive potency of *Mesua ferrea* Linn. leaf aqueous extract under ambient conditions. The thesis proceeds with the immobilization studies of two bio-medically important phytocompounds, *viz.*, curcumin and lycopene, reported in the fourth chapter. Sonication mediated directed assemblage as triads, tetrads and chains, magnetic responsiveness and synergistic free radical scavenging of poly(ethylene glycol)-iron oxide nanoparticles-curcumin' trio were documented. On the other hand, the aptness of the green chemistry tool of sonication (under statistically optimized

parameters) in conjunction with bio-catalysis was explored for the extraction of tomato peel lycopene. Anti-lipid peroxidation, cytocompatibility with normal L929 cells in contrast to anti-proliferative action against HeLa cells, and stimulatory effect on seed-germination of the (extracted) lycopene coupled biomimetic 'trifoliate' polyaniline (PAni) nanofibers were registered. Furthermore, DMol^3 was employed for the quantum molecular calculations of lycopene interacting with PAni (via non-covalent functionalization involving π–π stacking) and solvation study. The results attested the applicability of the prepared hybrid systems as multifunctional biomaterial. On the other hand, the subsequent chapter focuses on the use of Box-Behnken design technique for tuning the diameter of electrospun cellulose acetate (CA) fibers. The study pertained to three chosen process variables namely potential difference, distance between tip-to-collector and feed rate. The modulations in various physico-chemical attributes of cellulose acetate (CA) nanofibers in the presence of poly(ethylene glycol), electrospun under the same optimized processing parameters. In the perspective of transdermal drug delivery, ampicillin loaded eCA and eCAPEG were checked for the biocompatibility with peripheral blood mononuclear cells and differential antibacterial action against *Staphylococcus aureus*. In the concluding chapter of the thesis, an effort has been made to critically analyse and re-scrutinize the preparation strategies, bio-interfacial action, applications, the limitations, the major achievements and the projection of future prospects of the compiled works.

Keywords:

- Biomolecule immobilization
- Nanomaterials
- Polymers
- Sonication
- Green nanotechnology
- Biomaterial
- Electrospinning

DECLARATION

I do hereby declare that the thesis entitled '**Polymer assisted nanomaterials immobilized biomolecules and their potential applications**', submitted to Tezpur University in the Department of Chemical Sciences under the School of Science, in partial fulfilment for the award of the **Degree of Doctor of Philosophy in Science**, is a record of original research work carried out by me.

All sources of assistance have been assigned due acknowledgment.

I also declare that neither this work as a whole nor a part of it has been submitted to any other University or Institute for any other degree, diploma or award.

Place: Tezpur University
Date: 15/05/2013

(Rocktotpal Konwarh)

DR. NIRANJAN KARAK, M. Tech., Ph. D. (IIT Kgp.)
Professor and Head
Department of Chemical Sciences,
Tezpur University
(*A Central University established by an Act of Parliament*)
Napaam, Tezpur – 784028
Sonitpur, Assam (India)

+91-09957184354,
+91-3712-267007-5056
Fax: +91-03712-267006
Email: nkarak@tezu.ernet.in,
karakniranjan@yahoo.com

CERTIFICATE

This is to certify that the thesis entitled, '**Polymer assisted nanomaterials immobilized biomolecules and their potential applications**' submitted to Tezpur University in the Department of Chemical Sciences under the School of Science, in partial fulfilment for the award of the **Degree of Doctor of Philosophy in Science**, is a record of original research work carried out by **Rocktotpal Konwarh** under my personal supervision and guidance.

All help and support received by him from various sources have been duly acknowledged.

No part of this thesis has been submitted or reproduced elsewhere for the award of any other degree or diploma.

Niranjan Karak 15/05/13

Place: Tezpur University
Date:

(Dr. Niranjan Karak)
Professor & Head
Department of Chemical Sciences, School of Science.

TEZPUR UNIVERSITY
(*A Central University established by an Act of Parliament*)
Napaam, Tezpur-784028
District: Sonitpur, Assam, India

Ph.: 03712-267004, 03712-267005 Fax: 03712-267005, 03712-267006

CERTIFICATE

This is to certify that the thesis entitled **"Polymer assisted nanomaterials immobilized biomolecules and their potential applications"** submitted to Tezpur University in the Department of Chemical Sciences under the School of Science, in partial fulfilment for the award of the **Degree of Doctor of Philosophy in Science**, has been examined by us on …… and found to be satisfactory.

The committee recommends for the award of the degree of Doctor of Philosophy.

Principal Supervisor
Date:

External Examiner
Date:

CONTENT OF THE THESIS

LIST OF ABBREVIATIONS/SYMBOLS

μg: microgram

μL: microliter

μ_r: Retentivity

ALP: Anti-lipid peroxidation

AMG: Amyloglucosidase

Amp: Ampicillin

AMVN: 2, 2'-azobis (2,4-dimethylvaleronitrile)

BET: Brunauer-Emmett-Teller

BOD: Biochemical oxygen demand

BSA: Bovine serum albumin

CA: Cellulose acetate

CCMV: Cowpea chlorotic mottle virus

CEA: Carcino embryonic antigen

CH_2N_2: Cyanamide

CMC: Carboxymethyl cellulose

CNFs: Carbon nanofibers

CNTs: Carbon nanotubes

COD: Chemical oxygen demand

COSMO: COnductor like Screening MOdel

CRP: C-reactive protein

CVD: Chemical vapour deposition

List continued on the next page

DAPI: 4', 6-diamidino-2-phenylindole

df: Dilution factor

DFT: Density Functional Theory

DMEM: Dulbecco's Modified Eagle Medium

DMSO: Dimethylsulfoxide

DNA: Deoxyribonucleic acid

DNSA: 3,5-dinitrosalicylic acid

DPND: Directed patterning of nanoparticle dispersions

DPPH: 2, 2-diphenyl-1-picrylhydrazyl

DSC: Differential scanning calorimetry

eCA: Electrospun cellulose acetate

eCAPEG: Electrospun blended fiber of cellulose acetate and poly(ethylene glycol)

ELISA: Enzyme-linked immunosorbent assay

EMBR: Enzyme immobilized membrane bioreactor

fcc: face-centred cubic

FDH: Formate dehydrogenase

$FeCl_2 .4H_2O$: Iron (II) chloride tetrahydrate

$FeSO_4$: Iron sulphate

FTIR: Fourier Transform Infrared Spectroscopy

FWHM: Full Width at Half Maximum

GatDH: Galactitol dehydrogenase

GGA: Generalized gradient approximation

GOD: Glucose oxidase

GST: Glutathione-S-transferase

List continued on the next page

H_2O_2: Hydrogen peroxide

H_c: Coercivity

HIF-α: Hypoxia-Inducible Factor- α

HOMO-LUMO: Highest occupied molecular orbital and lowest unoccupied molecular orbital

HRP: Horseradish peroxidase

Hz: Hertz

IONPs: Iron oxide nanoparticles

JCPDS: Joint Committee on Powder Diffraction Standards

KBr: Potassium bromide

KOH: Potassium hydroxide

LMG: Leucomalachite green

Luc: Luciferase

MANP: Mesophase assembly of nanoparticles

MCF: Mesocellular siliceous foams

MDA: Malondialdehyde

MIC: Minimum inhibitory concentration

mL: Milliliter

M_n: Number average molecular weight

MNP-E: Magnetic nanoparticles-enzyme conjugates

M_r: Remnant magnetization

M_s: Saturation magnetization

MTCC: Microbial Type Culture Collection and Gene Bank

MTT: 3-(4,5-dimethylthiazol-2-yl)-2,5-diphenyl tetrazolium bromide

List continued on the next page

NAESS: Nano-Assembly platform using Encoded Solid Supports

NaOH: Sodium hydroxide

NCCS: National Center for Cell Science, Pune

ng: nanogram

nm: nanometer

NMR: Nuclear Magnetic Resonance

NTA: Nitrilotriacetic acid

Pa: Pascal

PAni: Polyaniline

PCR: Polymerase Chain reaction

PEG: Poly(ethylene glycol)

PEGA: Polyethylene glycol-polyacrylamide

PEG-Ag-IONPs: Poly(ethylene glycol) supported silver-iron oxide nanoparticles

PEG-IONPs: Poly(ethylene glycol) supported iron-oxide nanoparticles

PMMA: Polymethyl methacrylate

PNA: Peptide nucleic acid

PNC: Polymeric nanocomposites

pNPP: p-nitrophenyl palmitate

POMs: Polyoxometalates

PPL: Porcine pancreatic lipase

PVA: Polyvinyl alcohol

PVP: Polyvinyl pyrrolidone

PZC: Point of zero charge

RAR β: Retinoic acid receptor β

List continued on the next page

Rif: Rifampicin

RSM: Response Surface Methodology

S.D.: Standard deviation

SEM: Scanning electron microscope

SPAN: Self-doped polyaniline

SPIONs: Superparamagnetic iron oxide nanoparticles.

SPR: Surface plasmon resonance

SQUID: Superconducting Quantum Interference Device

SWCNT: Single wall carbon nanotubes

TBA: Thiobarbituric acid

TCA: Tris-chloro acetic acid

TDD: Transdermal drug delivery

TDS: Total dissolved solids

TEG: Tetraethylene glycol

TEM: Transmission Electron Microscope

TGA: Thermogravimetric analysis

THF: Tetrahydrofuran

USEPA: United States Environmental Protection Agency

Van-FLA: Van conjugated to fluorescein amine,

VRE: Vancomycin-resistant *Enterococci*

VSM: Vibrating Sample Magnetometer

XRD: X-ray diffraction

χ: Magnetic susceptibility

LIST OF TABLES

List continued on the next page

LIST OF FIGURES

List continued on the next page

List continued on the next page

List continued on the next page

List continued on the next page

List continued on the next page

ACKNOWLEDGMENT

The task of transcoding my Ph.D. journey in the form of the present thesis remains incomplete without forwarding a note of gratefulness to all those who have directly or indirectly helped me to churn out the best.

Unbound gratitude flows to *Prof. Niranjan Karak*, Department of Chemical Sciences, Tezpur University, for trusting and accepting me as a Ph.D. student under his guidance. Sharing a personal bond and a special rapport with him, his enthusiasm and passion for science complemented with an integral and futuristic view on research will be an inspiration forever. His guidance to set focused objectives and their realization by channeling man and material resources with time management skills would be his most ideal gifts to me. Our brain-storming discussions ranging from science to music and from poetry to patents, his never-tiring spirit to go through and correct the various manuscripts even at the dead of the night even after being assigned with truck- load of tasks, and most importantly the personal care, love and affection for me– I am going to miss. Just, want to say, *Thank you Sir*!! Your words shall remain the fulcrum to balance in the life's acts.

Proceeding ahead, I would like to extend my gratitude to the doctoral committee members. Thank you, *Prof. N.S. Islam* and *Dr. A.J. Thakur* for your constant monitoring of my progress, criticism and appreciation!

I was highly inspired by *Prof. M.K. Chaudhuri*, Vice Chancellor, Tezpur University for his dynamism and positive outlook. Words of encouragement as poured out by *Prof. A.K. Buragohain*, Registrar, Tezpur University shall also be cherished forever.

The experience of my Ph.D. programme in the Department of Chemical Sciences, Tezpur University would have never tasted so pleasing without the encouraging words of the faculty members and the staff, who never fail to exchange a smile in spite of

dealing with hundreds of academic/administrative assignments daily. And most importantly, thanks to the sportive and supportive student friends of the department.

I would like to thank whole-heartedly the members of our Advanced Polymers and Nanomaterials Laboratory. Demonstration and explanation of various techniques and concepts, intertwined with the unconditional help and support, offered by my senior research scholars- *Suvangshu* da, *Harekrishna* da, *Uday* da, *Gautam* da and *Buddha* da (all bearing the 'Dr.' as the prefix in their names) would be personally cherished forever. My Ph.D. programme was made vibrant in the lab, canteen and outside by the never daunted, hardworking and cooperative lab-mates- *Hemjyoti, Sujata, Shaswat, Beauty, Bibekananda, Suman* and *Satyabrat,* who were always found experimenting much before I had reached the lab in the morning hours. Gratitude is also extended to all the M.Sc. and M. Tech students who have completed their respective project works in our lab during my stay.

Gratitude is also extended to the faculty and staff members of the Departments of Molecular Biology and Biotechnology; Food Engineering and Technology; and Physics, Tezpur University for helping and permitting me to use their resources for executing different experiments, various characterization and analysis.

Words sound too poor while I offer my regards to *Prof. T.K. Maiti,* Dept. of Biotechnology, IIT-Kharagpur and *Dr. M.A. Laskar,* Department of Biotechnology, St. Anthony's College, Shillong. Miss K. Sanjana P. Devi and Miss Ruby Philip are thankfully acknowledged for helping me out in some of the bio-related experiments. I also extend my gratitude to the staff of CIF, IIT-Guwahati and RSIC, NEHU, Shillong for VSM and TEM analyses respectively.

I express my gratefulness to the Department of Biotechnology, Government of India for my junior and senior research fellowships. I am indebted to *Prof. A.K. Mohanty,* Bioproducts Discovery and Development Centre (BDDC), Department of Plant Agriculture, Crop Science Building, University of Guelph, Canada, for accepting me as a visiting researcher under Canadian Commonwealth Scholarship, Canadian Bureau for International Education, Foreign Affairs and International Trade, Canada, DFAIT. Gratitude is due to *Prof. M. Misra,* BDDC for introducing me to the wonderful area of electrospinning. The memories of attending safety workshops, lab trainings, discussions, outings, photo-sessions and most importantly *Star-Buck's* hot-chocolate shared among the members of the BDDC are indelible. The assistance received from

Vida, Vidhya and *Jay*, University of Guelph, in various analytical tools, is thankfully acknowledged.

Acknowledgments are extended to the proprietor of Sonu Computers, Napaam, Tezpur for the printouts and re-printouts of the various chapters of the thesis!!

Special thanks go out to *Mukti, Trideep, Papu, Dipankar, Gitartha, Sushanta, Paban, Mon, Rakesh, Kumar, Pankaj Losan, Akash, Reba, Dhruba, Dibakar, Debasish, Pankaj, Amlan, Vishal and many more* for being there for me.

I take this privilege to extend a bouquet of gratitude to my parents (*Ma* and *Deuta)* and my dearest brother for their constant support and morale boost-up ever-steering my career with a positive thrust.

And, lastly, thanks to all those whom I have actually forgotten to enlist on this page.

Date: 15/05/2013

(Rocktotpal Konwarh)

Chapter 1

Introduction

HIGHLIGHTS OF THE CHAPTER*

This chapter gives a comprehensive introductory peek into the framework for the execution of the present work *i.e.,* biomolecule- immobilization onto the *avant-garde* polymer supported nanomaterials. The basic idea is to confine/anchor the biomolecules of interest in or on an appropriate support for their stability and functional reuse. These strategies make these bio-active molecules much more efficient and cost effective for their industrial applications. Starting off with various immobilization strategies (including different green approaches) and their respective pros and cons, the chapter moves onto the assessment of the spectrum of polymeric and nanostructured immobilization platforms, a survey of the progress in biomolecule immobilization studies including the hunt for appropriate immobilization platform and protocols for efficient and easy immobilization over the last few years and the various characterization tools and strategies. In the backdrop of these discussions, the objectives and the strategies of the present work have been highlighted.

*Parts of this chapter are published in

1. Konwarh, R., & Karak, N. et al. *Biotechnol. Adv.* **31**, 421--437, 2013.
2. Konwarh, R., & Karak, N. *Adv. Colloid Interface Sci.* (Communicated)

1.1. Overview

Nature is the school for material scientists. Amongst others, the 'contact sport' of material science and life science has led to a myriad of innovations of the present day. [1] To cite for evidence, immobilization of biomolecules onto various classes of novel materials[2] have found applications across different domains. It is pertinent to mention that the soft and flexible nature yet well-organized architectures together with high specificity and efficiency (resulting in incredible functions) represent the hallmark features of biomolecules. However, their performance being optimal only under ambient conditions and maintenance of structural stability in limited environments restrain their practical utility. An ideal strategy to exploit their exclusive properties and cope with the issues of functionality and stability for practical applications is to design hybrids comprising of materials of biological origin immobilized onto suitable matrices.[2]

Biomolecule- immobilization refers to the technique of confining/anchoring them in or on an appropriate support for their stability and functional reuse.[3] The underlying objective is to make these bio-active molecules much more efficient and cost effective for their industrial applications. The various research publications and patents over the years highlight the different aspects of biomolecule immobilization *viz.*, hunt for appropriate immobilization platform and protocols for efficient and easy immobilization to manipulate the attributes of the immobilized biomolecules for various biomedical and industrial applications.[3,4]

It is relevant to mention that the unison of nanotechnology with the domain of polymer science has opened up multihued panorama of application-oriented utilities. In this context, polymeric nanocomposites have instigated tremendous excitement due to a colossal number of improved facets over the pristine polymer for a spectrum of applications.[5] These systems are of considerable interest in various research fields, due to their intriguing physico-chemical characteristics and their potential application in catalysis, microelectronics, sensing, magnetism, photonics, energy storage, packaging sectors, flame-resistant, surface-coating, high-strength advanced materials, biomaterials and so on.[6-10]

Today, various scientific literature databases host a number of references on polymeric nanocomposites with nano clay, carbon nanotubes (CNTs), carbon nanofibers (CNFs), graphene, nanocrystalline metals and a truck load of inorganic filler or fiber modifications. On the other hand, macromolecules like starch, chitosan and

poly(ethylene glycol) (PEG), various vegetable oil based polymers[7-10] are emerging as apt choices in the context of sustainability, biocompatibility and biodegradability for a plethora of applications. At this juncture, it is notable that mining of scientific literature from the database, SciFinder® yielded some pertinent data pertaining to biomolecule immobilization. A set of 2988 references could be traced in SciFinder® for the search query 'biomolecule immobilization' on 29th July 2012. On the other hand, addition of the term 'nano' and 'polymer' to the root query of 'biomolecule immobilization' yielded a return of 490 and 348 references respectively. The year-wise categorization of the references over the last 5 years (2008-2012) is depicted in Fig.1.1.

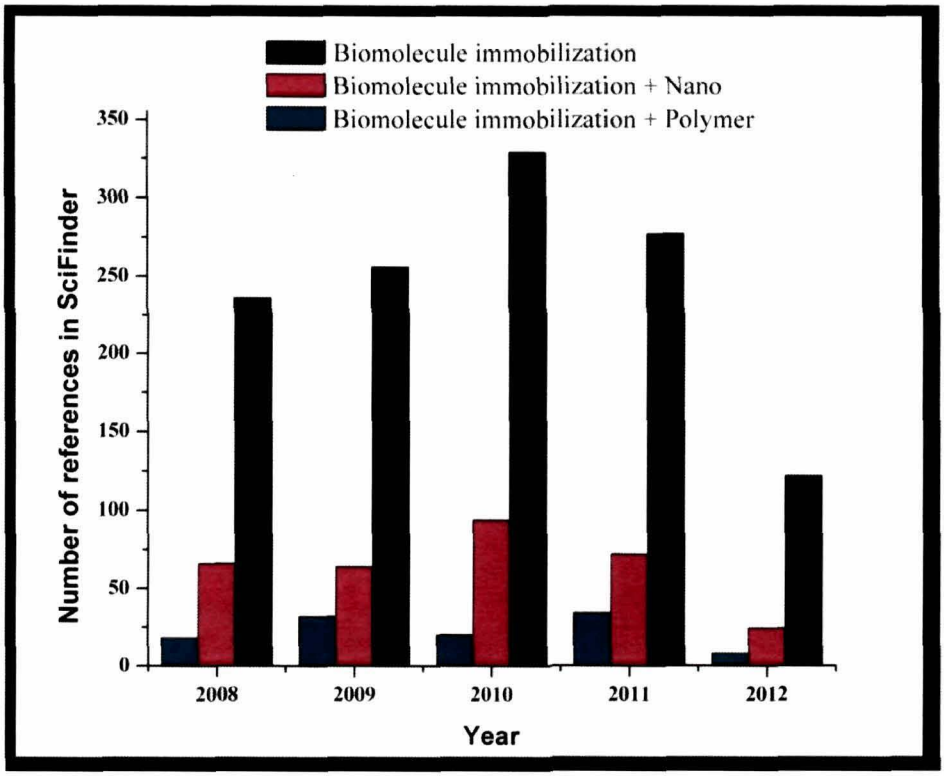

Fig.1.1. *Histogram showing the number of hits for the search queries- 'biomolecule immobilization', 'biomolecule immobilization + nano' and 'biomolecule immobilization + polymer' in SciFinder®*

Thus it can be easily agreed upon that that literature reports abound on biomolecule immobilization onto nanomaterials and polymers separately. However, only 13 references were returned for the search query 'biomolecule immobilization + polymer nanocomposite'. This may form the foundation for developing strategies for biomolecule immobilization onto polymer supported nanomaterials for advanced applications.

Nanomaterials (with their own unique properties owing primarily to the shape-size accord and quantum confinement) templated in polymeric matrices[5,6] are expected

to provide numerous advantages (compared to use of nanomaterials or polymers alone) like better stability of the conjugated biomolecule, higher probability of reproducible results with recyclability (for magnetic nanoparticles) and others. For example, a biocompatible/biodegradable polymer like PEG can not only be used for stabilization/capping of magnetic iron oxide nanoparticles (IONPs) within a narrow size spectrum[11] but this may also efficiently stabilize a biocatalyst in the polymer assisted nano-biocomposite. They may also lend opportunity to prepare and modulate precise structures by both top-down fabrications and bottom-up assembly for numerous applications like biosensing, catalysis etc. These days, research is also focused upon the development of multifunctional nanomaterials. For example, such nanostructured materials may have the ability to carry one or more therapeutic agents and used for biomolecular targeting through one or more conjugated antibodies or other recognition agents; imaging-signal amplification, by way of doping fluorophores or other contrast agents; and biobarrier avoidance, exemplified by poly(ethylene glycol) (PEG) to avoid macrophage uptake (Fig.1.2).[12]

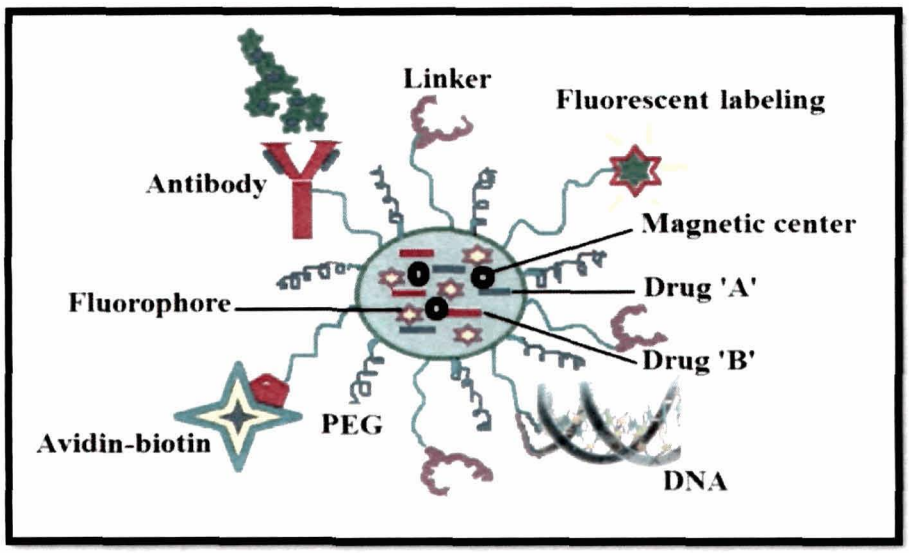

Fig.1.2. *A representation of multifunctional NP (adapted from reference 12)*

However, a very critical aspect to address is the methodology for preparing such hybrid systems. A surmounting pressure of 'going green' amongst the scientific fraternity has dictated the researchers to explore and exploit the nature's way of preparing nanomaterials[13] as well as opt for tools of green chemistry for biomolecule loading.[14] But, this may not be the complete story. Even such green materials need to undergo toxicity assessment before commercializing them for practical applications. Furthermore, optimization of process parameters (say, through tools like response surface methodology) for preparation of the immobilization platform and consequent

bio-conjugation can significantly improve the overall performance.[15] Research on bio-organic/inorganic nanohybrids[2] is gradually emanating as an interdisciplinary field resulting from the interfaces between biotechnology, materials science in particular polymer research, and nanotechnology. They are 'well-blessed children' from both the biological and material worlds[2], and should succeed in providing essences and advantages of the both for *avant-gárde* applications.

1.2. Strategies for biomolecule immobilization

There exists a plethora of prospective candidates for immobilization which includes- various biocatalysts, drugs, lipids, nucleic acids, ligands, natural compounds etc.[16] The methods of immobilization of these different molecules are almost the same. Although it has been stated that there is no general universally applicable method of certain molecule immobilization,[17] a number of literature reports and reviews[16,18] throw insight on the myriad techniques used for immobilization of various biomolecules, either alone or in combination with each other. In this context, the following discussion is focussed with special reference to some of the enzyme (one of the much focused upon biomolecules)-immobilization techniques.

It is pertinent to mention about the indispensable parameters that are to be considered while planning for biomolecule immobilization as described by Hanefeld et al.[3]

- *Biomolecule associated parameters (e.g.,* size of the biomolecule, conformational flexibility, stability under immobilization conditions etc.)
- *Carrier associated parameters (e.g.,* surface charges, surface functionalization, chemo-mechanical stability, surface area, porosity, particle size etc.)
- *Specific factors related to the immobilized system (e.g.* diffusion limitations, enzyme inhibition, precipitation of products, non-specific solute-support interaction etc.)

To elaborate further, attributes of adequate shape-size, mechanical property and high stability of the carrier in various solvent system aid in separation, easy control of reaction, flexibility of reactor design with fewer diffusion constraints. Operational stability, thermostability, conformational stability of the immobilized biocatalyst are desirable for high productivity and space-time yield of desired product. On the other hand, recyclability, broad applicability and reproducibility of the immobilized system ensure cost-effectiveness, tolerance in process variation and product quality. Lower

volume and rational design of the immobilization system facilitate lower cost for handling and avoidance of laborious screening. Easy disposal and safety for use are two important facets as well. Features of innovativeness and competitiveness are signature marks for commercialization of the immobilized biomolecules.

Moving on, Di Marco et al.[19] and Elnashar[16] have adequately focused on the various biomolecule immobilization techniques (Fig.1.3). This is presented in brief in the following section.

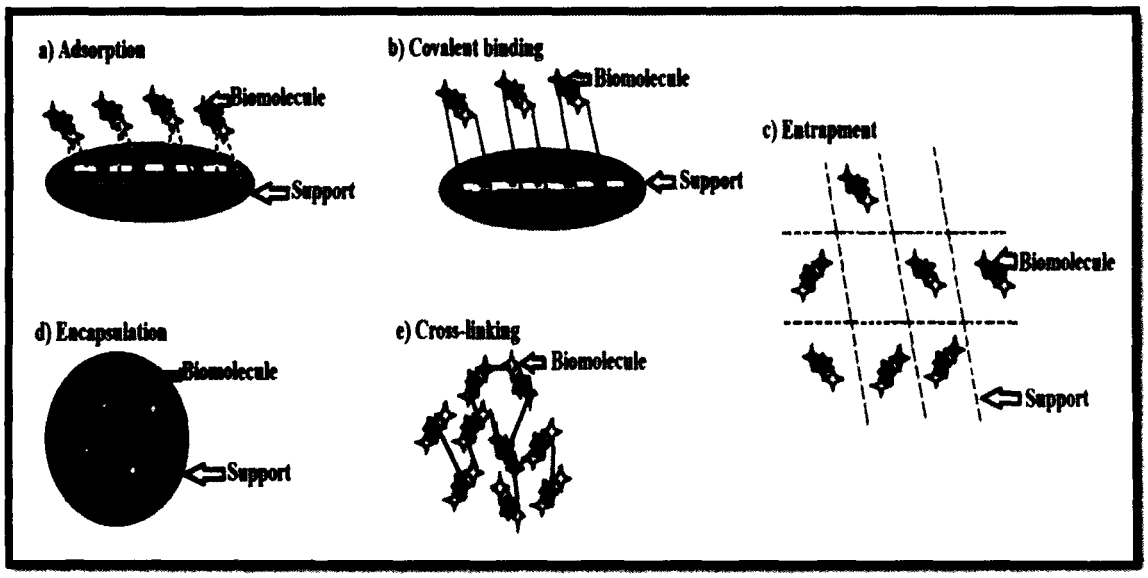

Fig.1.3. *Various strategies for biomolecule immobilization*

1.2.1. *Adsorption and ionic binding*

In this approach, non-covalent linkages (ionic or hydrophobic interactions, hydrogen bonding, and van der Waals forces) are used to attach the biocatalyst to the support, without any pre-activation step of the latter.[16] As far as adsorption is concerned, the following attributes are pertinent to mention:

- The prevailing surface chemistry of the support and the type of surface exposed amino acids (in case of biocatalysts) dictate the interactions.
- The matrices range from inorganic carriers (ceramic, alumina, activated carbon, kaolinite, bentonite, porous glass, nanoparticles etc.) and organic synthetic carriers (nylon, polystyrene), to natural organic carriers (chitosan, dextran, gelatin, cellulose, starch).

On the other hand, ionic binding of active molecules to supports containing ionic charges is stronger than physical adsorption.

- The maintenance of the optimal ionic strength and pH conditions is prerequisite to prevent the biomolecule leaching.

- ❖ Preferred supports for immobilization by ionic binding ranges from polysaccharide derivatives like diethylaminoethylcellulose, dextran and synthetic polymers like polyethylene vinyl alcohol to inorganic materials like silicates, bentonite etc.

1.2.2. *Covalent binding by chemical coupling*

The availability and reactivity of various functional groups of the biomolecules for covalent bonding and the stability of the covalent link, once formed dictates this approach.[16]

- ❖ Specific reagents (*e.g.*, cyanogen bromide, carbodiimide, aminoalkylethoxysilane, isothiocyanate, and epichlorohydrin, etc.) are used for the activation of the functional groups on the support.
- ❖ Often spacer arms on the support (conferring a greater degree of mobility to the immobilized biomolecule) are used instead of direct covalent bonding.
- ❖ Diazotation, amino bond, Schiff's base formation, amidation reactions, thiol-disulfide, peptide bond, and alkylation reactions are some of the common reaction procedures for the covalent coupling.
- ❖ A number of supports are available for covalent loading of biomolecules, *e.g.*, hydrophilic natural polymers with extensive hydroxyl groups- ideal for participating in covalent linkages.

1.2.3. *Entrapment and encapsulation*

The active components (like dyes, drugs, enzymes and other chemicals) are physically trapped into a film, gel, fiber, coating, or microencapsulation.[16]

- ❖ The bioactive moiety is mixed with a polymer like polyurethane, followed by the latter's crosslinking to form a lattice structure that traps the former.
- ❖ Spherical semipermeable polymer membranes with controlled porosity are employed for microencapsulation.

1.2.4. *Cross-linking*

Bi- or multifunctional reagents (*e.g.*, glutaraldehyde, glyoxal, diisocyanates, hexamethylenediisocyanate, toluene diisocyanate, etc.) are used to crosslink individual bio-catalytic units (enzymes, organelles or whole cells).[16]

- ❖ Amino groups of the lysine, the sulfhydryl groups of cysteine, phenolic OH groups of tyrosine, or the imidazol group of histidine are generally involved in crosslinking.
- ❖ Cross-linked biocatalysts often exhibit modulated conformation with a resultant loss of activity.

A comparative account of the various pros and cons of the immobilization approaches are enlisted in Table1.1. It is also relevant to mention that chemical modification of the matrix particularly in the case of biodegradable polymers, often lead to material degradation. Tremendous decrease in bioactivity and incorrect orientation of the biomolecules are additional challenges. To address these issues, the binding domains of lectins, immunoglobulin G (IgG) binding domains of protein G and protein A, and carbohydrate binding modules (present in many polysaccharide-degrading enzymes) may be used as affinity tags for immobilizing proteins to affinity adsorbents.[15]

Table1.1. *Pros and cons of the various conventionally used immobilization protocols*[16-19]

Technique (Reference)	*Advantage*	*Disadvantage*
Adsorption (Menaa et al.[20])	❖ Reversibility, which enables not only the purification of proteins but also the reuse of the carriers. ❖ Simplicity, which enables enzyme immobilization under mild conditions. ❖ Possible high retention of activity because there is no chemical modification. ❖ Cheap and quick method. ❖ No chemical changes to the support or enzyme occurs.	❖ High probability of leaching due to relatively weak interaction between the enzyme and the carrier, which can be destroyed by desorption forces such as high ionic strength, pH, etc. ❖ Contamination of product. ❖ Non-specific binding. ❖ Overloading on the support and steric hindrance by the support.
Covalent binding (Xie et al.[21])	❖ No leakage of enzyme. ❖ The enzyme can be easily in contact to substrate due to the localization of enzyme on	❖ Expensive supports ❖ The harshness of reaction conditions of coupling often leads to

Table continued on the next page

	support materials. ❖ Immobilization of enzymes through covalent attachment has also been demonstrated to induce higher resistance to temperature, denaturants, and organic solvents in several cases.	conformational change of the biomolecule. ❖ Loss of enzyme activity (*e.g.*, involvement of active centre in the binding may lead to mismatched orientation of enzyme).
Entrapment (Riaz et al.[22])	❖ Enzyme loading is very high	❖ Enzyme leakage from the support. ❖ Diffusion of the substrate to the enzyme and of the product away from the enzyme
Encapsulation (Patil et.al. [23])	❖ The enzymes could be encapsulated inside the cell. ❖ Possibility of co-immobilization where cells and/or enzymes may be immobilized in any desired combination to suit particular applications.	❖ Acute diffusion-associated problems that may result in rupture of the membrane if products from a reaction accumulate rapidly.
Cross-linking (Xie T. et al. [21])	❖ The immobilization is support-free. ❖ Cross-linking between the same enzyme molecules stabilises the enzymes by increasing the rigidity of the structure.	❖ Harshness of reagents used for crosslinking ❖ The enzyme may partially lose activity or become inactivated in case the crosslinking reagent reacts across the active site.

1.3. Green chemistry strategies for biomolecule immobilization

An increasing thrust on the global scientific fraternity is to opt for tools and techniques that confer 'green credentials' to its research output. Some of the green approaches for biomolecule- immobilization strategies that merit special mention are enlisted underneath:

1.3.1. *Biocatalytic immobilization*

Phosphopantetheinyl transferase Sfp catalysed site-specific mild, quantitative and rapid covalent immobilization (occurring in a single step without prior chemical modification of the target protein) of luciferase (Luc) and glutathione-S-transferase (GST) ybbR-fusion proteins onto polyethylene glycol-polyacrylamide (PEGA) resin has been reported with high activity retention of the immobilized proteins.[14]

1.3.2. *Ionic liquid*

Although costly, ionic liquids are considered green solvents of the future. Based on a biphasic catalytic system where the enzyme was immobilized into an ionic liquid *i.e.*, 1-butyl-3-methylimidazolium hexafluorophosphate, Rumbau and co-workers have reported a novel method which allowed recycling and re-using of horseradish peroxidase (HRP) in the biocatalytic synthesis of polyaniline.[24]

1.3.3. *Microwave technology*

Microwave irradiation has been used for the immobilization of papain and penicillin acylase using the adsorption technique into the mesocellular siliceous foams (MCFs).[25,26]

1.3.4. *Photoimmobilization technology*

HRP and glucose oxidase (GOD) have been immobilized onto the photoreactive cellulose membrane by ultraviolet and sunlight[27] with an important observation that sunlight exposure (with optimal intensity of 21,625 lux) gave better immobilization compared to 365 nm UV light.

1.3.5. *Sonication*

Recently, it has been found that alkaline phosphatase immobilized onto IONPs via sonication in presence of carbodiimide retained much higher activity when compared to immobilization through shaking.[28] Further, sonication has been reported to reduce the time of immobilization from 16 h to 10 min for tyrosinase conjugation onto amine functionalized carbon felt surface via glutaraldehyde-coupling. This also led to enhanced substrate sensitivity and operational stability.[29]

Streamlining the biomolecule immobilization protocols in lines of such greener routes and process optimization befitting the industrial and biomedical domains are highly anticipated.

Amongst the spectrum of technologies available for bioconjugation, probing into the prospects of sonication (a 'green chemistry' tool) mediated immobilization seems to be an interesting proposition. Although sonication has been used as an essential step in activation or functionalization of various nanomaterials including single wall carbon nanotubes (SWCNT)[30] for different biomedical applications, the prospects of biomolecule immobilization onto polymer supported nanomaterial/polymeric nanomaterial using sonication (one of the major focus of the present thesis, as noted in the subsequent chapters) have not been explored much. Before, proceeding further, it would be relevant to mention about the basics of ultrasonication at this juncture.

Generation of high frequency mechanical vibrations by stimulating piezoelectric crystals (with attached ultrasonic probes) with high frequency oscillating electrical currents forms the basis of ultrasonication.[31,32] When the probe contracts (on application of electrical current), negative pressure causes a liquid to flow up while the expansion of the crystals (on the reversal of the current) pushes the liquid. Due to mismatch in the pace of the liquid and the oscillation, small cavities are generated during the contraction. In general, cavitation pertains to the occurrence of vapour in a fluid attributed to local low pressures (generated by high local flow velocities).[31,32] The rarefaction and compression cycles dictate the size of the cavitation bubbles. During the expansion cycle, the transient cavitations rapidly implode and create microscopic shock waves (that is to say they end up in collapse within a short span of time). The stable cavitations resonate and survive the local pressure variations for a number of acoustic cycles in the applied sound field. Cavitational collapse produces intense local heating and high pressures. When collapse of a cavity occurs in a solution free of solid particles, heating is the only consequence. However, if implosion occurs near a solid surface, implosion is asymmetric. As water rushes to fill the void left by the imploding bubble shock pressures of 1-5 kPa can be generated. On the other hand, biomolecule immobilization relies on the fact that sonication can bring reactants to close proximity for interactions.

The surface intensity (I) *i.e.,* the power output per surface area of the sonotrode as a function of amplitude (A), pressure (p), reactor volume (V_R), temperature (T), viscosity (η) and others can be represented as[31, 32]:

$$I[W/mm^2] = f(A\ [\mu m],\ p\ [bar],\ V_R\ [mL],\ T\ [^oC],\ \eta\ [cP]...) \quad \text{.....(1.1)}$$

while the total power output, P_L [W] is the product of surface intensity (I) and surface area (S)

$$P_L\,[W] = I[W/mm^2] \times S\,[mm^2] \quad \text{.....(1.2)}$$

Consideration of the sonicated sample volume (V) and time of exposure (t) is prerequisite for making a sonication process scalable and reproducible.[31,32] Energy per volume dictates a particular process result (*e.g.*, particle size),

$$\text{Result} = f[E/V] \quad \text{.....(1.3)}$$

Where, the energy, E is given as:

$$E\,[Ws] = P\,[W] \times t\,[s] \quad \text{.....(1.4)}$$

Thus, it can be easily inferred that optimization of these process parameters is indispensable.

Furthermore, sonication has played quite an important role in material chemistry and particularly in the preparation of various nanostructured materials with different shape-size accord.[33] In this context, use of statistical tools like response surface methodology (RSM)[34] can be quite instrumental in optimizing the sonication parameters during the preparation of the immobilization platform as well as biomolecule loading.

In a recent review, Bezerra et al.[34] have focussed on the suitability of RSM in optimization studies. The prime objectives of RSM are:

(1) to choose the independent variables of major influence on the system post screening studies, delimit the experimental region in accordance to the study-objective and the researcher's experience;

(2) to select an experimental design and execute the experiments in the context of the selected experimental matrix;

(3) to fit a polynomial function of the experimental data via the latter's mathematic–statistical treatment;

(4) to assess the model's fitness;

(5) to verify the inevitability and option of executing a displacement in direction to the ideal/optimal region; and

(6) to obtain the optimum values of the variables under consideration.

Codification of the levels of the variable is important in RSM. Each studied real value is transformed into coordinates within a scale with dimensionless values. This should be proportional at its localization in the investigational domain. Codification facilitates the analysis of variables of varied orders of magnitude without the larger affecting the assessment of the smaller. The following equation can be applied to

transform a real value (z_i) into a coded value (x_i) according to a determinate experimental design:

$$x_i = (z_i - z_i^o / \Delta z_i)\, ß_d \quad \text{..... (1.5)}$$

where, z_i is the distance between the real value in the central point and the real value in the higher or lower level of a variable, $ß_d$ is the major coded limit value in the matrix for each variable, and z_i^o is the real value in the central point.

1.4. Nanomaterials and polymeric immobilization platforms- a focus on the present status.

The previous sections were suggestive of the existence of a plethora of immobilization platforms, the choice being dictated by the adopted immobilization strategy. In this context, the spectrum of inorganic nanomaterials and polymeric materials[35-38] demand a special merit.

- *Noble metals* like Au, Ag, Pt, Pd
- *Carbon based materials* like carbon nanofibers (CNFs), multiwalled nanotubes, single walled nanotube
- *Semiconducting materials* like CdSe, CdS, TiO_2, Si/SiO_2, PbS, InP
- *Nanoclay*
- *Magnetic materials* like Fe_3O_4, Co, $CoFe_2O_4$, FePt, CoPt and their composites
- *Lanthanide materials* like Gd_2O_3, Eu_2O_3
- Single *polymeric nanoparticles* such as gelatin, PGA, PBCA, PMMA, PACA, block copolymers such as PEG-*b*-PLGA and PEG-*b*-PDLLA, polymeric micelles such as PLA, PCL, PAsp, PGlu, PLys, PHis and dendrimers (PAMAM), polyurethane
- *Polysaccharides*: chitosan and chondroitin (animal origin), alginates (algal origin), pectin, guar gum (plant origin), dextran, xanthan gum (microbial origin),
- *Lipid materials* like liposomes, lipopolyplexes, solid lipid nanoparticles
- *Virus capsids and related cage-like proteins* (Cowpea chlorotic mottle virus (CCMV), vault nanocapsules, heat shock protein, hepatitis B cores, ferritin, MS2 and M13 bacteriophages)

The properties of the nanomaterials are markedly different from those of their bulk counterparts for two main reasons: the increased relative surface area and the quantum confinement effects.[39] The increase in the surface area also increases the nanoparticles' chemical reactivity and ability to interact with added functional

materials. The display of unique material properties by the nano-scaled materials (*e.g.,* surface plasmon resonance (SPR) and antibacterial potency of silver nanoparticles)[40] make them an opt choice as immobilization platform for development of multi-functional systems. The science of biomolecule immobilization has come a long way over the years and various scientific literature databases host a number of reports on immobilized biomolecules onto various nanomaterials and polymeric materials. In this context, delving into some of the recent patents (Table1.2) filed in various parts of the globe (a non-exhaustive list, retrieved from SciFinder® for the time-frame 2008-2012) would be enough to marshal in support of the diverse spectrum, status and possible scope of the topic under consideration. These can be bracketed together with the immense commercial prospects in the domain of biomolecule immobilization onto polymers and nanomaterials.

Table1.2. *Results retrieved from SciFinder for the search queries, 'Polymer + biomolecule immobilization' and 'Nano + biomolecule immobilization', with limiter sets of document type: patent and year range: 2008-2012*

Sl. No.	*Patent number, Date*	*Patent highlights*
1	US20080024117, 2008/01/31	An ultra-sensitive SQUID–based magnetoreduction measurement system using dextran-coated magnetic nanoparticles coupled to anti-goat C-reactive protein (CRP), monoclonal antibodies and anti-rabbit leucomalachite green (LMG) to assay human CRP, human coagulation factor IX, and LMG respectively.[41]
2	JP 2008043419, 2008/02/28	Polyvinyl alcohol (PVA) nanofiber nonwoven fabric, surface modified with hexamethylene diisocyanate and immobilized type I collagen as artificial cornea.[42]
3	WO 2008048209, 2008/04/24	Immobilization of biomolecules on the inner surface of nanofluidic channels and measurement of nanochannel conductance for detection of binding event.[43]
4	WO 2008131063, 2008/10/30	3-acryloxypropyl trimethoxysilane, carboxyethylsilanetriol, and (optionally) PEG-silane functionalized silica nanoparticles bound to antibody to detect *Staphylococcus aureus.*[44]
5	WO 2008140620, 2008/11/20	Double-stranded DNA co-loaded gold nanoparticles and co-immobilized capture molecules for ultra-sensitive

Table continued on the next page

		level detection of target analytes like proteins, DNA and peptides.[45]
6	WO 2008143351, 2008/11/27	Large-scale chemical surface nanopatterns to increase activity of biomolecules confined to fouling-area on a homogeneous surface.[46]
7	WO 2008012391, 2008/01/31	Treatment of surfaces (containing available hydroxyl groups and free from metals and metallic alloys) with orthophosphoric acid for immobilization of biomolecules, cellular membranes, liposomes, cells etc.[47]
8	WO2008062168, 2008/05/29	Biocatalyst-mediated activation of immobilized anti-inflammatory biomolecules for prospective application in prosthetic implants and scaffolds.[48]
9	US20080161200, 2008/07/03	Amine-reactive polymers coated onto amine modified substrates for immobilization of oligonucleotides.[49]
10	WO2009009188, 2009/01/15	Silica nanoparticles with water-dispersible groups, shielding groups and biomolecule binding groups.[50]
11	CN101392290, 2009/03/25	Use of magnetic nanoparticles affixed with colloid gold/avidin/aldehyde and solid-phase single base circular extension to detect single base difference.[51]
12	KR2009060143, 2009/06/11	Quantification of biomolecules using a frequency magnetic reader that measures number of magnetic nanoparticles marking the biomolecules immobilized on a strip type substrate.[52]
13	US20090208919, 2009/08/20,	Matrices for manipulation of biopolymers, including separation, purification, immobilization and archival or dry state storage of biomolecules and biopolymers.[53]
14	US20090258355, 2009/10/15	Application of Nano-Assembly platform using Encoded Solid supports (NAESS) to assemble nanomaterials at a colloidal substrate in a layer-by-layer fashion in which the interactions between layers have been encoded using biomolecules allowing for controlled interactions, purification of side products, modularity and construction of complex architectures like Janus particles.[54]
15	WO2009031804,	Polymer (prepared by polymerization of a) monomer

Table continued on the next page

	2009/03/12	having a surface-anchoring group, b) a monomer having a group that is repellant to unwanted proteins and c) a monomer having a reactive group for covalently binding to test biomolecules) for coating biochips and biosensors with anti-biofouling layers with good substrate anchoring behavior.[55]
16	DE102007049335, 2009/04/16,	Water-soluble polymers with chelators for reversible biomolecule binding and identification[56]
17	WO2009115938, 2009/09/24	Flow-through/porous polymeric membrane with spots (separated from each other by internal support) for biomolecule immobilization.[57]
18	KR2010030105, 2010/03/18	Radiation mediated immobilization of biomolecules and pattern formation on biodegradable polymer.[58]
19	US20100072080, 2010/03/25	Functionalized nanopipette with immobilized peptide ligand for biomolecule detection.[59]
20	WO2010066432, 2010/06/17	Use of polyelectrolyte layers in absorbent porous carrier for biomolecule immobilization and separation.[60]
21	CN101789295, 2010/07/28	Use of gold/silica/ferroferric oxide core-shell composite magnetic nanoparticles for detection of cellulase gene.[61]
22	WO2010115147, 2010/10/07	Use of metal nanoparticle-based biosensor for detecting fluorescently-labeled biomolecules and use in real time DNA sequencing.[62]
23	US20100255610, 2010/10/07	Use of a composition containing a surfactant and highly concentrated gold colloid nanoparticles coated with a protein ligand (*e.g.*, protein A, protein G etc,) for rapid biomolecule quantification assay.[63]
24	US20100304500, 2010/120/2	Mercaptoethanol molecules functionalized ZnS:Mn phosphorescent nanoparticles based biosensor for detecting avidin bio-conjugated antibodies.[64]
25	KR2010126928, 2010/12/03	Use of magnetic nanoclusters (which are magnetic nanoparticles, modified and linked post a series of biomolecule functionalization) for magnetophoretic biomolecule assay.[65]
26	KR2011012463, 2011/02/09	Immobilization of enzymes and biomolecules on nanocomposite of ferrocene-substituted polysiloxane

Table continued on the next page

		and chitosan.[66]
27	WO2011045394, 2011/04/21	Dendrimer functionalized and stabilized nanoparticle for conjugating a target analyte.[67]
28	US20110098445, 2011/04/28	Attachment of peptides and biomolecules onto luminescent semiconductor nanocrystals/quantum dots using covalent binding.[68]
29	KR2011065231, 2011/06/15	Encapsulation of gold nanoparticle and biomolecule oxidase within alginate matrix for detection of biomolecules.[69]
30	WO2011100638, 2011/08/18	Disordered array of nanosprings and nanowires as high surface area supports for biomolecule, chemical, drug and cell attachment.[70]
31	US20110236260, 2011/09/29	Barcode nano-wire for decoding a hard magnetic segment by using highly sensitive magnetic sensors and a bio-sensing system for a specific bio-analyte using the barcode nano-wire.[71]
32	US20110281288, 2011/11/17	Detection and quantification of troponin I using calmodulin-glutathione S-transferase associated glutathione/silicon nanowire field effect transistor.[72]
33	WO2011052205, 2011/05/05	Polymer-coated ferrite nanoparticles (with excellent water dispersibility) for biomolecule immobilization via surface exposed carboxyl groups derived from polyacrylic acid.[73]
34	WO2012085303, 2012/06/28	Materials with a nucleus of hybrid superparamagnetic nanoparticles and vinyl sulfone groups for biomolecule immobilization.[74]
35	CN102608188, 2012/07/25	Invention related to cleaning, activating and characterizing glassy carbon electrode, electrodepositing nanogold, dispensing 3D composite nanofilm, dispensing protein A, self-assembling carbofuran monoclonal antibody, and soaking in bovine serum albumin (BSA) solution to block the nonspecific binding sites; and establishing working curve of immunosensor, detecting performance (such as selectivity, stability and regenerability) of the immunosensor, and detecting

Table continued on the next page

		actual sample with the immunosensor.[75]
36	WO2012120387, 2012/09/13	Rapid quantification of biomolecules using the concept of liquid actuation and selective functionalization of surfaces in a nanochannel that creates a concentration gradient of transitory immobilized biomolecules across the nanochannel.[76]
37	WO2012140433, 2012/10/18	Use of lock-release immobilization technique for purifying, producing and storing biomolecules using diketone group containing polymer support.[77]
38	WO2012150373, 2012/11/08	Multifunctionalized nanoparticles conjugated to DNA/PNA (*i.e.*, peptide nucleic acid) with attached complementary molecule for applications such as fluorescent marking of human tumor cells, use with tumor antibodies to induce magnetic hyperthermia, magnetic capture and fluorescent marking of muscle larvae, and drug transport.[78]

It would be quite a mammoth task to present each of the diverse research findings on biomolecule immobilization in this chapter. And as such, the discussion (as presented in the subsequent section) has been streamlined specifically on the present status and gamut of applications of the materials used for the various studies reported in the present thesis.

1.4.1. *Iron oxide nanoparticles*

Amongst others, bio-conjugated magnetic nanoparticles (MNPs) have captured a unique niche of their own with multiple applications reported across different domains.[79] Fig.1.4 stands in testimony to this fact. Fig 1.4i depicts a straightforward strategy to detect bacteria in blood sample. Polyvalent interactions between vancomycin (Van) (conjugated to FePt nanoparticles) and D-Ala-D-Ala on the bacterial surface, followed by staining with fluorescent vancomycin (Van conjugated to fluorescein amine, Van-FLA) and observation using fluorescence microscope allows the easy detection of pathogens such as vancomycin-resistant enterococci (VRE) and other Gram-positive bacteria with high sensitivity.[80] Magnetite nanoparticles, decorated by bisphosphonate (BP) are effective agents for selective and rapid removal of radioactive toxins (e.g., upto 99% and 69% of UO_2^{2+} from water and blood) (Fig 1.4ii).[81] Use of recyclable nitrilotriacetic acid (NTA)-terminated highly specific magnetic nanoparticles

(synthesised using dopamine as a robust anchor) eliminates the pre-treatment of cell lysate for the effective and quick separation (Fig 1.4iii) of six histidine (6x His)-tagged protein.[82-83] On the other hand, the amenability for controlling size and external manipulation, and enhancement of contrast in magnetic resonace imaging, magnetic nanoparticles also fetch applications in drug delivery and medical imaging (Fig 1.4 iv and v).[79]

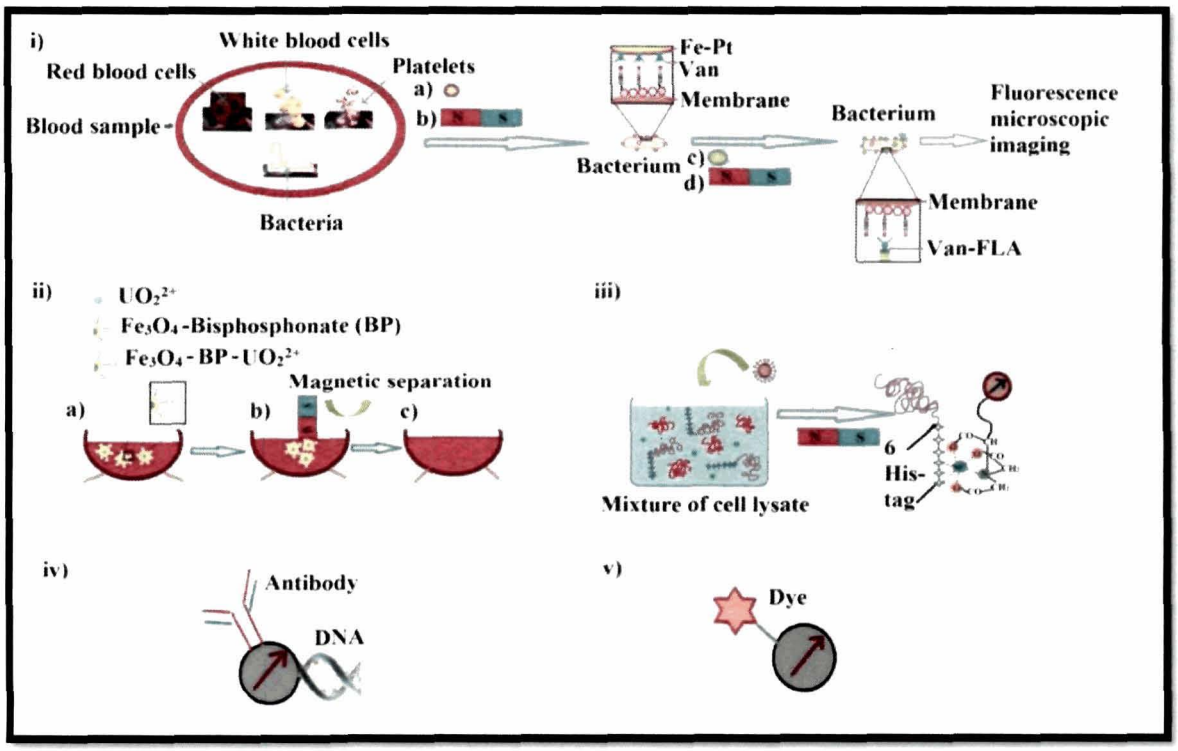

Fig.1.4. *Myriad utilities of biofunctionalized magnetic nanoparticles i) Detecting bacteria in blood samples: (a) addition of FePt@Van; (b) capturing bacteria assisted by a magnet; (c) addition of Van-FLA for staining the bacteria; and (d) magnetically separating stained bacteria from Van-FLA solution ii) Fe_3O_4-BP nanoparticles remove UO_2^{2+} from blood; (D) the amount of UO_2^{2+} in blood (I) before and (II) after the removal, and (III) the amount of UO_2^{2+} on the magnetic nanoparticles iii) NTA-terminated magnetic nanoparticles selectively binding to histidine-tagged proteins iv) Antibody or DNA bound MNP for specific binding or drug delivery v) Dye linked MNP for multimodal imaging* (Adapted from reference 79).

Amongst various magnetic nanoparticles, IONPs are the most commonly reported biomolecule- immobilization platform. The unique physico-chemical attributes and ability to operate at cellular and molecular niche of biological interactions endow special impetus to IONPs in the biomedical domain. This class of nanomaterial has been instrumental in a number of immobilization studies facilitating the recyclability of

various immobilized enzymes for industrial applications. As the present thesis also deals, in part, with the immobilization of different biomolecules like biocatalysts and phytocompounds onto iron oxide nanoparticles, it would of relevance to mention some of the critical aspects like magnetic properties of IONPs and the need for their stabilization.

A myriad of protocols are available for the preparation of IONPs with specific physical and chemical properties. The various pros and cons of the techniques like co-precipitation of iron salts, microemulsion formation, thermal decomposition of iron precursors, hydrothermal methods, sonochemical approach, sol-gel transition, chemical vapor deposition (CVD), flow injection, electrochemical techniques under oxidizing conditions, laser-induced pyrolysis of pentacarbonyl iron vapors and use of bioresources like fungi and bacteria for the production of IONPs have been extensively reviewed.[84]

The size and shape accord along with composition, crystallographic structure, magnetic anisotropic energy, vacancies and defects are the critical parameters for determining magnetic properties (such as coercivity, H_c and susceptibility, χ) of MNPs. Most importantly, surface chemistry can affect to a large extent the magnetometric parameters of nanoscaled iron oxide. Jun et al.[85] have evaluated these nanomagnetism scaling laws of engineered nanoparticles in a recent review.

Size seems to be a major player in affecting magnetic attributes of MNPs. The magnetic anisotropic energy barrier from a spin-up state to spin-down state of the magnet is proportional to the product of the magnetic anisotropic constant ($K\mu$) and the volume (V) of the magnet. Contrary to bulk materials, the thermal energy of MNPs can readily invert the magnetic spin direction (though, the spin-exchange coupling energy is not overcome). This behaviour is known as *superparamagnetism* where magnetic fluctuations lead to a net magnetization of zero. For colloidal material, the magnetic properties are dictated by the diameter of the crystal, its saturation magnetization, and its Ne´el relaxation time, τ_N. The agglomeration status of the particle can markedly influence τ_N through the dipolar intercrystal coupling aspect of the anisotropy. At the *blocking temperature (T_b)*, defined by the relationship, $T_b = K\mu V/25K$, occurs the transition from ferromagnetism to superparamagnetism. Above T_b, magnetic properties are lost by the nanoparticle ensemble. An external field induces spontaneous reorganization of spin directions and re-magnetizes the IONPs. Removal of the magnetic field causes the particle to lose their spin alignment with concomitant release of heat. Non-alignment of spin restricts inter-particle attraction, thereby, establishing the

requisite of ferromagnetism for synthesis of stable colloidal suspension. *Surface spin canting* (Fig.1.5) effects of nanoscaled iron oxide are reflected in the saturation magnetization value (m_s).

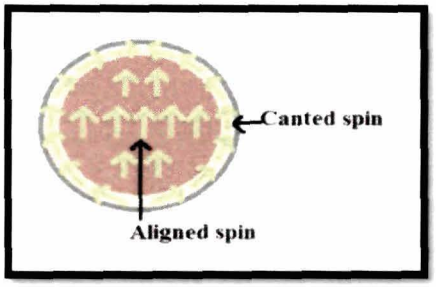

Fig.1.5. *Illustration of spin canting, the disorganization of spin close to the surface due to a lack of organization in crystallinity.*

These surface-associated magnetically disordered spin glass like layers arise due to spin-spin exchange coupling energy of the surface. It is pertinent to consider the following relation,

$$m_s = M_s [(r - d)]^3 \quad \text{.....(1.6)}$$

where r is the size, M_s is the saturation magnetization of bulk materials, and d is the thickness of disordered surface layer. This shows a linear relationship between $m_s^{1/3}$ and r^{-1}.

Furthermore, high crystallinity results in higher saturation magnetization. *Magnetic dopants* can affect the magnetism of MNPs to a large extent. Fe_3O_4 are characterized by a ferromagnetic spin structure. Fe^{2+}(d^6 configuration) and Fe^{3+}(d^5 configuration), occupying O_h sites align parallel to the external magnetic field and Fe^{3+} in the T_d sites of fcc-packed oxygen lattices align antiparallel to the field. The net magnetic moment per unit $(Fe^{3+})_{Td}$ $(Fe^{2+}\ Fe^{3+})_{Oh}O_4$ is approximately 4 μ_B. However, doping with M^{2+} species like, Mn, Co, Ni with electron configuration d^5, d^4, d^3, respectively, to replace O_h Fe^{2+} leads to modulation in the magnetic moment per unit. This has been estimated to be 5 μ_B, 3 μ_B and 2 μ_B with concomitant decrease in mass magnetization value at 1.5 T from 110 emu to 101, 99, and 85 emu per mass of magnetic atoms (emu/g (M^+ Fe)) for respectively for $MnFe_2O_4$, $CoFe_2O_4$, and $NiFe_2O_4$.[85]

At this juncture, it is pertinent to mention that steric or electrostatic stabilization of the IONPs is pre-requisite to ensure stable aqueous dispersion and countercheck agglomeration and precipitation. Biomolecules coupled onto bare, non-porous magnetic nanoparticles (MNPs) are often inactivated on exposure to proteases and high temperature.[86] Furthermore, agglomeration in aqueous medium with non-uniform and large particle size distribution and overall instability of the system often confront the

use of bare MNPs as carriers. The flocculation of IONPs is attributed to the surface iron atoms that behave as Lewis acids. Iron atoms coordinate with water, which dissociates readily leaving the iron oxide surface hydroxyl-functionalized.[87] The amphoteric hydroxyl groups may react with acids or bases and consequently the surface of the nanoparticles will be positive or negative depending upon the pH of the solution while the isoelectric point has been noted at pH 6.8.[87] The surface charge density (Σ) around this point of zero charge, PZC is not sufficient enough to keep the particles stable in water and as such aggregate. To ensure stable aqueous dispersion and countercheck agglomeration and precipitation, steric or electrostatic stabilization of the IONPs is thus pre-requisite. These particles are endowed with significant properties including improved dispersion, colloidal stability and reduction of toxicity[88] (that are lacking in the bare uncoated particles) on encapsulation or entrapment into organic polymers. This is complemented by their enhanced compatibility with organic ingredients, reduced susceptibility to leaching and surface-protection from external damages. Systems that are sterically stabilized tend to remain well-dispersed even under conditions where the zeta potential of the surfaces is significantly reduced. Furthermore, steric stabilization is effective at both high and low solid contents.

However, it pertinent to mention that saturation magnetization of IONPs decrease on steric stabilization and this has been ascribed to interactions of anchors with surface bound iron ions that have decisive role in magnetic properties of the IONP surface layer. Thus, the stability and size of IONPs have to be traded off against high saturation magnetization value.[89] Nevertheless, a spectrum of synthetic and natural polymers (Table1.3) has been used for the stabilization of iron oxide nanoparticles.[84] Polymeric encapsulation or coating of the MNPs has additional advantages over simple functionalization with other small organic compounds or other materials like amorphous or mesoporous silica.[90]

These may be summed as:

(1) Better colloidal stability in water through steric stabilization

(2) Conferring surface functionalities to the MNPs

(3) Facilitating the design of 'smart' or hybrid particles, (which may be used for stimulated and focused release of therapeutic agents)

(4) Greater shape-size tuning of the MNPs, (which directly affects their pharmacokinetics, bio-distribution and immune clearance).

Table1.3. *Few of the macromolecules used to coat IONPs* .[84]

Polymer used[Ref]	*Size and distribution of the coated IONPs/Applications*	*Advantage of using the corresponding polymer*
Polyethylene glycol (PEG)[91]	10–50 nm, narrow/ *In vivo* NMR imaging, *in vivo* contrasting	❖ Improves the biocompatibility, blood circulation time and internalization efficiency of the NPs, ❖ Easy to functionalise
Polyvinyl alcohol (PVA)[92]	10–50 nm, narrow/ *In vivo* imaging and drug delivery	❖ Prevents coagulation of particles, giving rise to monodisperse particles
Polystyrene[93]	10–20 nm, narrow/ Cellular imaging and DNA hybridisation	❖ Stable and uniform size particles in suspension
Polymethyl methacrylate (PMMA)[94]	10–50 nm, narrow/ DNA separation and amplification	❖ Novel, simple and labour-saving; ❖ Can be applied in automation system(s) to achieve high throughput detection of single nucleotide polymorphisms
Chitosan[95]	20–100 nm, broad/ Tissue engineering, hyperthermia	❖ A natural cationic linear polymer that is widely used as non-viral gene delivery system, ❖ Biocompatible, hydrophilic. ❖ Used in agriculture, food, medicine, biotechnology, textiles, polymers, and water treatment

Table continued on the next page

Dextran[96]	10–200 nm, narrow/ Isolation of *E. coli*, drug delivery, imaging	❖ Enhances the blood circulation time, ❖ Stabilises the colloidal solution
Starch[97]	10–20 nm, narrow/ Contrasting and imaging	❖ Natural polymer, biocompatible
Gelatin[98]	50–100 nm/ Isolation of genomic DNA, drug delivery	❖ Hydrophilic, natural biocompatible polymer. ❖ Improves the efficiency of drug loading.

Immobilization of biomolecules onto iron oxide nanoparticles has found applications across myriad of domains ranging from nano-remediation and catalysis to magnetically controlled drug delivery. Recently, Ansari and Hussain[99] have presented an extensive review on the use of magnetic and nonmagnetic nanoparticles for the immobilization of biocatalysts. The following table highlights some of the recent endeavours of biocatalyst-immobilization onto IONPs

Table1.4. *A few biocatalysts immobilized onto IONP-based systems.*[99]

Biocatalyst	*Immobilization platform*	*Application/ remarks*
Cholesterol oxidase[100]	Fe_3O_4	Analysis of total cholesterol in serum
Haloalkane dehalogenase [101]	Silica coated IONPs	Production of fusion proteins containing dehalogenase sequences with C-terminal polypeptide repeats
Laccase[102,103]	Zinc-tetra-amino-phthalocyanine Fe_3O_4, magnetic core-shell (Fe_3O_4-SiO_2) nanoparticles	Fiber optic biosensor, catechol biosensor
Urease[104]	Phosphonate grafted IONPs	Biosensors, analysis of urea content in blood, urine, alcoholic beverages, natural water and environmental wastewaters

Table continued on the next page

Lipase[105, 106]	Fe_3O_4	Hydrolysis of p-nitrophenyl palmitate (pNPP), biodiesel production
α-Amylase[107]	Cellulose coated magnetite nanoparticles	Starch degradation
ß-Galactosidase[108]	Chitosan-Fe_3O_4	Conversion of lactose into galacto-oligosaccharides
His(6)-tagged galactitol dehydrogenase (GatDH) and *formate dehydrogenase (FDH)*[109]	Chelated Co^{2+} modified Fe_2O_3	One-pot purification of two-enzyme system and production of rare sugar and chiral diol (L-tagatose and (S)-1,2-propanediol).

Furthermore, IONPs have been commercially used for automated immunomagnetic cell separation, drug delivery, nucleic acid purification, magnetic gene transfection, magnetic resonance imaging (MRI) contrast agents, hyperthermia and plethora of other applications by a number of companies like Chemicell, Ocean Nanotech, Estapor, Miltenyl Biotech, Invitrogen and Dynal Biotech, to name a few.[84] Amongst others, bioconjugated superparamagnetic IONPs (SPIONs) have instigated tremendous research interests as targeted contrast media for molecular and cellular imaging.[84] To cite for evidence, SPIONs-transferrin protein (for transferrin receptors)[110], SPIONs-mAb-610 (for surface antigen on colon carcinoma cell line)[111], SPIONs-PEG-anti-CEA (for carcino embryonic antigen)[112], SPIONs-mAb (anti-lymphocyte) (for lymphocyte)[113], SPIONs- $\alpha_v\beta_3$ (for tumoral angiogenesis)[114], SPIONs Herceptin (for Her2/neu positive cancer cells)[115].

Various studies on *in vitro* and *in vivo* drug delivery (Table1.5) using IONPs have been published in the recent years. Optimum surface charge, shape, size, colloidal stability in a biological environment, biocompatibility, saturation magnetization and route of elimination post-delivery of the drug (in the context of nanotoxicology) are some of the critical factors to be considered while employing IONPs for drug delivery.[84] Thus, IONPs loaded with biomolecules find plethora of applications across myriad of domains. In the subsequent section, the discussion is focused on silver nanoparticles that have gained impetus across the niches of microbiology, biotechnology, toxicology and multiple branches of material science

Table1.5. *A few SPIONs-based drug delivery studies*

Drug tested	*Coating on SPIONs*	*In vitro or in vivo*
Mitoxantrone[116]	Phosphated starch	*In vivo (mice)*
Dexamethasone acetate[117]	Poly(lactic-*co*-glycolic acid)	*In vitro and In vivo (*intra-articular)
Doxorubicin[118]	Amphiphilic block copolymers of maleimide terminated poly(ethyleneglycol)-block-poly(D,L-lactide) and methoxy-terminated poly (ethylene glycol)-block-poly(D,L-lactide)	*In vitro*
Taxol[119]	Poly(acrylic acid)	*In vitro*
Aspirin[120]	Cross-linked chitosan	*In vitro*
Tammoxifen[121]	Polyethylene glycol fumarate	*In vitro*

1.4.2. *Silver nanoparticles*

Noble metal nanoparticles like gold, silver and copper have been used in myriad of domains like catalysis, optoelectronics, photonics, and surface-enhanced Raman Scattering detection and biological labelling.[122.123] Furthermore, coherent existence of free electrons in the conduction band due to small particle size is responsible for their respective surface resonance band- dependent on the particle size, adsorbed species on the surface, chemical surrounding and dielectric constant.[124] Amongst others, use of silver ion or metallic silver as well as silver for burn treatment, preparation of antimicrobial stainless steel, textile, medical devices, sunscreen lotions, water treatment, development of biosensors etc. is constantly attested by the ever-increasing number of scientific reports and industrial patents (source: SciFinder®, Google Scholar and Scopus). Colloidal silver is characterized by remarkable attributes of good conductivity, chemical stability, catalytic and antimicrobial activity[125] which fetch it applications from surface enhanced spectroscopy (SERS) to preparation of multifaceted antimicrobial polymeric nanocomposites for biomedical stents.[126]

Conventionally, stable, colloidal dispersions of silver nanoparticles (Ag NPs) in water or organic solvents have been prepared through chemical reduction using various

reductants like borohydride, citrate, ascorbate, and elemental hydrogen.[13] However, of late, the growing trend is to 'go green' in the context of preparation of nanomaterials.[13] Sharma et al.[13] have highlighted the green approaches of preparing Ag NPs in the perspective of three important requisites of green chemistry:

(1) Selection of solvent medium

(2) Selection of environmentally benign reducing agent

(3) Selection of non-toxic substances for the stability of the silver nanoparticles

Based on these, they have classified these approaches into five broad classes:

1.4.2.1. *Polysaccharide method*: Ag NPs are prepared using an environmentally benign solvent and polysaccharide as a capping agent, or in some cases polysaccharides serve both a reducing and capping agent. To cite for evidence, use of starch as a capping agent and β-D-glucose as reducing agent in a gently heated system for preparation of Ag NPs.[127]

1.4.2.2. *Tollens method*: The basic Tollens reaction involves the aldehyde-mediated reduction of $Ag(NH_3)^{+}_2$ (aq.), a Tollens reagent.

$$Ag(NH_3)^{+}_2\,(aq) + RCHO \rightarrow Ag\,(s) + RCOOH\,(aq) \qquad \text{.....(1.7)}$$

Thus, Ag NPs with controlled size can be produced in single step approach. Using modified Tollens approach, silver ions were reduced by saccharides in presence of ammonia, yielding silver films with particle sizes from 50-200 nm, Ag hydrosols with particles in order of 20-50 nm, and multi-shaped Ag NPs.[128, 129]

1.4.2.3. *Irradiation method*: Ag NPs can be prepared using various irradiations (e.g., laser, microwave and gamma radiolysis). For example, Chen et al.[130] reported the preparation of uniform and stable (for two months at room temperature) Ag NPs by using microwave irradiation of a carboxymethyl cellulose and silver nitrate solution.

1.4.2.4. *Polyoxometalates (POMs) method*: POMs can be effectively used for the preparation of Ag NPs owing to the former's water solubility and capability to undergo stepwise, multielectron redox reactions without disturbing their structure. Ag NPs have been synthesized by illuminating a de-aerated solution of $POM/S/Ag^{+}$ (POM: $[PW12O40]^{3-}$, $[SiW12040]^{4-}$; S: prpan-2-ol or 2,4-dicholorphenol).[131] Here, POMs played the role of photocatalyst, reductant and stabilizer.

1.4.2.5. *Biological Approach*: Several microbial species can serve as production-factories of silver nanoparticles.[13] On the other hand, use of bio-extracts (acting as reservoirs of biocatalysts, polypeptides, polysaccharides, vitamins etc.) for reduction of silver ions is environmentally benign, yet chemically complex.[13] For example, rapid formation of Ag NPs has been reported through the Ag^{+} reduction of culture

supernatants of *Klebsiella pneumonia, Escherichia coli, and Enterobacter cloacae.*[132] Several phytoextracts from live alfalfa, broths of lemongrass, geranium leaves, *Capsicum annum* L.; isolated/purified organics like glutathione, L-Valine-based oligopeptides etc. have been effectively used for the synthesis of Ag NPs.[133-138]

Amongst the plethora of properties (like SPR, catalytic etc.), antimicrobial activity (including the potency to prevent HIV binding to host cells) of silver nanoparticles is a highly focused upon area of research.[139-146] Numerous propositions have been forwarded on the mechanism of the antimicrobial action of silver nanoparticles including disruption of membrane integrity, penetration into the cells, generation of reactive oxygen species (ROS) and disruption of the DNA replication machinery etc., dictated by the shape-size accord of the nanoparticles, aerobic versus anaerobic condition and most importantly the release of silver ions.[13]

On the other hand, silver nanoparticles have also gained considerable interest as immobilization platforms for a number of biomolecules.[147] To cite for evidence, Hsu et al.[148] have reported the covalent immobilization of glucose oxidase (GOD) onto thiol-modified Ag NPs for amperometric glucose biosensor. The electrostatic integration of Ag NPs with bovine hemoglobin has been reported to decrease the α-helices content of the latter from 72.5% to 66.2%.[149] Multiplexed detection of oligonucleotide targets has been reported by using silver nanoparticles functionalized with oligonucleotides and Raman labels coupled with SERS spectroscopy.[150] Recently a mixed monolayer of 11-mercaptoundecanoic acid (MUA)/6-mercapto-1-hexanol (molar ratio of 1:3) was used as a bifunctional linker for conjugating protein IgG onto the surface of silver nanoparticles.[151] On the other hand, silver nanoclusters have been linked with biotin using a monolayer consisting of 1-octanethiol (1-OT)/MUA.[152] In an interesting report, silver nanoparticles conjugated to amyloid-derived diffusible ligands (ADDL) were used to develop a SPR biosensor for assaying Alzheimer's disease.[153]

At this juncture, it is pertinent to mention that the plethora of applications reported for silver nanoparticles nowhere parallels the toxicity analysis- a prerequisite prior to commercialization of the Ag NPs based systems.[154] Lima et al.[154] have forwarded few critical points to ponder upon in their recent review on the cytotoxicity and genotoxicity of silver nanoparticles.

(1) Toxicity analysis of Ag NPs is complex which may be ascribed to the varied kinds of synthesis protocols, differences in size, presence or absence of capping agents and most importantly the diversity in toxicity evaluation tests.

(2) Ag NPs are less toxic when compared to silver ions.

(3) Biogenically prepared Ag NPs are less toxic as compared to the chemically synthesized nanoparticles.

(4) Human cells have been found to display greater resistance to toxic effects of Ag NPs in comparison with other organisms.

(5) A comprehensive and detailed toxicity analysis of Ag NPs is pre-requisite on different strata of the ecosystem ranging from microbes and plants to higher organisms.

In the next section, the discussion is on the use of polyaniline for prospective biomolecule immobilization.

1.4.3. *Polyaniline*

Intrinsically conducting polymers or electro-active conjugated polymers (extended π-conjugation along the backbone of the polymer) like polyaniline (PAni), polypyrrole (Ppy), polythiophene etc. have instigated tremendous research interests in the context of their unusual electrical, electronic, magnetic and optical properties.[155] In this context, polyaniline, belonging to the semi-flexible rod polymer family demands a special merit. A precise control over free volume, solubility, electrical conductivity and optical properties of PAni (Fig.1.6) is possible via simple and reversible acid/base doping/dedoping chemistry.[156]

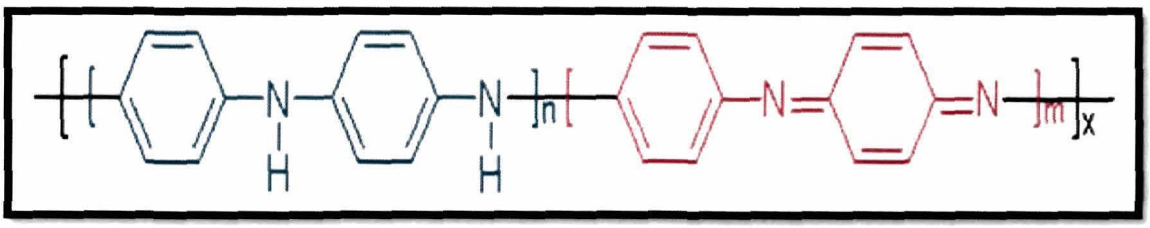

Fig.1.6. *Structure of PAni, where x equals half the degree of polymerization (DP) and n+m =1*

PAni can be found in one of the three idealized oxidation states[157]:

(1) *Leucoemeraldine* (n=1 and m=0): clear and colorless, fully reduced state, poor conductor.

(2) *Emeraldine* (n=m=0.5): blue for emeraldine base (neutral) and green for emeraldine salt (highly conducting). Protonation (/doping of the imine nitrogens by an acid) of the emeraldine base facilitates delocalization of the otherwise trapped diiminoquinone- diaminobenzene state.

(3) *(Per)nigraline* (n=0 and m=1): blue/violet, fully oxidised state, poor conductor.

One-dimensional (1-D) polyaniline nanostructures like nanowires, rods and tubes are endowed with the advantages of both low-dimensional systems and organic conductors. Such 1-D nanostructures have been synthesised by chemical approach, electrochemical strategies which involves the polymerization of the monomer using either a 'hard' (*e.g.*, zeolite channels, anodized alumina etc.) or 'soft' (*e.g.*, surfactants, micelles, liquid crystals) templates and physical methods like electrospinning and mechanical stretching.[158] In this context, a special mention must be made of organic/aqueous interfacial synthetic approach, the advantages of which are enlisted underneath:

- ❖ Template free easy synthesis and purification.
- ❖ Uniformity in the fibers' samples with fiber diameter in the nanoscale range.
- ❖ Scalability and high reproducibility of the synthetic approach.
- ❖ Generation of water-dispersible nanofibers (suitable for biological applications), which facilitate eco-friendly and facile processing.

Among others, polyaniline is often used as immobilizing platform for biomolecules and has been a material of choice in the development of biosensors.[159] For example, in 2009, Du et al.[160] reported a simple electrode modification method wherein PAni/chitosan and horseradish peroxidase (HRP) were dropped onto a glassy carbon electrode to develop a hydrogen peroxide (H_2O_2) biosensor with a linear range of 1×10^{-5} to 1.5×10^{-3} and a limit of detection of 5×10^{-7} M. On the other hand, materials like PAni/carbon nanofiber composite have been used to detect analytes like catechol[161] while gold nanoparticles (with immobilized ssDNA complementary to target DNA of *Staphylococcus aureus)* modified PAni nanofibers (with bound HRP) on gold electrode have been suitably applied to differentiate *S. aureus and S. epidermis.*[162] However, it is important to note that the intractability of polyaniline has limited its utilization in commercial biosensors, especially in its pure, inherently conductive form. In other words, PAni's redox activity is greatly restricted to acidic environments, restraining its application in the biological milieu which is generally in the neutral pH. This has been addressed by the use of SPAN *i.e.*, self-doped PAni (produced through co-polymerization of aniline and *m*-aminobenzenesulfonic acid in an aqueous solution) which has better activity and stability at neutral pH. For example, SPAN nanofibers patterned with gold microspheres have been used to modify a glassy carbon electrode to detect a gene fragment from cauliflower mosaic virus 35S gene.[163] Furthermore, processability of polyaniline can be tremendously improved via dispersion in a suitable matrix.[164]

A number of biomolecules have been immobilized onto PAni and PAni-based films and nanowires/fibrous systems through physical adsorption, covalent immobilization or electrochemical approach for the development of biosensors (Table 1.6).[165]

Table1.6. *Biomolecule immobilized PAni based biosensors*

Immobilization platform	*Immobilized biomolecule*	*Analyte*
Physical Adsorption		
Glassy carbon-PAni[166]	Cholinesterase	Pesticide
PAni/multiwall nanotube (MWNT)[167]	Choline oxidase	Choline
PAni graphite oxide nanocomposite in carbon paste electrode[168]	DNA	DNA
Covalent immobilization		
PAni[169]	DNA	DNA
PAni[170]	Cholesterol oxidase, esterase , peroxidase	Cholesterol oleal and cholesterol
Electrochemical approach		
PAni-*co*-fluoro aniline[171]	Glucose oxidase	Glucose
PAni[172]	Horseradish peroxidase	H_2O_2
PAni-polyvinyl suphonate[173]	Horseradish peroxidase	H_2O_2
PAni polythiophene[174]	Glucose oxidase	Glucose
ZrO_2 microparticles/SPAN/electrode[175]	ssDNA	DNA

1.4.4. *Electrospun cellulose acetate nanofibers*

Amongst others, cellulose acetate (CA) (acetate ester of cellulose) has a wide array of applications ranging from cigarette filters to high absorbent diapers, semi-permeable membranes for separation processes and fibers and films for biomedical utiliites. CA fibers have remained focal point of research in multiple industries including the textile and more recently in the biomedical domain. Cellulose acetate exhibits a wide range of properties[176] attesting its importance in polysaccharide research. The most common level of degree of substitution of ~2.45 -2.5 confers good solubility (in wide varieties of solvent systems) and melt properties[177]. Puls et al.[178] have pointed out the eco-compatibility of cellulose acetate based materials assessed in terms of their biodegradability as a function of the synergy between photodegradation, biodegradation and physical design of consumer products. Recently, Sousa et al.[179] have

presented a dynamical study (by dielectric relaxation spectroscopy, DRS), focussed on the subglass mobility in cellulose acetate under two structurally/morphologically different forms: the initial polymeric state and structured membrane. CA fiber has comparatively high modulus and adequate flexural and tensile strength.[180] Grafting with functional groups like –COOH, $-SO_3H$ and $-NH_2$ endows another interesting property to CA *i.e.*, surface complexation with heavy metal ions.[181] Exploring the multi-fold material properties of cellulose acetate in the nanoscale regime is an interesting proposition. Amongst others, electrospinning has conferred a whole new perspective to the application of CA fibers. The simple and highly efficient technique of electrospinning is apt for producing polymer nanofibrous membranes with high surface-to-volume ratio and high surface roughness.[182] Before delving into the prospects of electrospun CA for biomolecule immobilization, it would be of relevance to peruse the basics of electrospinning.

Electrospinning has been associated with the epithet of 'fascinating fiber technology'.[183] It has been used as a successful tool to spin a myriad of synthetic and natural polymers into 30-2000 nm fibers extending upto many kilometres in length. A typical electrospinning apparatus is schematically illustrated through the central image while the prospective applications[184-193] of electrospun CA are shown in the peripheral images of Fig. 1.7.

The basic apparatus consists of a syringe pump, a high voltage supply and a collector. Application of an electric field using high voltage source causes induction of charges within a polymer solution (held at a needle tip at a certain distance from the collector by surface tension), resulting in charge repulsion. The latter overcomes the surface tension with eventual initiation of a jet. As pointed out by Reneker and Chun,[194] the jet comprises of four regions: the base, the jet, the splay and the collection. In the base region emerges the Taylor cone, the shape of which depends on the complex balance between the surface tension of the liquid and the force of the electric field. Solutions with higher conductivity are more conducive to jet formation. The polymer jet is accelerated and stretched due to the electric forces with eventual decrease in the diameter corresponding to increase in its length. During the flight of the jet, the solvent evaporates and an appropriate collector can be used to capture the polymer fibers.

It has also been hypothesized that radial charge repulsions lead to 'splaying' of the jet into a number of small fibers of nearly equal diameter and charge per unit length.[194] The number of splays eventually dictates the final diameter of the electrospun fibers.

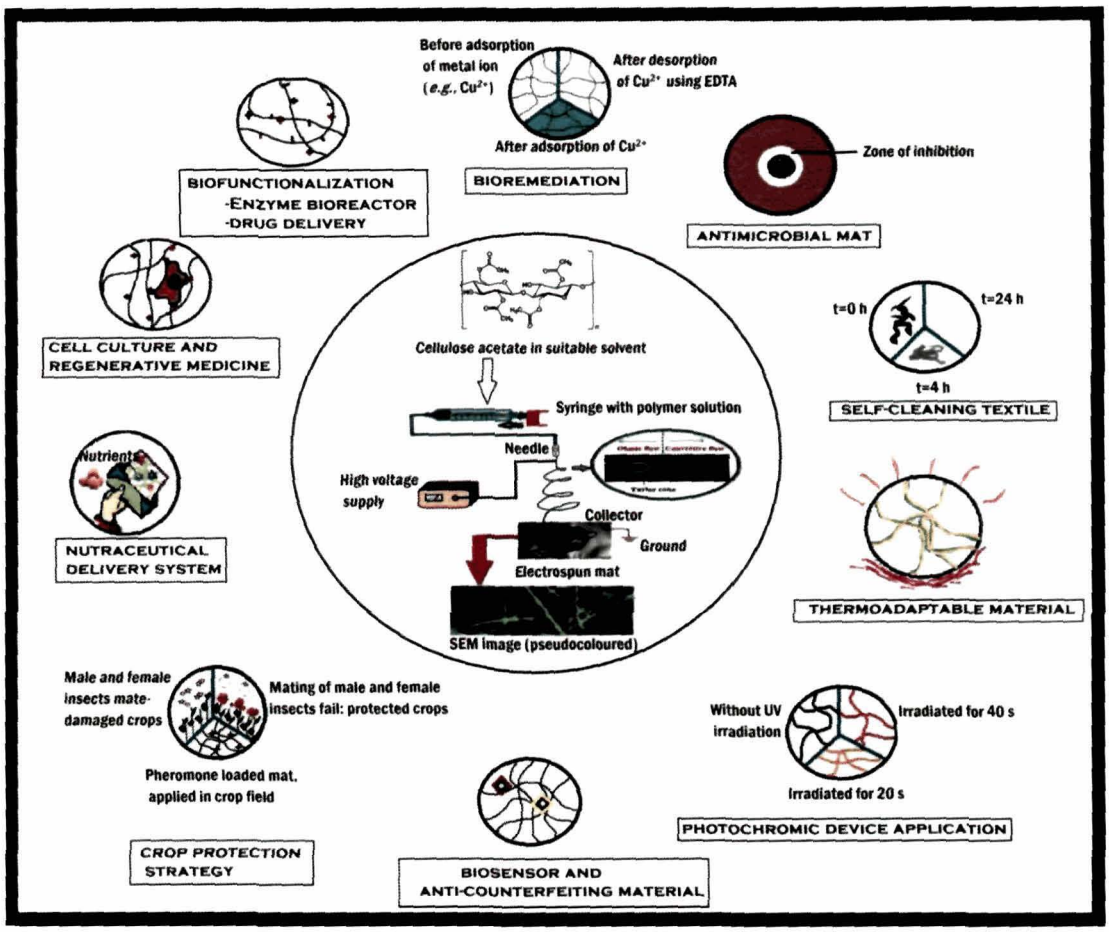

Fig.1.7. *Schematic representation of electrospinning cellulose acetate nanofibers (at the centre) and myriad of biotechnological applications (peripheral images)*

However, high speed photography has revealed that the 'splay' is in fact a single, rapidly whipping jet,[195,196] the behaviour of which depends upon three instabilities: the classical Rayleigh instability and two 'conducting' modes- dictated either by surface tension or electric forces.[197,198] Electrospinning process can be manipulated by three classes of parameters:

(1) *Solution properties* (conductivity/solution charge density, surface tension, viscosity/concentration, polymer molecular weight, dielectric constant and dipole moment)

(2) *Machine parameters* (field strength/ voltage, distance between tip and collector, flow rate, needle tip design and placement, collector composition and geometry)

(3) *Ambient parameters* (temperature, humidity and air velocity)

Optimization of such process parameters using statistical tools like RSM could be interesting proposition in the context of minimizing the diameter of CA nanofibers for increasing the active surface area for biomolecule loading.

The following section focuses on the immobilization of various biomolecules onto electrospun CA fibers. Electrospun CA nanofibers have instigated tremendous interest as immobilization matrix for a number of bioactive moieties including biocatalysts and drugs on one hand while the prospects for tissue engineering are being realised gradually on the other. Few of the representative immobilized biomolecules are shown in Fig.1.8.

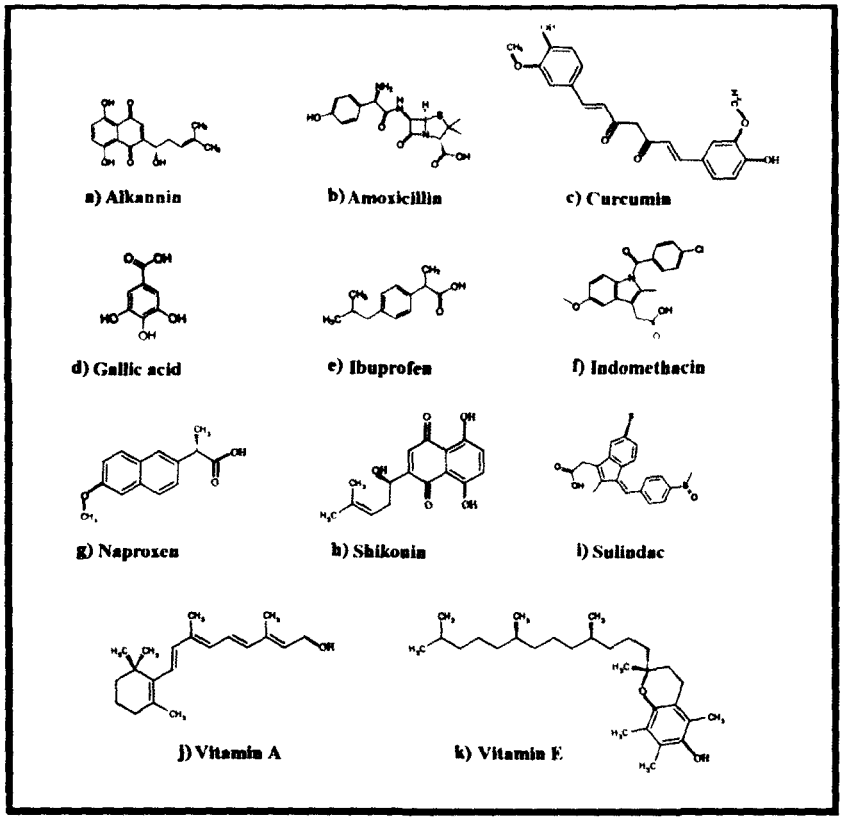

Fig.1.8. *A few representative biomolecules that have been used to functionalize electrospun CA fibers*

Amongst others, Taepaiboon et al.[184] work merits a special mention, where in the research team has immobilized Vitamin A and vitamin E (that exhibit multifarious biological action and protective roles) onto electrospun CA nanofibers (247-265 nm) with smooth and round cross-sectional morphology.

On the other hand, electrospun CA nanofibers on hydrolysis and subsequent oxidation by $NaIO_4$ (to generate surface aldehyde groups under statistically optimized parameters) acted as suitable immobilization platform for *Candida rugosa* lipase.[199] The authors have reported significant increment in thermostability and durability post

immobilization in comparison to the free counterpart. In yet another system, using glutaraldehyde as the coupling agent, *Candida rugosa* lipase was covalently attached to cellulose membrane (containing pentaethylenehexamine (PEHA) as spacer) regenerated from electrospun CA.[200] The authors have reported a high activity (9.83×10^4 U/m^2) of this biphasic enzyme-immobilized membrane bioreactor (EMBR) for the reaction model involving the hydrolysis of olive oil.

A number of recent works focus on the use of electrospun CA mats for transdermal drug delivery (TDD). TDD refers to topically (using skin as the port of entry) administered medicaments in the form of patches that deliver drugs for systemic effects at a predetermined and precisely controlled rate, improves patient compliance and reduce inter and intra patients' variability.[201] In this context, naproxen (NAP), indomethacin (IND), ibuprofen (IBU), and sulindac (SUL) have been loaded onto electrospun ultrafine fiber (263-297 nm) mats of CA.[202] The release profile of the drugs, as tested by total immersion method followed the trend: NAP > IBU > IND > SUL. Coaxially electrospun CA and PVP membranes have been assessed for the controlled release application of amoxicillin in gastrointestinal administration and for transdermal patches.[203] Suwantong's group[204] has reported curcumin loaded smooth electrospun CA nanofibers (within a size spectrum of 314-340 nm), compatible with normal human dermal fibroblasts, vouching for use as topical or transdermal patch. An important study in this domain is the loading of wound-healing mediators, asiaticoside (in the form of crude extract or pure substance) and curcumin onto electrospun CA fiber mats.[205] An interesting observation was the differential attachment, proliferation and morphology of fibroblast cells cultured onto these drug-loaded nanofibers that were stable upto 4 months on storage.

In an effort to overcome the poor water solubility (11.5 mg/mL) of gallic acid (3,4,5-trihydroxybenzoic acid) (endowed with multiple bio-protective action) and promote its release into the skin, the suitability of electrospun CA fibers was assessed.[206] Diffusion mediated monotonous release of silymarin has been observed from silymarin-loaded electrospun CA fibers (550-900 nm).[207] A zero-order release profile of ketoprofen (a benzophenone-derived non-steroidal anti-inflammatory drug) from drug-loaded electrospun CA fibers produced by using a modified coaxial electrospinning process (comprising of the use of a sheath solvent) has been recently reported.[208]

Alkannin, shikonin (A/S) (naturally occurring hydroxynaphthoquinones with well-established spectrum of wound healing, antimicrobial, anti-inflammatory,

antioxidant and antitumor activity) were loaded onto electrospun cellulose acetate nanofibers without considerably affecting the morphology and the mean diameter size.[209] Electrospun CA nanofiber fabrics containing an N-halamine antimicrobial agent of bis(N-choloro-2,2,6,6-tetramethyl-4-piperidinyl) sebacate (CI-BTMP) showed better antimicrobial efficacy than solution cast films containing identical amounts of CA and CI-BTMP. Furthermore, the composite fiber fabrics also displayed excellent mammal cell viability.[210]

Bioconjugated electrospun CA fibers have also been fabricated for crop protection and insect control. 2,6-dicholoro-4-nitroaniline (DCNA) is widely used to countercheck *Rhizopus* rot on sweet potato roots, fruits of cherries, peaches and foliage diseases of vegetable crops caused by *Botrytis* spp. and *Sclerotina* spp. In this context, smooth DCNA loaded electrospun CA nanofibers have been fabricated successfully.[211] With the objective of harnessing the various functional properties (including antibacterial, antifungal and mosquito-repellence) of Citronella (*Cymbopogon nardus*) essential oil, Silveira et al.[212] have reported its successful loading onto electrospun CA fibers. The ecological hazards associated with applications of insecticides for crop protection needs no further elaboration. As an answer to this issue, applications of pheromones – the chemical substances for message relay among insects, is considered to be a novel approach to control insect infestation. In this context, the application of beaded electrospun CA fiber mats loaded with as high as 33 weight percentage of pheromones in the crop fields has been proposed recently.[213]

Thus, one can easily conclude that biomolecule immobilization onto various classes of nanomaterials and polymeric platforms opens up multiple avenues for exploration. However, one of the prime requisites is the elucidation of the physico-chemical properties of the immobilization platforms prior to and post biomolecule immobilization. From the perspective of the immobilized biomolecule, there are several properties to be investigated (*e.g.,* modulation of enzyme kinetics)[3] and myriad of assays are available to determine the modulation (if any) of the respective biological activities, post immobilization. This is, however, not discussed in this chapter because each of these assays is biomolecule-specific and this fact would be attested by the content of the subsequent chapters.

1.5. Characterization tools and techniques

Characterization of the bioconjugated hybrids demands a concert of multiple techniques to address the physicochemical features in addition to the immobilization metrics of interest. There are a number of issues pertinent to purification and characterization of the bioconjugated hybrids. Sapsford et al.[214] have extensively reviewed the myriad of techniques used to determine these physicochemical metrics of the nanostructured immobilization platform which encompasses concentration; size and size distribution; shape and aspect ratio; aggregation; purity/contamination; composition; surface characteristics including surface area and surface charge/zeta potential; and stability. Post bio-conjugation the various tools used to characterize the nanomaterials also assist in confirmation of and type of biomolecule coupling. However, there emanates a number of other critical issues.

(1) Ratio of immobilization platforms: biomolecule and ratio distribution.

(2) Stability of the bio-conjugated hybrid system during preparation and proposed application.

(3) Structure and orientation of the biomolecule post coupling.

(4) Hydrodynamic radius and the distance of separation between the nanomaterial and the biomolecule.

(5) Activity/affinity/avidity of the biomolecule post attachment.

The nature of the conjugation method to a large extent dictates the eventual properties of the bioconjugated system. To cite for evidence, carbodiimide (EDC) chemistry (used for amide bond linkage between the pervasive amines or carboxyls on enzymes and the cognate target functionality on the immobilization matrix) may lead to heterogeneous orientation of the attached biomolecule, cross linking and aggregation.

The following section highlights some of the tools used for purification and characterization of the bioconjugated hybrids. It is pertinent to mention that not all tools are applicable for all types of nanomaterials. Furthermore, sample manipulation prior to analysis, such as drying or suspension in ultrapure liquids may often result in non-physiological states and modulated matrix-bioconjugate characteristics. This calls for caution as far as interpretation of the results are concerned. A plethora of separation-based, scattering, microscopy, spectroscopy, mass spectroscopy, and thermal techniques are used for the characterization of the bioconjugated hybrid system.

1.5.1. *Separation techniques*

A number of tools used for the separation and purification of bioconjugated immobilization systems from both unconjugated-biomolecules and unmodified

immobilization platforms are based on commonly utilized methods as noted underneath.

1.5.1.1. *Centrifugation*: Tools of ultracentrifugation and gradient centrifugation are rapid and easily adapted to various materials. On the other hand, analytical centrifugation can be instrumental in determining size, size distribution, shape, structural and conformational information, and stoichiometry. Although the technique is non-destructive (thus making the sample amenable for extraction and further characterization), self-association of the materials may lead to misinterpretation of separation profiles.[215, 216]

1.5.1.2. *Electrophoresis*: The simple, sensitive and cost-effective to use tools of slab gel (agarose, polyacrylamide (PAGE-native), sodium dodecyl sulphate-PAGE (denatured)) and capillary electrophoresis (CE) may be used to separate and purify bioconjugated systems (that may be analysed further using other techniques) and elucidate hydrodynamic radius and zeta potential. To cite for evidence, agarose gel electrophoresis has been used to purify pyramidal nanostructure assemblies prepared from different sized gold nanocrystals functionalized with complementary single stranded DNA.[217]

1.5.1.3. *Field-flow fractionation (FFF)*: Dependent on the nature of the applied field (direct or asymmetric cross flow, sedimentary, electrical, thermal gradient, magnetic and dielectrophoretic), FFF can be used to determine size and size distribution and purify the bioconjugated systems. Effective mass, hydrodynamic radius, density and volume can be determined using sedimentary and flow fields. On the other hand thermal FFF aids in separation based upon size and surface potential. In this context, asymmetric flow-FFF has been used to separate DNA/chitosan nanocomposite (for therapy) from chitosan.[218] Furthermore, amount of unbound polycation, hydrodynamic size, and size distribution were elucidated using customized instrumentation allowing UV-visible, multiangle light scattering (MALS) and dynamic light scattering (DLS) detection.

1.5.1.4. *Chromatography*: High resolving power, simplicity and cost-effectiveness have made chromatographic techniques (standard liquid chromatography, high performance liquid chromatography and hydrodynamic chromatography) as tools of choice for purification of bio-conjugated system and investigation of post-production stability and impurities.[219] These techniques however suffer from nonspecific interaction with the stationary phase.

1.5.2. Spectroscopic technique

1.5.2.1. ***UV-Visible spectroscopy*****:** This is one of the most commonly used cost effective, simple and fast tools to characterize a myriad of bio-conjugated hybrid system and nanomaterial: biomolecule ratio. This tool exploits the intrinsic optical properties of nanomaterials to determine their concentration, size and even shape while modulations in the spectra is often correlated to the state of aggregation. The same may be used for determination of the concentration of the biomolecules.

1.5.2.2. ***Circular dichroism*** **(CD)** *(UV to visible CD, vibrational CD and synchrotron CD)***:** Being a non-destructive technique, analysis of liquid samples prepared in physiological environment yield convincing information on the conformation and stability of the biomolecule. However non UV-absorbing buffers is a prerequisite.

1.5.2.3. ***Infrared spectroscopy*** *(standard IF, Fourier transform-IR and attenuated total reflection-IR):* The appearance of characteristic fingerprint IR bands confirms the coupling of biomolecule to the immobilization matrix with an insight into the conformation of the biomolecule post bio-conjugation. However, strong absorbance by moisture is a common confrontation in IR spectroscopy.

1.5.2.4. ***Fluorescence spectroscopy*** *(standard fluorescence, wavelength and time resolved)*: In this, fluorescence resonance energy transfer (FRET) (dependent on a donor fluorophore and an acceptor species) merits a special mention with respect to its sensitivity to molecular distance. This sensitive tool can provide insight into biomolecule conformational information, attachment to immobilization matrix and average coupling ratio. However, the requirement is of either intrinsic or extrinsic fluorescence, thereby necessitating labelling.

1.5.2.5. ***Nuclear Magnetic resonance*** *(2D NMR, NOE NMR, TROSY NMR)*: Though the technique is non-destructive and yields physical, chemical, structural and environmental information about the biomolecule, it suffers from certain limitations. There are exclusive requisites of deuterated solvents, high samples' concentrations for this relatively expensiveness technique. Most importantly only certain nuclei are NMR active.

1.5.3. *Scattering techniques*

1.5.3.1. ***X-Ray diffraction (XRD)*****:** This tool is particularly important in characterization of polymeric nanocomposites. Although it generates limited information about the nature of interaction between the immobilization support and

the biomolecule, XRD can be instrumental in determining size and structure of the former prior to and post bio-conjugation and polymorphic information. Small angle X-ray scattering (SAXS) is used to yield macromolecular size, shape, distance and the overall packing structure of crystalline samples (as thin films) along with information on aggregation. However, X-rays often damage biological entities. Data analysis is complex and demands appropriate modelling approach.

1.5.3.2. ***Small angle neutron scattering (SANS)*****:** This has been instrumental in determining size, shape and orientation of crystalline samples and probing 'labile' biological sample. Although it is limited by the availability of neutron sources, isotopic sensitivity can be instrumental to elucidate structure.

1.5.3.3. ***Raman Spectroscopy*** *(Resonance Raman (RR), Surface Enhanced Raman (SERS) and Surface Enhanced Resonance Raman (SERRS)):* Although relatively weaker than Rayleigh scattering, Raman signals can provide complementary data to IR, insight into biomolecular investigation and isotope composition.

1.5.3.4. ***Zeta (ζ) potential*****:** Particle stability and surface charge are measured using this tool.

1.5.3.5. ***Dynamic Light Scattering (DLS)*** (or Photon Correlation Spectroscopy (PCS) or Quasi Elastic Light Scattering, (QRLS)): This non-destructive, rapid, sensitive, simple and relatively cheap technique can be used to measure hydrodynamic dimensions in any liquid media or solvent of interest. However, it suffers from restricted ability to measure polydisperse samples, biasedness toward larger particles and assumption of spherical shape of the particles.

1.5.4. *Microscopy techniques*

Both scanning and transmission electron microscopic imaging have proven instrumental in characterizing biomolecule conjugated hybrid systems. However, both these instruments are expensive and technical expertise is a must to derive at proper conclusions.

1.5.4.1. ***Scanning electron microscopy (SEM)*****:** Besides determining surface structure and nanomaterial composition, SEM is often used to analyse nanomaterial core and analysing their size and shape. Baring environmental SEM (ESEM) (used to image biomolecules, although with reduced resolution), dry samples are required for analysis.

1.5.4.2. ***Transmission electron microscopy (TEM)*****:** This is often used to analyse the size, shape and aspect ratio of myriad of nanomaterials (in the dry state) within a

small angle of view (thereby requiring visualization and analysis of a number of fields). It is to be noted that ionizing radiation can damage the sample. In this regard, cryogenic TEM may be used.

1.5.4.3. ***Atomic force microscopy (AFM)*****:** This technique is applicable to semiconducting wet and soft samples on various substrates and capable of 3D mapping of the sample surface (though only small areas). Furthermore, biomolecular interaction can be resolved using functionalized tips.

1.5.4.4. ***Near—field scanning optical microscopy (NSOM)***: Currently considered as a 'specialist' technique, NSOM is used for high-resolution surface analysis of nanoparticles under ambient conditions.

Sapsford et al.[214] have also highlighted the use of certain emergent techniques like ***CytoViva*** and ***Hyperspectral imaging, Quartz Crystal Microbalance, Acorn Area Analysis*** for characterization of bioconjugated hybrids.

On the other hand, elucidation of the magnetometric parameters may be critical in many applications. Hysteresis plots of the immobilization platform (*e.g., polymeric supported IONPs)* prior to and post biomolecule loading may be traced in instruments like ***vibrating sample magnetometer (VSM).*** On the other hand, ***thermo-gravimetric analysis (TGA)*** and ***differential scanning calorimetry (DSC)*** may be used for the analysis of the thermal properties of various polymeric nanomaterials/polymeric nanocomposites (*e.g., for electrospun nanofibrous mats).*

A special mention must be made of various **computational tools and theoretical analyses** (*e.g., density functional theory (DFT) calculations)*[220] for addressing of a number of issues:

(1) The stable geometry and adsorption energies for covalent and noncovalent interaction of a chosen biomolecule and the immobilization platform,

(2) Modulation in electronic properties of the immobilization platform in terms of variation in HOMO–LUMO (highest occupied molecular orbital and lowest unoccupied molecular orbital) energy gap, and global reactivity descriptors,

(3) Frontier orbital contribution to the electronic charge distribution in the bioconjugated system,

(4) Charge transfer between the immobilized biomolecule and the immobilization platform, and finally

(5) Solubility of the hybrid system in aqueous media that can provide a general insight into its biocompatibility.

Thus, it can be safely concluded from this discussion that comprehending the biomolecule-immobilization platform interactions demands the use of multiple instrumentation and analytical approaches.

1.6. Scope of Investigation

The perusal of the discussion presented in the previous sections would bring a simple fact to the light *i.e.,* an immense scope of exploration for multiple prospective applications exists on the ever-widening avenue of biomolecule immobilization which is intersected by research from the various domains of life science, physics, mathematics, chemistry and material science.

In this perspective, the compiled works reported in the present thesis geared off with certain queries presented underneath:

(1) What could be appropriate immobilization platforms for certain commercially important biocatalysts like keratinase, amyloglucosidase and lipase to confer them with higher industrial applicability and efficiency?

(2) What are the prospects of opting for polymer assisted nanomaterials, prepared through green routes, as immobilization platforms?

(3) How 'green' are the biopolymer–assisted nanomaterials, prepared using bioresources, in terms of their bio-nano interfacial action?

(4) What are the prospects of using sonication (a green chemistry tool), amongst others, for immobilization of medically important phytocompounds like curcumin (extracted from turmeric) and lycopene (extracted from tomato) onto polymer supported nanomaterials/polymeric nanomaterial?

(5) Can statistical tools like response surface methodology aid in tuning of the shape-size accord of nanomaterials (*e.g.,* diameter of electrospun nanofibers) as well as in the optimization of biomolecule-immobilization process?

(6) How does biomolecule loading alter different properties (like magnetic and antimicrobial) of the immobilization platform?

(7) What could be the possible modulations in the bio-physico-chemical properties of the immobilized biomolecule and feasibility for application-oriented utility?

The objectives of the present work, as presented in the subsequent section have the underpinning in the afore-stated scopes.

1.7. Objectives of the present work

The main objective of the proposed research is to develop bio-conjugated polymeric nanocomposites for practical applications. This is associated with the following sub-objectives:

(1) To prepare polymer assisted nanomaterials with impetus on green approach.

(2) To immobilize bio-molecules of interest like enzymes onto the prepared polymeric nanocomposites to obtain the bio-conjugated systems.

(3) To optimize the process parameters for preparation protocol of the nanomaterials as well as the process of bio-conjugation.

(4) To characterize the polymer assisted nanomaterials before and after immobilization of the bio-molecule by using different analytical and instrumental techniques like UV-visible spectroscopy, FTIR spectroscopy, XRD, SEM, TEM, etc.

(5) To evaluate different properties like magnetic, optical, electrical and biological, etc. of the characterized nanomaterials before and after immobilization of bio-molecules.

(6) To use the immobilized systems in various possible applications.

1.8. Technical program/plan of research

The plan of work for the proposed research:

(1) A state-of-art literature survey on the field of polymeric assisted nanomaterials, biocompatible polymers, bionanoconjugates and the interaction behaviour of various nanomaterials with biomolecules will be conducted.

(2) Polymer like poly(ethylene glycol) and starch assisted nanomaterials like magnetic iron oxide nanoparticles, anti-microbial silver nanoparticles etc. will be prepared by *in-situ* wet chemical technique.

(3) The potency of some bioresources like *Mesua ferrea* L. for the preparation of nanomaterials will be assessed.

(4) Bio-molecules like enzymes (*e.g.*, keratinase, amyloglucosidase) and other biologically relevant compounds like curcumin, lycopene etc. will be conjugated onto polymer assisted nanomaterials through various approaches (*e.g.*, using covalent couplers like cyanamide for enzyme coupling).

(5) *In-silico* statistical optimization (using soft-wares like Minitab, USA) of the various parameters of the preparation protocol of the nanomaterials (like sonication) and the immobilization process will be carried out.

(6) Characterization of the polymeric nanocomposites before and after biomolecule immobilization using tools like UV-visible spectroscopy, FTIR, SEM, TEM, XRD, VSM and performance evaluation like anti-microbial potency as function of shape-size-concentration accord of the nanofillers will be performed.

(7) Evaluation of changes in properties (like biological, optical, magnetic etc.) of the immobilized bio-molecule in comparison to its free counterpart like enzyme stability, reusability, activity etc. will be done.

(8) Evaluation of the practical application(s) of the studied systems will be tried.

(9) Preliminary toxicity evaluation of the prepared nanosystem across various domains of life to complement their practical utility assessment will be conducted.

The proposed research work would involve a few collaborations and receipt of co-operation from the Departments of Physics, Molecular Biology and Biotechnology, Food Engineering and Technology, Tezpur University; Department of Biotechnology, St. Anthony's College, Shillong; IIT Guwahati; North Eastern Hill's University, Shillong and others depending on the requirement.

References

1. Gao, J., et al. *Acc. Chem. Res.* **42,** 1097--1107, 2009.
2. Forano, C. & Prévot, V. Enzyme-based bioinorganic materials, in *Bio-inorganic hybrid nanomaterials: strategies, syntheses, characterization and applications*, E. Ruiz-Hitzky et al., eds., Wiley-VCH Verlag GmbH & Co. KGaA, Weinheim, Germany, 2008, Chapter 15.
3. Hanefeld, U., et al. *Chem. Soc. Rev.* **38,** 453--468, 2009.
4. Khan, A.A., & Alzohairy, M.A. *Res. J. Biol. Sci.* **5,** 565--575, 2010.
5. Paul, D.R., & Robenson, L. M. *Polymer* **49**, 3187--3204, 2008.
6. Karak, N. *Fundamentals of polymer: raw materials to finish products*, PHI learning Pvt. Ltd., Delhi, 2009.
7. Das, G., et al. *Adv. Sci. Lett.* **4**, 1--9. 2012.
8. Deka, H., et al. *Carbon* **48**, 2013--2022, 2010.
9. Konwar, U., et al. *Prog. Org. Coat.* **68**, 265--273, 2010.
10. Konwar, U., et al. *Polym. Degrad. Stabil.* **94**, 2221--2230, 2009.
11. Boyer, C., et al. *NPG Asia Mater.* **2,** 23--30, 2010.
12. Ferrari, M. *Nat. Rev. Cancer* **5**, 161--171, 2005.
13. Sharma, V.K., et al. *Adv. Colloid Interface Sci.* **145**, 83--96, 2009.
14. Wong, L.S., et al., *J. Am. Chem. Soc.* **130**, 12456--12464, 2008.
15. Ray, S., & Lalman, J.A. *Chem. Eng. Commun.* **169**, 116--125, 2011.
16. Elnashar, M.M. *J. Biomater. Nanobiotechnol.* **1**, 61--77, 2010.
17. Cao, L. *Curr. Opin. Chem. Biol.* **9**, 217--226, 2005.
18. Katzbauer, B., et al. *Bioprocess Eng.* **12**, 173--179, 1995.
19. Di Marco, M., et al. *Int. J. Nanomedicine* **5**, 37--49, 2010.
20. Menaa, B., et al. *Biophys. J.* **95,** L51--L53, 2008.
21. Xie, T., et al. *Afr. J. Biotechnol.* **8**, 4724--4733, 2009.
22. Riaz, A., et al. *Aust. J. Basic & Appl. Sci.* **3**, 2883--2887, 2009.
23. Patil, J.S., et al. *Digest J. Nanomat. Biostruct.* **5**, 241--248, 2010.
24. Rumbau, V., et al. *Macromolecules* **39**, 8547--8549, 2006.
25. Wang, A.M., et al. *J. Biosci. Bioeng.* **106**, 286--291, 2008.
26. Wang, A.M., et al. *J. Biosci. Bioeng.* **107**, 219--224, 2009.
27. Kumar, S., & Nahar, P. *Talanta* **71**, 1438--1440, 2007.
28. Saiyed, Z.M., et al. *J. Biotechnol.* **131**, 240--244, 2007.
29. Wang, Y., & Hasebe, Y.J. *Environ. Sci. (China)* **23**, 1038--1043, 2011.

30. Liu, Z. *Nat. Protoc.* **4**, 1372--1382, 2009.

31. Suslick, K.S. Sonochemistry, in *Kirk-Othmer Encyclopedia of Chemical Technology*, 4th ed., J. Wiley & Sons, New York, 1998, 517--541.

32. http://www.hielscher.com/ultrasonics/nano_00.htm, accessed on 30 July, 2012

33. Gedanken, A. *Ultrason. Sonochem.* **11**, 47--55, 2004.

34. Bezerra, M.A., et al. *Talanta* **76**, 965--977, 2008.

35. Veerapandian, M., & Yun, K.S. *Appl. Microbiol. Biotechnol.* **90**, 1655--1667, 2011.

36. Veerapandian, M., & Yun, K.S. *Dig. J. Nanomater. Bios.* **4**, 243--262, 2009.

37. Faraji, A.H., & Wipf, P. *Bioorgan. Med. Chem.* **17**, 2950--2962, 2009.

38. Gaucher, G., et al. *J. Control Release* **143**, 2--12, 2010.

39. Hansen, S.F. *Wiley Interdiscip. Rev. Nanomed. Nanobiotechnol.* **2**, 441--449, 2010.

40. Ravindran, A., et al. *Colloid Surface B*, in press. doi: 10.1016/j.colsurfb.2012.07.036

41. Hong, R.C.Y., Hung, A.C. J., Horng, H.E., Yang, H.C. and Yang, S.Y. *Ultra-sensitive magnetoreduction measurement system and ultra-sensitive, wash-free assay using the same,* **US Patent No. 20080024117,** January 31, 2008.

42. Kobayashi, N. *Artificial cornea containing transparent nanofibers and biomolecules,* **JP Patent No. 2008043419**, February 28, 2008.

43. Yang, P., Karnik, R., Castelino, K., Fan, R. and Manjumdar, A. *Functionalization of nanofluidic channels with immobilization of biomolecules on the inner surface of the channel and measuring nanochannel conductance for detection of a binding event,* **WO Patent No. 2008048209**, April 24, 2008.

44. Jing, N., Schultz, W.J., Guo, C. and Legatt, M.L. *Methods of use of solid support material for binding biomolecules and their preparation,* **WO Patent No. 2008131063**, October 30, 2008.

45. Huber, M. *Ultrasensitive biomolecule detection using double stranded DNA co-loaded gold nanoparticles and co-immobilized capture molecules,* **WO Patent No. 2008140620,** November 20, 2008.

46. Himmelhaus, M. and Sivashankar, K. *Chemical surface nanopatterns to increase activity of surface-immobilized biomolecules,* **WO Patent No. 2008143351**, November 27, 2008.

47. Rodriguez, R.P., Bareda, G.G., Fernandez, J.A.G., Astigarraga, E.A., Aranzabe, A.G., Marcaide, A.R. and Gomez, D.P. *Method for surface treatment of solid substrates,* **WO Patent No. 2008012391**, January 31, 2008.

48. Todd, S.J., Ulijin, R.V. and Gough, J. *Enzyme-triggered activation of immobilized anti-inflammatory biomolecules, and use in prosthetic implants and bioscaffolds,* **WO Patent No. 2008062168**, May 29, 2008.

49. Yu, H., Pourmand, N. and Wang, S.X. *Biomolecule immobilization on biosensors,* **US Patent No. 20080161200**, July 3, 2008

50. Jing, N., Schultz, W.J., Guo, C., Legatt, M.L. and Zhang, Y. *Uses of water-dispersible silica nanoparticles for attaching biomolecules,* **WO Patent No. 2009009188,** January 15, 2009.

51. Li, S., He, N. and Liu, H. *Detecting single base difference by magnetic separation and solid-phase single base circular extension,* **CN Patent No. 101392290**, March 25, 2009.

52. Hong, H.B., Yoon, H.J. and Jung, M.A. *Method for quantificationally detecting biomolecule by using magnetic nanoparticle and frequency mixing magnetic reader,* **KR Patent No. 2009060143**, June 11, 2009.

53. Utermohlen, J.G. and Hogan, M.E. *Particle matrix for dry state storage of biomolecules and biopolymers,* **US Patent No. 20090208919**, August 20, 2009.

54. Maye, M.M. Gang, O., Nykypanchuk, D. and Van Der Lelie, D. *Methods for preparation of nanoscale clusters,* **US Patent No. 20090258355**, October 15, 2009.

55. Jon, S.Y., Park, S., Sung, D.K. and Yang, H. *Multifunctional polymeric layers for biochips and biosensors,* **WO Patent No. 2009031804**, March 12, 2009.

56. Fabis, R. and Springer, B. *Water-soluble polymers having chelators for reversible binding and identification of biomolecules,* **DE Patent No. 102007049335**, April 16, 2009.

57. Punyadeera, C.K., Van Lieshout, R.M.L., Hermans, K, Prenen, A.M., Bastiaansen, C.W.M. and Broer, D.J. *Membranes suited for immobilizing biomolecules,* **WO Patent No. 2009115938**, September 24, 2009.

58. Choi, J.H., Jung, C.H., Hwang, I.T., Kim, D.G. and Noh, Y.C. *Method for immobilizing biomolecules and forming patterns on biodegradable polymer material using radiation,* **KR Patent No. 2010030105**, March 18, 2010.

59. Karhanek, M., Webb, C.D., Umehara, S. and Pourmand, N. *Functionalized nanopipette biosensor with immobilized peptide ligand,* **US Patent No. 20100072080**, March 25, 2010.

60. Scheper, T., Sohling, U., Ralla, K., Kasper, C., Burzlaff, A., Daehne, L., Senst, S. and Baude, B. *Adsorbent porous carrier with polyelectrolyte layers for immobilizing and separation of biomolecules,* **WO Patent No. 2010066432**, June 17, 2010.

61. Tang, L., Zeng, G., Yin, J., Luo, J., Yuan, X., Du, C., Peng, Y. and Pang, Y. *Gold/silica/ferroferric oxide core-shell composite magnetic nanoparticles for detection of cellulase gene, and preparation method and application thereof,* **CN Patent No. 101789295,** July 28, 2010.

62. Sun, H. and Oldham, M. *Metal nanoparticles-based biosensor for detecting fluoroscently-labeled biomolecules, and use in real-time DNA sequencing,* **WO Patent No. 2010115147,** October 07, 2010.

63. Sigillo, E.C., Chien, J.C., Pomeroy, M.C. and Saltalamacchia, C.A. *Rapid biomolecule quantification assay employing highly concentrated, protein ligand-coated gold colloid nanoparticles,* **US Patent No. 20100255610**, October 07, 2010.

64. Mohagheghpour, E., Moztarzadeh, F. and Rabiee, M. *Fabrication of nano-biosensor for biomolecular recognition,* **US Patent No. 20100304500**, December 02, 2010.

65. Kim, H.S., Kim, J.M., Park, J.G. and Han, Y.G. *Magnetophoretic biomolecule assay method using magnetic nanoclusters,* **KR Patent No. 2010126928,** December 03, 2010.

66. Shin, U.S., Nagarale, R.K. and Lee, J.M. *Nanocomposite of ferrocene-substituted polysiloxane and chitosan and its manufacture method,* **KR Patent No. 2011012463**, February 09, 2011.

67. Gubala, V., Le Guevel, X. and Nooney, R. *Biomolecular labels, involving nanoparticles functionalised with dendrimers,* **WO Patent No. 2011045394**, April 21, 2011.

68. Mattoussi, H.M., Dawson, P.E., Uyeda, H.T., Medintz, I.L. and Scheinost, J.C. *Covalent attachment of peptides and biological molecules to luminescent semiconductor nanocrystals,* **US Patent No. 20110098445**, April 28, 2011.

69. Park, C.B., Lim, S.Y. and Lee, J.S. *Method for detecting biomolecule using alginate matrix encapsulating gold nanoparticle and biomolecule oxidase,* **KR Patent No. 2011065231**, June 15, 2011.

70. Beaux, M.F.II., Corti, G., McIlroy, D.N. and Norton, M.G. *Nanostructured high surface area supports for biomolecule, chemical, drug, and cell attachment applications and methods of making the same,* **WO Patent No. 2011100638,** August 18, 2011.

71. Kim, C., Sudha Rani, V., Jeong, J-R. and Yoon, S.S. *Digital barcode nano-wire and system for bio-sensing using the same,* **US Patent No. 20110236260**, September 29, 2011.

72. Chen, Y-T., Pan, C-Y. and Lin, T-W. *Reusable nanowire field effect transistor system for detecting biomolecular interactions,* **US Patent No. 20110281288**, November 17, 2011.

73. Handa, H., Hatakeyama, M., Sakamoto, S. and Kishi, H. *Polymer-coated ferrite microparticles and production method for same,* **WO Patent No. 2011052205**, May 5, 2011.

74. Fernandez Gutierrez, A., Santoyo Gonzalez, F., Medina Castillo, A.L., Morales Sanfrutos, J. and Megia Fernandez, A. *Polymer compounds having immobilizing properties,* **WO Patent No. 2012085303**, June 28, 2012.

75. Sun, X., Du, S., Wang, X., Liu, J. and Li, Q. *Preparation method of current-type immunosensor for pesticide residue detection,* **CN Patent No. 102608188**, July 25, 2012.

76. Durand, N., Maerki, I., Broillet, S., Mayor, A. and Lasser, T. *Rapid quantification of biomolecules in a selectively functionalized nanofluidic biosensor and method thereof,* **WO Patent No. 2012120387,** September 13, 2012.

77. Evans, D. *Lock-release immobilization technique for purifying, producing and storing biomolecules using diketone group containing polymer support,* **WO Patent No. 2012140433,** October 18, 2012.

78. Del Pino Gonzalez de la Higuera, P.A., Grazu Bonavia, M.V., Martinez de la Fuente, J., Sanchez Espinel, C. and Santos Martinez de Laguna, R. *Multifunctionalized nano- or microparticles joined to PNA/DNA chains with attached biomolecules,* **WO Patent No. 2012150373,** August 8, 2012.

79. Jinhao, G., et al. *Acc. Chem. Res.* **42**, 1097--1107, 2009.

80. Gao, J. H., et al. *Adv. Mater.* **18**, 3145--3148, 2006.

81. Wang, L., et al. *J. Am. Chem. Soc.* **128**, 13358--13359, 2006.

82. Xu, C. J., et al. *J. Am. Chem. Soc.* **126,** 9938--9939, 2004.

83. Xu, C. J., et al. *J. Am. Chem. Soc.* **126**, 3392--3393, 2004.

84. Morteza, M., et al. *Adv. Drug Deliver. Rev.* **63**, 24--46, 2011.

85. Young-wook, J., et al. *Acc. Chem. Res.* **41**, 179--189, 2008

86. Johnson, A.K., et al. *J. Nanopart. Res.* **10**, 1009--1025, 2008.

87. Laurent, S., et al. *Chem. Rev.* **108**, 2064--2110, 2008.

88. Bourgeat-Lami, E., & Lang, J. *J. Colloid Interface Sci.* **197**, 293--308, 1998.

89. Amstad, E., et al. *Nanoscale* **3**, 2819--2843, 2011.

90. Boyer, C., et al. *NPG Asia Mater.* **2**, 23--30, 2010.

91. Sun, C., et al. *Small* **4**, 372--379, 2008.

92. Mahmoudi, M., et al. *J. Phys. Chem. B* **112**, 14470--14481, 2008.

93. Xu, F.H., et al. *Nanotechnol.* **20**, 40, 2009.

94. He, N., Wang, Z., & Li, S. DNA separation and amplification of Fe_3O_4/PMMA/SiO_2 nanoparticles with core-shell structure, in The 231st ACS National Meeting, Atlanta, GA, 2006, p.162-ANYL.
95. Bravo-Osuna, I., et al. *Eur. J. Pharm. Sci.* **30**, 143--154, 2007.
96. Lacava, L.M., et al. *Biophys. J.* **80**, 2483--2486, 2001.
97. Saboktakin, M.R., et al. *Carbohyd. Polym.* **78**, 292--295, 2009.
98. Intorasoot, S., et al. *Anal. Biochem.* **366**, 291--292, 2009.
99. Ansari, S.A., & Husain, Q. *Biotechnol. Adv.* **30**, 512--523, 2012.
100. Kouassi, G.K., et al. *J. Nanobiotechnol.* **3**, 1--9, 2005.
101. Johnson, A.K., et al. *J. Nanopart. Res.* **10**, 1009--1025, 2008.
102. Huang, J., et al. *Int. J. Nanomed.* **2**, 775--784, 2007.
103. Zhang, Y., et al. *Huan Jing Ke Xue*, **28**, 2320--2325, 2007.
104. Sahoo, B., et al. *J. Mol. Catal. B: Enzym.* **69**, 95--102, 2011.
105. Huang, S.H., et al. *Biotechnol. Prog.* **19**, 1095--1100, 2003.
106. Mak, K.H., et al. *Sci. Technol. Vision* **5**, 19--23, 2009.
107. Namdeo, M., & Bajpai, S.K. *J. Mol. Catal. B: Enzym.* **59** 134--139, 2009.
108. Pan, C., et al. *J Mol Catal B: Enzym* **61**, 208--15, 2009.
109. Demira, A.S., et al. *J. Biotechnol.* **152**, 176--183, 2011.
110. Zhao, M., et al. *Nat. Med.* **7**, 1241--1244, 2001.
111. Cerdan, S., et al. *Magn. Reson. Med.* **12**, 151--163, 1989.
112. Li, Z., et al. *Adv. Mater.* **8**, 1001--1005, 2005.
113. Bulte, J.W., et al. *Magn. Reson. Med.* **25**, 148--157, 1992.
114. Zhang, C., et al. *Cancer Res.* **67**, 148--157, 2007.
115. Lee, J.H., et al. *Nat. Med.* **13**, 95--99, 2007.
116. Butoescu, N., et al. *Arthritis Res. Ther.* **11,** R72 (10 pp), 2009.
117. Butoescu, N., et al. *Eur. J. Pharm. Biopharm.* **72** 529--538, 2009.
118. Nasongkla, N., et al. *Nano Lett.* **6**, 2427--2430, 2006.
119. Santra, S. et al. *Small* **5**, 1862--1868, 2009.
120. Gong, X., et al. *Adv. Funct. Mater.* **19,** 292--297, 2009.
121. Mahmoudi, M., et al. *J. Phys. Chem. C* **113**, 8124--8131, 2009.
122. Smith, A.M., et al. *Phys. Chem. Chem. Phys.* **8**, 3895--3903, 2006.
123. Kearns, G.J., et al. *Anal. Chem.* **78**, 298--303, 2006.
124. Mulvaney P. *Langmuir* **12**,788--800, 1996.
125. Frattini, A., et al. *Mater. Chem. Phys.* **94**,148--152, 2005.
126. Panagiotis, D., et al. *Adv. Colloid Interface Sci.* **166,** 119--135, 2011.

127. Raveendran, P., et al. *J. Am. Chem. Soc.* **125**, 13940--13941, 2003.

128. Sato, Y., et al. *Langmuir* **19**, 6857--6861, 2003.

129. Kvítek, L., et al. *J. Mater. Chem.* **15**, 1099--1105, 2005.

130. Chen, J., et al. *Mater. Chem. Phys.* **108**, 421--424, 2008.

131. Troupis, A., et al. *Angew Chem. Int. Ed.* **41**, 1911--1914, 2002.

132. Shahverdi, A.R., et al. *Process Biochem.* **42**, 919--923, 2007.

133. Gardea-Torresdey, J.L., et al. *Langmuir* **19**, 1357--1361, 2003.

134. Shankar, S.S., et al. *Biotechnol. Prog.* **19**, 1627--1631, 2003.

135. Shankar, S.S., et al. *Chem. Mater.* **17**, 566--572, 2005.

136. Mantion, A., et al. *Soft Matter* **4**, 606--617, 2008

137. Lee, K.J., et al. *Nanotechnol.* **18**, 33560 (5 pp), 2007.

138. Rai, M., et al. *Biotechnol. Adv.* **27**, 76--83, 2009.

139. Guin, D., et al. *J. Phys. Chem. C* **111**, 13393--13397, 2007.

140. Alt, V., et al. *Biomaterials* **25**, 4383--4391, 2004.

141. Russell, A.D., & Hugo, W.B. *Prog. Med. Chem.* **31**, 351--370, 1994.

142. Lee, H.Y., et al. *Chem. Commun.* 0, 2959--2961, 2007.

143. Jeong, S., et al. *J. Mater. Sci.* **40**, 5407--5411, 2005.

144. Chou, W-L., *Polym. Adv. Technol.* **16**, 600--607, 2005.

145. Sun, R.W.Y., *Chem. Commun.* **40**, 5059--5061, 2005.

146. Petkova, G.A. et al. *Nanoscale Res. Lett.* **7**, 287 (10 pp), 2012.

147. Zhang, Y.J., et al. *Chinese Sci. Bull.* **57**, 238--246, 2012.

148. Hsu, F.Y., et al. *J Chin. Chem. Soc.* **58**, 756--760, 2011.

149. Shen, X.C., et al. *Acta Chim Sin*, **64**, 469--474, 2006.

150. Cao, Y.W., et al. *Science* **297**, 1536--1540, 2002.

151. Huang, T., et al. *Anal. Chem.*, **79**, 7708--7718, 2007.

152. Zhu, S.L., et al. *Sensor. Actuat. B-Chem.* **134**, 193–198, 2008.

153. Haes, A.J., et al. *Nano Lett.* **4**, 1029--1034, 2004.

154. Lima, R. D., et al. *J. Appl. Toxicol.* **32**, 867--879, 2012.

155. Vidal, J.C., et al. *Microchim. Acta* **143**, 93--111, 2003.

156. Kim, M., et al. *ACS Appl. Mater. Interface* **4**, 4603--4609, 2012.

157. Feast, W.J., et al. *Polymer* **37**, 5017—5047, 1996.

158. Huang, J., et al. *J. Am. Chem. Soc.* **125**, 314--315, 2003.

159. Matlock-Colangelo, L., & Baeumner, A.J. *Lab Chip* **12**, 2612--2620, 2012.

160. Du, Z. et al. *Mater. Sci. Eng. C* **29**, 1794--1797, 2009.

161. Zhang, J., et al, *Biosens. Bioelectron.* **24**, 1858--1863, 2009.

162. Spain, E. R., et al. *Biosens. Bioelectron.* **26**, 2613--2618, 2011.

163. Wang, X., et al. *Biosens. Bioelectron.* **26**, 2953--2959, 2011.

164. Khalil, A., et al. *IEEE Sens. J.* **9**, 1942--1951, 2009.

165. Tarushee, A., et al. *Biomaterials* **28**, 791--805, 2007.

166. Ivanov, A.N., et al. *IEEE Sens. J.* **3**, 333--40, 2003.

167. Fengli, Q., et al. *Anal. Biochem.* **344**, 108--14, 2005.

168. Hahm, J-I., *Nano Lett.* **4**, 51--4. 2004.

169. Zhu, N., et al. *Electrochim. Acta* **51**, 3758--3762, 2005.

170. Singh, S., *Sensor Actuat. B-Chem.* **115**, 534--541, 2006.

171. Sharma, A., et al. *J. Appl. Polym. Sci.* **91**, 3999--4006, 2004.

172. Mathebe, N.G.R., et al. *Talanta* **64**, 115--20, 2004.

173. Iwuoha, E.I., et al. *Biosens. Bioelectron.* **12**, 749--761, 1997.

174. Xue, H., et al. *Synth. Met.* **124**, 345–349, 2001.

175. Yang, T., et al. *J. Electroanal. Chem.* **656**, 140--146. 2011.

176. Edgar, K. Organic cellulose esters, in *Encyclopedia of Polymer Science and Technology.* H.F. Mark, ed. Wiley, New York, 2004, 129--158.

177. Fischer, S., et al. *Macromol. Symp.* **262**, 89--96, 2008.

178. Puls, J., et al. *J. Polym. Environ.* **19**, 152--165, 2011.

179. Sousa, M., et al. *J. Phys. Chem. B* **114**, 10939--10953, 2010.

180. Aoki, D., et al. *Biomacromolecules* **8**, 3749--3757, 2007.

181. Liu, C.X., & Bai, R.B. *J. Membr. Sci.* **284**, 313--322, 2006.

182. Pham, Q.P., et al. *Tissue Eng.* **12**, 1197--1211, 2006.

183. Bhardwaj, N., & Kundu, S.C. *Biotechnol. Adv.* **28**, 325--347, 2010.

184. Taepaiboon, P., et al. *Eur. J. Pharm. Biopharm.* **67**, 387--397, 2007.

185. Tian, Y., et al. *Carbohyd. Polym.* **83**, 743--748, 2011.

186. Chen, C., et al. *Appl. Energ.* **88**, 3133--3139, 2011.

187. Son, W.K., et al. *Carbohyd. Polym.* **65**, 430--434, 2006.

188. Bedford, N.M., & Steckl, A.J. *ACS Appl. Mater. Interfaces* **2**, 2448--2455, 2010.

189. Rubenstein, D.A., et al. *J. Biomater. Sci. Polym. E* **21**, 1713--1736, 2010.

190. Hellmann, C., et al. *Polym. Adv. Technol.* **22**, 407--413, 2011.

191. Wongsasulak, S., et al. *J. Food Eng.* **98**, 370--376, 2010.

192. Liu, S., et al. *Mater. Lett.* **64**, 2427--2430, 2010.

193. Hendrick, E., et al. *J. Eng. Fiber Fabr.* **5**, 21--30, 2010.

194. Renekar, D.H., & Chun, I. *Nanotechnol.* **7**, 216--223, 1996.

195. Shin, Y.M., et al. *Appl. Phys. Lett.* **78**, 1149--1151, 2001.

196. Shin, Y.M., et al. *Polymer* **42**, 9955--9967, 2001.

197. Hohman, M.M., et al. *Phys. Fluids* **13**, 2201 (20 pp), 2001.

198. Hohman, M.M., et al. *Phys. Fluids* **13**, 2221 (16 pp), 2001.

199. Huang, X-J., et al. J. Mol. Catal. B: Enzy. **3**-4, 95--100, 2011.

200. Chen, P-C., et al. *Cellulose* **18**, 1563--1571, 2011.

201. Kumar, C.G. *IJPT* **3**, 1367--1381, 2011.

202. Tungprapa, S., et al. *Polymer* **48**, 5030--5041, 2007.

203. Castillo-Ortega, M.M., et al. *J. Appl. Polym. Sci.* **116**, 1873--1878, 2010.

204. Suwantong, O., et al. *Polymer* **48**, 7546--7557, 2007.

205. Suwantong, O., et al. *J. Biomed. Mater. Res.* A **94**, 1216--1225, 2010.

206. Phaechamud, T., & Phiriyawirut, M. *Res. J. Pharm. Biol. Chem. Sci.* **2**, 85-98, 2011.

207. Phiriyawirut, M., & Phaechamud, T. *J. Nanosci. Nanotechnol.* **12**, 793--799, 2012.

208. Yu, D-G., et al. *Carbohyd. Polym.* **90**, 1016--1023, 2012.

209. Kontogiannopoulos, K.N., et al. *Int. J. Pharm.* **409**, 216--228, 2011.

210. Sun, X., et al. *ACS Appl. Mater. Interfaces* **2**, 952--956, 2010.

211. Thitiwongsawet, P., et al. *AJCHE* **10**, 41--47, 2010.

212. Silveira JVW, Millás ALG, Tessarolli LF, Bittencourt E, Ago M, Rojas OJ. Production of electrospun cellulose acetate fiber mats as carriers of citronella essential oil. Abstracts of Papers, 239th ACS National Meeting, San Francisco, CA, United States, March 29, 2012: CELL-305.

213. Hellmann, C., et al. *Polym. Adv. Technol.* **22**, 407--413, 2011.

214. Sapsford, K.E., et al. *Anal. Chem.* **83**, 4453--4488, 2011.

215. Ribeiro, C., et al. *Int. J. Pharm.*, **367**, 204--210, 2009.

216. Saini, V., et al. *Small* **2**, 262--269, 2008.

217. Mastroianni, A.J., et al. *J. Am. Chem. Soc.* **131**, 8455--8459, 2009.

218. Ma, P.L., et al. *Biomacromolecules*, **11**, 549--554, 2010.

219. Claridge, S. A., et al. *Nano Lett.* **8**, 1202--1206, 2008.

220. Saikia, N., & Deka, R.C. *J. Mol. Model.* **19**, 215--226, 2013.

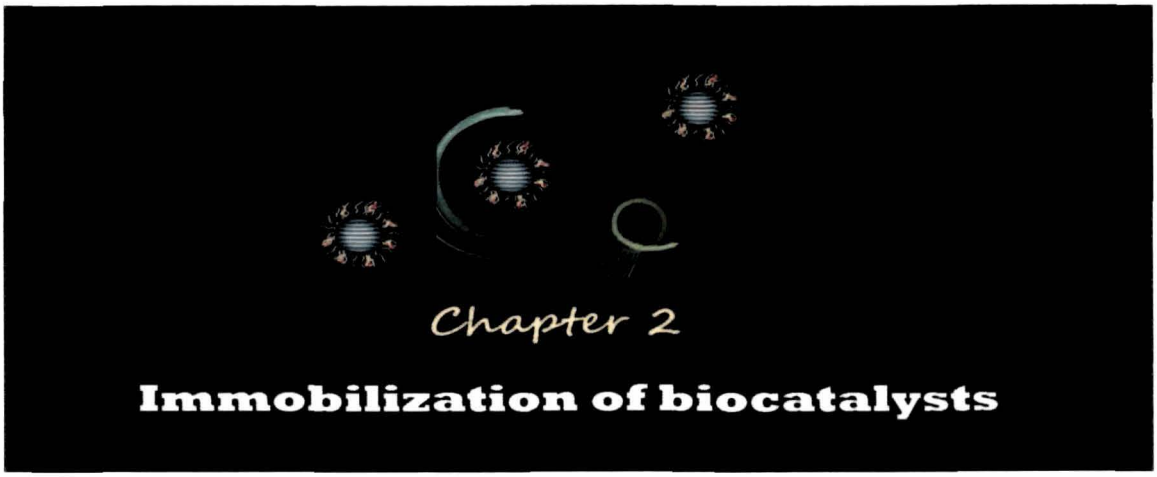

Chapter 2

Immobilization of biocatalysts

HIGHLIGHTS OF THE CHAPTER*

Immobilization of biocatalysts onto suitable platforms is a common strategy for increasing the former's stability, functional reuse and cost effectiveness in both industrial and biomedical domains. In this context, subchapter 2A deals with the immobilization of *Bacillus subtilis* keratinase onto poly(ethylene glycol) supported iron oxide nanoparticles for prospective depilatory (hair-removal) applications in leather industry. On the other hand, subchapters 2B and 2C respectively deal with the immobilization of *Aspergillus niger* amyloglucosidase (for starch saccharification and starch de-staining) and porcine pancreatic lipase (exhibiting compatibility with commercial detergents for oil de-staining) onto antibacterial and magnetically recyclable poly(ethylene glycol) supported silver-iron oxide exotic nanostructures, as characterized by various spectroscopic and analytic tools. The preparation of the silver nanoparticles is based on the reductive potency of various bio-resources. The immobilization studies have relied on the use of the green chemistry tool of sonication in tuning the physico-chemical properties including the morphological modulations of the immobilization platform and thermostability, storage stability, reusability and kinetic parameters of the immobilized enzymes.

*Parts of this chapter are published in

1. Konwarh, R., & Karak, N., et al. *Nanotechnol.* **22**, 225107 (10 pp), 2009.
2. Konwarh, R., & Karak, N., et al. *Appl. Microbiol. Biotechnol.* **87,** 1983--1992, 2010.
3. Konwarh, R., & Karak, N., et al. *Ultrason. Sonochem.* (Communicated)
4. Konwarh, R., & Karak, N. *Adv. Colloid Interface Sci.* (Communicated)

2A. KERATINASE IMMOBILIZATION ONTO PEG-IONPs

2A.1. Introduction

A concert of material-science and enzyme technology can be instrumental in addressing a number of global environmental issues such as solid waste management, amongst other things. As an answer to recalcitrant keratinous wastes such as chicken feathers, keratinase echoes the tremendous potential to wheel a number of industrial sectors. These microbial enzymes are predominantly extracellular, although cell-bound and intracellular enzymes have also been described.[1] Amongst the reported utilities, generation of poultry feed and semi slow-release nitrogen fertilizer, production of biofuels, cleaning up of drains clogged with keratinous wastes and prion degradation by broad-spectrum keratinase PWD1 (Versazyme) and selective dehairing without collagenolysis are instigating tremendous interest.[2] It is pertinent to mention that immobilization study of this class of biocatalyst has not been explored so far. Therefore, conjugating keratinase onto polymer supported magnetic nanoparticles (MNPs) would imply highly prospective industrial applications.

As noted in Chapter 1, magnetic nanoparticles-enzyme conjugates (MNP-Es) have attested applications across myriad of domains. The high surface to volume ratio favours high binding capacity and high catalytic specificity of the conjugated enzyme. In addition, magnetic field susceptibility provides a mechanism for efficient recovery of the enzyme complex and thereby preventing the enzyme contamination[3] of the final product. Enzyme stability[4] is maximized with nano-scaled support with additional advantages of possible modulation of the catalytic specificity, lower transfer resistance to solve diffusion problem and lower operational cost. Polymer coatings/dispersions of particles enhance compatibility with organic ingredients, reduce susceptibility to leaching, and protect surfaces from external damages. Eventually, there is improvement in dispersion, stability and reduction of toxicity.[5]

Thus, in this work, the supportive role of poly(ethylene glycol) supported iron-oxide nanoparticles (PEG-IONPs) as immobilization platform for *Bacillus subtilis* keratinase has been delved into for activity enhancement, recyclability and stability with exploration of its prospective hair saving applicability in leather industry.

2A.2. Experimental

2A.2.1. *Materials used for the preparation of the immobilization platform*

Iron (II) chloride tetrahydrate ($FeCl_2 .4H_2O$) (≥ 99.0%, BDH, molar mass: 198.8 g/mol) was used to prepare iron oxide nanoparticles. Ferrous chloride (occurring as the mineral lawrencite in nature) is used as an electrolytic agent in metallurgy and as a mordant in dyeing.[6] It finds application in the synthesis of pentasubstituted acylferrocenes.[6] It is pertinent to mention that in biological research, it is often used as a source of Fe^{2+} ion. It has been found to block calcium influx though N-methyl-D-aspartate receptor channels in immature rat cortical neurons.[6] Furthermore, it has been used to investigate the interaction between hypoxia-inducible factor (HIF-α) and the von hippel-Lindau ubiquitylation complex.[6] Aqueous solutions of ferrous chloride are readily oxidized.[6]

The preparative protocol as outlined in the subsequent section involved the *in-situ* dispersion of the particles in polymer matrix *i.e.,* poly(ethylene glycol). The methodology involved the use of potassium hydroxide (KOH) (Merck, molar mass: 56.1 g/mol) and hydrogen peroxide (H_2O_2) (Ranbaxy, 30% v/v) respectively. KOH is a caustic reagent, often used to neutralize acids. It readily absorbs carbon dioxide and water from air and deliquesces.[7] It finds applications in manufacture of soap, electroplating, photoengraving, mercerizing of cotton and lithography.[7] It is used in intercalation studies of anti-cancer drugs to nucleic acids and in the analysis of bone and cartilage samples by histology.[7] On the other hand, hydrogen peroxide, a powerful corrosive and oxidising agent finds a spectrum of applications ranging from highly effective disinfectants to bleaches.[8] Diluted hydrogen peroxide solutions with water tend to be light sensitive. Interestingly, cellular metabolism generates H_2O_2 as a natural component in tissues.[8]

Poly(ethylene glycol) (number average molecular weight, M_n=6,000 g/mol, PEG_{6000} , GS Chemicals) was used for the stabilization of iron oxide nanoparticles. PEG (with the general formula - $H(OCH_2CH_2)_nOH$)) is a condensation polymer of ethylene oxide and water. PEG is soluble in water (100 mg/mL), as well as other polar solvents such as acetone, alcohols, and chlorinated solvents. Although PEGs are susceptible to oxidative degradation in presence of air, aqueous PEG solutions are stable at room temperature.[9] As noted in the first chapter, PEG is often used in developing biocompatible nanomaterials.[10] PEG has been also been used as fusing agent in

enhancing the effect of macrophages on hybridoma, in the separation and purification of biomolecules and in induction of cell hybridization. [9] On the other hand, the stabilization of various proteins by PEGylation is highlighted at appropriate places (including this chapter) of the thesis.

On the other hand, prior to immobilization of the biocatalyst *i.e.,* keratinase, the PEG-IONPs were surface functionalized using cyanamide (CH_2N_2) (Sigma, molar mass: 42.040 g/mol). The presence of both nucleophilic and electrophilic site within the same molecule facilitates a plethora of cyanamide mediated reactions (including condensation reactions where in it behaves as a dehydration agent). It finds wide applications in agriculture and manufacture of pharmaceuticals and other organic compounds. Modest toxicity of cyanamides has been reported in humans.[11]

All the chemicals and reagents were used as received· Millipore water was used through the experiment.

2A.2.2. *Protocol for the preparation of PEG-IONPs*

PEG-IONPs were prepared as described by Rossi et al.,[12] with slight modification. Briefly, 2% (w/v) PEG and 0.1 M $FeCl_2.4H_2O$ (25 mL) were prepared in Millipore water separately and the latter dispersed in the polymer solution with constant mechanical stirring. 1.0 M KOH aqueous solution was added drop wise to the above mixture, with constant stirring at room temperature. During the addition of KOH solution, the colour of the mixture gradually turned dark green. Addition of 250 µL of 3% (v/v) H_2O_2 to the above dark green suspension yielded a black dispersion that was attracted by a permanent magnet. After separating the matrix supported particles by centrifugal decantation, they were washed with distilled water followed by washing with acetone (Merck). The sample was then vacuum dried at 45 ^{0}C for 24 h.

2A.2.3. *Keratinase immobilization*

Alkaline keratinase produced by *Bacillus subtilis* was collected from the Department of Molecular Biology and Biotechnology, Tezpur University. For immobilization, 25 mg of PEG-IONPs was suspended in 0.5 mL of freshly prepared cyanamide solution (20 mg per mL of 0.5 mL of tris-HCl (Merck), pH 8.0) and sonicated for 15 min at room temperature using a standard sonotrode (having a tip-diameter of 3 mm) in a high-intensity ultrasonic processor (UP200S, Hielscher Ultrasonics GmBH, Germany). Further, sonication was done for 30 min at 4 ^{0}C (ice-bath) after adding 0.5

mL of the enzyme followed by centrifugation at 3000 rpm for 10 min. The post-precipitate supernatants were collected in fresh microfuge tubes. It is to be noted that cyanamide used for the immobilization process may stabilize the enzyme by cross linking it or its subunits and enzyme aggregates may remain in the solution. So, after the centrifugation step, the enzyme-bound PEG-IONPs (keratinase-PEG-IONPs) were subjected to magnetic decantation. The separated nanoparticles were then washed twice and finally suspended in 0.5 mL of 100 mM tris-HCl (pH 8.0). The percentage of binding was estimated by determining the keratinase activity for both the post-precipitate supernatant and the immobilized enzyme fraction.

2A.2.4. *Enzyme activity measurement*

Keratinase activity was measured spectrophotometrically by using 1% (w/v) keratin (HIMEDIA, India) as a substrate. The immobilized enzyme supernatant (50.0 µL) was mixed with 950.0 µL of 100 mM tris-HCl (pH 8.0) containing 1% (w/v) keratin and incubated for 15 min at 45 ^{0}C. The reaction was stopped by addition of 0.5 mL ice cold 10% (w/v) tris-chloro acetic acid (TCA) (Merck). The mixture was allowed to stand at 4 ^{0}C for 20 min and then centrifuged at 10,000 rpm for 10 min to remove the precipitate. The mixture supernatant was decanted to a fresh tube and 2.0 mL of 2% (w/v) Na_2CO_3 (99.5%, E. Merck, India) in 0.1 N NaOH (Merck) was added and incubated at room temperature for 10 min followed by addition of 0.5 ml Folin Ciocalteaus' reagent (Merck) (1:2 aqueous dilution). After 30 min, absorbance was measured at 660 nm. From a standard curve of tyrosine, keratinase activity was calculated. One unit of keratinase activity was defined as the amount of enzyme, which liberated 1 µmol of tyrosine per min per mL at 37 ^{0}C. Specific activity is defined as unit of enzyme activity per mg protein. Protein concentration was determined by the method of Lowry et al.,[13] using bovine serum albumin (BSA) as a standard.

2A.2.5. *Optimization of process parameters*

The step-wise optimization process was carried out for the following parameters governing the *in-situ* preparation of IONPs in PEG matrix. The efficiency of the polymer supported nanoparticles was evaluated in terms of activity enhancement of the enzyme immobilized onto it. Influence of temperature, pH of the reaction mixture before addition of H_2O_2, concentration of polymer and mole ratio of polymer to iron ($FeCl_2.4H_2O$) were the parameters chosen for the optimization process. Preparation of

iron oxide nanoparticles was executed under three different temperatures: 0 ^{0}C, 25 ^{0}C and 50 ^{0}C. The reaction mixture adjusted to pH 7.2, 8.2, 9.2, 10.2 and 11.2 were examined to evaluate the effect of pH on the synthesis efficiency and consequently on the enhancement of enzyme activity. The polymer concentration (w/v) was varied as 1%, 2%, 5% and 10% of the total medium volume. Taking 0.05 M, 0.1 M and 0.2 M $FeCl_2.4H_20$ in PEG at a concentration, determined to be the optimum in the previous step, the mole ratio of polymer to iron (0.031:1, 0.062:1, 0.121:1) was varied. Response Surface Methodology (RSM) was used to estimate the main effects on the response *i.e.*, the enzyme immobilization to the PEG-IONPs and evaluated in terms of enzyme activity. Three factors with three levels consisting of 31 experimental runs were used to analyse the experimental data including five replicates at the centre point. This allows better estimate of the experimental error and to provide extra information about the specific activity of the coupled enzyme in the interior of the experimental region.[14] The temperature (C_1), pH of the reaction system before addition of H_2O_2 (C_2), and polymer to iron molar ratio (C_3) were chosen as the experimental factors or the independent variables capable of influencing the activity (Y) of keratinase immobilized onto PEG-IONPs. Analysis was done using coded values (-1 for C_1=23 ^{0}C, C_2=7.2 and C_3=0.031:1; 0 for C_1=25 ^{0}C, C_2=8.2 and C_3=0.062:1; 1 for C_1=27 ^{0}C, C_2=9.2 and C_3=0.121:1). Using this design, the experimental data were fitted according to the equation (2A.1) as a second order polynomial equation including individual and cross effect of each variable.

$$Y = a_0 + a_1C_1 + a_2C_1^2 + a_3C_2 + a_4C_2^2 + a_5C_3 + a_6C_3^2 + a_7C_1{*}C_2 + a_8C_1{*}C_3 + a_9C_2{*}C_3 \quad \textbf{.....(2A.1)}$$

Where, Y= keratinase activity (response), C_1 = temperature, C_2 = pH of reaction system before addition of H_2O_2, C_3 = mole ratio of polymer to iron and a_0, a_1, a_2, a_3, a_4, a_5, a_6, a_7, a_8, a_9 are the regression coefficients. Analyses were carried out in duplicate. The data tabulated were (Table2A.1) the average of the measurements. Multiple regression analysis and response surface plots were generated using Minitab 15® software.

2A.2.6. *Physico-chemical characterization tools*

UV-visible spectra were analyzed in Hitachi (Tokyo, Japan) U2001 UV spectrophotometer. FTIR spectra were recorded in a Nicolet (Impact 410, Madison, WI) FTIR spectrophotometer by using KBr pellets. The X-ray diffractogram was recorded in 'Miniflex', (Rigaku Corporation Japan) X-ray diffractometer at room temperature (ca. 23 ^{0}C). A scanning rate of 5.0^{0} min^{-1} over the range of 2θ = 10-70 ^{0} was used. Hysteresis loop tracer (model HLT-III, Seshtechno) was used to study the magnetic behavior before

and after enzyme immobilization onto the PEG-IONPs. Size and distribution of the nanoparticles were studied using JEOL, JEMCXII transmission electron microscope (TEM) at an operating voltage of 80 kV.

Table2A.1. *Observed and predicted values of response {keratinase specific activity (Units/mg protein)}*

Temperature (C_1)	*pH of reaction mixture (C_2)*	*Polymer to iron ratio (C_3)*	*Observed Response*	*Predicted Response*
-1	-1	-1	109.830	107.505
-1	-1	0	116.670	119.053
-1	-1	1	115.860	114.156
-1	0	-1	107.960	108.374
-1	0	0	116.630	119.920
-1	0	1	114.000	115.023
-1	1	-1	106.080	104.638
-1	1	0	117.560	116.184
-1	1	1	112.030	111.286
0	-1	-1	111.400	111.948
0	-1	0	127.679	129.893
0	-1	1	118.598	118.598
0	0	-1	109.540	112.666
0	0	1	121.110	119.314
0	1	-1	107.570	108.780
0	1	0	117.230	120.325
0	1	1	113.600	115.426
1	-1	-1	110.670	109.187
1	-1	0	119.200	120.733
1	-1	1	116.700	115.835
1	0	-1	108.800	109.754
1	0	0	120.360	121.299
1	0	1	114.830	116.400
1	1	-1	106.800	105.717
1	1	0	118.360	117.261

Table continued on the next page

1	1	1	109.890	112.361
0	0	0	124.454	124.212
0	0	0	123.345	124.212
0	0	0	125.234	124.212
0	0	0	125.232	124.212
0	0	0	124.453	124.212

2A.2.7. *Thermostability, storage stability and reusability of loaded enzyme*

Thermal stabilities of free and bound keratinase were checked by measuring their residual activities post 30 min incubation in the temperature range of 35-85 ^{0}C. Thermal stability of free and bound keratinase was also examined by assaying their residual activities post incubation at 45 ^{0}C (determined as optimum for the free enzyme) for the required period. Activities of free and bound keratinase were determined post storage at 4 ^{0}C or 25 ^{0}C. The measurements were performed at intervals of 4 days within a period of 24 days. The reusability of bound keratinase was examined by conducting the activity measurement at 25 ^{0}C. After each activity measurement, the bound keratinase was separated magnetically and washed several times followed by activity measurement.

2A.2.8. *Depilatory action*

The de-hairing action of the free and the immobilized enzyme was tested as described previously[15] with slight modifications. Briefly, goat skin was procured from the local butcher and washed several times to remove the blood stain and other materials adsorbed onto it. It was then cut into 5×5 cm^2 pieces with a sterilized blade and placed onto three petridishes. 15 mL of distilled water (negative control), free enzyme (positive control) and immobilized enzyme (test sample) were poured into the petridishes and incubated at 45 ^{0}C. The keratinase-PEG-IONPs were recovered after 12 h of incubation using a magnetic field and were washed and stored at 4 ^{0}C for further use. The skin was washed with water and the depilatory action of the free and the immobilized enzyme system was checked. The activity of the recycled enzyme was checked post dehairing.

2A.3. Results and discussion

2A.3.1. *Optimization of the process parameters*

The first objective was to optimize the reaction parameters for preparation of PEG-IONPs with the aim of increasing the enzyme activity loaded onto the system. As can be seen in Fig.2A.1a, the system prepared at 25 ^{0}C supported the maximal activity of the enzyme immobilized onto it. Only 83.8% of the enzyme activity was recorded for the system synthesized in ice-cold condition as compared to that at 25 ^{0}C. The plausible reason may be the attainment of the activation energy at 25 ^{0}C for the reactants and the polymer to interact and coalesce optimally for the formation and uniform dispersion of the MNP, assisted by magnetic stirring and sonication at later stages. It was interesting to note the standing/dispersion stability of the system in water decreased with decrease in temperature of the reaction system.

As far as the pH is concerned, a gradual decrease in the activity of the immobilized enzyme (Fig.2A.1b) was recorded corresponding to the increase in the pH of the reaction mixture before addition of H_2O_2. Increase in alkalinity in the reaction system up to pH 11.2 resulted in decrease of activity by 13.93% of the immobilized enzyme as obtained under the system with pH of 7.2. A negative effect on the stabilization of the MNP was observed with the increase of pH of the medium as supported by the increase of λ_{max} value in UV-spectra. This may be due to the decrease in the steric stabilization, conferred upon by the polymer at lower pH while the electrostatic stabilization attributed to the negative hydroxyl group (base) becomes pre-dominant with increase in pH.

Settling as agglomerate under the action of gravity was a major challenge during the preparation process. The instability of the system was observed with increase in PEG content. Furthermore, the enzyme activity was maximal for the system with 2% (w/v) PEG content and least for 10% (w/v) (Fig.2A.1c). The increase in the concentration of PEG implies an increase in the viscosity of the reaction medium and as such a greater hindrance to the uniform dispersion of the iron oxide nanoparticles and consequently an impediment to the enzyme immobilization.

With this value of polymer content as optimum to support IONPs' preparation, variation of polymer to iron ratio showed that immobilized enzyme onto the system with 0.062:1 molar ratio of PEG to $FeCl_2.4H_2O$ resulted in the highest enzyme activity (Fig.2A.1d). This may be attributed to the optimum stabilization of the IONPs by the polymer. Maximum keratinase specific activity (U/mg) was obtained with the data set of pH 7.2, reaction mixture temperature of 25 ^{0}C, and PEG: iron molar ratio of 0.062:1. The

parameters of equation (2.A.1) were determined by multiple regression analysis. The overall second-order polynomial equation for keratinase activity is represented as

$$Y = 124.212 + 0.689C_1 - 1.585C_1^2 + 3.324C_2 - 3.602C_2^2 - 2.302C_3 - 8.222C_3^2 - 0.151C_1*C_2 - 0.001C_1*C_3 - 0.001C_2*C_3 \quad \text{.....(2A.2)}$$

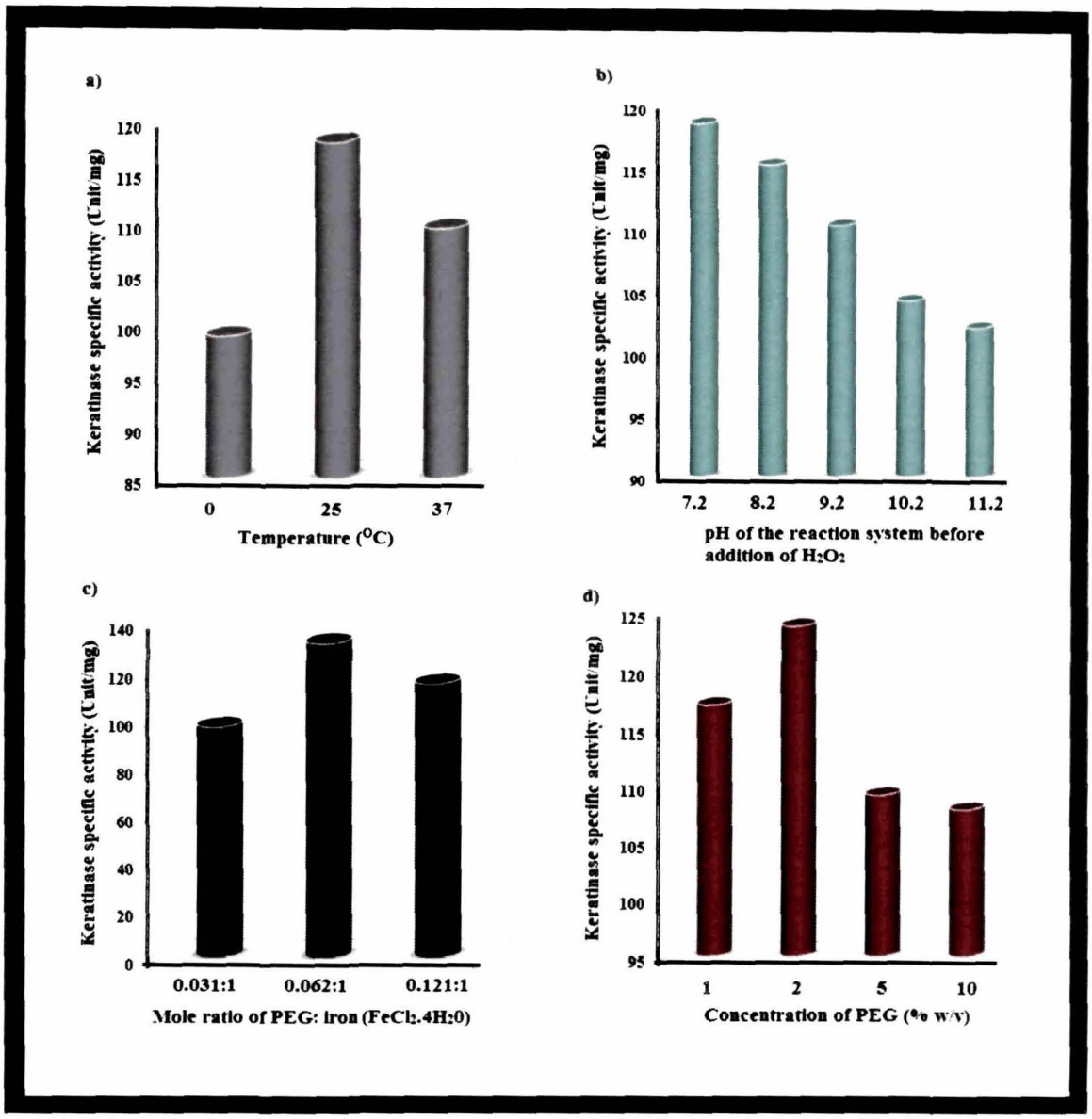

Fig.2A.1. *Effect of a) temperature, b)pH of the reaction system before addition of H_2O_2, c) mole ratio of PEG: iron ($FeCl_2$:$4H_2O$) and d) concentration of PEG (% w/v) on the specific activity of the immobilized enzyme*

All the three variables (temperature, pH of the reaction system before addition of H_2O_2, and polymer to iron mole ratio) chosen had quadratic effect on the activity of the immobilized enzyme (Fig.2A.2). The model contained a three two-way interactions (pH*temperature, pH*PEG: iron molar ratio, and temperature*PEG: iron molar ratio). For each of these interactions, p-value was more than 0.05 (chosen α value) (Table

2A.2). That is, these cross-interactions were found not to have a significant effect on the enzyme activity.

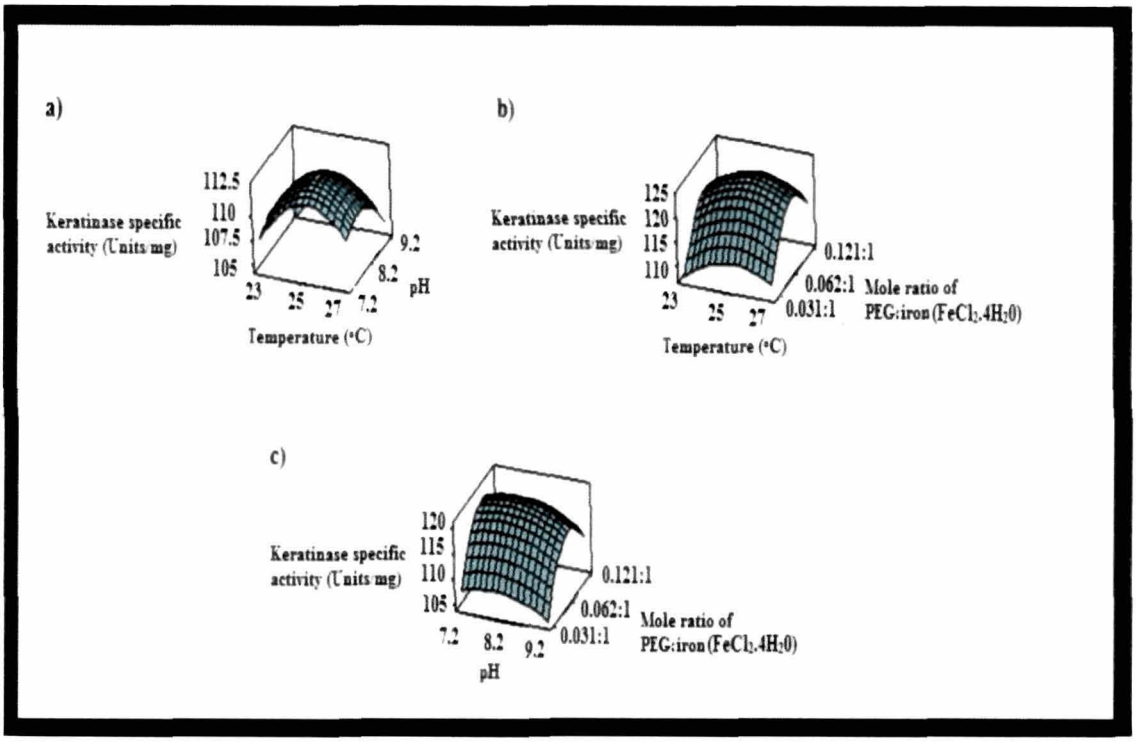

Fig.2A.2. *Response surface plots showing keratinase-specific activity versus a) temperature versus pH, b) temperature versus PEG:iron molar ratio and c) pH versus PEG:iron molar ratio*

The immobilized enzyme onto the optimized system showed almost four fold enhancement in activity compared to the free enzyme. Free enzyme showed a specific activity of 37 units/mg while the immobilized enzyme recorded a specific activity of 128.97 units/mg. Keratinase activity estimation in the post-precipitate supernatant revealed that the binding of the enzyme to the PEG-IONPs was about 91% for the optimized system.

Response surface methodology and the experimental design that was applied, given the limits imposed by the nature of the experiment, revealed themselves to be efficient in the determination of the optimal conditions for the preparation of PEG-IONPs s. As the optimum had been located, the experimental domain and the spacing of levels were adequately chosen. The choice of a second order polynomial regression model was also satisfactory, and the estimation of coefficients by multiple linear regressions was a priori much more explanatory than that obtained by any classical analysis of variance.

Table2A.2. *Model coefficients estimated by multiple regressions (model adequacy checking)*

Factor	*Coefficient*	*t-value*	*p-value*
Constant	124.212	162.969	0.000<0.05
C_1	0.689	1.369	0.008<0.05
C_2	-1.585	-3.148	0.005<0.05
C_3	3.324	6.601	0.000<0.05
C_1*C_1	-3.602	-4.467	0.000<0.05
C_2*C_2	-2.302	-2.855	0.009<0.05
C_3*C_3	-8.222	-10.197	0.000<0.05
C_1*C_2	-0.151	-0.245	0.809>0.05
C_1*C_3	-0.001	-0.001	0.999>0.05
C_2*C_3	-0.001	-0.001	0.999>0.05

2A.3.2 *Physico-chemical characterization of PEG-IONPs before and after keratinase immobilization*

The UV-visible absorption spectroscopy was employed to characterize the PEG-IONPs (Fig.2A.3).

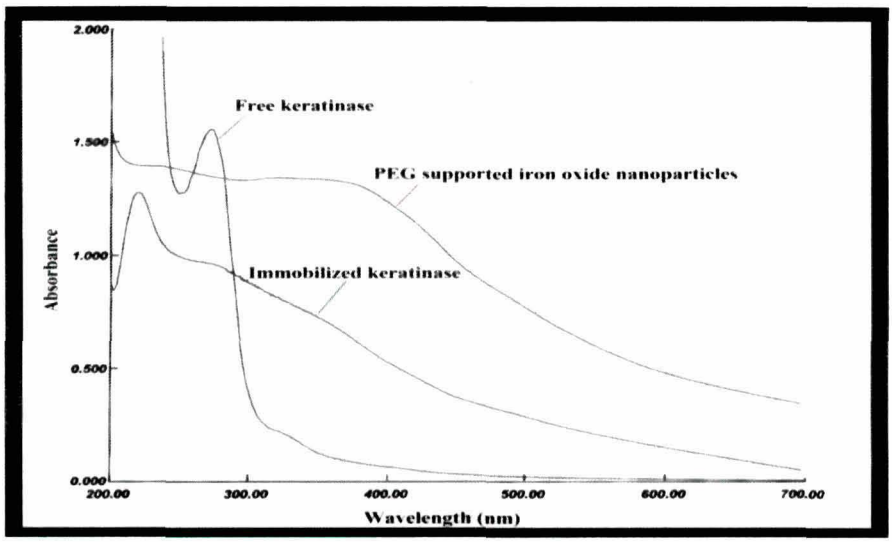

Fig.2A.3. *UV-visible spectra for PEG-IONPs, free and immobilized enzyme.*

A broad and featureless absorption band seen at ~330-390 nm originated primarily from the absorption and scattering of light by the IONPs while the enzyme showed typical UV absorption peak at about 280 nm. It was interesting to note that the enzyme immobilization onto the polymer-assisted iron oxide nanoparticles led to shifting of both these peaks from lower energy level to higher energy level. This was

indicative of PEG-assisted metal-oxide–enzyme interaction with plausible structural modulation of the enzyme upon immobilization.

FTIR imaging revealed that upon immobilization of enzyme on the PEG-assisted IONPs, there was broadening of the band at 3430 cm^{-1} compared to PEG-IONPs. This was indicative of hydrogen bonding between the $-NH_2$ group of enzyme with the hydroxyl group of PEG. In addition to the above, the band for the carbonyl group of the free enzyme at 1637 cm^{-1} split to two at 1629 and 1638 cm^{-1} which corresponded to the free and hydrogen bonded carbonyl for the immobilized enzyme. The above observations of UV and FTIR spectroscopic analyses indicated possible PEGylation of the enzyme.

A characteristic peak was obtained for the polymer at $2\theta=28.56^0$. The reflection planes were consistent with the standard pattern for Fe_3O_4 (Fig. 2A.4).[16] The average crystallite size was determined by Scherrer's equation:

$$D= K\alpha/\{\beta \cos \theta\} \quad \text{.....(2A.3)}$$

where D is the crystalline domain size, K (Scherrer constant)=0.9 in this case, α = 1.574 $\times 10^{-10}$ m is the wavelength of the X-ray, β is the line broadening at half the maximum intensity (FWHM) in radians and θ is the diffraction angle.

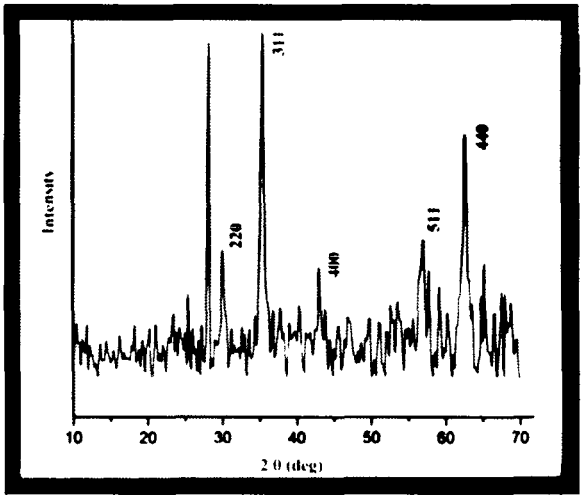

Fig.2A.4. *X-ray diffractogram of the PEG-IONPs.*

The crystalline average domain size for the PEG-IONPs without and with enzyme was found to be 9.57 nm and 14.56 nm respectively. This may be suggestive of the fact that the enzyme immobilization was a surface phenomenon. These results tallied with that of the TEM image. The average particle size was 12.56 nm with particle-size window extending between 5 nm to 17 nm. It was also interesting to note that the highest fraction of particles had a diameter of 12.5 nm (Fig.2A.5).

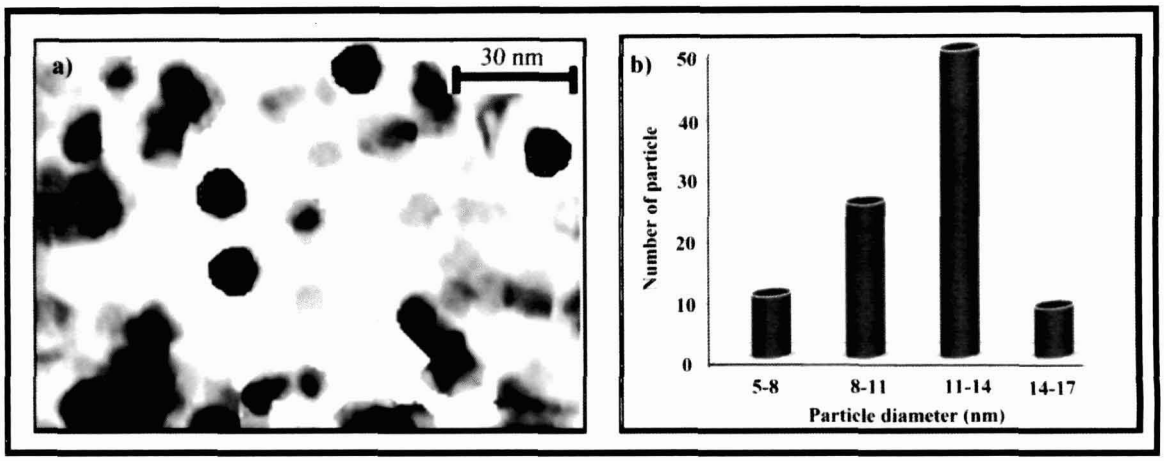

Fig.2A.5. *a) TEM micrograph and b) histogram showing the size distribution of keratinase-PEG-IONPs*

The magnetic behaviour of the prepared system was demonstrated by their physical attraction towards a magnetic bead. Hysteresis loop tracer (Model HLT-III, Sestechno) was used to study the magnetic behaviour before and after enzyme immobilization onto PEG-IONPs. The magnetization value at the applied low field (178 G) remained the same for the system with and without enzyme immobilization (Fig. 2.A.6). The hysteresis loop did not show saturation up to this field indicating that the specimen could withstand to relatively larger field strength.

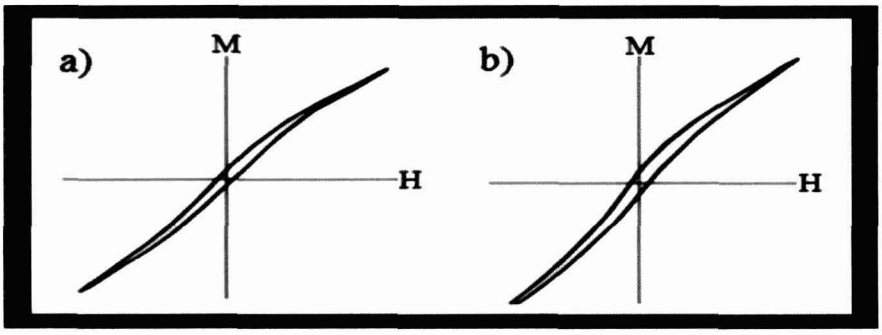

Fig.2A.6. *Low Field hysteresis (178 G) loop (M in emu/g and H in G) of PEG-IONPs a) before and b) after keratinase immobilization.*

The coercivity values (H_c) for both the samples *i.e.*, the bare and the enzyme coupled nanoparticles, were 9.28 G and 9.7 G respectively. One can calculate low field magnetic susceptibility from the linear regimes of the hysteresis plot around zero field. In the present case, χ was estimated as 0.367 for both the samples *i.e.*, iron oxide with and without enzyme. Similarly, the retentivity, (μ_r=339.5 emu/g) as calculated was found to be same for both the samples. The above results indicated that the quality of the polymer-supported magnetic nanoparticles was retained post biocatalyst loading. The binding of magnetic particles to bioactive substances involves a number of

interactions including the interactions between organic ligand, and the interactions between the amino acid side chains of proteins and the metal centre. Such bindings pave the way for the coupling of bio-molecular entities for enhancing the latter's stability.

2A.3.3. *Effect on the immobilized biocatalyst*

As mentioned previously, the immobilization had led to a quadruple increment in the enzyme activity. This may be primarily attributed to better substrate-enzyme interaction upon immobilization with availability of higher surface area on the IONPs and possible structural modulation or better exposure of the active site. This, however, needs molecular probing for a deeper insight. Nevertheless, it was interesting to probe into the additional advantages arising from the immobilization process. A range of biocatalysts used in organic synthesis has been made soluble in non-aqueous solvents and stabilized against denaturation therein through surface attachment of PEG molecules.[17-19] In order to judge and assess the protection (if any) conferred by PEG-assisted MNP to the immobilized keratinase, three criteria were chosen - thermo-stability, storage stability and recyclability.

After predetermined thermal inactivation, the residual activities were determined to check the thermo-stability of immobilized enzyme and free enzyme. As shown in Fig.2A.7a, the enzyme activity of the unbound keratinase declined to almost 54.66% when incubation temperature was raised to 85 ^{0}C. However, the bound keratinase still had a residual activity of 89% at 85 ^{0}C. Interestingly, the immobilized enzyme showed an activity of about 95.5% after an incubation period of 4 h at 45 ^{0}C while it was only 80% for the free enzyme. This excellent thermostability may be attributed to the protection conferred by the polymer. Literature shows that several enzymes display substantially enhanced thermostability post PEGylation.[20-22] It has been assessed that the surface hydrophobic character of biocatalysts is stressed on binding of PEG. This leads to a considerable improvement of enzyme thermal stability. The creation of a hydrophobic shield prevents the destabilising interactions between hydrophobic clusters of the enzyme and surrounding water to occur. [23]

Knowledge about storage stability of an enzyme is prerequisite to judge its industrial applicability. As depicted in Fig.2A.7b, a rapid decline was observed in the activity of free keratinase just after 8 days of storage at 25 ^{0}C, while free enzyme stored at 4 ^{0}C retained 56% of its activity post 24 days storage. In contrast, the immobilization

led to a considerable retention of initial activity of both the systems stored at 4 ^{0}C and 25 ^{0}C respectively analyzed for a 24-day storage period.

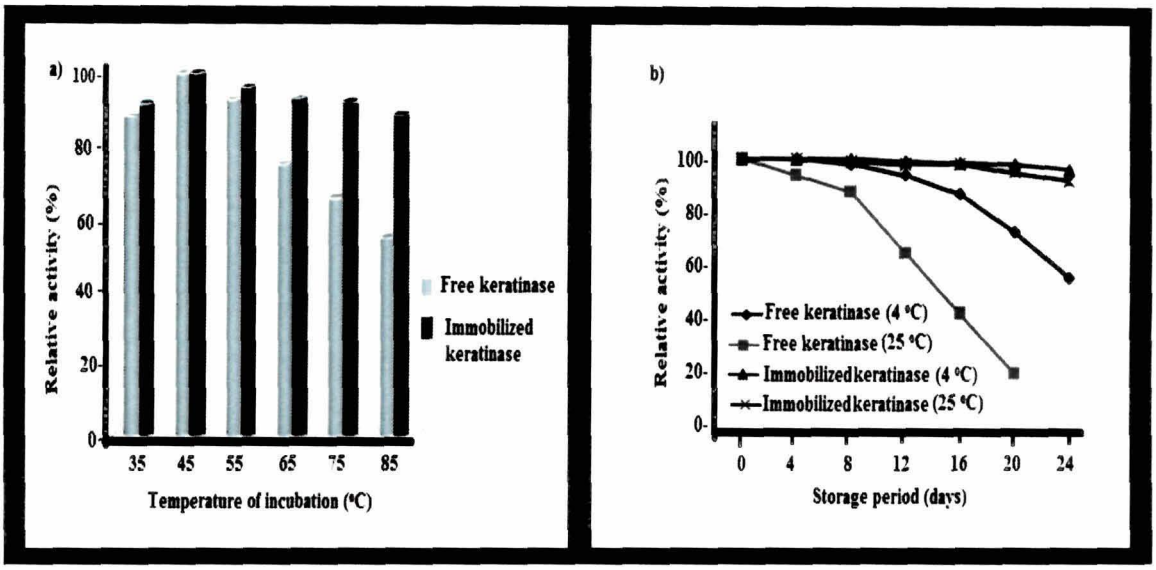

Fig.2A.7. *a) Thermostability and b) storage stability of the free and immobilized keratinase*

The experiment revealed that storage stability of the bound keratinase was improved in comparison to free keratinase. The covalent immobilization definitely held the enzyme in a stable position in comparison to the free counterpart. The immobilization is believed to have minimized possible distortion effects imposed from aqueous medium on the active site of the immobilized enzyme. It's interesting to note that lysine and cysteines are amongst the most reported targets for PEGylation.[24, 25] The involvement of surface exposed cysteines in oxidative protein denaturation processes, as shown in several cases of biocatalysts[26-28] makes these residues very interesting targets for protein stabilization via PEGylation. This may be due to the formation of complex through the hydroxyl group of PEG with the amino or the carboxylic group of the enzymes.

Reusability of immobilized enzymes is an important consideration for their practical application. As shown in Fig.2A.8, no significant loss in the activity of bound keratinase was recorded after being reused for five times. This was indicative of structural stabilization of the enzyme in the system by the polymer and thereby minimizing the possibilities of leaching of the bio-catalyst. This feature of excellent reusability holds tremendous promise in the domain of enzyme biotechnology. Chemical tailoring of proteins with synthetic macromolecules such as poly(ethylene glycol) (PEG) has attracted substantial interest in various niches of biotechnology.[23, 24,

[29] These also provide a promising route towards novel biomaterials.[30] These features get well reverberated in the reported system.

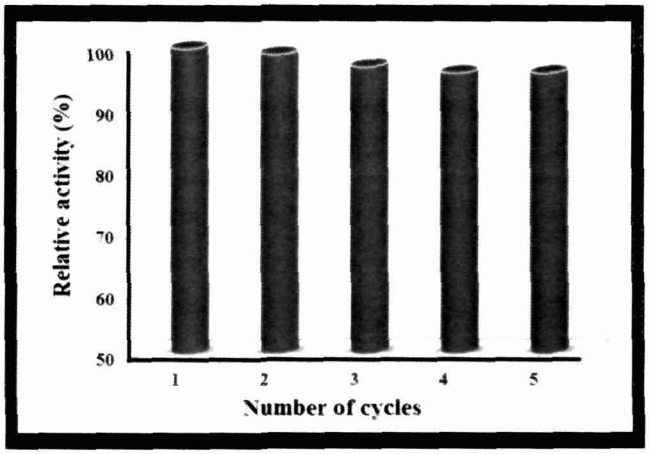

Fig.2A.8. *Recyclability efficiency plot*

Thus, the various characterization tools had elucidated the successful immobilization of the enzyme onto the PEG-IONPs. The response surface methodology was instrumental in optimizing the process parameters. The results also vouched for the fact that use of covalent immobilization along with statistical optimization can be instrumental in designing strategies to minimize the loss of enzyme by desorption (percentage of enzyme binding was found to be 91% onto the PEG-IONPs), a crucial factor to be addressed for cost-efficiency in industries.

2A.3.4. *Prospective application in leather industry*

Leather processing technology involves a series of operations, amongst which pre-tanning contributes to the major amount of pollution (approximately 70%). Sodium sulfide, lime and solid wastes generated as a result of pre-tanning are mainly responsible for increased biochemical oxygen demand (BOD), chemical oxygen demand (COD) and total dissolved solids (TDS).[31] The demand of the hour is to promote biocatalytic leather processing. This is in accordance to the dictates of green chemistry that calls for minimization of waste-generation, shunning the use of toxic chemicals and supporting the use of biocatalysts among other things. Keratinolytic proteases lacking collagenolytic and having mild elastolytic activities are increasingly being explored for the depilating process. They cause selective breakdown of keratin tissue in the follicle, thereby pulling out intact hairs without affecting the tensile strength of leather.[31] In order to assess the commercial applicability of the immobilized enzyme-system, the de-hairing of goat-skin was tested. As shown in the Fig.2A.9, the immobilized enzyme led to selective de-hairing without damaging the tissue underneath. The image also shows that

the keratinase bound to PEG-IONPs has a couple of advantages over the free enzyme. Firstly, a much cleaner saving of the goat-skin was achieved using the immobilized enzyme as compared to the free counterpart in the context of 12 h incubation-time period.

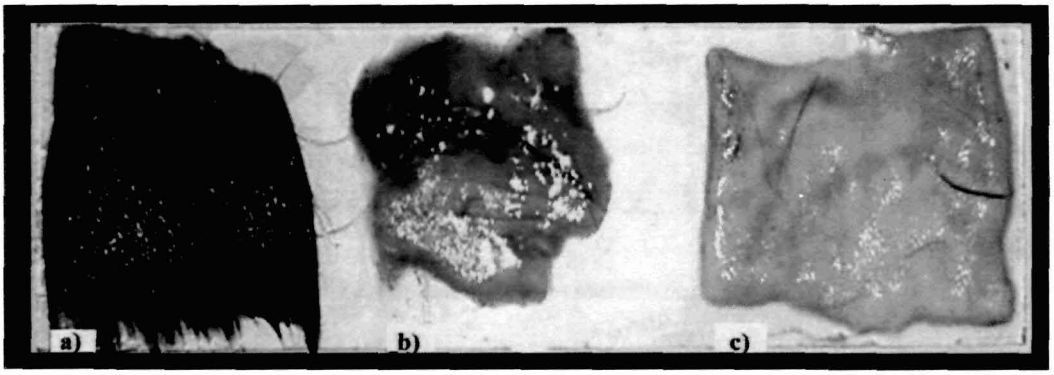

Fig.2A.9. *Dehairing test: a) distilled water treated goat-skin (negative control), b) free enzyme treated (positive control) and c) immobilized enzyme treated (test sample)*

This was also indicative of enhancement of the enzyme action upon immobilization. The activity of the recyled enzyme was measured after dehairing. The relative activity was found to be about 98.5%, taking 100% activity for the immobilized enzyme before dehairing. Furthermore, the magnetic susceptibility of the immobilized system facilitated the recovery of the enzyme and thereby, paving its way for reusability. The prospects of applying the system on the commercial scale are bright as because the removed hair of the leather factories may be siphoned as raw material into other industries involved in production of films, glues and compostable packaging materials from keratinous wastes.[32] Thus, the reported polymer-assisted iron oxide immobilized keratinase could serve as a multifaceted, environmentally clean hair-saving technology.

2A.4. Conclusion

Enhancement of catalytic efficacy of keratinase, an industrially important enzyme by immobilizing onto polymer supported nanomaterial, with concomitant improvement in thermostability, storage stability and recyclability opens up avenues to a panorama of biotechnological applications. The leather-industry-oriented utility of the immobilized enzyme was successfully tested for the de-hairing of animal-skin. Establishment of the biocompatibility of the present system is prerequisite prior to exploration of plausible pharmaceutical application.

2B. AMYLOGLUCOSIDASE IMMOBILIZED ONTO PEG-SILVER-IONPs

2B.1. Introduction

Amyloglucosidase (AMG) (1, 4-α-D glucan glucanohydrolase, EC 3.2.1.3.) is an industrially important biocatalyst.[33] It is a multi-domain, exo-acting enzyme that catalyses the hydrolysis of starch and related substrates from the non-reducing ends mainly by cleaving α-1,4-glycosidic linkages and a few α-1,6 linkages, but at a very slow pace.[34] Immobilization on to polyaniline polymer,[35] mesoporous and hydrophilic novel bead carriers containing epoxy groups,[36] chemical ligation onto carbon nanotubes[37] etc., are some of the recently reported immobilization studies on AMG. The nature of the carrier and degree of purity of the enzyme dictate the binding efficiency and properties of immobilized AMG. Amount of enzyme lost from the immobilization systems, diffusion limitations and the net increment in the enzyme activity are critical issues in these immobilization protocols.[36] Immobilization onto a polymeric nanocomposite platform, endowed with multiple attributes like antimicrobial potency and magnetic recyclability can further facilitate the value addition of this commercial enzyme.

As noted in subchapter 2A, coupling onto polymer assisted iron oxide nanoparticles seems to be an attractive avenue to improve performance of biocatalysts addressing industrial sustainability requirements like magnetic recyclability and thermostability along with activity augmentation. On the other hand, with myriad of synthesis protocols[38] and numerous applications,[39] silver nanoparticles have carved a unique niche of their own in the domain of nanobiotechnology. The anti-microbial action[40] of silver nanoparticles justifies their inclusion in a wide variety of products. Silver nanoparticles based systems are gaining special significance in the context of the emerging concept of 'green technology'.[40] The present work reports the tapping of a bio-resource namely *Mesua ferrea* L. (locally known as 'Nahar' in North-East India) leaf aqueous extract for the preparation of nanoparticles of this noble metal. The extract from the various parts of this plant are traditionally known to have a variety of medical uses. Several *in vivo* studies have validated these ethnopharmaceutical practices.[41]

In this subchapter, the immobilization of AMG onto poly(ethylene glycol) (PEG) supported silver-iron oxide nanoparticles (PEG-Ag-IONPs) has been documented. This

was an attempt to combine the innate advantages of polymeric nanocomposite, an advanced class of material with the catalytic potential of an industrial enzyme. The study has been focused on enzyme activity enhancement and assessment of its magnetic recyclability, stability, anti-microbial potency and the prospects for inclusion in detergent formulation and starch saccharification.

2B.2. Experimental

2B.2.1. *Materials used for the preparation of the immobilization platform*

The materials used for the preparation of PEG-IONPs have already been illustrated in section 2A.2.1. A wet chemical reduction of silver nitrate ($AgNO_3$, Qualigens®) was used for the generation of the silver nanoparticles. Silver nitrate (that occurs as acanthite in nature) is used in photography, manufacture of mirrors, silver plating and preparation of indelible inks.[42] Furthermore; it is often exploited for the staining of proteins, nucleic acids and glycoconjugates in gels.[42] It is used as a source of silver ions in various toxicological studies. On the other hand, *Mesua ferrea* L. leaves were collected from the Tezpur University campus in the month of September 2010. Various components of the leaf extract like friedelin and triterpenes of the friedelin group, namely canophyllal, canophyllol and canophyllic acid[41] could be envisaged as the active components responsible for the generation of the silver nanoparticles. Sonication mediated mixing of these two classes of nanoparticles was used for the generation of the immobilization platform *i.e.*, PEG-Ag-IONPs. However, it is pertinent to mention that cyanamide was not used for the functionalization of the nanoparticles in this study. Sonication (a green chemistry tool) was exploited for the adsorption of the biocatalyst *i.e.*, amyloglucosidase onto the PEG-Ag-IONPs.

2B.2.2. *Preparation of PEG-Ag-IONPs for AMG immobilization*

PEG-IONPs were prepared as described previously in section 2A.2.2 with a minor variation. Instead of mechanical stirring, a sonication step (2 min, 60% amplitude and 0.5 cycle) was introduced for mixing the iron chloride and PEG solution. Other steps remained essentially the same.

For the preparation of the silver nanoparticles, about 20 matured *M. ferrea* L. leaves were washed with water. Aqueous extract of the crushed leaves, prepared in about 50 mL of water was filtered through a muslin cloth. 200 μL of 0.1 M $AgNO_3$ was

taken in 7.5 mL of 5% (w/v) PEG solution, prepared in Millipore water and 6 mL of the *M. ferrea* leaf extract was added as the reducing agent. The pH of the reaction mixture was adjusted to 11.5. The nanoparticles, well distributed within a narrow size range (1-12 nm, with average diameter of 5 nm), were obtained under statistically optimized sonication parameters of 3 min, 60% amplitude and 0.5 cycle by using RSM (where the response was either red or blue shift in the λ_{max} position in UV-visible spectrum, taken as the indicator of the size of silver nanoparticles). Equal volume (250 µL) suspensions of the silver and iron oxide nanoparticles were taken in an eppendorf tube for sonication for 3 min at 60% amplitude and 0.5 cycles. The polymer assisted nanosystem before and after enzyme immobilization was analysed using different characterization tools as described in subsequent section.

2B.2.3. *Immobilization of amyloglucosidase (AMG)*

For immobilization, 0.5 mL of *Aspergillus niger* amyloglucosidase (Fluka, Sigma) (1 mg mL^{-1}) in acetate buffer (0.05 M, pH 4.5) was added to 50 mg of PEG-Ag-IONPs followed by sonication for 15 min at 4 ^{0}C (ice-bath). This was followed by centrifugation at 3000 rpm for 10 min after which the mass was magnetically decanted. The post-precipitate supernatant was collected in fresh microfuge tube while the precipitate was washed twice and finally suspended in 0.5 mL of acetate buffer (0.05 M, pH 4.5). The percentage binding was estimated by determining the amyloglucosidase activity for both the post-precipitate supernatant and the immobilized enzyme fraction.

2B.2.4. *Enzyme activity determination*

3, 5-dinitrosalicylic acid reagent (DNSA) was used for determination of the AMG activity.[43] Starch was used as the substrate. One unit of AMG activity was defined as the amount of enzyme required to produce 1 µM of glucose in 5 min at 25 ^{0}C. Protein concentration was determined by Lowry's method[13] with bovine serum albumin (BSA) as a standard. The specific activity of the immobilized enzyme was defined as the number of µM of glucose which were liberated in one minute by one gram of the immobilizate at its optimum temperature.

2B.2.5. *Physico-chemical characterization*

UV-visible spectra were analyzed in Hitachi (Tokyo, Japan) U2001 UV spectrophotometer. Fourier Transform Infrared Spectroscopy (FTIR) spectra were

recorded in a Nicolet (Impact 410, Madison, WI) FTIR spectrophotometer by using KBr pellets. Lakeshore Vibrating Sample Magnetometer (VSM) (Model 668) was used to study the magnetic behaviour of the samples. Size and distribution of polymer assisted nanoparticles were studied in transmission electron microscope (TEM) (JEOL, JEMCXII, Japan) at operating voltage of 100 kV.

2B.2.6. *Determination of optimum temperature, pH, K_m and V_{max} of the immobilized AMG*

The effect of temperature on the enzyme activity of the free and immobilized samples was studied in the temperature range from 30 ^{o}C to 85 ^{o}C with 1% (w/v) soluble starch in acetate buffer (50 mM pH 4.5). The effect of pH on the enzyme activity was determined with 1% (w/v) soluble starch in 50 mM sodium citrate-phosphate buffer of an appropriate pH at 25 ^{o}C. The Michaelis constant, K_m and maximal rate, V_{max} were determined by measuring the initial production rate from 0.1-4% (w/v) soluble starch in 50 mM acetate buffer at respective pH and temperature optima of the free and immobilized AMG.

2B.2.7. *Determination of thermostability and reusability*

Thermal stability of the free and bound AMG was checked by measuring their residual activities post incubation for 15 min in the temperature range of 30-85 ^{o}C. Residual activity of the free and the coupled enzyme was also assayed after incubating at their respective optimum temperature for about 4 h. Activities of free and bound AMG were determined post storage at 4 ^{o}C or 25 ^{o}C. The measurements were performed at intervals of 5 days within a period of 30 days. The reusability of the bound AMG was assessed by evaluating the activity at the optimum temperature post repeated magnetic separation and washing with phosphate buffer.

2B.2.8. *Starch saccharification*

Saccharification of 20% (w/v) soluble starch prepared in 0.1 M phosphate buffer was studied at the respective optimum temperature for the free and the immobilized AMG for 24-48 h. Reducing sugars in the starch hydrolysate were estimated by DNSA reagent.[43] The percent starch saccharification was calculated according to previously reported protocol. [44]

2B.2.9. *Determination of potency for detergent formulation inclusion*

For the starch de-staining test (washing performance), cotton cloth pieces (size: 4.5×4.5 cm^2) were stained with 0.2 mL of aqueous starch solution. The stock solutions of four commercially available detergents, namely Surf Excel Blue (Hindustan Unilever Ltd.), Active Wheel Gold (Hindustan Unilever Ltd.), Ariel OxyBlue (Procter and Gamble), and Tide (Procter and Gamble) were prepared in distilled water (2.0 gL^{-1}). Two stained cloth pieces were taken for each detergent. One piece was washed with detergent alone, while another piece was washed with detergent in the presence of immobilized AMG at the optimum temperature for 20 min with continuous stirring. Similarly, one stained piece was washed with distilled water and immobilized AMG. Each washed cloth piece was manually rinsed twice with distilled water. The washing performance in each case was determined according to a method reported previously by Dhingra et al.[45] Minimum amount of starch content indicated effective washing.

2B.2.10. *Determination of anti-microbial potency*

The antimicrobial potency of the PEG-Ag-IONPs with and without AMG was tested against a panel of microorganisms including *Staphylococcus aureus* MTCC96, *Bacillus subtilis* MTCC736, *Pseudomonas aeruginosa* PN1. The antibacterial tests were performed as described elsewhere[46] using agar-well diffusion method after some modification. All the microorganisms mentioned above were incubated (37 ^{0}C, 24 h) by inoculation into Mueller Hinton broth.[47] The Mc Farland 0.5 standard[48] was used as turbidity standard for the preparation of the culture suspensions. Mueller Hinton Agar (20 mL) was poured into each sterilized Petri dish (10 mm x 90 mm) followed by inoculation with 100 µl of bacterial cultures. To test the antibacterial potency, the samples were filter sterilized through a 0.22 µm membrane filter. The spherical silver nanoparticles, PEG-Ag-IONPs and AMG immobilized polymer supported nanoparticles at various concentrations were introduced directly into the wells (6 mm) in agar plates. The plates were incubated at 37 ^{0}C for 24 h. At the end of the incubation period, minimum inhibitory concentration (MIC) for the respective samples was determined. The experiments were performed in triplicates with ampicillin (50 µg) as positive control.

2B.3. Results and discussions

2B.3.1. *Preparation and characterization of the polymer assisted nanosystem with and without AMG*

The strategy adopted to prepare the immobilization system is presented in Fig. 2B.1. The 'green' method of preparing silver nanoparticles generated spherical particles within a distribution range of 1-12 nm and average diameter of 5 nm (Fig.2B.1a).

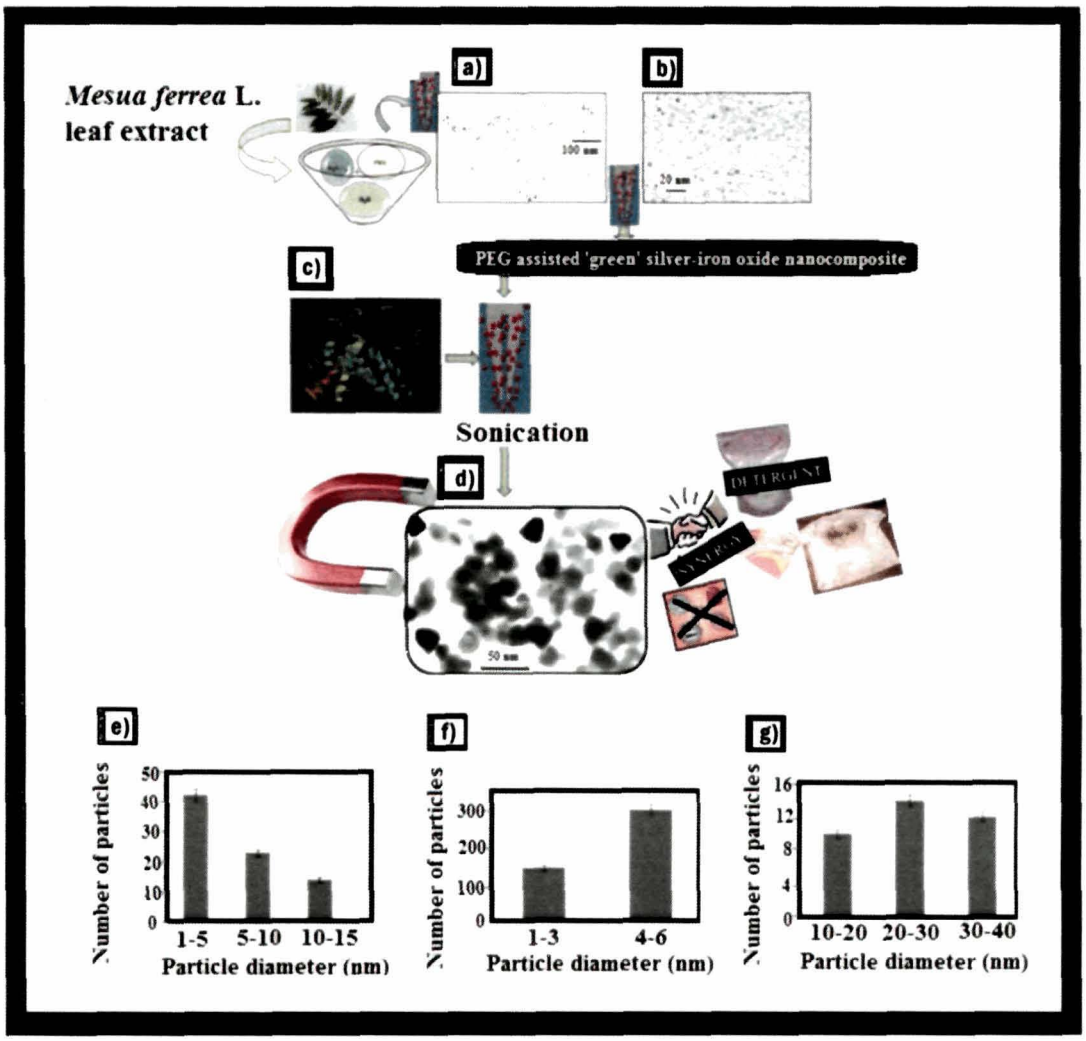

Fig.2B.1. *Sonication mediated strategy for immobilization of AMG a) TEM micrograph of the spherical silver nanoparticles, b) TEM micrograph of the PEG assisted iron oxide magnetic nanoparticles, c) structure of amyloglucosidase, d) TEM micrograph of the AMG immobilized system with illustrations of its multiple attributes. Histogram showing the particle size distribution of e) silver nanoparticles, f) PEG assisted iron oxide magnetic nanoparticles and g) AMG conjugated PEG assisted nanoparticles*

In the present protocol for generation of iron oxide nanoparticles, the step involving sonication had a profound effect as can be seen from the dense population of particles in the range of 2-5 nm (Fig.2B.1b). This was in sharp contrast to the size range

of the nanoparticles (5-17 nm) which were obtained earlier (subchapter 2A). Now when the two sets of nanoparticles were subjected to sonication for immobilization of the enzyme (Fig.2B.1c), the nanoparticles obtained were of greater shape-size diversity (Fig.2B.1d) with maximal particles of triangular shape (20-30 nm), a critical factor to decide the anti-microbial potency. The magnetic property, anti-microbial property and the synergy of the immobilised system with commercial detergents is graphically represented in Fig.2B.1d. The results of the particle size distribution from TEM analysis is presented in the histograms (Fig.2B.1e-g).

The characteristic surface Plasmon resonance peak at around 400 nm for the spherical silver nanoparticles alone shifted to higher wavelength with a broad featureless absorption band at around 330-450 nm when IONPs nanoparticles were present in the system (Fig.2B.2).

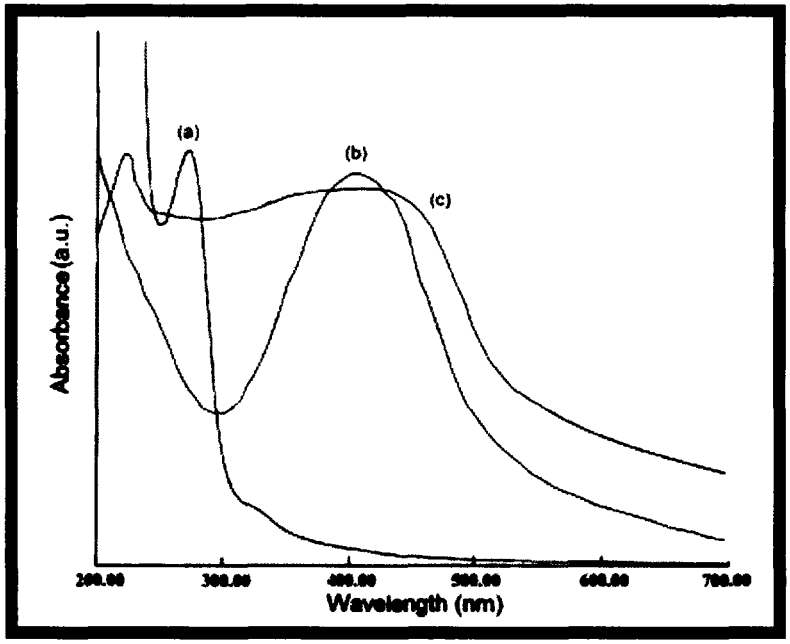

Fig.2B.2. *UV-visible spectra of a) AMG in free state, b) silver nanoparticles with characteristic surface Plasmon peak at around 400 nm and c) AMG conjugated PEG assisted nanoparticles*

The characteristic UV peak for the free enzyme shifted from 280 nm to about 230 nm upon immobilization. Thus, the UV-visible spectroscopic analysis gave the first indication of enzyme immobilization onto the polymer-assisted nanosystem as evident from the shifting of the silver surface Plasmon peak and enzyme's peak from the lower energy levels to higher energy levels. The shifts in the UV-visible spectra peak position of the enzyme and the silver nanoparticles indicated the PEG-assisted metal-metal-oxide-enzyme interaction. The broadening of the silver surface resonance peak was also

indicative of larger and greater particle shape diversity of the nanoparticles in the immobilization system. Interaction of the *M. ferrea* extract and poly(ethylene glycol) together with the influence of sonication might be responsible for the diversity in the shape and size of the nanoparticles in the immobilization system.

In the FTIR spectra, there was a broadening of the band at 3470 cm^{-1} upon immobilization of the enzyme onto the PEG-assisted silver-iron oxide nanoparticles, compared to the system without enzyme. This was indicative of hydrogen bonding between the $-NH_2$ group of the enzyme and the hydroxyl group of PEG. In addition to the above, the carbonyl peak of the free enzyme at 1639 cm^{-1} split into two peaks at 1642 and 1563 cm^{-1} upon coupling. This splitting was illustrative of the free and hydrogen-bonded carbonyl for the immobilized enzyme. The above observations indicated PEGylation of the enzyme.

Unlike covalent coupling (using cyanamide for keratinase) as documented in the previous subchapter 2A, the efficacy of sonication was exploited for biocoupling in this case. The sonication induced collision between the polymer supported nanoparticles and the enzyme moiety in solution had a profound effect on the morphology of the nanoparticles. On coming to closer proximity, the establishment of H-bonding between the hydroxyl groups of the PEG chains and the surface hydroxyl group of the iron oxide nanoparticles with the enzyme moiety was facilitated. The preponderance of H-bonding, among other possible secondary interactions is an important factor in the reported bio-conjugation. The binding of magnetic particles to bioactive substances also involves the chelating interactions between the biological moiety and the metal's centres.

Lakeshore VSM was used to study the magnetic behaviour of the PEG-Ag-IONPs before and after enzyme coupling in comparison to the PEG assisted IONPs. The M–H hysteresis loops of the various systems were recorded at room temperature (Fig.2B.3). The M_S (saturation magnetization) was found to be highest (76.065 emu g^{-1}) for the PEG assisted IONPs (Fig.2B.3a) while it decreased by almost 50% for the PEG assisted Ag-MNP system (M_S= 37.785 emu g^{-1}) (Fig.2B.3b) and the enzyme immobilized system (36.093 emu g^{-1}) (Fig.2B.3c). The remnant magnetization (M_r) showed a similar trend. The coercivity values for the various systems did not show a significant variation. The decrease recorded in few of the magnetometric values for the enzyme immobilized system in comparison to the IONPs is attributed to the presence of diamagnetic components like polymer supported silver nanoparticles and the biocatalyst in the system.

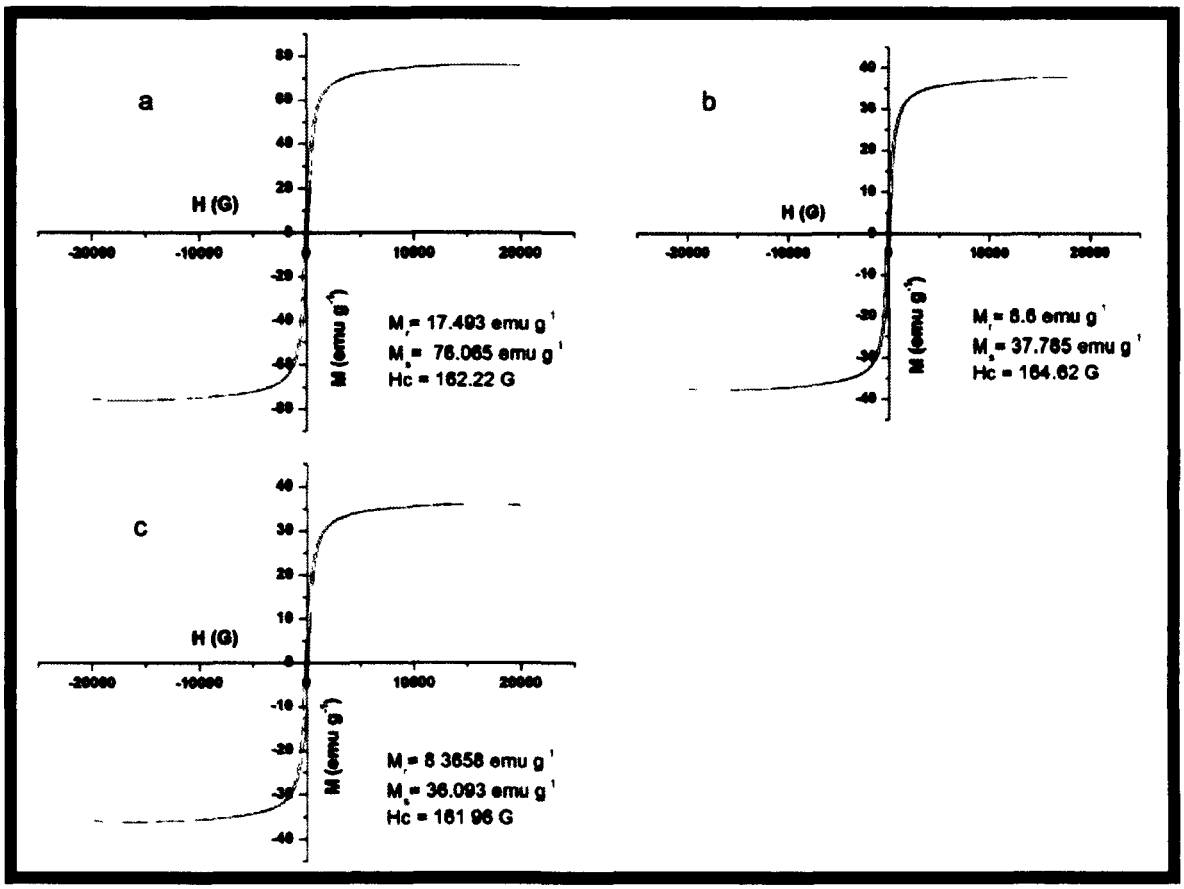

Fig.2B.3. *Hysteresis plot of a) PEG-IONPs, b) PEG-Ag-IONPs and c) enzyme immobilized system*

It is to be noted that the immobilization of the enzyme onto the PEG-Ag-IONPs did not alter the magnetic quality of the immobilization system to a great extent. Magnetic field susceptibility and consequently the recyclability of the biocatalyst make the reported system attractive in terms of industrial economy.

Carefully designed immobilization system can be instrumental in devising strategies to minimize the loss of enzyme by desorption. About 86% binding of the enzyme onto the immobilization system was documented.

2B.3.2. *Effect on the immobilized biocatalyst*

The immobilized enzyme showed multi-fold enhancement in activity compared to the free counterpart. The free enzyme showed a specific activity of 69 U mg^{-1} while the immobilized enzyme recorded a specific activity of 807 U mg^{-1} (Fig.2B.4).

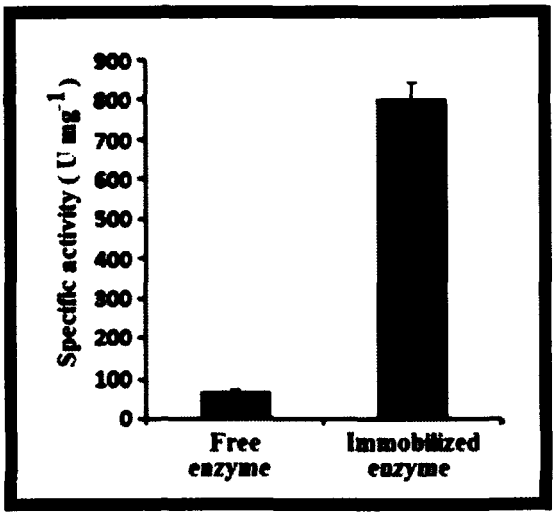

Fig.2B.4. *Specific activity of free and immobilized enzyme*

The changes in kinetic properties of the enzyme after immobilization are determined by four factors: change in enzyme conformation and its microenvironment, steric, bulk and diffusional effects.[49] Table 2B.1 enlists few of the kinetic parameters of the free and the immobilized system.

Table2B.1. *Comparative data on the kinetic parameters of the free and immobilized AMG*

Parameters	*Free*	*Immobilized*
pH optimum	4.5	4.5
Temperature optimum (^{0}C)	60	70
K_m (mM)	6	3
V_{max} (nM min^{-1})	0.03	0.08

The Michaelis constant, K_m indicates the substrate concentration at which half the active sites are filled. Furthermore, a low K_m indicates strong enzyme-substrate binding and vice versa. The K_m value depends on the substrate used and the environmental conditions such as pH, temperature, and ionic strength.[50] The maximal rate, V_{max}, reveals the turnover number of an enzyme. The K_m value decreased by almost 50% for the immobilized enzyme compared to the free counterpart. The increment in the V_{max} indicated greater efficiency of the immobilized enzyme.

Recently modulation of the binding affinity of α-chymotrypsin with *N*-succinyl-alanine-alanine-proline-phenylalanine-*p*-nitroanilide substrate by tetraethylene glycol (TEG) functionalized gold nanoparticles via an excluded volume mechanism has been reported to increase the enzyme activity.[51] In a similar way, it has been proposed that macromolecular crowding potential of PEG is responsible for increasing the effective concentrations of the enzyme and the substrate.[52, 53] The greater surface area of the

immobilization system in the nano dimension with possible structural modulation may be viewed as the reason for better substrate-enzyme interaction, through exposure of the active site.

There was no apparent change in the optimum pH of 4.5 for the enzyme before and after immobilization. However, the immobilization process had shifted the optimum temperature to 70 ^{o}C, an increment of 10 ^{o}C over that of the free enzyme (60 ^{o}C) (Fig.2B.5).

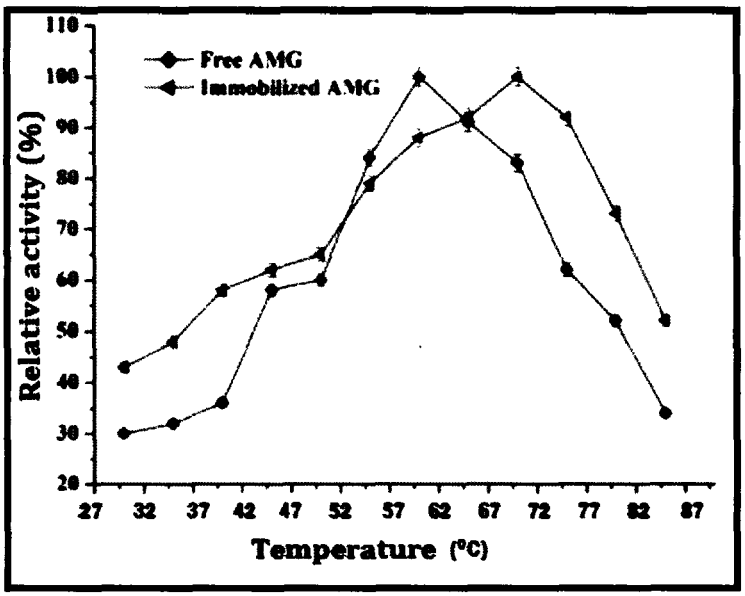

Fig.2B.5.*Thermostability plot of free and immobilized enzyme*

This could be safely attributed to the structural stabilization of the enzyme in the system. The shifting of the optimum temperature to higher values with greater activity even at higher temperature is indicative of the potentials of the system for various industrial applications.

After predetermined thermal inactivation, the residual activities were determined to check the thermo-stability of the immobilized enzyme and the free enzyme. As shown in Fig.2B.5, the enzyme activity of the free AMG declined to almost 34% when incubation temperature was raised to 358 K. However, the immobilized AMG still had a residual activity of 52% at the same temperature. Interestingly, the immobilized enzyme and the free enzyme showed an activity of about 92% and 76 % respectively after an incubation period of 4 h at their corresponding optimum temperature (343 K and 333 K). As depicted in Fig.2B.6, a rapid decline was observed in the activity of the free AMG just after 5 days of storage at 298 K while it retained 79% of its activity post 30 days storage at 277 K.

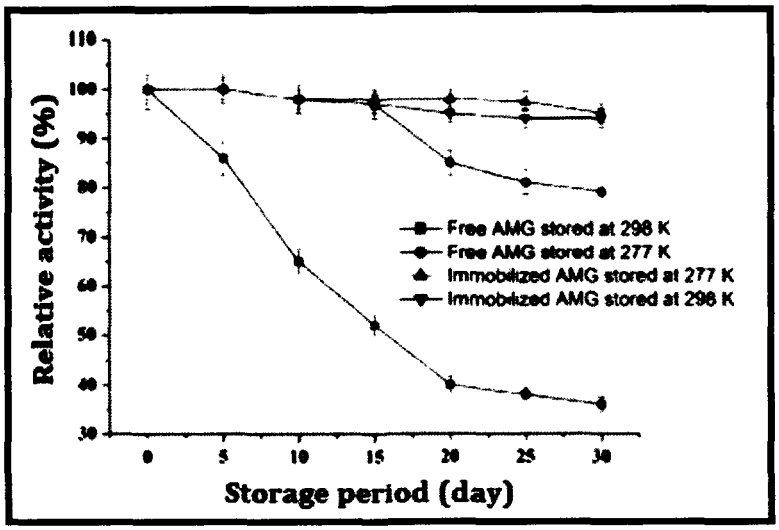

Fig.2B.6. *Storage stability plot of free and immobilized enzyme at two different temperatures*

In contrast, both the immobilized systems stored at 277 K and 298 K for the 30-day storage period retained considerable initial activity (about 95%). The results justified that the storage stability of the enzyme improved upon immobilization.

Repetitive use of the enzyme under identical experimental conditions showed very little bioleaching with retention of initial activity up to 96% after 8 cycles of use (Fig.2B.7). Thus, the immobilized enzyme showed better thermostability, storage stability and multiple cycle use in contrast to the free enzyme. It is quite likely that PEGylation had induced structural modulation of the enzyme as a result of immobilization. As already noted in subchapter 2A, PEGylation has been instrumental for protecting a host of biocatalysts against denaturation.[18, 21]

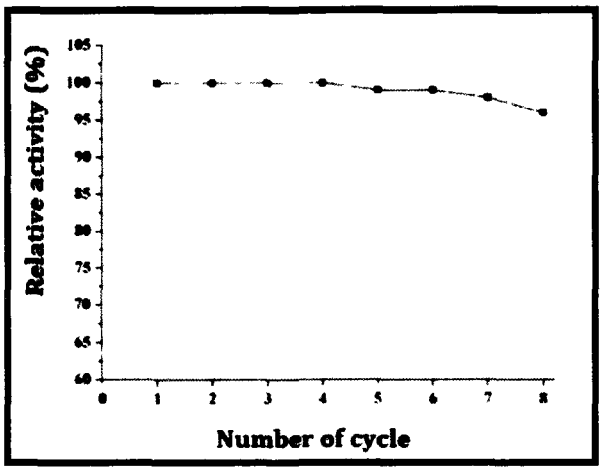

Fig.2B.7. *Recyclability efficiency plot of the immobilized enzyme*

Stabilization has been proposed to originate from solvation of the bound PEG chains with water molecules, thereby restricting local molecular mobility which in turn

led to a decrease in the unfolding rate of the protein.[22] Improvement of the storage stability is another attractive feature of the system. With a possibility of holding the immobilized enzyme in a more stable position than the free counterpart, the coupling reduces the distortion effects imposed from aqueous ambience on the active site of the enzyme.

At this point, it's pertinent to mention that the biocompatible poly(ethylene glycol) not only stabilized the nanoparticles within a narrow size spectrum but also protected the biocatalyst. This may be viewed as the result of probable PEGylation of surface exposed residues like cysteines known for their involvement in oxidative denaturation of proteins. The chelation type interaction between the nanoparticles' metal centre and the biomolecule further stabilized the whole system that helped in reducing the bio-leaching. A number of anti-oxidants are naturally pooled in leaf extracts to prevent thermal, photo or oxidative denaturation of various biochemical entities. These components may be instrumental in improving the storage stability of the enzyme.

2B.3.3. *Prospective application for food and detergent industry*

The domain of enzyme biotechnology has opened up new possibilities for advanced application oriented products in the food industry. There are several reports on the use of amylase and amyloglucosidase for starch saccharification.[54-56] The increased percent saccharification and the magnetic recyclability (without losing the enhanced action) of the immobilized system make it a better candidate (compared to the free enzyme) for application. An attempt was made to probe into the possible utility of the immobilized system in starch industry. The free enzyme showed about 62 % saccharification after 24 h. This increased by another 8% after 48 h. The immobilized system had yielded about 79% saccharification after 24 h. This increased upto 91% post 48 h. Furthermore, after magnetic recycling of the immobilized system, 90% saccharification was registered during the second and third rounds of use.

On the other hand, detergents normally contain surfactants (anionic, cationic, non-ionic and amphoteric), builders, co-builders, bleach, bleach activators and special additives, such as fluorescent brightener, filler, corrosive inhibitors, antifoaming agents and enzymes (in case of only enzyme fortified detergents) and perfumes.[57] However, due to ethical obligations and professional confidentiality, the chemical composition of these marketed detergents and the overall ionic state of the

surfactants used are generally not stated. The synergy of the detergents and the immobilized enzyme has been reflected clearly in the starch de-staining test. The reported system not only protects the enzyme from the inhibitory effects of ionic surfactants but also is expected to prevent the degradation due to proteases- the likely constituents in enzymatic detergent formulations. This is supported by the repeated separation of the nanosystems even after 5 washing cycles with a simple laboratory magnet and its reuse without losing the enhanced enzyme activity.

Starch stained pieces of cloth were washed with the selected detergents alone and in the presence of immobilized AMG, followed by the determination of the residual starch. For the interpretations, the minimal residual starch indicated better washing. The washing performance of the detergents was in the following order: Surf Excel Blue > Tide > Ariel OxyBlue > Active Wheel Gold > distilled water when used alone (Table2B. 2). However, better washing performance was noted when the detergents were used in combination of the immobilized AMG. The immobilized enzyme helps in the rapid removal of the starch stain, thereby indicating a synergistic effect with the various components of the detergents. It is to be noted that when individual results are compared, the difference may be attributed to the unique washing performance of the detergent alone.

Table2B.2. *Colorimetric determination of residual starch content for the assessment of the washing performance of the detergents with and without the immobilized enzyme*

Detergent used	*Residual starch content*			*Ranking of Detergent*	
	**System A* (x_1)	***System B* (x_2)	$\{(x_1-x_2)/x_1\} \times 100$	*System A*	*System B*
Surf Excel Blue	0.557	0.311	44.165	1st	1st
Active Wheel Gold	0.976	0.779	20.18	4th	4th
Ariel OxyBlue	0.763	0.520	31.84	3rd	3rd
Tide	0.665	0.442	33.53	2nd	2nd

* Detergent alone, **Detergent with immobilized AMG

The anti-microbial action of the immobilized system is primarily attributed to the presence of the silver nanoparticles. The MIC values (Table2B.3) registered a dip for the nanocomposite (with and without the enzyme) in comparison to the silver nanoparticles alone.

Table2B.3. *Anti-bacterial potency of the polymeric nanocomposites with and without AMG*

Test organism	*Minimum Inhibition Concentration (MIC) (μg/mL)*		
	PEG-Ag NPs	*PEG-Ag-IONPs*	*Immobilized AMG onto PEG-Ag-IONPs*
S. aureus MTCC96	6.32	3.16	3.16
B. subtilis MTCC736	6.32	6.32	6.32
P. aeruginosa PN1	25.3	15.1	15.1

The presence of the enzyme did not alter the MIC value. Furthermore, antimicrobial action was more pronounced against the Gram positive bacteria than the Gram negative bacteria. Various mechanisms have been put forward to explain the anti-microbial action of Ag nanoparticles.[40] These include alteration of the cell membrane permeability primarily by immediate dissipation of the proton motive force and interaction with sulphur and phosphorus containing macromolecules like DNA and thereby affecting the replication machinery.[40] It has also been reported that triangular silver nanoparticles are more efficient in counteracting the bacterial proliferation.[40] The {111} facets have high-atom-density, which is favourable for the reactivity of Ag. A triangular nanoplate has a high percentage of {111} facets whereas spherical and rod-shaped Ag nanoparticles predominantly have {100} facets along with a small percentage of {111} facets.[58] In the present system, the morphology directing action of the various components may be envisaged to be responsible factors for the generation of relatively more nanoparticles of triangular shape. This might be responsible for the decrease in the MIC values compared to that of the spherical nanoparticles. The differential interaction of the nanoparticles with the molecular moieties at the surface of the two groups of the bacterial species -Gram positive and Gram negative might be responsible for the observed differences in the anti-microbial effect. The basic architectural differences between the cell walls in the two groups of bacteria may also have a role in determining the anti-microbial activities of the nanoparticles. The anti-microbial potential of the PEG assisted silver iron oxide nanosystem is retained even after the enzyme coupling. This further supports its inclusion in commercial detergent formulation.

2B.4. Conclusion

The excellent thermostability, storage stability, magnetic field recyclability and catalytic action (evaluated for starch saccharification) of the anti-microbial AMG immobilized system was complemented by the washing performance synergy with commercial detergents. Thus, the immobilized system represented the multi-faceted advantages of coupling an industrially important biocatalyst onto polymer supported nanomaterials, prepared through greener route.

2C. LIPASE IMMOBILIZED ONTO PEG-SILVER-IONPs

2C.1. introduction

The recent demonstrations of catalytic promiscuity has conferred a special niche to lipases (triacylglycerol acylhydrolase, EC 3.1.1.3)- one of the much focussed upon industrially relevant biocatalysts.[59] Amongst others, porcine pancreatic lipase (PPL) (a globular protein of a single chain of 449 amino acids with a molecular weight of 50-52 kDa and a molecular volume of 4.6×2.6×1.1 nm^3) has fetched enormous applications across myriad of domains.[60] Comparatively cheaper compared to commercial microbial and animal lipases, PPL is widely used in a plethora of biotransformation reactions both in aqueous (*e.g.*, regioselective hydrolysis, pre-treatment of lipid-rich wastewaters, resolution of racemates, degradation of engineering thermoplastics etc.) and organic media (for preparation of flavours and fragrances, biodiesel, emulsifiers and cosmetics etc.).[60] PPL has also been used in the treatment of congenital pancreatic triglyceride lipase deficiency.[60]

Various materials like celite, nano-sized magnetite, chitosan, amberlite, macroporous anion exchange resins, polyacrylamide beads, hydrophilic polyurethane composite, sepiolite and amorphous $AlPO_4$ and so on have been used for immobilization of PPL via physical adsorption, covalent attachment and entrapment strategies.[60] It is pertinent to mention that multimodalities and multi-functionalities (like antimicrobial potency with magnetic susceptibility of polymeric nanocomposites) of the immobilization platform increase the spectrum of applications of the immobilized enzyme. In this context, as noted in subchapter 2A, the utility of keratinase immobilized onto polymer assisted iron oxide nanoparticles was demonstrated as a recyclable hair saving technology with prospective application in the leather industry. On the other hand, the utilities of amyloglucosidase, immobilized onto polymeric nanocomposite for food and detergent industries were documented in subchapter 2B.

In the light of the above discussion, an endeavour was made to immobilize PPL onto PEG supported silver-iron oxide nanoparticles (PEG-Ag-IONPs) using the green chemistry tool of 'sonication'. The reduction potential of aqueous extract of orange peel (that could be envisaged as interplay of a number of active components including ascorbic acid, vitamin A, flavonoid fractions and various other flavones)[61] has been exploited for the generation of the silver nanoparticles. As noted earlier, sonication

mediated coupling of an enzyme moiety onto polymeric nanocomposite can generate exotic nanostructures, the plausible alterations in the physico-chemical attributes including the morphology, magnetometric parameters, antibacterial potency of the immobilizing platform along with the thermostability, recyclability and storage stability of the immobilized PPL for prospective application in the detergent industry were delved into.

2C.2. Experimental

2C.2.1. *Materials used for the preparation of the immobilization platform*

The starting materials for the preparation of the immobilization platform were same as mentioned in section 2B.2.1. However, aqueous extract of orange peels was used for the reduction of the silver salt. The epicarp or the peels (representing a store house of a myriad of pectins, sugars and flavonoids)[61] of oranges were collected from the fruit juice vendor of Tezpur University campus.

2C.2.2. *Preparation of the immobilization platform*

PEG-IONPs were prepared as described in section 2B.2.1. On the other hand, the reductive potency of aqueous extract of orange peel was exploited to prepare PEG assisted silver nanoparticles (PEG-AgNPs). In brief, about 0.2 g of orange peel was washed with de-ionized water and ground using a domestic blender. Post stirring for about 20 min in 50 mL of water at 50 ^{0}C, the aqueous extract was filtered through a muslin cloth at ambient temperature. 200 µL of 1 M $AgNO_3$ was taken in 7.5 mL of 2% (w/v) PEG solution with 6 mL of the extract. The pH was adjusted to basic condition by adding adequate amount of 2 M KOH. PEG supported particles were washed with Millipore water and acetone post centrifugal decantation. Equal volume (250 µL) suspensions of the PEG-IONPs and PEG-AgNPs in 1 mM Tris/HCl buffer (pH 7.5) were taken in an eppendorf tube for sonication for 3 min at 60% amplitude and 0.5 cycles. The PEG-Ag-IONPs were analysed using various characterization tools prior to and post biocatalyst immobilization as detailed in the subsequent sections.

2C.2.3. *Immobilization of lipase and activity determination*

1 mL of lipase (5 mg mL^{-1}) in 1 mM Tris/HCl buffer (pH 7.5) was added to 50 mg of PEG-Ag/IONPs followed by sonication. Response surface methodology (executed

using the software Minitab 15, USA) was used to optimize the sonication parameters, *viz.*, cycles, amplitude and time of sonication for the maximal lipase loading onto the PEG-Ag/IONPs. The RSM study revealed that sonication under 40% amplitude and 0.6 cycles for 7 min was optimal for the maximal lipase loading. Post sonication under these parameters at 4 ^{0}C (ice-bath), the enzyme immobilized PEG-Ag-IONPs were centrifuged at 3000 rpm for 10 min and magnetically decanted. The post-precipitate supernatant was collected in fresh tubes. The precipitate was washed twice and finally suspended in 1 mM Tris/HCl buffer (pH 7.5). It is to be noted that the percentage binding was estimated by determining the lipase activity for both the post-precipitate supernatant and the immobilized enzyme fraction.

Protein concentration was determined by the method of Lowry et al.[13] with bovine serum albumin (BSA) as standard. The biocatalyst – PPL was procured from SISCO Research Laboratory Pvt. Ltd. Tributyrin (a prodrug of natural butyrate with broad anticancer and synergistic action with many therapies) was used as the substrate for testing the lipase activity. Titrimetric determination of lipase activity at pH 7.5 and 298 K using 0.11 M emulsified triacylbutyrylglycerol (tributyrin) in 1 mM Tris/HCl buffer containing 0.1 M NaCl, 5 mM $CaCl_2$ was carried out according to previously reported protocol.[62]

2C.2.4.*Physico-chemical characterization*

UV-visible spectra were recorded in Hitachi (Tokyo, Japan) U2001 UV spectrophotometer. Lakeshore Vibrating Sample Magnetometer (VSM) (Model 668) was used to study the magnetic behaviour of the samples. Size and distribution of PEG-Ag-IONPs prior to and post enzyme loading were studied in JEOL, JEM 2100 transmission electron microscope (TEM) at an operating voltage of 200 kV.

2C.2.5. *Determination of optimum temperature, pH, K_m and V_{max} of the immobilized lipase*

The optimum temperature of the free and immobilized samples was determined by studying the enzyme activity in the temperature range of (298–358) K. The effect of pH on the enzyme activity at the respective optimum temperature was also recorded. The Michaelis constant, K_m and maximal rate, V_{max} were determined by measuring the initial butyric acid production rate under the respective pH and temperature optima of the free and immobilized lipase.

2C2.6. *Determination of thermostability, storage stability and reusability*

Thermal stability of free and bound lipase was checked by measuring their residual activities after incubation for 15 min in the temperature range of 298-358 K. Residual activity of the free and the coupled enzyme was also assayed after incubating at their respective optimum temperature for about 4 h. Activities of free and bound lipase were determined post storage at 277 K or 298 K. The measurements were performed at intervals of 5 days for a month. Post magnetic separation and washing with buffer solution, the reusability of the bound lipase was assessed by evaluating the activity against fresh substrate at the optimum temperature and pH.

2C.2.7. *Determination of anti-microbial potency*

The antibacterial potency (in terms of minimum inhibitory concentration, MIC) of the PEG-AgNPs and PEG-Ag-IONPs with and without lipase was tested against *Staphylococcus aureus* MTCC96, *Bacillus subtilis* MTCC736, and *Pseudomonas aeruginosa* PN1 according to a previously described protocol, mentioned in section 2B.2.9. The experiments were performed in triplicates with ampicillin (50 μg) as positive control.

2C.2.8. *Prospective application in the detergent industry*

The immobilized PPL was assessed for oil de-staining according to a previously reported protocol (involving assessment for compatibility with commercial detergents).[63] In brief, cotton cloth pieces (size 4.5 × 4.5 cm^2) were stained with 0.2 mL of mustard oil. The stock solutions of four commercially available detergents, namely Active Wheel Gold, Ariel OxyBlue, Tide and Surf Excel Blue (same as given in section 2B.2.8) in distilled water (2.0 g L^{-1}) were prepared. Two stained cloth pieces were taken for each detergent. One piece was washed with detergent alone, while another piece was washed with detergent in presence of the immobilized PPL (25 mg/g of the detergent) at the optimum temperature for 15-20 min with continuous stirring to ensure the maximal contact of the latter with the oil stain. In parallel lines, one stained piece was washed with distilled water and immobilized PPL. Controls involving combinations of detergents and free enzyme were also maintained. Post rinsing with distilled water, the residual oil (if any) on the washed piece was extracted in 10 mL of petroleum ether, transferred to a round bottom flask containing 25 mL alc. KOH (0.5 M). Post refluxing in a boiling water bath for 30 min and cooling to room temperature (~ 27 ^oC), the reaction content was titrated against 0.5 M HCl against reagent blank (without

any oil). 1% phenolphthalein was used as an indicator. The measured volume of HCl was proportional to the unused KOH. Higher the volume of HCl used in titration, lesser was the residual oil and better the washing performance.[63]

2C.3 Results and Discussion

Although immobilization studies of lipase based on covalent coupling,[64] entrapment[65] or cross-linking reactions[66] have apparent advantages over adsorption, the latter is still the most commonly preferred method.[67] This is ascribable to mild reaction conditions of immobilization, easy and cheaper technique amenability for recycling without much activity loss. However, a serious practical snag is the stripping off of the biocatalyst from the carrier because of the weak adhesion forces between the former and the latter.[67] In the present study, the suitability of the green chemistry tool of sonication to aid in the adsorption of lipase onto polymer supported nanomaterials and the modulations in the bio-physico-chemical properties of the bioconjugated polymer assisted nano-platform were assessed.

2C.3.1. *Preparation and characterization of the immobilization platform prior to and post biocoupling*

The preparation of the immobilization platform in the present study was based on sonication mediated mixing of the PEG-AgNPs (prepared using the reductive potency of orange peel, Fig.2C.1a) and PEG-IONPs (prepared using a wet chemical process, Fig. 2C.1b). The spherical PEG-AgNPs (Fig.2C.1c) were distributed within a spectrum of (1-3) nm. On the other hand, well dispersed, dense population of 2-5 nm sized PEG-IONPs (with maximal particles of about 4 nm diameter) were observed in TEM imaging (Fig. 2C.1d).

Recently, a shielding model has been developed to explain the correlation between the size effects of nanoparticles and the kinetic responses of the immobilized enzyme. It has been reported that smaller gold nanoparticles promoted the catalytic efficiency of *Candida rugosa lipase* by increasing its kinetic affinity (*i.e.*, lower K_m values) toward the substrate *p*NPP.[68] Dictated by this observation, the sonication parameters of frequency, amplitude and cycle (using response surface methodology, RSM, as executed in Minitab 15) were optimized for minimal size of the resulting PEG-Ag-IONPs obtained post mixing of the PEG-IONPs and PEG-AgNPs. Successful fusion of PEG-Ag NPs and

PEG-IONPs to generate hybrid PEG-Ag-IONPs, distributed within a size spectrum of (6.5-14) nm and average diameter of 10.25 nm (Fig.2C.1e) under optimized sonication parameters marshals in support of the green chemistry tool of sonication as an apt strategy to tailor nanomaterial assembly. It has been demonstrated that the control of cavitation involving the control of interfaces at the microsecond timescale and use of different surfactants make it possible to prepare multicomponent metallic nanostructures having properties markedly different from those fabricated by conventional means.[69] Studies show that hybrid assemblies of different nanostructures, requiring a fine balance of entropic and energetic interactions is a kinetically limited process, where in critical roles of suitable additives, high dielectric constant of spherical nanoparticles, and large Hamaker constant have been illustrated.[70] Nevertheless, a detailed mechanistic approach would be required to understand the coalescing and assemblage particularly the balance of entropic and energetic interactions between the two classes of the nanoparticles, each one stabilized by poly(ethylene glycol) chains via steric interference.

This was followed by sonication mediated immobilization of the biocatalyst. RSM revealed that sonication parameters of 7 min under 40% amplitude and 0.6 cycles were optimal for the maximal lipase loading (76%). A large number of literature reports vouch for aggregation of biomolecule-functionalized nanoparticles.[71] In the present report, post lipase (Fig.2C.1f) immobilization nanorods could be observed (Fig.2C.1g). The majority of the nanorods were as long as 98 nm while the shortest were found to be around 12 nm with width of 10 nm. It is pertinent to mention that the sonication (under the same parameters) if executed in the absence of the enzyme led to agglomerated mass. Thus the lipase molecules (which themselves are in the nanoscale regime) seem to have a major surface –chemistry modulating and morphology directing action.

The shape-size accord of nanomaterials is influenced by the interplay of a plethora of factors: magnitude of intensive variables (like temperature, pressure etc.), the extent of contributions to the chemical potential by the enthalpic and entropic interactions, the consequence of mixing on the internal degrees of freedom of the constituents, the extent of dispersion of the constituents and most importantly, the intricacy of surface and intermolecular interaction.

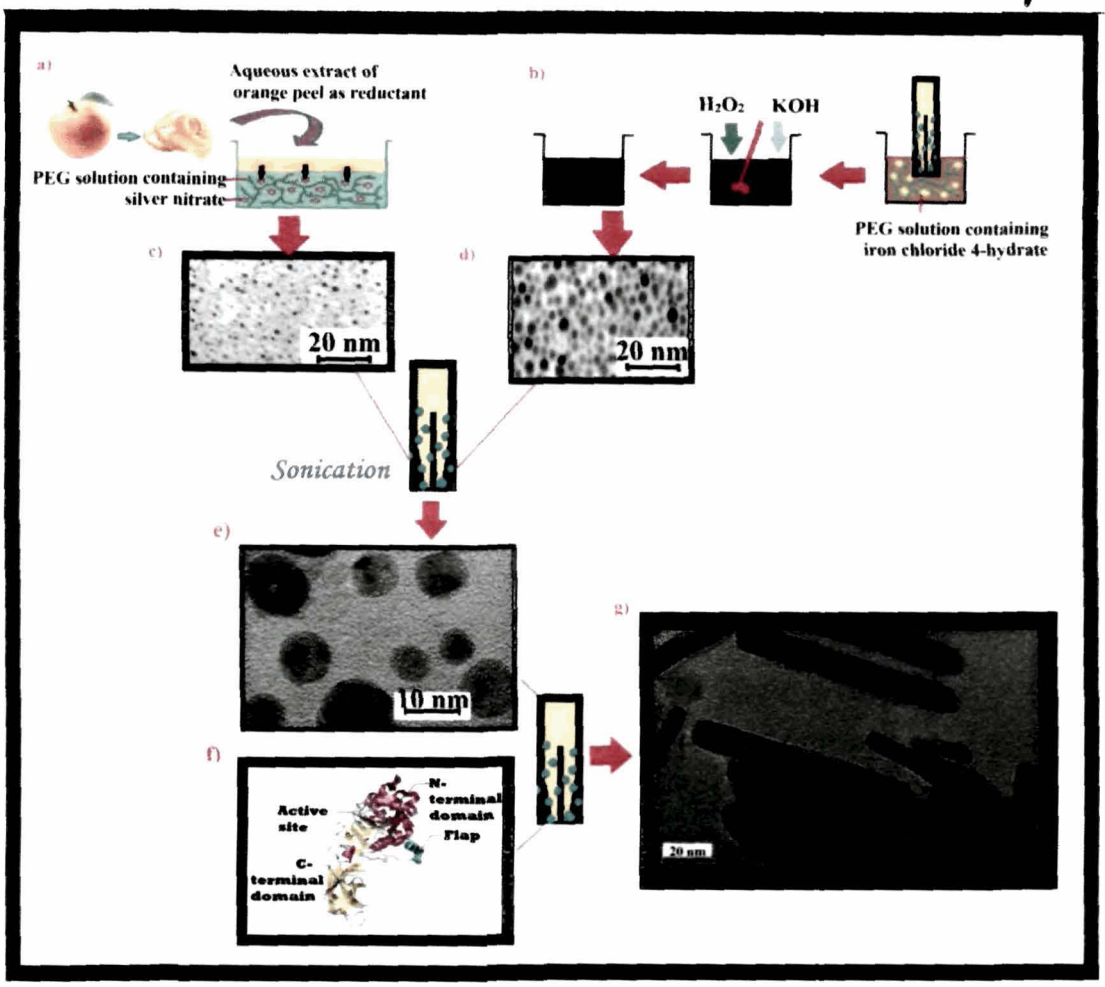

Fig.2C.1. *Immobilization protocol, a) Bioresource based preparation of the PEG-AgNPs, b) Preparation of the PEG-IONPs nanoparticles, Sonication mediated mixing of c) PEG-Ag NPs and d) PEG-IONPs to obtain the immobilization platform e) PEG-Ag-IONPs, Sonication mediated immobilization of f) PPL to obtain the immobilized system g) PPL-PEG-Ag-IONPs.*

The HRTEM imaging of the biocatalyst conjugated rod-shaped nanostructure is shown in Fig.2C.2a. The blow-up of the boxed area in Fig.2C.2b gives an impression that the biocatalyst immobilized hybrid nanoparticles come into close proximity and fuse at the boundaries. It was difficult to associate any preferential crystallographic orientation in the nanorod (vouched by the pseudo-coloured HRTEM image, Fig.2C.2c, obtained in Fiji- image processing software). This random orientation may be due to lipase adsorbed nanoparticles' rotation, coming to closer proximity and deformation during sonication. The messy, though spot-like diffraction pattern (inset in Fig. 2C.2b) further vouched for a process involving particle boundary deformation.[72] Furthermore, amorphous aggregation regimes (marked in green with orange bordered arrows) could be observed interspersing the nanoparticles.

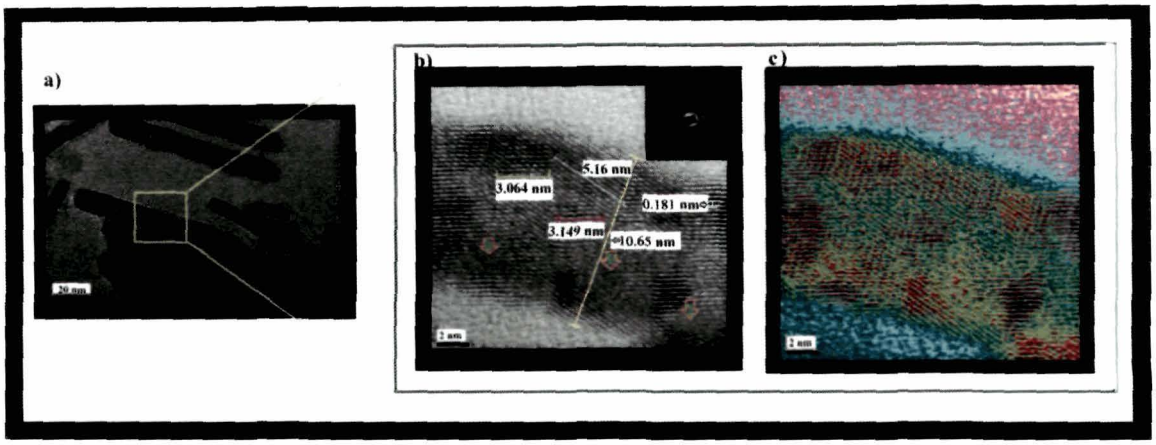

Fig.2C.2. *a) HRTEM image of PPL-loaded PEG-Ag-IONPs, b) blow-up image of the nanorods with inset showing the diffraction pattern, c) pseudo-coloured (in Fiji) HRTEM image of the blow-up area.*

Hierarchical nanostructures grow either by monomer addition or through dynamic particle attachment events. The evolution of the nanorods in the present case may be interpreted in lines of the following discussion, schematically illustrated in Fig.2C.3(i-iii). In a highly illustrative study, it has been shown that direction-specific interactions dictate iron oxide crystal growth via oriented attachment.[73] On the other hand, real time transmission electron microscopy imaging of solution growth of Pt_3Fe nanorods from nanoparticle building blocks with surface co-adsorbed oleylamine and oleic acid has been reported recently.[74] The complex interactions between the nanoparticles during the formation of nanorods involve van der Waals forces, hydrophobic attractions, and charge-charge interactions along with dipolar interactions (both electrostatic and magnetic).[74] A complicated process involving a number of steps *viz.*, shape-directed nanoparticle assembly, straightening, orientation correction, and mass redistribution with prominence of dipolar nanoparticle interactions have been identified for the dynamic growth of Pt_3Fe nanorods in solution using TEM.[74] In the present case, sonication brings the biocatalyst moieties in close proximity to the hybrid nanoparticles and facilitates in their surface adsorption. The enzyme adsorbed PEG-Ag-IONPs diffuse freely and undergo continuous rotation and interaction until they find a perfect lattice match.[73] As the nanoparticles separation distance decreases to a critical value, they acquire a drift velocity (which increases with decrease in separation distance).[74] It has been shown that a consequent sudden jump over less than 1 nm leads to lateral atom-by-atom addition initiated at the contact point, followed by interface

elimination (that follows a rate dictated by the curvature dependence of the Gibbs free energy).[73]

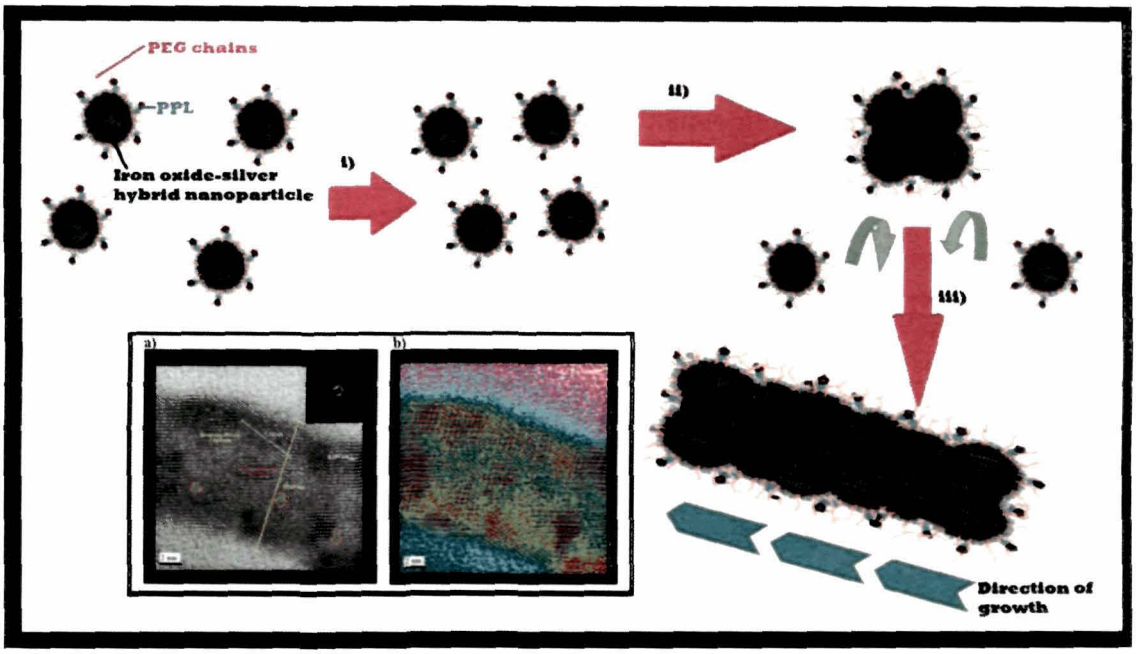

Fig.2C.3. *Plausible mechanism of the evolution of the PPL-loaded PEG-Ag-IONPs nanorods*

Highly direction-specific interactions have been shown to drive crystal growth via oriented attachment (as vouched by measurements of translational and rotational accelerations). A special issue that demands attention is the preferential end add-on over the attachment in the middle of nanoparticle chain. This may be attributed to the strong anisotropic potential energy between a nanoparticle and nanoparticle chain compared to the interaction potential energy between two approaching nanoparticles.[74] Surface chemistry possibly modulated by the adsorption of specific bioactive species *i.e.,* PPL (without excluding the plausible role of surface adsorbed phytoextract components) and interaction with the PEG chains under specific sonication parameters could be envisaged for the structural modulations in the present case.

The lipase cargo on the hybrid nanoparticles (as determined by Lowry's protein assay in the original lipase solution, supernatant and washing post immobilization) was found to be around 74%.

Magnetic behaviour (Fig.2C.4) of the immobilization platform prior to and post PPL loading was studied at room temperature using Lakeshore VSM. PEG-IONPs showed the highest saturation magnetization, M_s of about 78.09 emu g^{-1} (Fig.2C.4a) while it was about 35.7 emu g^{-1} and 31.2 for PEG-Ag/IONPs with (Fig.2C.4b) and without (Fig.2C.4c) PPL loading respectively. A similar trend was registered for the remnant magnetization (M_r) while considerable variations in the coercivity values were

not documented. Such modulations in the magnetometric parameters were in parallel lines as observed in the previous subchapters. Nevertheless, the reusability of the PPL-loaded system (that is ascribable to the magnetic field susceptibility), as described in the later section makes it commercially attractive.

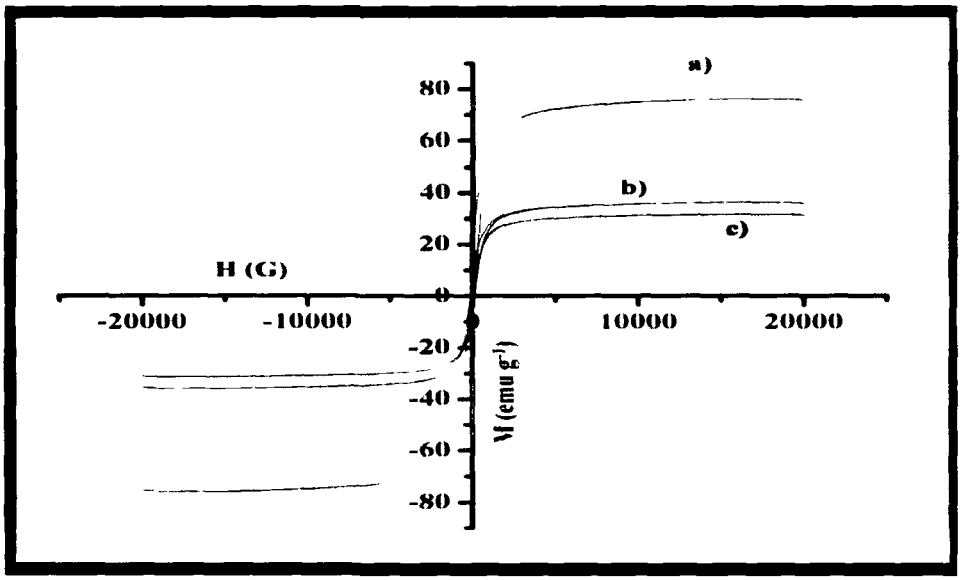

Fig.2C.4. *M–H hysteresis curves of a) PEG-IONPs, b) PEG-Ag-IONPs and c) PPL-PEG-Ag-IONPs*

UV-visible spectra attested the successful immobilization of the biocatalyst and were indicative of the PEG-assisted metal/metal-oxide-enzyme interaction. The spherical PEG-AgNPs (Fig.2C.5a) showed the characteristic surface plasmon resonance (SPR) peak at around 407 nm. On the other hand, the PEG-Ag-IONPs (Fig.2C.5b) exhibited a broad featureless peak at around 330-420 nm. Surface aromatic amino acid residues (of proteins) like tyrosine, tryptophan and phenylalanine absorb strongly in the UV spectral region. The free PPL (Fig.2C.5c) showed characteristic peaks in this region. However, immobilization of PPL (Fig.2C.5d) led to slight shift in the energy level and increase in the intensity of these absorption peaks. The immobilized system also showed a broad peak around 400 to 600 nm. It has been previously reported that sonication under specific parameters (*and not under all conditions*) led to increase in enzyme activity with greater surface exposure of the aromatic amino acid residues (and substantial decrease of α-helix structure and parallel increase in β –sheets) of PPL resulting in its unfolding.[75] The modulations in the helical movement of the lid (that blocks the hydrophobic tunnel in closed conformation) away from the enzyme surface and consequent exposure of the active site on sonication has been proposed for the increased activity.[75] The increase in the PPL activity in the present case (as noted in the

subsequent section) could be explained in parts in this context. However, this needs to be critically analyzed in the light of the stabilizing action of PEG on the structure of biocatalysts, as highlighted in the subsequent section.

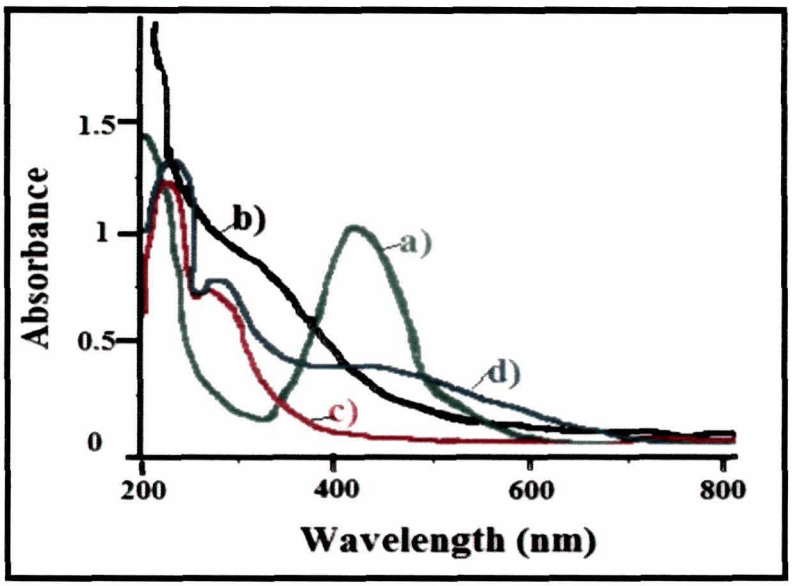

Fig.2C.5. *UV-visible spectra of a) PEG-Ag NPs, b) PEG-Ag-IONPs, c) PPL in its free state and d) PPL-PEG-Ag-IONPs*

2C.3.2. *Properties of the immobilized PPL*

Dyal et al.[76] had demonstrated the prevention of desorption and protection of lipase from denaturation post covalent immobilization onto γ–Fe_2O_3 nanoparticles. However, they had reported a serious limitation of loss in enzyme activity. This could be attributed to the burial of the active site or restriction from assuming the conformation needed to initiate the catalysis. In the present investigation, the free enzyme showed a specific activity of 40 U/mg while it was about 110 U/mg for the immobilized PPL. The pH optimum for the free and immobilized biocatalyst was 7.5 and 8.5 respectively (Fig.2C.6a). Interestingly, the immobilized PPL retained a much higher relative activity at higher pH. On the other hand, the optimum temperature for the immobilized PPL shifts to 313 K while 308 K was the optimal for the free enzyme (Fig.2C.6b).

Furthermore, a higher activity was retained for the immobilized PPL in comparison to the free counterpart at temperatures higher than their respective optimal temperature. To vouch for this, the citation of enhanced activity recovery and widened adaptive pH and temperature range of lipase immobilized onto poly(glycidyl methacrylate)-grafted Fe_3O_4/SiO_x nanoparticles is pertinent.[77] On the other hand, about 91% activity was retained for the immobilized PPL post 8 cycles of use (Fig.2C.7).

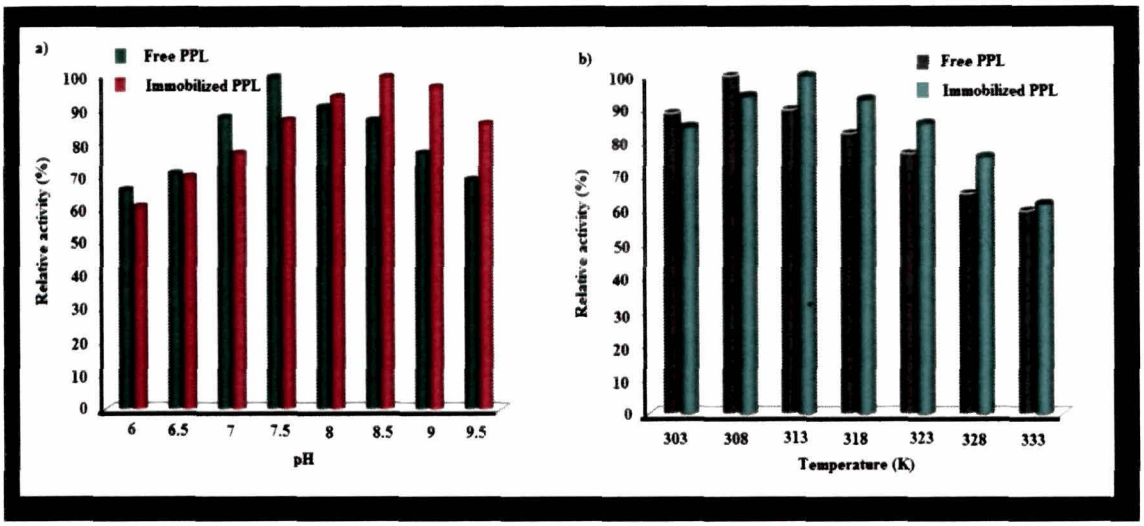

Fig.2C.6. *Effect of a) pH and b) temperature on the activity of free and immobilized PPL.*

It was interesting to note an overall increase in the activity, thermostability and storage stability of the porcine lipase post immobilization complemented by its excellent recyclability. As noted in the previous subchapter, a plethora of biocatalysts and biomolecules have been reported to be stabilized by poly(ethylene glycol).[18-21] Solvation of the hydrophilic region of bound PEG chains and interaction of the hydrophobic regions of PEG with the hydrophobic clusters on the biomolecule has been proposed for the stabilizing action of PEG.[22]

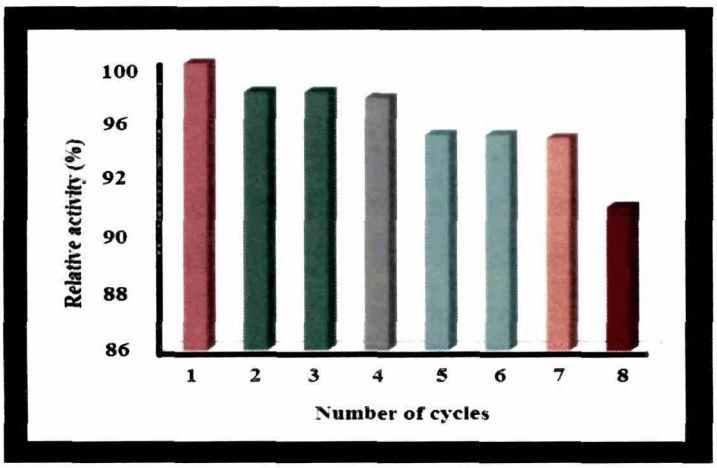

Fig.2C.7. *Recyclability plot of the immobilized PPL*

PPL seems to be held in a more stable position in its immobilized state which possibly reduces the ambient distortion effects on the active site. On the other hand, PEG-lipase complex was found to exhibit 16 times higher lipase activity in relation to the native enzyme powder in fluorous solvent (FC-77). The localization of substrates around lipase molecules, induced by adsorption of the substrates to the PEG layer of the complex, has been forwarded as the possible mechanism for the enhanced catalytic

activity.[78] Interestingly, in a study pertaining to *Candida rugosa* lipase (Lip1) partitioning in aqueous two-phase systems of PEG-potassium phosphate, Bassani et al.[79] have reported a decrease of the partition coefficients with PEG molecular mass. The enzyme-partition was dictated by the excluded volume effect and not by the enzyme-polymer interaction. Furthermore, neither the secondary and tertiary structure of the biocatalyst nor the latter's activity was modulated by the polymer.[79] Thus, it appears that an intricate balance between the effects of sonication (mentioned previously) and PEGylation dictated the enhanced activity and stability of the immobilized PPL in the present case. The plausible chelating interactions between the biocatalyst and the metal's centers could also be envisaged, amongst others, for the enhanced stability. Furthermore, the probable adsorption of natural components of the orange peel onto nanoparticles' surface might have exerted a protector influence on the loaded PPL.

2C.3.3. *Antibacterial efficacy and detergent compatibility*

Table 2C.1 shows the antibacterial potency of the PEG-AgNPs, PEG-Ag-IONPs and PPL-PEG-Ag-IONPs. The MIC value of the PEG-Ag-IONPs and lipase immobilized system was almost half that of the PEG-AgNPs against all the three bacterial species. Lipase immobilization did not affect the antibacterial potency of the PEG-Ag-IONPs as vouched by the MIC values.

Table2C.1. *Antibacterial potency of the polymeric nanocomposites with and without PPL*

Test Organism	*MIC (μg/mL)*		
	PEG-AgNPs	*PEG-Ag-IONPs*	*PPL-PEG-Ag-IONPs*
S. aureus MTCC96	15	7.5	7.5
B. subtilis MTCC736	15	7.5	7.5
P. aeruginosa PN1	45	25	25

It is pertinent to mention at this juncture that a long standing debate whether it's the silver nanoparticles or the release of silver ions that are responsible for the antibacterial action seems to be solved recently.[80] As noted in the previous subchapter (as well as focussed in the next chapter), different factors like size, shape, surface charge, solution chemistry, surface coating and solubility of Ag NPs have been reported for the latter's toxicity. Xiu et al.[80] have reported that these are indirect effectors that eventually dictate the release of Ag^+, the definitive molecular toxicant, suggesting a negligible particle-specific antibacterial activity and requisite of aerobic conditions for

Ag^0 oxidation and Ag^+ release.[80] In the present investigation, the iron oxide nanoparticles seem to possibly modulate and augment the silver ion release and thereby resulting in the decrease MIC value for the PEG-Ag-IONPs. Another striking observation was the differential action against the gram positive and gram negative bacterial species. As mentioned in the previous subchapter, this may be attributed to the differential interaction of the prepared systems with the surface moieties of the differently architectured cell walls of the two classes of the bacteria. This however, needs a further study, complemented by the tools of molecular biology and computational chemistry. The antibacterial action of the immobilized system was complemented by its excellent oil-destaining potency, vouched by a synergistic action with a panel of commercial detergents (Table2C.2).

Table2C.2. *Titrimetric determination of residual oil content in test cotton cloth post washing with different detergents with and without immobilized PPL*

Detergent used	*Amount of HCl used in titration (mL)*		*Ranking of Detergent*	
	Detergent alone (System A)	*Detergent + immobilized PPL (System B)*	*System A*	*System B*
Surf Excel Blue	22.2	24.8	1st	1st
Active Wheel Gold	21.2	23	4th	4th
Ariel Oxy Blue	21.8	23.8	3rd	3rd
Tide	22	24.1	2nd	2nd

From the table, it can be well perceived that detergents (when used alone) did not differ much as far as their washing performance was concerned. The oil de-staining potency of the detergents in the absence or presence of the immobilized lipase exhibited the same trend: Surf Excel Blue>Tide>Ariel Oxy Blue> Active Wheel Gold.

Presence of immobilized PPL improved the washing performance of Surf Excel Blue by 11.71% while it was about 8.46% for Active Wheel Gold. It is pertinent to note that the washing performance of the detergents also improved in the presence of free PPL (although it reached only a maximum of 5% in the case of Surf Excel Blue). However, the exhaustive nature of the free PPL precludes its inclusion in commercial detergents. This practical snag is aptly addressed by the retention of high activity even after post repetitive reuse. An immediate scope of investigation lies in the evaluation of the compatibility of the prepared immobilized PPL with immobilized proteases for prospective inclusion in commercial detergents.

2C.4. Conclusion

Sonication mediated immobilization of porcine pancreatic lipase led to the genesis of exotic polymer supported nanorods with magnetic recyclability and commendable antibacterial potency. Immobilized PPL, with enhanced catalytic activity and modulated pH and temperature optima demonstrated compatibility and synergy with a panel of commercial detergents in oil de-staining, thereby attesting commercial prospects to the developed system.

References

1. Gupta, R., & Ramnani, P. *Appl. Microbiol. Biotechnol.* **70,** 21--33, 2006.
2. Brandelli, A., et al. *Appl Microbiol Biotechnol.* **85,** 1735–1750, 2010.
3. Saiyed, Z. M., et al. *Biomagn. Res. Technol.* **1,** 2 (8 pp), 2003.
4. Kouassi, G. K., et al., *J. Nanotechnol.* **3,** 1, 2005.
5. Bourgeat-Lami, E., & Lang, J. J. *J. Colloid Interface Sci.* **197**(2), 293--308, 1998.
6. Iron (II) chloride tetrahydrate-Sigma Aldrich Product information. http://www.sigmaaldrich.com/etc/medialib/docs/Sigma-Aldrich/Product_Information_Sheet/220299pis.Par.0001.File.tmp/220299pis.pdf, 2012
7. Potassium hydroxide- Sigma Aldrich Product information. http://www.sigmaaldrich.com/etc/medialib/docs/Sigma/Product_Information_Sheet/2/h0904pis.Par.0001.File.tmp/h0904pis.pdf, 2012.
8. Hydrogen peroxide- Sigma Aldrich Product information. http://www.sigmaaldrich.com/etc/medialib/docs/Sigma/Product_Information_Sheet/2/h0904pis.Par.0001.File.tmp/h0904pis.pdf, 2012.
9. PEG- Sigma Aldrich Product information http://www.sigmaaldrich.com/etc/medialib/docs/Aldrich/Product_Information_Sheet/p3265pis.Par.0001.File.tmp/p3265pis.pdf, 2012.
10. Boyer, C., et al. *NPG Asia Mater.* **2,** 23--30, 2010.
11. Schep, L., et al. *Clinic. Toxicol.* **472,** 58--60, 2009.
12. Rossi, L. M., et al. *Anal. Bioanal. Chem.* **380,** 606--613, 2004.
13. Lowry, O.H., et al. *J. Biol. Chem.* **193,** 265--75, 1951.
14. Haaland, P.D. (ed.). *Experimental Design in Biotechnology,* Marcel Dekker Inc., New York, 1989.
15. Rai, S.K., & Mukherjee, A. K. *Bioresour. Technol.* **100,** 2642--2645, 2009.
16. Wing, J., et al. *Adv. Mater.* **16,** 136--40, 2004.
17. Al-Azzam, W., et al. *J. Pharm. Sci.* **94,** 1808--19, 2005.
18. Castellanos, I. J., et al. *J. Pharm.Sci.* **94,** 327--40, 2005.
19. Inada, Y., et al., *Trends Biotechnol.* **13,** 86--91, 1995.
20. Gaertner, H. F., & Puigserver, A. *J. Enzyme Microb. Technol.* **14,** 150--5, 1992.
21. Garc´ıa-Arellano, H., et al. *Bioconjug. Chem.* **13,** 1336--44, 2002.
22. Hern´aiz, M. J., et al. *Enzyme Microb. Technol.* **24,** 181--90, 1999.

23. Longo, M. A., & Combes, D. *J. Biotechnol.* **58**, 21--32, 1997.

24. Roberts, M. J., et al. *Adv. Drug Deliv. Rev.* **54**, 459--76, 2002.

25. Veronese, F. *Biomaterials* **22**, 405--17, 2001.

26. Furlinger, M., et al. *Eur.J. Biochem.* **251**, 955–63, 1998.

27. Slavica, A., et al. *Appl. Environ.Microbiol.* **71**, 8061--8, 2005.

28. Slusarczyk, H., et al. *Eur. J.Biochem.* **267**, 1280--9, 2000.

29. DeSantis, G., & Jones, J. B. *Curr. Opin. Biotechnol.* **10**, 324--30, 1999.

30. Tiller, J. C., et al., *Biotechnol. Bioeng.* **73**, 246--52, 2000.

31. Thanikaivelan, P., et al. *Trends Biotechnol.* **22**, 181--8, 2004.

32. Schrooyen, P.M.M., and Radulf, O., *Keratin-based products, compositions, their modifications, and casting process*, **US Patent No. 20040210039**, October 21, 2004.

33. Vijayakumar, G.R., et al. *Eur. Food Res. Technol.* **220**, 272--277, 2005.

34. Pandey, A., et al. *Biotechnol. Appl. Biochem.* **31**, 135–152, 2000.

35. Silva, R.N., et al. *Process Biochem.* **40**, 1155--1159, 2005.

36. Bai, Y., et al. *Appl. Microbiol. Biotechnol.* **83**, 457--464, 2009.

37. Cang-Rong, J.T., & Pastorin, G. *Nanotechnol* **20**, 255102 (20 pp), 2009.

38. Mulfinger, L., et al. *J. Chem. Educ.* **84**, 322, 2007.

39. Nair, L.S., & Laurencin C.T. *J. Biomedical Nanotechnol.* **3**, 301--316, 2007.

40. Sharma, V.K., et al. *Adv. Colloid Interface Sci.* **145**, 83--96, 2009.

41. Dweck, A.C., & Meadows, T. *Int. J. Cosmetic Sci.* **24**, 1--8, 2002.

42. Silver Nitrate- Sigma Aldrich Product information http://www.sigmaaldrich.com/etc/medialib/docs/Sigma/Product_Information_Sheet/1/s7276pis.Par.0001.File.tmp/s7276pis.pdf, 2012.

43. Bernfeld, P. *Method Enzymol* **1**, 149--158, 1955

44. Mishra, R., & Maheshwari, R. *J. Biosciences* **21**, 653--672, 1996.

45. Dhingra, S., et al. *Indian J Chem Techn* **13**, 119--121, 2006.

46. Turkoglu, A., et al. *Food Chem.* **101**, 267--273, 2007.

47. Jorgensen, J.H., & Turnidge, J.D. Antibacterial susceptibility tests: dilution and disk diffusion methods, in *Manual of Clinical Microbiology*, P.R. Murray et al. eds., ASM Press, Washington, DC, 1999, 1526--1543.

48. Andrews, J.M. *J. Antimicrob. Chemoth.* **56**, 60--76, 2005.

49. Kennedy, J.F., & White, C.A. Principles of immobilization of enzymes, in *Handbook of Enzyme Biotechnology*, A. Wiseman et al. eds., John Wiley and Sons, New York, 1985, 147--207.

50. Rodwell, V.W., & Kennelly, P.J. Enzymes: Kinetics, in *Harper's Illustrated Biochemistry*, R.K. Murray et al. eds., Lange Medical Books/McGraw-Hill, New York, 2003, 60--71.
51. Jordan, B.J., et al. *Nanotechnol.* **20**, 434004 (5 pp), 2009.
52. Dominak, L.M., & Keating, C.D. *Langmuir* **24**, 13565--13571, 2008.
53. Vergara, A., et al. *Macromolecules* **39**, 4500--4506, 2006.
54. Soni, S.K., et al. *Indian J. Exp. Biol.* **33**, 957--961, 1995.
55. Adeni-Awg, D.S. et al. *Biomed Res. Int.* 935852 (8 pp), 2013.
56. Kaur, P., & Satyanarayana, T. *World J. Microb. Biot.* **20**, 419--425, 2004.
57. Tyebkhan, G. *Indian J. Pediatr.* **69**, 767--769, 2002.
58. Wiley, B.Y., et al. *Chem. Eur. J.* **11**, 454--463, 2005.
59. Kapoor, M., & Gupta, M.N. *Process Biochem.* **47**, 555--569, 2012,.
60. Mendes, A.A., et al. *J. Mol. Catal. B. Enz.* **78**, 119--134, 2012.
61. Li, S., et al. *J. Chromatogr. B* **846**, 291--297, 2007.
62. Hermoso, J., et al. *J. Biol. Chem.* **271**, 18007--18016, 1996.
63. Sharma, M., et al. *Indian J. Biotechnol.* **7**, 328--332, 2008.
64. Jiang, Y., et al. *AIChE J.* **58**, 1203--1211, 2012.
65. Gupta, P., et al. *Res. J. Microbiol.* **6**, 281--288, 2011.
66. Kalantari, M., et al. *J. Mater. Chem.* **22**, 8385--8393, 2012.
67. Tan, T., et al. *Biotechnol. Adv.* **28**, 628--634, 2010.
68. Wu, C-S., et al. *Chem. Commun.* **47**, 7446--7448, 2011.
69. Dmitry, G., et al. *Annu. Rev. Mater. Res.* **40**,345--62, 2010.
70. Nagaoka, Y., et al. *Small*, **8**, 843--846, 2012.
71. Katz, E., & Willner, I. *Angew. Chem. Int. Ed.* **43**, 6042--6108, 2004.
72. Huang, Z., et al. *Sci. Rep.* **1**, 148 (5 pp), 2011.
73. Li, D., et al. *Science* **336**, 1014--1018, 2012.
74. Liao, H-G., et al. *Science* **336**, 1011--1014, 2012.
75. Liu, L., Li, L., Sun, J., Liu, P., Zhang, X., & Zhang, J. Influence of ultrasonic treatment on the activity and conformation of porcine pancreas lipase, in 5th International Conference on Bioinformatics and Biomedical Engineering (iCBBE 2011), Wuhan, China, 1--4.
76. Dyal, K., et al. *J. Am. Chem. Soc.* **125**, 1684--1685, 2003.
77. Lei, L., et al. *Mater. Chem. Phys.* **125**, 866--871, 2011.
78. Maruyama, T., et al. *Org. Biomol. Chem.* **21**, 524--527, 2004.

79. Bassani, G., et al. *Colloid Surf. B* **75**, 532--537, 2010.

80. Xiu, Z-M., et al. *Nano Lett.* **12**, 4271--4275, 2012.

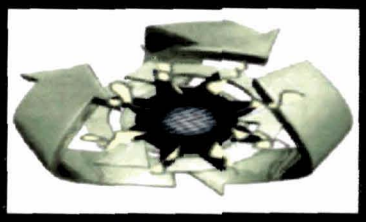

Chapter 3

Preparation of polymer-assisted silver nanoparticles by greener route and bio-nano interfacial action

HIGHLIGHTS OF THE CHAPTER*

In this chapter, bio-resource based preparation and characterization of silver nanoparticles dispersed in starch matrix (instead of PEG as reported in the previous chapter) is scrutinized. Evaluation of phytotoxicity on *Cucumis sativus,* compromise on amplification of a 263 base pair mammalian DNA sequence in PCR and anti-microbial potency (descripted in subchapter 3A) attested the differential action of starch templated silver nanostructure with branched morphology (~440 nm, along the long axis with average branch diameter of 11.5 nm) (generated on aging) and spherical silver nanoparticles (average diameter, 5.4 nm), prepared using the reductive potency of *Mesua ferrea* Linn. leaf aqueous extract under ambient conditions. On the other hand, subchapter 3B focuses on the anti-lipid peroxidation (using goat liver homogenate), DPPH scavenging, synergy with Rifampicin against *Bacillus subtilis* MTCC 736 and cytocompatibility with THP-1 cell line, of starch templated silver nanoparticles (3-12 nm), prepared using the reductive potency of aqueous extract of orange peel. Thus, this chapter gives a peek into few *in vitro* actions of starch assisted silver nanoparticles (prepared used bio-resources) as a function of the shape-size-surface chemistry accord.

*Parts of this chapter are published in

1. Konwarh, R., & Karak, N., et al. *Carbohyd. Polym.* **83**, 338--345, 2010.
2. Konwarh, R., & Karak, N., et al. *Colloid Surf. B* **87**, 1983--1992, 2010.
3. Konwarh, R., & Karak, N. *Adv. Colloid Interface Sci.* (Communicated)

3A. BIO-NANO INTERFACIAL ACTION OF SONICATED AND AGED STARCH-SILVER NANOPARTICLES PREPARED THROUGH A GREEN ROUTE

3A.1. Introduction

The accord of the medical world and material science is continually strengthened by the ever widening spectrum of applications of Ag NPs. However, many of the conventional methods[1] for their generation rely on the use of organic solvents and toxic reducing agents like sodium borohydride and N, N-dimethylformamide. For cleaner preparation of these noble metal nanoparticles, various biomimetic approaches are being explored.[2,3] As highlighted in Chapter 1, green technology, in the niche of nanomaterial preparation stands for switching to environmentally benign starting materials, water as the reaction medium, a biodegradable polymer as the stabilizing template and minimal wastage in terms of energy and raw materials.[4]

It is pertinent to mention that carbohydrate templated AgNPs have carved a unique niche in the domain of nanobiotechnology[5] with an immense spectrum of applications particularly as antimicrobial bio-polymer nanocomposite. As noted in the previous chapters, macromolecules, when used for encapsulation or entrapment of inorganic particles ensures enhanced compatibility, reduced leaching and protection of the surfaces from damage with concomitant improvement in dispersion and stability of the nanoparticles.[6]

In subchapter 2B of the previous chapter, the exploitation of *Mesua ferrea* L. aqueous leaf extract as reducing agent, adjusted to basic pH was reported for the preparation of PEG-AgNPs. The leaf components including friedelin and triterpenes of the friedelin group, namely canophyllal, canophyllol and canophyllic acid are envisaged as active components for the generation of the nanoparticles.[7]

Delving into the action at bio-interface of silver nanoparticles, prepared using a bioreductant and assisted by a green/biobased polymer seems to be interesting proposition in the contexts of green nanotechnology and nanotoxicology. The templating attribute of starch- a bio-based polymer in lieu of the previously reported polymer *i.e.*, PEG is reported in this work. The right-handed helical conformation of

starch in aqueous solution, with extensive number of hydroxyl groups can facilitate the complexation of metal ions to the molecular matrix. The green capping and stabilizing attribute, morphology-directing action and effective reductive potency of starch under microwave-assistance or hydrothermal energy for generation of nanoparticles have already been exploited.[8-12] In this work, the use of starch as templating matrix and the reductive potential of *Mesua ferrea* L. leaf aqueous extract are reported for the preparation of AgNPs at ambient temperature, eliminating the additional energy input. The effects of aging and sonication on the shape-size accord of AgNPs were assessed. Statistical optimization of the various sonication parameters has been devised to obtain narrow-sized Ag NPs, as indicated by λ_{max} position in the UV-visible spectra.

Preparation of nanoparticles through 'green' routes also demands adequate eco-toxicological testing and establishment of biocompatibility before their commercialization, particularly for biomedical-niche applications. Limited phytotoxicity studies have reported both positive and negative effects of nanoparticles on higher plants. Seed germination and root elongation is a rapid and widely used acute phytotoxicity test with several advantages: sensitivity, simplicity, low cost and suitability for unstable chemicals or samples.[13, 14] It is expected that starch (a biopolymer that is commercially extracted from plant sources) supported nanomaterial should be biocompatible with plant species. However, this may not be the case always. In order to evaluate this, the phytotoxicity of the prepared samples (the unsonicated/aged and the sonicated) was assessed on *Cucumis sativus* (cucumber), a plant among the 10 recommended species by USEPA (1966) for the determination of ecological effects of pesticides and toxic substances.

Polymerase Chain reaction (PCR) is used to amplify a single or few copies of a piece of DNA across several orders of magnitude, generating a library of copies of the particular DNA sequence. Compromise with the replication fidelity of DNA in PCR is a recently reported tool to assess preliminary genotoxicity of nanoparticles. It has been reported that silver nanoparticles of food storage material interfere with DNA replication fidelity and bind with DNA, visualized through atomic force microscopy.[15] In the present investigation, a mammalian 263 base pair target sequence was used in order to assess the potential toxicity of the prepared samples. Furthermore, the starch templated silver nanoparticles were assessed for their antimicrobial potency.

Thus, in this subchapter, the templating behaviour of a biomacromolecule *i.e.*, starch for silver nanoparticles under different conditions is reported. The correlation of

shape, size and concentration of the biomacromolecule templated silver nanoparticles with their bio-action has been delved into.

3A.2. Experimental

3A.2.1. *Materials for the preparation of starch supported silver nanoparticles*

The materials used for the preparation of the nanoparticles were the same as descripted in section 2B.2.1. However, soluble starch (Qualigens®) was used for the stabilization of the nanoparticles instead of PEG. It is pertinent to mention that starch (derived from Middle English *sterchen*, meaning to stiffen), a bio-macromolecule of glucose units, consists of two types of molecules – the helical amylose (Fig.3A.1a) and the branched amylopectin (Fig.3A.1b). It acts as the prime energy store in plants. The present work was executed to exploit this unique structure of starch in stabilizing silver nanoparticles prepared using the reducing potency of *M. ferrea* Linn. leaf extract under ambient conditions.

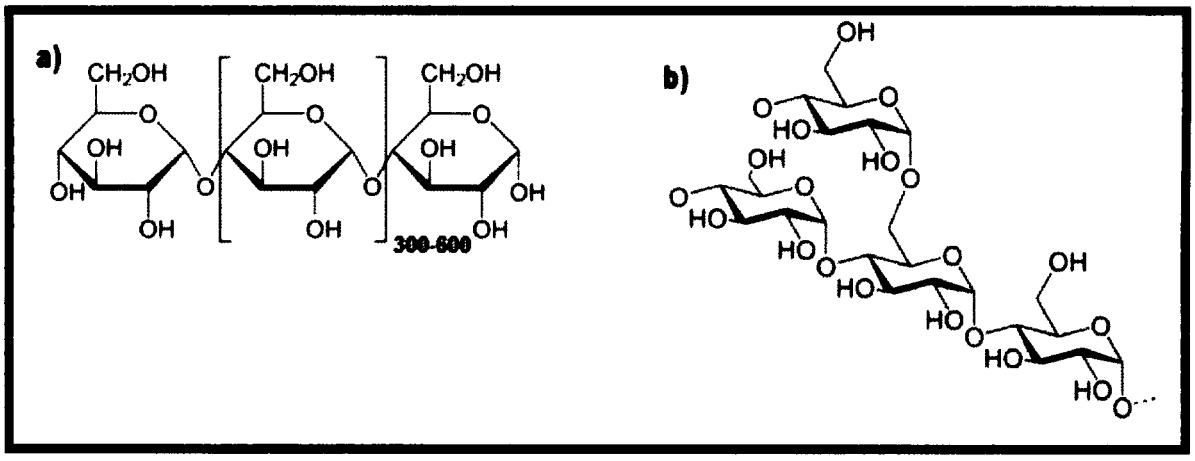

Fig.3A.1. *Structure of a) amylose and b) amylopectin*

3A.2.2. *Preparation of starch-AgNPs*

The polymer assisted silver nanoparticles were prepared according to the protocol given in section 2B.2.2 with a minor modification that involved the use of 5% (w/v, g/mL) soluble starch instead of PEG. The other steps remained essentially the same.

3A.2.3. *Statistical optimization of sonication parameters*

Ultrasonication was carried out with standard sonotrode (tip-diameter of 3 mm) in a high-intensity ultrasonic processor (UP200S, Hielscher Ultrasonics GmbH, Germany) in a beaker submerged in thermostatic bath at 4 ^{0}C. RSM was used to estimate the main effect of sonication on response *i.e.*, the λ_{max} peak position. Three factors with three levels consisting of 32 experimental runs were used to analyze the experimental data including five replicates at the center point.[16] Time of sonication (C_1), cycles (C_2) and amplitude percent (C_3) were chosen as the experimental factors or the independent variables capable of influencing the λ_{max} peak position (Y). Analysis was done using coded values (-1 for C_1=1 min, C_2=0.1 and C_3=30%; 0 for C_1=3 min, C_2=0.5 and C_3=60%; 1 for C_1=5 min, C_2=0.9 and C_3=90%). Using this design, the experimental data were fitted according to the equation (3A.1) as a second order polynomial equation including individual and cross effect of each variable.

$$Y = a_0 + a_1C_1 + a_2C_1^2 + a_3C_2 + a_4C_2^2 + a_5C_3 + a_6C_3^2 + a_7C_1{*}C_2 + a_8C_1{*}C_3 + a_9C_2{*}C_3 \quad \textbf{(3A.1)}$$

Where a_0, a_1, a_2, a_3, a_4, a_5, a_6, a_7, a_8, a_9 are the regression coefficients. Analyses were carried out in duplicates. The data tabulated (Table3A.1) were the average of the measurements. Multiple regression analysis, response surface plots and statistical analyses were performed using Minitab 15 Statistical Software® (Minitab Inc., PA, USA). After separating the matrix supported particles by centrifugal decantation, they were washed with Millipore water to remove the excess base and unreacted silver ions.

3A.2.4. *Instrumentation*

UV-spectra were recorded in Hitachi (U-2001, Tokyo, Japan) UV spectrophotometer. FTIR spectra for the samples were recorded in a Nicolet (Impact 410, Madison, WI) FTIR spectroscopy by using KBr pellets. Size and distribution of NPs were studied using JEOL, JEMCXII transmission electron microscope (TEM) at operating voltage of 100 kV.

3A.2.5. *Effect of the nanoparticles on amplification of DNA sequence in PCR*

The effect of AgNPs on PCR was performed by employing a human 263 base pair target sequence: F: 5′-GATTAGCATACTTAGACTACTAACCTCCATG-3′

R: 5′-GATCAACTTCTGGAAAAAGCATTCCCAC-3′.

The PCR consisted of an initial denaturation at 95 ^{0}C for 1 min, followed by 32 cycles of 30 s at 95 ^{0}C, 1 min at 58 ^{0}C and 1 min at 72 ^{0}C, and a final extension of 5 min at 72 ^{0}C. The amplicons were then run on 2% agarose gels pre-stained with ethidium

bromide. 50 base pair molecular marker (Fermentas) was used to analyse the size of the bands. It is to be noted that the execution of this experiment was performed in accordance to the guidelines set by Tezpur University Ethical Committee.

Table3A.1. *Observed and predicted values of response (λ_{max} peak position)*

Time of sonication (min)(C_1)	*Cycle (C_2)*	*Percent Amplitude (C_3)*	*Observed Response*	*Predicted Response*
-1	-1	-1	413.8	414.1
-1	-1	0	413.6	413.6
-1	-1	1	414.0	414.3
-1	0	-1	412.9	412.6
-1	0	0	412.5	412.1
-1	0	1	413.0	412.9
-1	1	-1	415.7	415.8
-1	1	0	415.4	415.4
-1	1	1	416.2	416.2
0	-1	-1	411.2	411.2
0	-1	0	411.0	410.8
0	-1	1	411.9	411.6
0	0	-1	410.0	409.6
0	0	1	410.6	410.0
0	1	-1	412.6	412.8
0	1	0	412.3	412.4
0	1	1	413.0	413.3
1	-1	-1	415.6	415.5
1	-1	0	415.4	415.2
1	-1	1	415.9	416.0
1	0	-1	413.6	413.8
1	0	0	413.2	413.5
1	0	1	414.0	414.4
1	1	-1	416.9	416.9
1	1	0	417.1	416.6
1	1	1	417.8	417.6

Table continued on the next page

0	0	0	409.0	409.2
0	0	0	408.8	409.2
0	0	0	408.9	409.2
0	0	0	408.8	409.2
0	0	0	409.9	409.2

3A.2.6. *Phytotoxicity analysis on Cucumis sativus*

The average germination rates of the *Cucumis sativus* seeds (confirming to the standard of Seed Act 1966) were greater than 92% as shown by a preliminary study. Seeds were kept in a dry and dark place at room temperature before use. These were surface sterilized in a 10% sodium hypochlorite solution for 10 min (USEPA 1996), followed by rinsing thrice with Millipore water. They were then soaked in Millipore-water or nanoparticle suspensions for about 2 h. One piece of filter paper was put onto each petri dish, and 5 mL of the test samples (unsonicated versus sonicated) was put into the respective petri dishes. Seeds were then transferred onto the filter paper, with 15 seeds per dish at 1 cm or larger distance between each seed. Petri dishes were covered and sealed with tape, and placed in an incubator. After 5 days of incubation in the dark under room temperature, more than 90% of the control seeds had germinated and developed roots that were at least 18 mm long. Then, the germination was halted, seed germination rate was calculated, and seedling root length was measured.

To examine which process (seed soaking or incubation after the soaking) primarily retarded the various developmental stages of the seedlings, three treatments were used: (A) both seed soaking and incubation were performed in nanoparticle suspensions; (B) seeds were soaked in nanoparticle suspensions for 2 h, and were then transferred into Petri dishes with 5 mL Millipore-water for incubation after being rinsed three times with Millipore-water; and (C) seeds were incubated in Petri dishes with 5 mL nanoparticle suspensions after being soaked in Millipore-water for 2 h. The germinated seeds were then transferred to beds prepared with sandy loam soil enriched with yard manure and compost. The shoot length was measured after 5 days. All studies were done in triplicates and results expressed as average of these. In conjunction to the above tests, the seeds were also soaked and incubated in the aqueous leaf extract to check any phytotoxic effect of the latter.

3A.2.7. *Evaluation of anti-microbial potency of starch-Ag NPs*

The samples were individually tested against a panel of microorganisms including *Staphylococcus aureus* MTCC96, *Bacillus subtilis* MTCC736, *Pseudomonas aeruginosa* PN1 and *Candida albicans.* The antibacterial tests were performed as described elsewhere[17] after some modification. Antimicrobial activity of samples was determined by the agar-well diffusion method. All the microorganisms mentioned above were incubated (37 ^{0}C, 24 h) by inoculation into Mueller Hinton broth. *C. albicans* was incubated in Sabouraud dextrose broth (30 ^{0}C, 48 h). The culture suspensions were prepared and adjusted by comparing against 0.4–0.5 Mc Farland turbidity standard tubes. Mueller Hinton Agar and Sabouraud dextrose Agar (20 mL) were poured into each sterilized petri dish (10 mm x 90 mm) after injecting cultures (100 µl) of bacteria and yeast and distributing medium in petri dishes homogeneously. For the investigation of the antibacterial and anticandidal activity, the samples were filtered through a 0.22 µm membrane filter. The two prepared samples at various concentrations were introduced into the wells (6 mm) in agar plates directly. Plates injected with the yeast cultures were incubated at 30 ^{0}C for 48 h, and the bacterial cultures were incubated at 37 ^{0}C for 24 h. At the end of the incubated period, minimum inhibitory concentration (MIC) for the respective samples was determined. Studies were performed in triplicates *against positive control of ampicillin (50 µg) for bacteria and Nystatin (10 µg) for Candida.*

3A.3 Results and discussion

3A.3.1. *Preparation and characterization of the starch supported 'green' branched and spherical silver nanoparticles*

No absorption peak was observed in UV-visible spectrum of Ag^{+} solution before addition of leaf extract, *i.e.,* reduction, which may be attributed to Ag^{+} ion's d^{10} configuration.[18] After the reduction process, nucleation is followed by auto-catalytic particle growth. Myriad parameters like particle size, shape, dielectric constant of the medium and surface adsorbed species determine the position and shape of the plasmon absorption.[19] UV-visible spectra give considerable information about the growth and shape-size accord of nanoparticles. It is pertinent to mention that the plasmon peak and the full-width of half-maximum (fwhm) depend on the extent of colloidal aggregation.[20]

Colloidal aggregation resulting in larger particle size often leads to red shift in the spectrum. However, the presence of polymer in the solution hinders the excessive nucleation and decreases the rate of growth. Recently starch stabilization of nanoparticle surfaces has been attributed to formation of nanoscopic domains with hydrophobic interior, which associates with the nano-particle surface, while the amylose hydrophilic surface is expected to confer solubility and steric stabilization.[21]

The formation and growth of Ag nanoparticles was not completed even after 72 h of aging. A progressive increase in the intensity of the SPR band at around 400–420 nm with aging time till 24 days could be seen (Fig.3A.2a). To monitor stability of the silver colloid, the UV-visible absorption of the colloid was recorded after different time-periods. There was no apparent change in peak position for three weeks, except for the increase of absorbance.

The influence of pH (Fig.3A.2b) could be directly visualized via the gradual colour change from almost transparent at pH 6.0 to light yellow at pH 8.0 and finally to deep brown at pH 13 (Fig.3A.2b inset). In acidic pH, the association among the active compounds of the leaf extract through H-bonding is expected to be more pronounced which stabilizes the structures and as a result of which these compounds are not effectively utilized in reduction process. This feature is reversed with increase in basicity. With the increase of pH upto 11.5, the intensity of the peak at 410 nm kept on increasing which indicated the progressive generation of the nanoparticles. However, further increase in the basicity of the medium resulted in a red shift of the peak position towards 430 nm, indicative of larger particle size due to overgrowth. It is important to note that very high alkaline condition of the medium may lead to weakening of the association (H-bonding) even for the starch matrix and thereby diminishing its templating potential to support small sized nanoparticles. This may explain the red-shift for the nanoparticles formed above pH 11.5. The samples prepared at pH 11.5 have been used for various analyses described underneath.

It was also interesting to note the decrease in intensity of the peak at 410 nm for the samples prepared corresponding to the progressive aging of the leaf extract used for reduction (Fig.3A.2c). The fresh extract gave the highest peak followed by that stored in the refrigerator at 4 ^{0}C and the least intense peak was observed for the extract stored at room temperature (ca. 25 ^{0}C). The influence of aging of the leaf extract may be bracketed together with the likely progressive aerial oxidation of the active reducing

components of the leaf extract, manifested via a dip in the SPR peak intensity of the generated silver nanoparticles.

It is important to mention that no characteristic silver's SPR peak was observed when starch alone was used at ambient conditions without the input of external thermal energy. This additional energy is required for the breakdown of starch to generate active -OH groups through release of glucose units for the reduction.

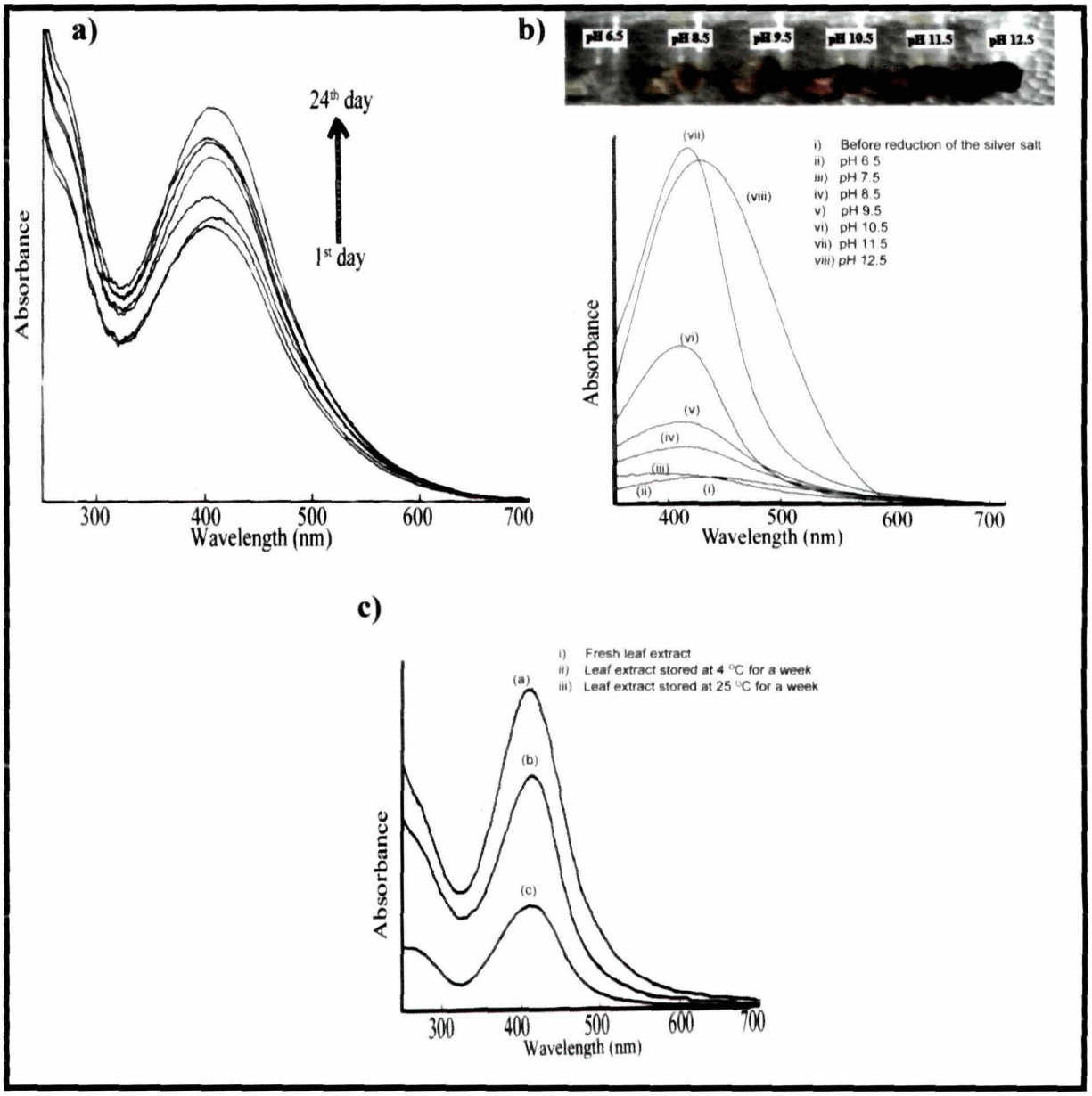

Fig.3A.2. *UV spectra of the starch templated silver nanoparticles (a) aged up to 24 days, (b) with variation of pH (the inset shows the colour variation of the silver nanoparticles at different pH) and (c) on aging and storage temperature of the leaf extract*

However, the monovalent silver ion is primarily reduced by -OH group of the active components of the leaf extract, which is oxidized to corresponding carbonyl

group, as indicated by the IR spectra (Fig.3A.3). The distribution of 72 h aged starch assisted silver nanoparticles within a size window of (1-24 nm) and average particle size of 8.75 nm (Fig.3A.4a) was indicative of non-coherent nucleation–a probable outcome of an interfacial mechanism of the reduction process.

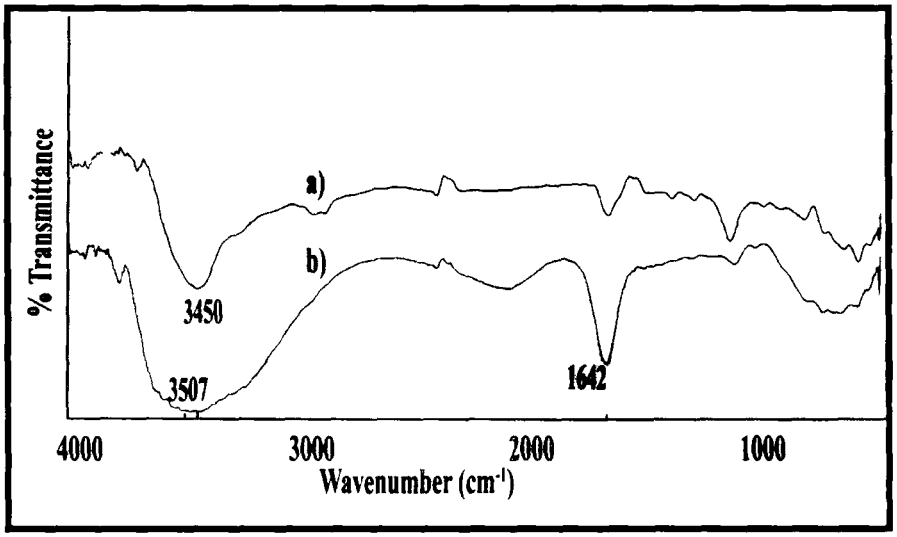

Fig.3A.3. *FTIR spectra of (a) Mesua ferrea L. aqueous leaf extract and (b) Mesua ferrea L. leaf extract and starch mixture after reduction of metallic silver*

During non-coherent or heterogeneous nucleation, the time dependence of the transformation rate is determined by the relative magnitudes of the nucleation and growth rates. Aging for about 24 days showed the formation of nanobranches with diameter of 11.5 nm, generating a branched structure with 440 nm length along the long axis (Fig.3A.4b). The leaf extract components and starch matrix interacted as evident from the FTIR spectra, indicated by the broadening of the band at around 3600-3200 cm^{-1} (Fig.3A.3). As such this complex structure may have acted as the morphology directing agent, promoted together by gradual nucleation.

With greater passage of the aging period (in the absence of any external agitation of the system), the interaction with the *Mesua ferrea* leaf extract components and the helical conformation and templating effect of starch might have directed the growth of nanobranches emanating from the central nanoparticle core, thereby generating the branched structure.

TEM images of the colloidal samples were recorded after evaporation of the solvent resulting in the non-extended conformation of the polymer. This might have also facilitated a greater aggregation. It is to be noted that the UV-vis spectrum of the system subjected to aging, as recorded in Fig. 3A.2a, is resulting from the solution phase or finely dispersed phase of the sample. The branched structure was most probably

absent in the sample used for recording the UV-visible spectra as its presence was expected to exhibit considerable red shift.

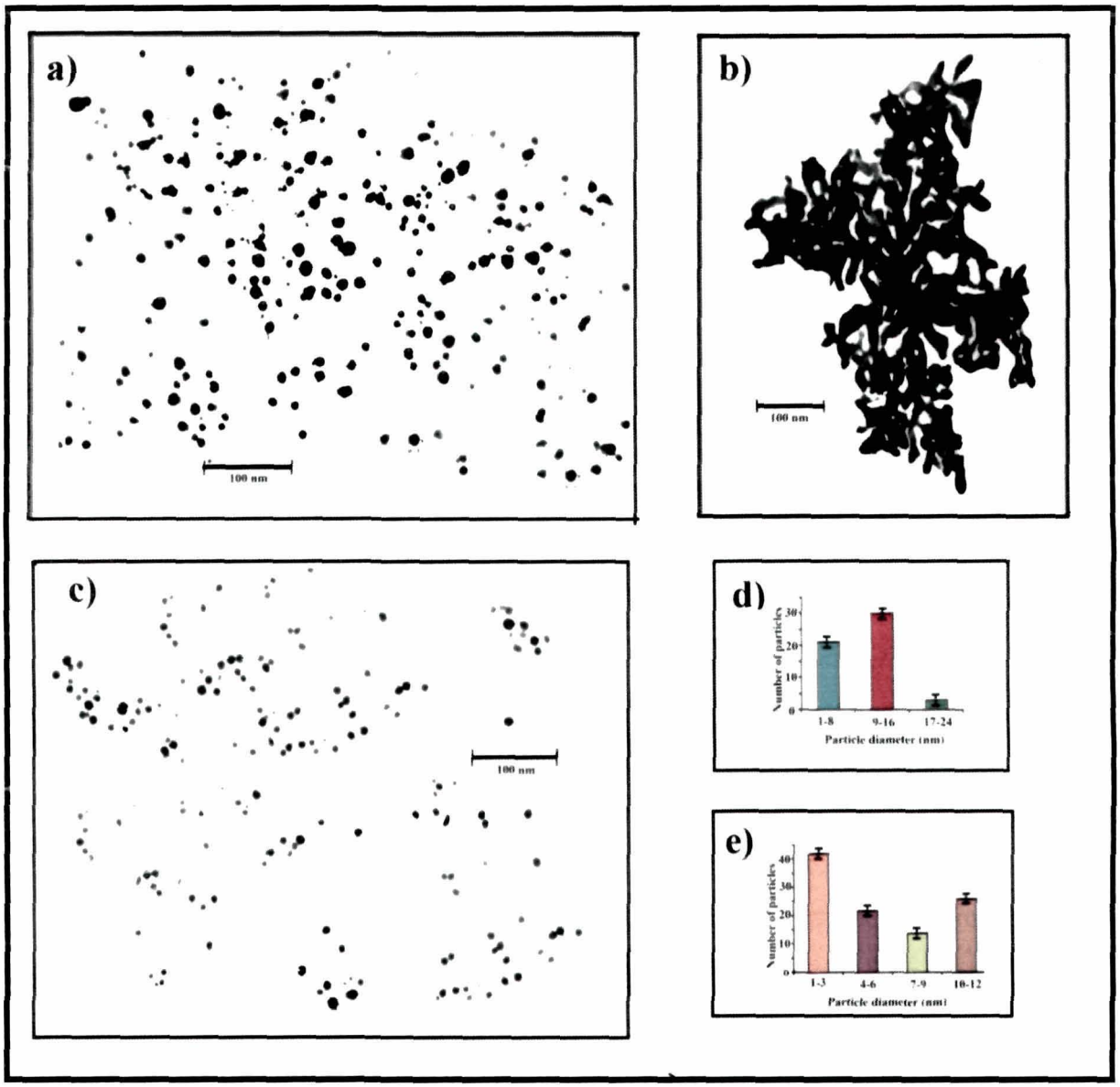

Fig.3A.4. *TEM image of starch supported silver nanoparticles obtained (a) on aging for 72 h (the particle size distribution, shown in (d)), (b) on aging for 24 days (branched silver nanostructure) and (c) under statistically optimized sonication parameters (the particle size distribution, shown in (e))*

It is established that the atoms in nanostructured metals tend to relax towards minimum free energy content from the grain boundaries and grain boundary joints. In these interfacial regions, orientational transitions, non-equilibrium atomic densities and coordination numbers reside.[22] The inter-crystalline volume represents a region of stored excess energy with respect to the bulk of a grain. The structure of grain joints

is unstable even at ambient temperature and tends to evolve towards a more ordered state, affecting the density of crystalline defects, grain size, crystallographic orientation and grain boundary structure. Under annealing, the nanosized crystallites may even start to grow in a random fashion; some of them act as nuclei and preferentially start to grow at the expense of the surrounding nanocrystalline material. Thus the present study leaves scope for the material scientists to delve into and validate these probabilities for the carbohydrate templated 'green' silver nanoparticles.

The separation or combination between two particles, exhibiting constant Brownian motion in a continuous solution is governed by the inter-particular net repulsive or attractive energies as well the nature of interfacial zone. To produce good silver particle dispersion in a solution, a change in the inter-particle interfacial region by either chemical or physical methods is necessary. Thus, an analysis of the effect of sonication, a physical strategy, on directing the shape- size parameters of the prepared nanoparticles was made. The influence of sonication with three variable parameters, namely, duration of sonication (min), cycle and percent amplitude on the shift of λ_{max} position in the UV-visible spectra of the samples was analysed statistically using response surface methodology (RSM).

The parameters of equation (3A.1), given in the experimental section were determined by multiple regression analysis. The overall second-order polynomial equation is represented as

$$Y = 409.2 + 0.689C_1 + 3.6C_1^2 + 0.811C_2 + 2.4C_2^2 + 0.228C_3 + 0.617C_3^2 - 0.083C_1*C_2 + 0.067C_1*C_3 + 0.05C_2*C_3 \quad \text{.....(3A.2)}$$

All the three chosen variables exerted both linear and quadratic effect on the λ_{max} position of the sample analyzed (Fig.3A.5). The model contained three two-way interactions (time of sonication*cycles, time of sonication*percent amplitude and cycles*percent amplitude). For each of these interactions, p-value was more than 0.05 (chosen α value) (Table3A.2) and as such these cross-interactions did not have a significant effect on determining the λ_{max} position.

The model yielded a R^2 value that could explain up to 98.76% of the sample variance, indicating a good fit of the data with the devised model. Minimum particle size was expected for the data set of 3 min of sonication, 0.5 cycle and 60% amplitude. Fig. 3A.4c shows the spherical shaped silver nanoparticles, homogenously distributed within a size window of 1–12 nm, with average diameter 5.4 nm, obtained under optimized sonication parameters with maximum number of particles between 1-3 nm.

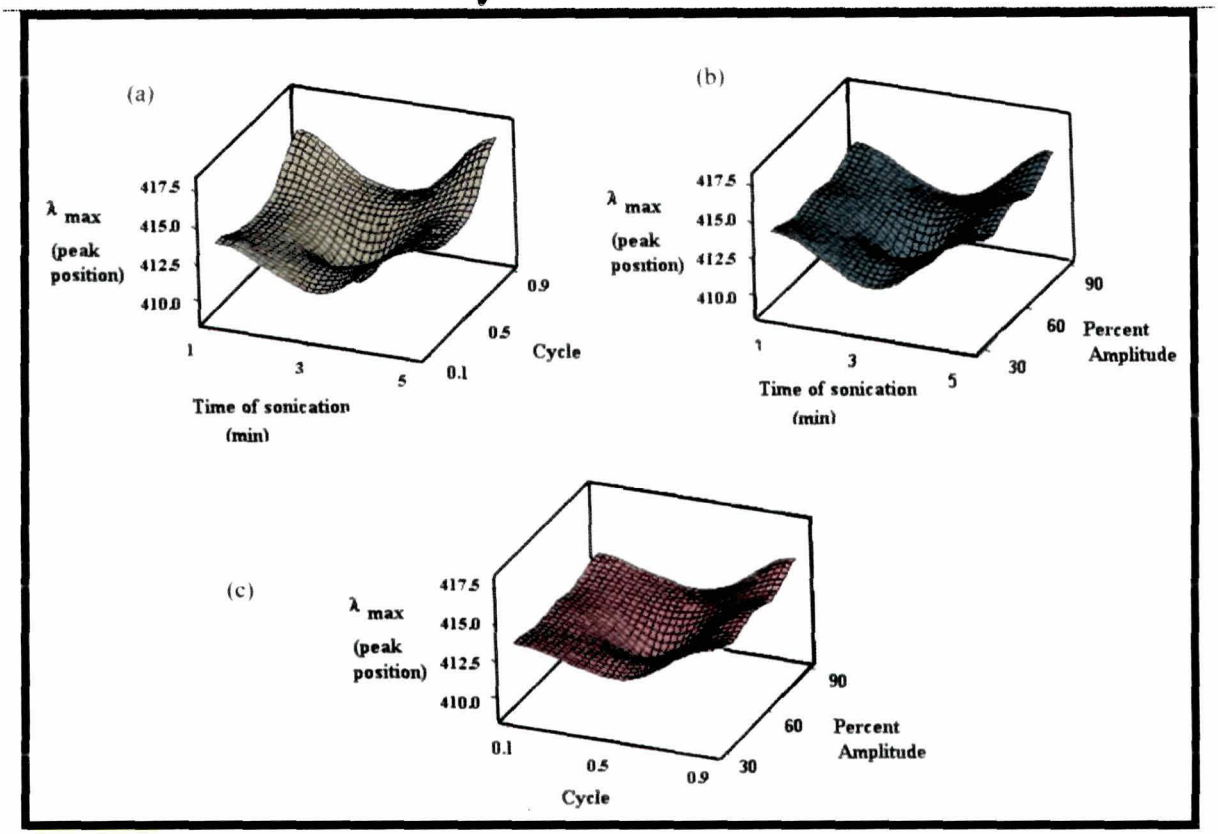

Fig.3A.5. *Response surface plots showing λ_{max} position versus (a) time of sonication versus cycles, (b) time of sonication versus percent amplitude and (c) cycles versus percent amplitude*

Sonication is a common strategy to obtain well dispersed nanoparticles within a narrow size window. However, it is critical to control the timing and amplitude. Too much energy input in the system can lead to increased inter-particular collision, resulting in formation of larger agglomerates and consequent red shift in the UV-visible spectrum. On the other hand, the aid for dispersion may be limited if optimal energy is not supplied to the system.

Table3A.2. *Model coefficients estimated by multiple regressions (model adequacy checking)*

Factor	*Co-efficient*	*t-value*	*p-value*
Constant	409.2	3450.79	0.000<0.05
C_1	0.689	8.282	0.000<0.05
C_2	0.811	9.751	0.000<0.05
C_3	0.228	2.738	0.012<0.05
C_1*C_1	3.6	27.284	0.000<0.05

Table continued on the next page

C_2*C_2	2.4	18.189	0.000<0.05
C_3*C_3	0.617	4.674	0.000<0.05
C_1*C_2	-0.083	-0.818	0.422>0.05
C_1*C_3	0.067	0.654	0.520>0.05
C_2*C_3	0.05	0.491	0.628>0.05

RSM aided in optimizing the sonication-parameters to obtain narrow-sized particles, correlated with observed blue shift. The choice of a second order polynomial regression model was satisfactory, and the estimation of coefficients by multiple linear regressions was a priori much more explanatory than that obtained by any classical analysis of variance.

It was interesting to note the stability of the system even for the samples analysed after 4 months of preparation and storage at room temperature as indicated by the retention of the peak sharpness and position at 408 nm with almost no red shift.

3A.3.2. *Action at the bio-interface*

The premonition of a differential shape-size influence of the prepared starch assisted silver nanoparticles on the action at the bio-interface dictated the assessment for phytotoxicity, anti-microbial action and the consequence of incubation of the samples with mammalian DNA sequence in PCR.

The preliminary genotoxicity test of the prepared silver nanoparticles, assessed through effect on PCR amplification showed a concentration dependent inhibition. Silver[23, 24] tends to have a high affinity for phosphorous- and sulfur-containing compounds such as DNA. As compared to the branched structure, the smaller sized particles in the sonicated sample with greater surface area may bind more efficiently with the DNA and as such interference with the replication machinery may be more profound than the former. This plausibility may be even complemented by their probable interaction with the polymerase enzyme. These need further insight and detailed *in-vivo* studies. In the presence of silver nanoparticles up to a concentration of 14 nM, there was no inhibition (for both the samples) of the PCR amplification when compared to the control band (Fig.3A.6a). The concentration of both the samples when increased to 50 μM showed complete inhibition. Therefore, on decreasing the concentration (Fig.3A.6b) for the unsonicated sample to 3.5 and 7 μM, the amplification was significantly less (R_1 and R_2) than the control (C) (without treatment with the silver nanoparticles) with no amplification at 14 μM (R_3).

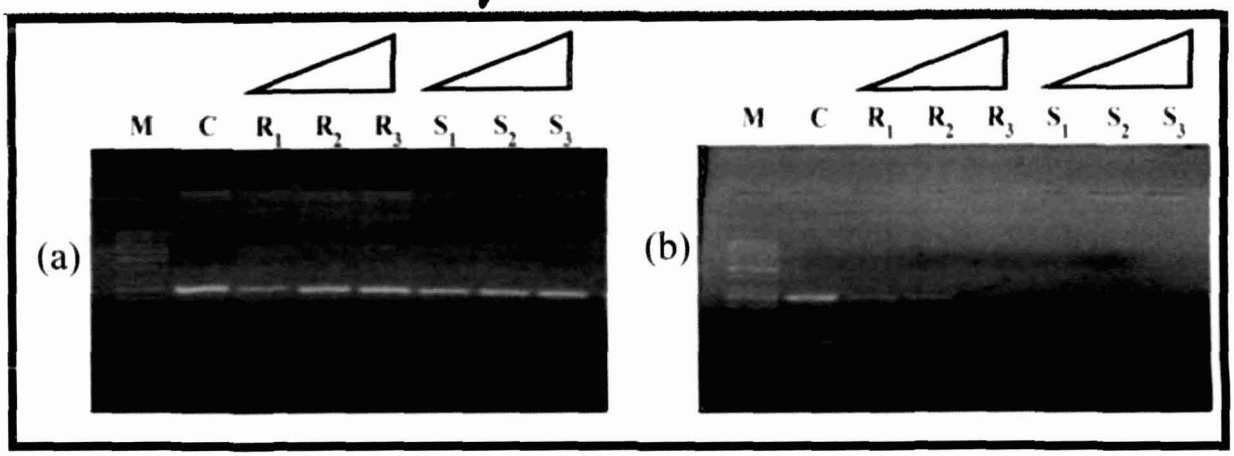

Fig.3A.6. *Gel electrophoresis of PCR amplified products. M, marker; C, control (untreated DNA); lanes (R_1, R_2 and R_3) and (S_1, S_2 and S_3), samples treated with (a) 3.5, 7, 14 nM and (b) 3.5, 7, 14 μM of branched and spherical silver nanoparticles respectively*

However, the same concentrations for the sonicated sample were completely inhibitory for the amplifications (S_1, S_2 and S_3) (Fig.3A.6b). As far as the aqueous leaf extract is concerned, no inhibitory action was noted in PCR. Nevertheless, this preliminary study did unveil the potential of the nanoparticles to become a risk factor especially when used at higher concentrations. Further tests into the effect of the silver nanoparticle on humans are important.

Plant seeds showing emergence of radicle or cotyledon coming out of the seed coat were recorded as being germinated in the present experiment. Prior to membrane invagination in plant cells, exotics penetrate through the semi-permeable cell wall, primarily composed of polymeric carbohydrates with pore size less than several nanometers.[25] Investigation of the modulation of the phyto-physiology due to such possible penetration of the silver nanoparticles was an interesting proposition. From the phytotoxicity assessment, it could be inferred that minor variations did exist in the interaction and penetration of the samples through the seed coat. The size and shape factors of the samples could be correlated to the average germination rate of the seeds. As shown in Table 3A.3, the sonicated sample decelerated the average germination rate as compared to that for the unsonicated sample.

Interestingly, the three treatments (as descripted in the experimental section) did show minor variations. Treatment B for both the samples showed germination rate parallel to that of the control (without any treatment). However, treatments A and C inhibited the germination rate to greater extent and in particular for the sonicated

sample. In order to further validate whether the process of soaking or incubation led to inhibition, the soaking time was increased from 2 to 8 h and almost similar rate of inhibition was found. Thus, the incubation parameters seemed to be more critical than soaking conditions in deciding the phytotoxicity profile of the nanomaterials.

Table3A.3. *Phytotoxicity assessment of the prepared nanomaterials - ramified/unsonicated (R) and sonicated (S) silver nanoparticles on germination and growth of Cucumis sativus*

	In the Laboratory conditions				*In Field conditions*			
Process (for details, please refer to the text)	*Average germination rate (%) of the seeds*		*Average radicle length (mm) after 5 days incubation*		*Average survival rate (%) of seedlings 5 days post-transplantation*		*Average shoot length (cm) 5 days post-germination*	
	R	**S**	**R**	**S**	**R**	**S**	**R**	**S**
A	94	87	18	16	100	100	14	13
B	97	96	20	19	100	100	15	13.5
C	95	89	18.	17	100	100	14	12.5

The differential effect on the seed germination may be attributed to smaller size and spherical shape of the AgNPs in the sonicated sample that could be mobilized into the plant cells with greater ease as compared to the branched structure. Roots being the initial targets to confront with excess concentrations of pollutants, toxic symptoms seem to appear more in roots rather than in shoots.[26] Radicles, after penetrating the seed coats, could contact the nanoparticles directly. The tested samples did not show statistically significant variations in the root elongation. However, probably more internalization of the sonicated AgNPs did affect the radicle length to a greater extent in comparison to the unsonicated sample. Similar trend was noted for shoot-length elongation. However, no significant variations were noted for the survival percentage of the seedlings post-transplantation. It is to be noted that the aqueous leaf extract did not influence the seed-germination and the growth of the cucumber seedlings post transplantation.

However, certain questions still remain unanswered. Will the effect of the prepared samples and the consequences of the internalization and bio-distribution be

same for both dicot and monocot plants? Does the penetration of Ag NPs into the root cells help the plants to ward off soil pathogens or lead to the loss of beneficial microflora peripheral to the roots? Furthermore, investigation is needed to clarify the contribution of dissolution to the toxicity of metal-based nanoparticles.

The prepared samples exhibited anti-microbial activity against a panel of test-organisms. A number of interesting results emanated from the experiment. The antimicrobial action was more pronounced against Gram positive bacteria (*Staphylococcus aureus* and *Bacillus subtilis*) than Gram negative bacteria (*Pseudomonas aeruginosa*). The samples showed anti-candidal activity as well. The MIC of the sonicated sample (6.32, 6.32, 25.3 and 12.65 μg/mL) was less as compared to the unsonicated sample (12.65, 25.3, 37.95 and 32.5 μg/mL) against *Staphylococcus aureus, Bacillus subtilis, Pseudomonas aeruginosa* and *Candida albicans* resepectively. Various mechanisms[27] have been propounded for the anti-microbial action of Ag NPs. These include, setting the cell membrane permeability out of gear primarily by immediate dissipation of the proton motive force and interaction with sulphur and phosphorus containing macromolecules like DNA and thereby affecting the replication machinery. The smaller particles in the sonicated sample with larger surface area not only might interact with the membrane surface but are likely to be more penetrating than the larger branched structure. Considering the surface area of prepared silver nanostructures, it was expected that if alteration of the membrane permeability is the main route of anti-microbial action, the spherical particles should have been multi-times potent than the branched structure. The MIC values of the sonicated sample were expected to be significantly less when compared to that of the branched structure. The MIC data showed that the shape of the nanoparticles has a critical role to play. The branched architecture might have helped in confining of the microorganisms for a longer duration than the mobile spherical particles. Furthermore, antimicrobial action was more pronounced against Gram positive bacteria than Gram negative bacteria. This may be due to the differential interaction of the AgNPs with the molecular moieties at the surface of the two groups of the bacterial species and probably the overall different cell-wall architecture influences the anti-bacterial action. The above results shore up the inclusion of these silver nanoparticles in various materials like paints and industrial coatings. However, further toxicity assessment of these prepared samples is a must.

3A.4. Conclusion

In the present work the morphology directing action of starch-*Mesua ferrea* L. aqueous leaf extract complex was documented to generate branched nanostructure, obtained on aging. On the other hand well dispersed silver nanoparticles (obtained upon statistical optimization of sonication parameters) hold promise for multitude of application-oriented utilities. The shape-size-concentration accord of the prepared starch templated silver nanoparticles was attested by the differential effect on various biosystems (*Cucumis sativus*, mammalian DNA and bacterial and fungal species). The reported system supports the switching over to bioresources (*viz.*, starch and bioreductant in this case) for achieving easy and inexpensive shape-size tuning of nanoparticles. However, the results show that mere opting of greener route may not be the dead end but calls for compilation of comprehensive toxicity profile.

3B. BIORESOURCE MEDIATED PREPARATION OF STARCH-SILVER NANOPARTICLES: ACTION AT BIO-INTERFACE

3B.1. Introduction

The recent global impetus is on making the nanoscale-research greener[27, 28] and this aspect has already been highlighted in the first chapter as well as in the previous subchapter, 3A. In subchapter 2C of the previous chapter, the exploitation of orange peel aqueous extract as reducing agent, adjusted to basic pH was reported for the preparation of poly(ethylene glycol) (PEG) supported AgNPs. In continuance of the previous endeavours, the reductive potential of orange peel (a common waste material of the food processing industry) has been exploited to prepare starch supported silver nanoparticles under ambient conditions. The compositional abundance of pectins, flavonoids, ascorbic acid, sugars, carotenoids, limonene and various other flavones[29, 30] in the epicarp of various *Citrus* species has been reported. Different *in vitro* assays in brain homogenates have been used to establish the excellent antioxidant potency of the various polar fractions of orange peel.[30] These components may be envisaged for the effective reductive potential of orange peel to generate silver nanoparticles by a greener route.

Free radicals, leading to oxidative stress can cause biological havoc. Jain et al. [31] have reported that antimicrobial gel formulation containing silver nanoparticles elicit oxidative stress with subsequent triggering of the cellular anti-oxidant system. On the contrary, a crucial role of novel Ag^+-loaded zirconium phosphate nanoparticle in diabetic wound healing has been documented.[32] Thus, investigating the free radical scavenging potency of the green silver nanoparticles forms an interesting proposition. Furthermore, tunable antibacterial coatings with silver nanoparticles, generated through *in situ* route, which support mammalian cell growth, have been developed.[33] Establishing the biocompatibility of the reported 'green' silver nanoparticles is important in the context of their biomedical utility.

This work is concerned with the utilization of the reduction potency of orange peel for the preparation and characterization of the starch supported silver nanoparticles. Furthermore, their anti-lipid peroxidation activity, free radical

scavenging potency, anti-bacterial action using *Bacillus subtilis* as the test organism and the cytocompatibility with human leukemic monocytic cell line (THP-1) are also evaluated.

3B.2. Experimental

3B.2.1. *Materials for the preparation of starch supported silver nanoparticles*

The materials used for the preparation of the nanoparticles were the same as mentioned in 3A.2.1. The reductive potency of aqueous extract of orange peel (as descripted in section 2C.2.1) exploited for the generation of the Ag NPs.

3A.2.2. *Preparation of starch-Ag NPs*

The polymer assisted silver nanoparticles were prepared according to the protocol given in section 2C.2.2 with a minor modification that involved the use of 5% (w/v, g/mL) soluble starch instead of poly(ethylene glycol). The other steps remained essentially the same.

3A.2.3. *Instrumentation*

UV-spectra of the samples were analysed in Hitachi (U-2001, Tokyo, Japan) UV spectrophotometer. FTIR spectra for the samples were recorded in a Nicolet (Impact 410, Madison, WI) FTIR spectrometer by using KBr pellets. An X-ray diffractometer, 'Miniflex' (Rigaku Corporation Japan), was used for the analysis of film sample at room temperature (approx. 23 ^{0}C). The scanning rate of 5.0^{0} min^{-1} over the range of 2θ =10–90^{0} was used. Size and distribution of nanoparticles were studied using JEOL, JEMCXII transmission electron microscope (TEM) at operating voltage of 100 kV.

3B.2.4. *Anti-lipid peroxidation assay*

Goat liver, used for anti-lipid peroxidation (ALP) assay, was collected from slaughter house immediately after slay and the experiment was conducted within 1 h after the collection. Mammalian liver was rinsed with phosphate buffered saline (PBS) to get rid of the residual blood, and 0.9 mL of 1.5 g L^{-1} KCl solution was added to 100 mg liver tissue to make 100 g L^{-1} homogenates of liver, then stored at -20 ^{0}C .The anti-lipid peroxidation assay in the goat liver homogenate was measured according to the method used by Mandal and Chaterjee[34] after slight modification. 2.8 mL of 10% goat liver

homogenate, 0.1 mL of 50 mM $FeSO_4$ and various volumes of the polymer supported green silver nanoparticles were mixed together with a micro-stirrer. The mixture was then incubated for 30 min at 37 ^oC. 1 mL of this mixture was taken with 2 mL of 10% TCA-0.67% TBA in acetic acid (50%) to stop the reaction. This was followed by boiling for 1 h at 100 ^oC and subsequent centrifugation at 10,000 rpm for 5 min. Absorbance of the supernatant was recorded at 535 nm against the reagent blank. Identical experiments were performed to determine the absorbance of the control (without the nanoparticles and $FeSO_4$) and induced (without the nanoparticles) peroxidation. Vitamin C was used as the standard in this study. ALP percentage was clculated using the following formula

$$\%ALP = \{(Abs_a - Abs_t) / (Abs_a - Abs_c)\} \times 100 \quad \text{..... (3B.1)}$$

Where, Abs_a =Absorbance of Fe^{2+} induced peroxidation, Abs_t=Absorbance of test sample and Abs_c=Absorbance of control

3B.2.5. *DPPH scavenging assay*

Antioxidant activity was also measured by using the modified DPPH method as reported previously.[35] 20 µL, 50 µL, 100 µL, 150 µL and 200 µL of the polymer supported nanoparticles were mixed with 2 mL of 100 µM DPPH solution. The samples were vortexed and allowed to scavenge DPPH in dark for 30 min. The absorbance of the supernatants post centrifugation at 9200 g for 2 min was measured at 517 nm in UV-visible spectrophotometer. In all the cases, measurements were done in triplicates. The scavenging percentage was calculated using the formula:

$$DPPH\ scavenging = \{(A_C - A_S) / A_C\} \times 100 \quad \text{....(3B.2)}$$

where A_C and A_S are absorption of blank DPPH and sample mixed DPPH at 517 nm, respectively.

3B.2.6. *MTT assay*

The human leukemic monocytic cell line (THP-1) was obtained from the National Center for Cell Sciences (NCCS), Pune, India and used for the cytotoxicity analysis. THP-1 cell line was maintained in RPMI-1640.[36] For this test, briefly, 1×10^5 cells mL^{-1} at the exponential growth phase were placed in a flat-bottomed 96-well polystyrene-coated plate and were incubated for 24 h in a CO_2 incubator at 5% CO_2 and 37 ^oC. 14.1 µM, 56.4

μM and 98.7 μM of the starch supported nanoparticles were introduced into the medium. Each concentration was added to the plate in triplicates. After termination of the incubation period, 100 μL of MTT solution (5 mg mL^{-1}) was added to the wells. The plates were wrapped in aluminium foil and incubated for 4 h in the CO_2 incubator. This was followed by dissolution of formazon crystals formed in the respective wells in 100 μL of DMSO and 25 μL of glycine buffer (to adjust the pH). Absorbance at 540 nm was recorded in ELISA plate reader (Eppendorf Biophotometer Plus Hamburg, Germany). Wells with complete medium, nanoparticles, and MTT, but without cells were used as the blank for each case. All experiments were performed twice in triplicates, and the average of all the experiments has been shown as a cell-viability percentage in comparison with the control experiment, while silver untreated controls were considered as 100% viable.

3B.2.7. *Anti-bacterial assay*

Bacillus subtilis MTCC 736 was used to evaluate the antimicrobial potency of the prepared nanoparticles. Nutrient agar (1.5%) was prepared by dissolving 5 g of peptone, 5 g of beef extract, 8 g of NaCl and 15 g of agar in 1 L of water, followed by autoclaving under 15 lbs pressure at 121 ^{0}C for 20 min. The media was poured onto sterilized petri plates and allowed to solidify. In similar lines, the soft agar was prepared (0.7%) and when it had acquired a temperature of about 35 ^{0}C, it was inoculated with the bacterial culture in the ratio of 1:10 (v/v). About 25 μL of the inoculum was poured onto the agar plates. After the agar had solidified, wells were punched as per the requirement. The silver nanoparticles at various concentrations (Table3B.1) were vortexed with desired Rifampicin concentration for 15 min. These combinations were injected into the wells with Rifampicin (1 mg mL^{-1}) as the positive control. After 24 h of incubation at 37 ^{0}C, the plates were checked for zones of inhibition. All experiments were done in triplicates.

3B.3. Results and Discussion

3B.3.1. *Preparation and characterization of the starch- silver nanoparticles*

In the present study, the first objective was to use the aqueous extract of orange peel to prepare starch supported AgNPs. The UV-visible spectra supported the successful green-route mediated generation of the silver nanoparticles. No absorption

peak was observed in UV-visible spectrum of Ag^+ solution before reduction. This is attributed to Ag^+ ion's d^{10} configuration. However, addition of the reducing agent adjusted to basic pH, led to gradual generation of silver nanoparticles as indicated by the progressive increase (till 45 min) in the absorbance intensity at around 400–410 nm in the UV-visible spectra. This is due to silver's surface plasmon resonance (SPR) (Fig. 3B.1). It is to be noted that the plasmonic coupling of metal nanoparticles with light augment a number of useful optical phenomena that finds application in ultra-sensitive biomolecular detection and lab-on-a-chip sensors.[36]

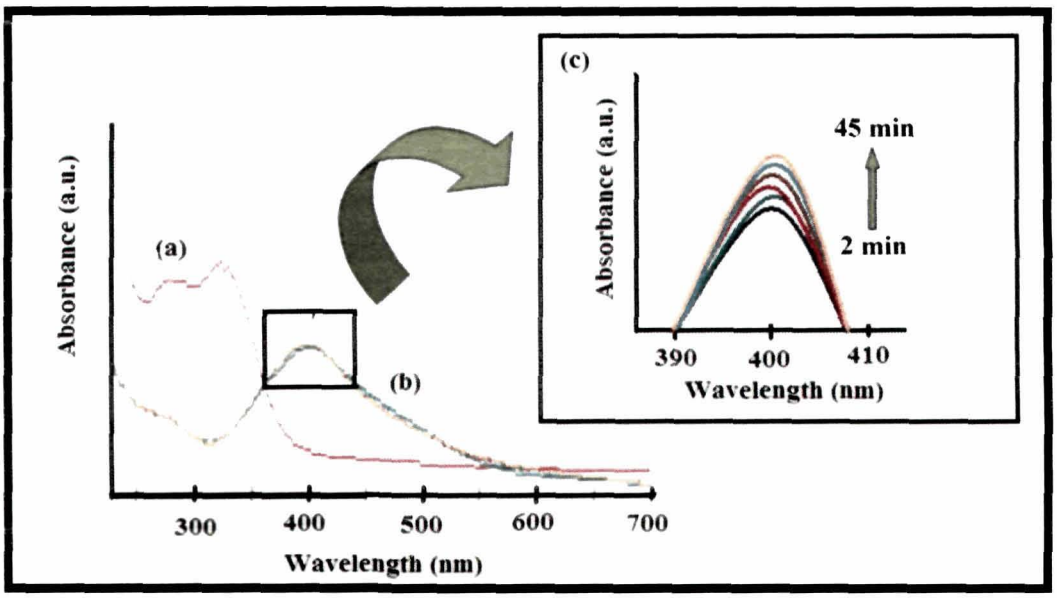

Fig.3B.1.*UV-vis spectra of (a) Orange peel extract and (b) starch templated Ag NPs, showing the Surface Plasmon Resonance at 404 nm. The inset (c) shows the progressive time course evolution of silver nanoparticles.*

It has been reported that the time required for completion of the reaction during biosynthesis of metal nanoparticles, (*i.e.*, complete reduction of the metal ions) using bacteria and fungi ranged from 24 to 124 h.[28] Gold nanoparticles, though of considerable size diversity (20-40 nm), have been prepared using *Geranium* leaves in 60 min, while a basic solution had reduced the time from 72 h to 1 h for the preparation of protein stabilized spherical silver nanoparticles by *Coriolus versicolor*.[28] Here the rapid generation of the nanoparticles (in about 45 min) owing to the excellent reducing potential of the orange extract and their polymeric stabilization within a narrow size spectrum with fine particle formation (discussed in the sections for TEM and XRD analyses) has clear advantages over the previously reported systems.

It is important to note that no characteristic silver's SPR peak was observed when starch alone was used at ambient conditions without the input of external thermal energy. This additional energy is required for the breakdown of starch to generate active –OH groups through release of glucose units for the reduction of the metal ions. In the present case, the monovalent silver ion was primarily reduced by –OH group of the active components of the peel extract, which was oxidized to corresponding carbonyl group.

As mentioned earlier, orange peel represents a complex storehouse of myriad of biomolecules (Fig.3B.2).

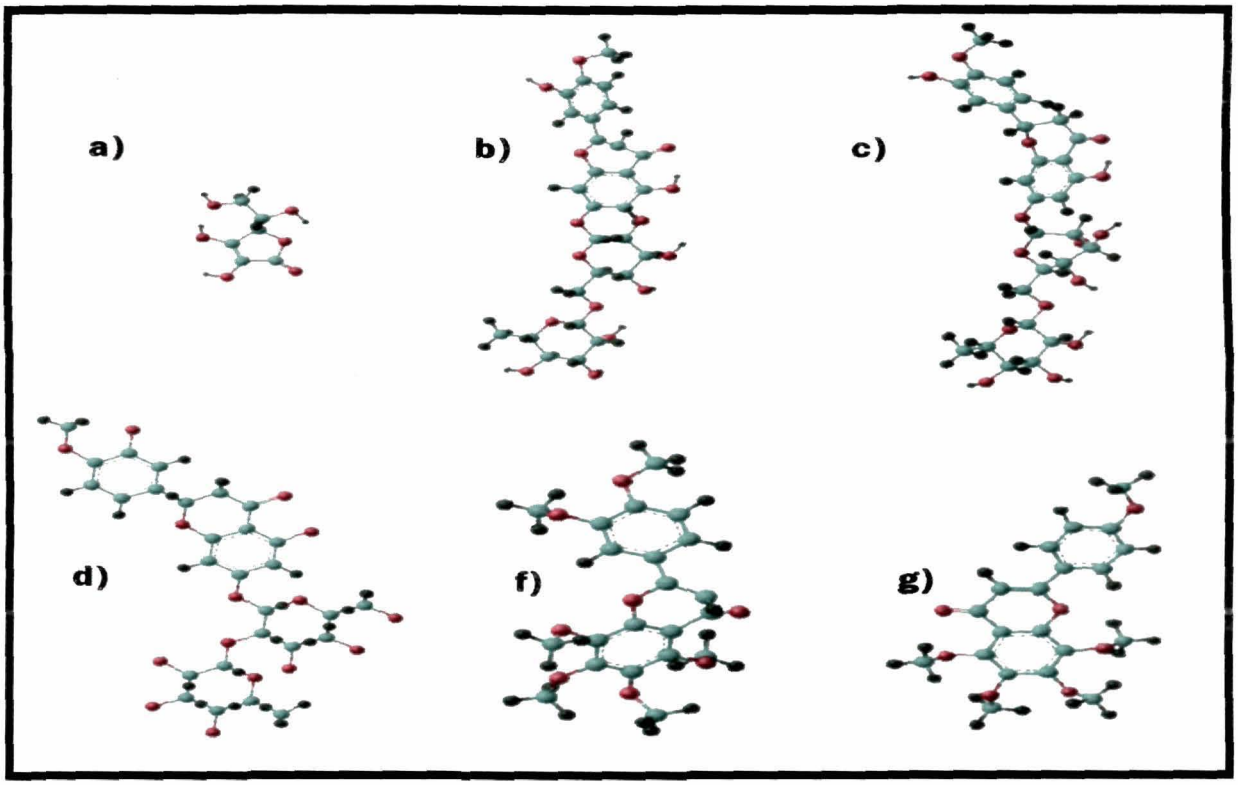

Fig.3B.2. *Few of the biomolecules present in the orange peel–a) Ascorbic acid, b) Diosmin, c) Hesperidin, d) Neohesperidin, e) Nobiletin and f) Tengeritin*

This includes ascorbic acid, vitamin A, flavonoid fractions, including hesperidin, neohesperidin, diosmin and various other polymethoxylated flavones like nobiletin and tangeritin (rarely found in other plants). It is very much likely that the reduction process of metallic silver is interplay of number of active components of the orange peel. For simplicity, let us consider the role of ascorbic acid as an effective reductant, illustrated in Fig. 3B.3.

$$2\,Ag^{+} + C_6H_8O_6 \rightleftharpoons 2\,Ag^{0} + C_6H_6O_6 + 2\,H^{+} \quad \text{...(3B.3)}$$

The silver ions in the starch matrix are predominantly stabilized by electrostatic interaction, while the narrow size and good dispersion of the silver nanoparticles in the

polymeric support is primarily attributed to steric stabilization. Furthermore, pH played an important role in dictating the reducing potency of the orange extract. It is pertinent to mention that under acidic conditions the active components of the peel extract are not effectively utilized for the reduction process. This may be due to their structural stabilization and association predominantly through H-bonding.

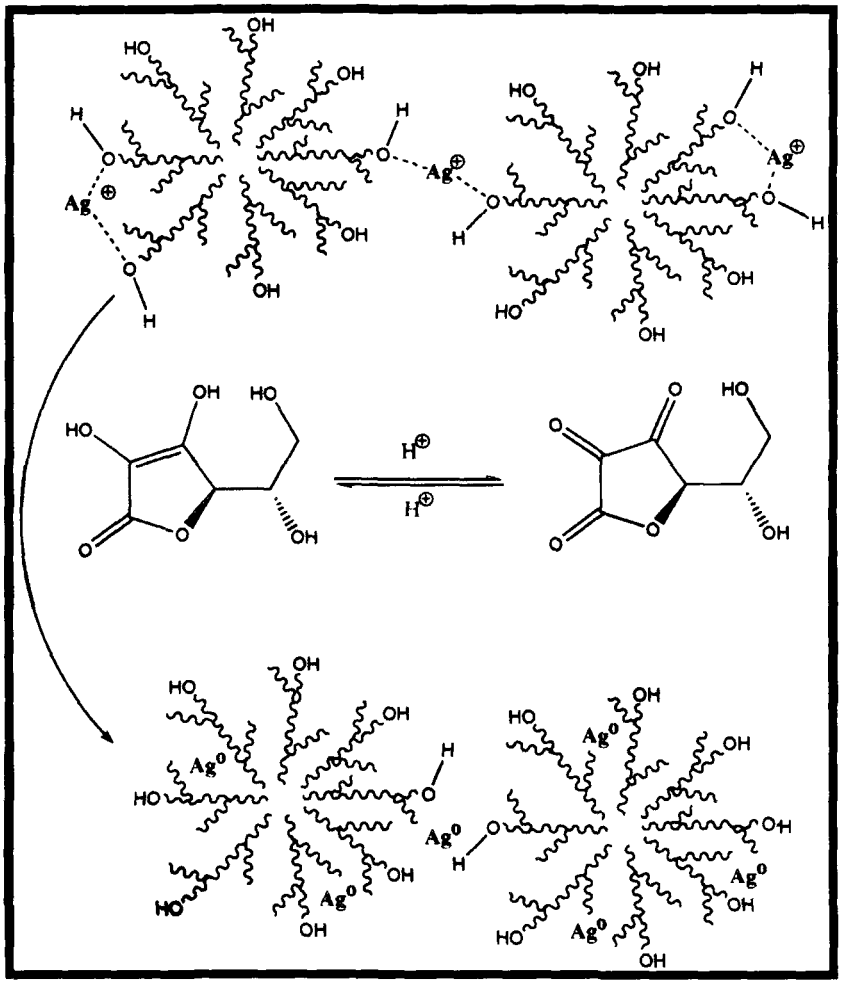

Fig.3B.3. *Probable mechanism of reduction of silver ion in starch matrix using ascorbic acid as representative effective reductant present in orange peel.*

The reduction potency of ascorbic acid (the biomolecule under consideration as effective reducing agent) also decreases under acidic condition for another reason. The nitrate group[37] (of the silver salt) at low pH, is a stronger oxidant than Ag^+ and can oxidize ascorbic acid as shown underneath.

$$NO_3^- + 4\,H_3O^+ + 3\,e^- \rightleftharpoons NO\uparrow + 6\,H_2O \qquad E_o = 0.96\ V \qquad \text{....(3B.4)}$$

$$Ag^+ + 1\,e^- \rightleftharpoons Ag^0 \qquad E_o = 0.799\ V \qquad \text{....(3B.5)}$$

$$NO_3^- + H_2O + 2\,e^- \rightleftharpoons NO_2^- + 2\,OH^- \qquad E_o = 0\ V \qquad \text{....(3B.6)}$$

However, these components are free to take part in the reduction under alkaline conditions due to dissociation of H-bonding. It was interesting to note that when no base was added to the system, the silver ion was not reduced by the extract at all, implying that there is an energy barrier for this reduction. Chou et al.[38] have proposed a two-step reaction mechanism to illustrate the role of alkaline ion in the synthesis of nanosized silver colloids using either formaldehyde or dextrose as the reducing agent. The alkaline ion reacted initially (the first stage) with silver ion to form Ag_2O. Its conversion to silver is instantaneous and the solution becomes acidic. In the next stage, the decrease in the silver ion concentration was gradual and continuous. The results observed in the present system could also be interpreted in similar lines. The UV-visible absorbance spectrum could be visualized just after 2 min post addition of all the reacting materials. However, after this the increase in the intensity was gradual and continuous.

There was corresponding increase in the UV-visible spectral peak intensity at 404 nm with the increase of pH up to 11. This was indicative of the progressive generation of the nanoparticles. Further increase in the basicity of the medium resulted in a red shift of the λ_{max} peak position indicative of larger particles. Very high alkaline medium may weaken the association (H-bonding) even for the starch matrix (also noted in the section 3A.3.1). This possibly diminishes the templating potential of the biopolymer to support small sized nanoparticles and may be bracketed together with the observed red-shift for the nanoparticles formed at pH above 11. The samples prepared at pH 11 have been used for various analyses described underneath. The common problem of agglomeration of nanoparticles upon storage was not observed in the present study due to the stabilization by the polymeric chains. This was indicated by the retention of the peak sharpness and position at 404 nm with almost no red shift (analysed after 3 months of preparation) on storage at room temperature. The X-ray diffractogram (Fig.3B.4) of the sample agreed well with the literature values for silver nanoparticles.

All the distinct peaks at 2 theta values of about 38, 44.5, 64.5, 77.5 and 82 representing the 111, 200, 220, 311 and 222 Braggs reflections of fcc structure of silver, confirms the formation of Ag nanoparticles.[39] These indexed peaks were compared with the JCPDS data file (4-783) indicating the presence of metallic silver in the *fcc* lattice. The average crystallite size was determined by Scherrer's formula (equation 2A.3). The

crystalline average domain size for the polymer assisted silver nanoparticles was found to be 5.29 nm

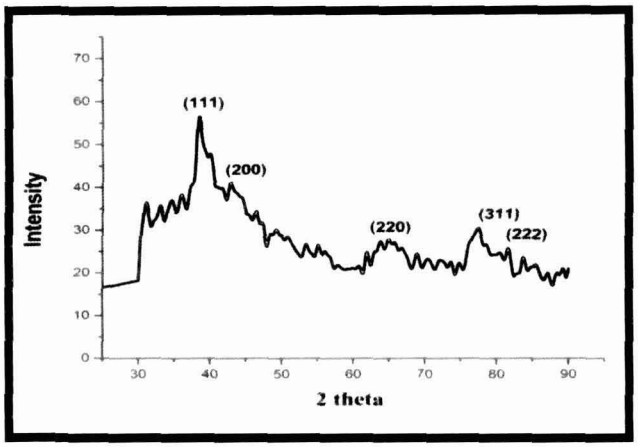

Fig.3B.4. *XRD pattern of the starch-Ag NPs*

TEM imaging (Fig.3B.5) shows well-dispersed spherical particles of 3-12 nm size. It was also interesting to note that the highest fraction of particles had a diameter of 6 nm.

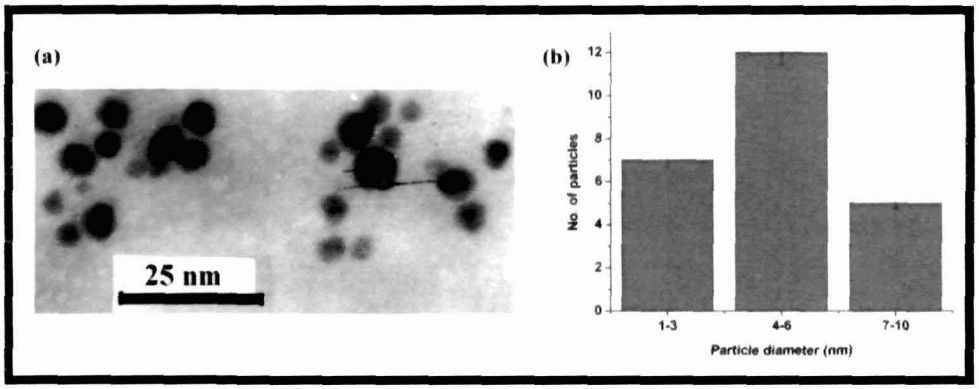

Fig.3B.5. *(a) TEM micrograph and (b) histogram showing the particle size distribution. Results represent mean ± S.D. of observations under three different fields*

3B.3.2. *Action at the bio-nano interface*

The free radical scavenging, antimicrobial potency and the cytocompatibility of the silver nanoparticles were evaluated in the present study. Fig.3B.6 highlights the linear correspondence of the percent anti-lipid peroxidation and the increasing volume of the silver nanoparticles. This raises the prospects of incorporating the prepared nanoparticles for development of topical antimicrobial formulation with added facet of free radical scavenging. The free radical scavenging potency of the silver nanoparticles is shown in Fig. 3B.7.

Numerous anti-oxidants of the orange peel act synergistically. During the preparation of the nanoparticles, these biomolecules are pooled into the system. These may get adsorbed onto the active surface of the noble metal nanoparticles reported here.

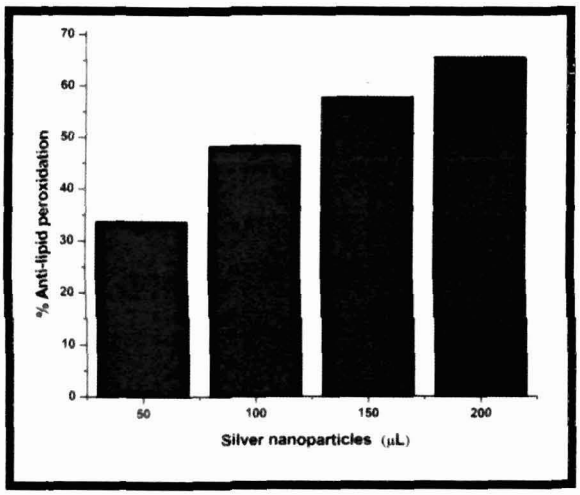

Fig.3B.6. *Anti-lipid peroxidation assay using goat liver tissue homogenate. Results represent mean ± S.D. of triplicate determination.*

With a high surface area to volume ratio and an ambient electrostatic field with anti-oxidant bio-moieties on the surface, these silver nanoparticles develop a high tendency to interact with and reduce DPPH like species.

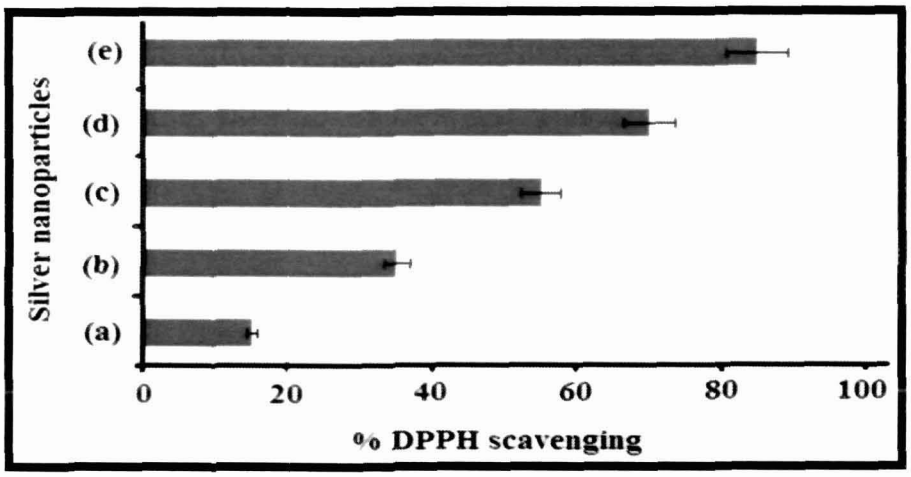

Fig.3B.7. *DPPH scavenging by (a) 20 μL, (b) 50 μL, (c) 100 μL, (d) 150 μL and (e) 200 μL of the starch supported Ag NPs. Results represent mean ± S.D. of triplicate determination*

Interestingly, Paul et al.[35] have recently documented anti-oxidant activity for iron oxide particles as a surface dependent property. The nanochemistry involved in this free radical scavenging attribute of nanoparticles needs further investigation but nevertheless, this facet of the noble metal nanoparticles can have profound impact in the domain of nanomedicine.

Nano-silver targets a broad spectrum of Gram-negative and Gram-positive bacteria including antibiotic-resistant strains.[40] It has been demonstrated that silver reactivity is favored by (111) facets.[41] Spherical silver nanoparticles (generally with cubooctahedral, multiple-twinned decahedral, or quasi-sperical morphology) have (100) facets along with a small percentage of (111) facets.[42] Spherical silver nanoparticles with (111) facets (which is also a characteristic feature of the nanoparticles reported here) attach directly to the bacterial surface of the cell membrane and are located inside bacteria.[43] Shahverdi et al.[44] have reported that the antibacterial activities of penicillin G, amoxicillin, erythromycin, clindamycin, and vancomycin were increased in the presence of Ag NPs against *Staphylococcus aureus* and *Escherichia coli*. The antimicrobial action of the prepared nanoparticles was tested against *Bacillus subtilis*. The antimicrobial potency of the silver nanoparticles was also investigated in presence of the antibiotic–rifampicin (Rif) in the wells of the agar plates. Rifampicin inhibits DNA-dependent RNA polymerase in bacterial cells, especially those that are Gram stain positive, by binding its beta-subunit, thus preventing transcription and subsequent translation.

Fig.3B.8 depicts representative culture plates showing antibacterial test. The mean zones of inhibition ± standard deviation observed in the anti-bacterial test have been represented in the Table3B.1. In the present study the antibiotic (20 μg) *i.e.*, the positive control produced a mean zone of inhibition of 20 mm (Fig.3B.8a1). The smaller zone of inhibition (14 mm) produced by the polymer templated nanoparticles (Fig. 3B.8a2) may be attributed to their lesser diffusion than the antibiotic in the agar plates.

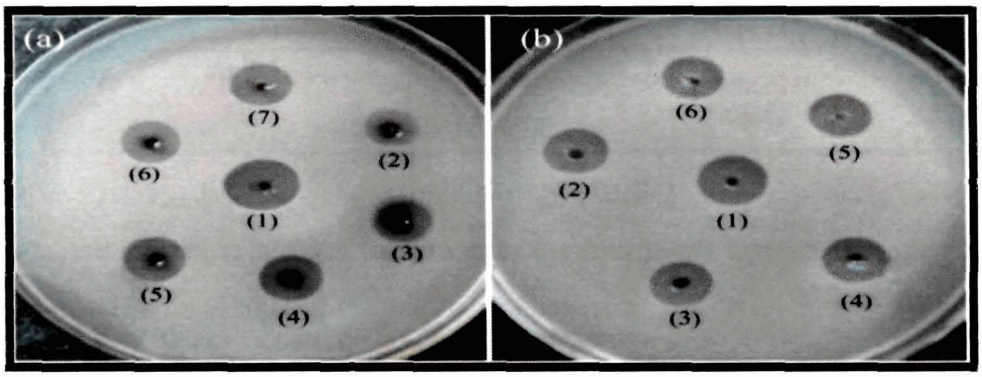

Fig.3B.8. *Representative culture plate showing antibacterial test: Combination of antibiotic, rifampicin (Rif) and silver nanoparticles (a) both at different concentrations, (b) with constant concentration of the nanoparticles and increasing concentration of the antibiotic at the peripheral wells. The central well contained Rif as positive control*

Next, the synergy of the antibiotic with the nanoparticles was investigated. The concentration of the nanoparticle was progressively increased while that of the antibiotic was decreased in the wells.

Table3B.1 *Mean zone of inhibition (mm) ± standard deviation of various combinations of antibiotic and silver nanoparticles*

Plate no. / Well number	*Antibiotic (μg)*	*Silver nanoparticles (μg)*	*Mean Zone of inhibition (mm) ± standard deviation*
(a)/(1)	20	0	20 ± 0.00
(a)/(2)	0	20	14 ± 0.5
(a)/(3)	12	8	16 ± 1.0
(a)/(4)	10	10	17 ± 0.5
(a)/(5)	8	12	17 ± 0.5
(a)/(6)	4	16	16 ± 1.0
(a)/(7)	16	4	17 ± 0.5
(b)/(1)	20	0	20 ± 0.0
(b)/(2)	1	20	17 ± 0.5
(b)/(3)	2	20	17 ± 0.5
(b)/(4)	3	20	17 ± 0.5
(b)/(5)	4	20	17 ± 0.5
(b)/(6)	5	20	17 ± 0.5

It is very much likely that the antibiotic gets adsorbed onto the active surface of the nanoparticles. This further reduces the mobility of the starch supported nanoparticles since diffusion is indirectly proportional to the mass. Even though the coupled system was expected to have a higher antimicrobial potency, the latter never reached that of the positive control. Irrespective of the increment in the rifampicin concentration, all the combinations produced a zone of inhibition of 17 mm (Fig.3B.8b). These observations suggest that a combination of antibiotic and the polymer templated nanoparticle may not merely show synergistic antimicrobial potency. Also, the probable interaction of the starch template and the agar medium might further restrict the diffusion of the particles. The interaction of the partners and the overall diffusion bears a relation with their respective concentrations, available active surface area and nanoscale surface chemistry, which merits further investigation.

The cytotoxicity of the nanoparticles on THP-1 cells was examined in terms of the former's effect on the latter's proliferation by the MTT assay. Untreated cells as well as cells exposed to different concentrations of the silver nanoparticles for 24 h were subjected to the MTT assay for cell viability determination. MTT assay, first described by Mosmann[45] is based on the ability of mitochondrial dehydrogenase enzyme from viable cells to cleave the tetrazolium rings of the pale yellow MTT and form dark blue formazan crystals, largely impermeable to cell membranes, thus resulting in its accumulation within healthy cells. Solubilisation of the cells results in the liberation of the crystals. The number of surviving cells is directly proportional to the level of the formazon product formed that can be quantified photometrically. After 24 h post treatment, the THP-1 cells showed excellent viability (almost 100 %) even up to 98.7 μM concentration of the nanoparticles (Fig.3B.9).

These results indicate that the phytochemicals present in the aqueous orange extract provide a non-toxic coating on the nanoparticles. It is critical to mention that THP-1 cells have Fc and C3b receptors and lack surface and cytoplasmic immunoglobulins. The response of a single cell-line towards a particular nanomaterial is not representative of all the plausible outcome of the events at the bio-nano material interface. The safe utility of the reported silver NPs demands *in vivo* assessments and greater risk analysis.

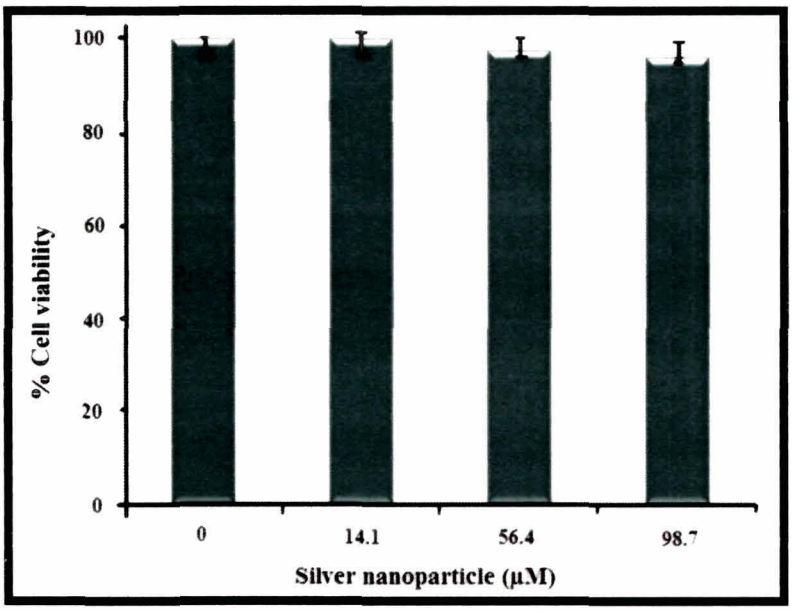

Fig.3B.9. *MTT assay for cytocompatibility of the silver nanoparticles with THP-1 cell line. Results represent mean ± S.D. of triplicate determination.*

3B.4. Conclusions

The reported system highlights a common by-product of the food sector *i.e.*, orange peel that normally finds applications in the cosmetic industry can be useful even in the domain of nanotechnology. The biopolymer templated silver nanoparticles synthesised in the ambient conditions shows tremendous potential for applications in a number of niches. These nanoparticles with free radical scavenging, biocompatibility and antimicrobial potency may be exploited for various biomedical applications including development of catheters, topical antimicrobial gel formulations and so on.

References

1. Chen, X., & Schluesener. H.J. *Toxicol. Lett.* **176**, 1--12, 2008.
2. Philip, D. *Spectrochim. Acta A Mol. Biomol. Spectrosc.* **73**, 374--381, 2009.
3. Guidelli, E.J., et al. *Spectrochim. Acta A Mol. Biomol. Spectrosc.* **82**, 140--145, 2011.
4. Wong, S., & Barbara, K. *Nanotechnol.* **23**, 290201 (2 pp), 2012.
5. Babu, V.R., et al. *Carbohyd. Polym.* **81**, 196--202, 2010.
6. Bourgeat-Lami, E., & Lang, J.J. *J. Colloid Interface Sci.* **197**, 293--308, 1998.
7. Govindachari, T.R., et al. *Tetrahedron* **23**, 1901--1910, 1967.
8. Bozanic, D.K., et al. *Eur. Phys. J. E* **22**, 51--59, 2007.
9. Raveendran, P., et al. *J. Am. Chem. Soc.* **125**, 13940--13941, 2003.
10. Singh, M., et al. *Mater. Lett.* **63**, 425--427, 2009.
11. Vigneshwaran, N., et al. *Carbohyd. Res.* **341**, 2012--2018, 2006.
12. Lu, Q., et al. *Langmuir* **21**, 6002--6005, 2005.
13. Yang, F., et al. *Biol. Trace Elem. Res.* **110**, 179--190, 2006.
14. Lin, D., & Xing, B. *Environ. Sci. Technol.* **42**, 5580--5585, 2008.
15. Yang, W., et al. *Nanotechnol.* **20**, 085102 (7 pp), 2009.
16. Haaland, P.D. (ed.). *Experimental Design in Biotechnology*, Marcel Dekker Inc., New York, 1989.
17. Turkoglu, A., et al. *Food Chem.* **101**, 267--273, 2007.
18. Ulkur, E., et al. *Burns*, **31**, 874--877, 2005.
19. Zhao, J., et al. *Accounts Chem. Res.* **41**, 1710--1720, 2008.
20. Yamamoto, S., et al. *Anal. Sci.*, **20**, 1347--1352, 2004.
21. Singh, M., et al. *J Nanopart. Res.* **13**, 69--76, 2011.
22. Bicelli, L.P., et al. *Int. J. Electrochem. Sci.*, **3**, 356--408, 2008.
23. Hatchert, D.W., & White, H.S. *J. Phys. Chem.-U.S.* **100**, 9854--9859, 1996.
24. Basu, S., et al. *J. Colloid Interface Sci.* **321**, 288--93, 2008.
25. Carpita, N., et al. *Science* **205**, 1144--1147, 1979.
26. Sresty, T.V.S., & Rao, K.V.M. *Environ. Exp. Bot.* **41**, 3--13, 1999.
27. Sharma, V.K., et al. *Adv. Colloid Interface Sci.* **145**, 83--96, 2009.
28. Korbekandi, H., et al. *Crit. Rev. Biotechnol.* **29**, 279--306, 2009.
29. Li, S., et al. *J. Chromatogr. B* **846**, 291--297, 2007.

30. Guimarães, R., et al. *Food Chem. Toxicol.* **48**, 99--106, 2010.

31. Jain, J. *Mol. Pharmaceutics* **6**, 1388--1401, 2009.

32. Mohammad, G., et al. *Dig. J. Nanomater. Bios.* **3**, 159--162, 2008.

33. Vasilev, K., et al. *Nano Lett.* **10**, 202--207, 2010.

34. Mandal, T.K., & Chatterjee, S.N. *Radiat. Res.* **83**, 290--302, 1980.

35. Paul, S., et al. *J. Magn. Magn. Mater.* **321**, 3621--3623, 2009.

36. Zhao, J., et al. *Nanomedicine-U.K.* **1**, 219--228, 2006.

37. Suber, L., & Plunkett, W.R. *Nanoscale* **2**, 128--133, 2010.

38. Chou, K-S., et al. *Mater. Chem. Phys.* **94**, 429--433, 2005.

39. Monti, O.L.A., et al. *J. Phys. Chem. B* **108**, 1604--1612, 2004.

40. Percival, S.L., et al. *Int. Wound J.* **4**, 186--191, 2007.

41. Hatchett, D.W., & Henry, S.J. *Phys. Chem.* **100**, 9854--9859, 1996.

42. Wiley, B., et al. *Chem. Eur. J.* **11**, 454--463, 2005.

43. Morones, J.R., et al. *Nanotechnol.* **16**, 2346--2353, 2005.

44. Shahverdi, A.R., et al. *Nanomed-Nanotechnol.* **2**, 168--171, 2007.

45. Mosmann, T. *J. Immunol. Methods* **65**, 55--63, 1983.

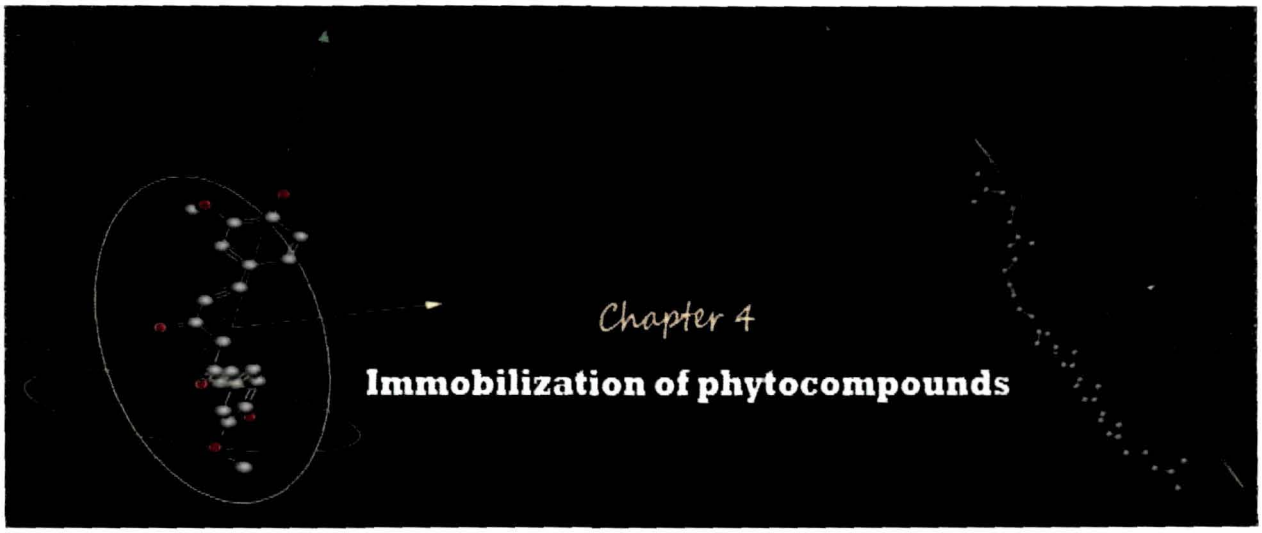

Chapter 4

Immobilization of phytocompounds

HIGHLIGHTS OF THE CHAPTER*

The spectrum of distinctive properties, unique molecular architecture and multi-potent efficacies of biomolecules extracted from the plant kingdom needs no further elaboration. In this context, two of the bio-medically important phytocompounds, *viz.*, curcumin and lycopene were chosen for the immobilization study. Subchapter 4A is focused on the directed assemblage, magnetic responsiveness and synergistic free radical scavenging of poly(ethylene glycol)-iron oxide nanoparticles-curcumin' trio. On the other hand, anti-lipid peroxidation; cytocompatibility with normal L929 cell line in contrast to anti-proliferative action against HeLa cells; and stimulatory effect on seed-germination of tomato peel lycopene (extracted by the coupled tools of green chemistry- sonication and biocatalysis) coupled onto biomimetic 'trifoliate' polyaniline (PAni) nanofibers forward the system as multifunctional biomaterial, as presented in the subchapter 4B. Furthermore, DMol^3 was employed for the quantum molecular calculations of lycopene interacting with PAni (via non-covalent functionalization involving π–π stacking) and solvation study. These systems may find prospective applications in the medical domain.

*Parts of this chapter are published in

1. Konwarh, R., & Karak, N., et al. *Colloid Surf. B* **81**, 578--586, 2010.
2. Konwarh, R., & Karak, N., et al. *Ultrason. Sonochem.* **19**, 292--299, 2012.
3. Konwarh, R., & Karak, N., et al. *J. Mat. Chem.* **22**, 15062--15070, 2012.
4. Konwarh, R., & Karak, N. *Adv. Colloid Interface Sci.* (Communicated)

4A. CURCUMIN IMMOBILIZATION ONTO PEG-IONPs

4A.1. Introduction

The unique architecture of curcumin {(1E, 6E)-1,7-bis(4-hydroxy-3-methoxy phenyl)-1,6-heptadiene-3,5-dione} endows special attributes to this wonder molecule. Curcumin is a homodimer of feruloyl-methane containing a methoxy group and a hydroxyl group, a heptadiene with two Michael acceptors, and an α, β-diketone. The importance given to this phytocompound, extracted from *Curcuma longa*, related curcuminoids and their conjugates is attested by the ever-increasing *in-vitro* and *in-vivo* tests being reported in various research journals.[1] Different studies have shown that curcumin has diverse biological and pharmacological activities including anti-inflammatory, antibacterial, antifungal, antiviral, and anticoagulant potency.[2] Be it the gradual unfolding of the modulation of various signaling pathways in the 'crab' disease or the elucidation of probable mechanism of its antimicrobial action- all these findings are carving out newer research lines in the bio-medical domain.[3-7] The utility of curcumin, attributed with multiple therapeutic actions is however, limited by its color, poor water solubility, and relatively low *in vivo* bioavailability. The recent quest for a 'super-curcumin' has led to synthesis of myriad of curcumin analogues, through numerous molecular tinkerings and formulations with various oils and with inhibitors of metabolism (*e.g.*, piperine), liposomal and polymeric nanoparticles encapsulations[8] and conjugation of curcumin prodrugs.[2] PEGylation has been an instrumental avenue to increase the water-solubility, stability and bioactivity of curcumin.[9-11]

Another special attribute is its anti-oxidant potency. The mechanism of its free-radical scavenging has been dealt with in a number of publications.[2] More recently, in two separate studies,[12, 13] it has been established that it acts as an antioxidant through the phenolic hydroxyl group and the free radical scavenging mechanism is dictated by the nature of the free radical itself. On the other hand, literature shows that the photodegradation of curcumin is augmented in presence of nanoparticles and metal salts.[14, 15] Another interesting domain of investigation is its heavy metal-chelation capacity[16-18] bearing probable correlation with its cytoprotective potency in various *in-vivo* studies.[17]

Various computational and analytical reports are being published on its interaction behavior with iron. ^{1}H NMR data state that the dissociated β-diketo moiety of the ligands is involved in metal chelation.[18]

On the other hand, the research on iron and iron oxide based nanoparticles has captured attention in the recent years as efficient drug delivery system with numerous biomolecule immobilization studies being reported time and again.[19] Recently, IONPs have been reported as potent free-radical scavengers.[20] The presence of a biomolecular moiety like curcumin in the vicinity of the nanoparticles is supposed to influence the latter's intrinsic property. For instance, such molecular modulation may be well echoed in the magnetometric parameters of IONPs. Studies of such property-modulations seem to be interesting in the context of biomolecule immobilization. As noted in the second chapter, it is important to mention that the complexation with nanomaterials may be just another way of tuning the properties of a biomolecule itself as metallic interaction is supposed to have a profound role in dictating the structure-property accord of the coupled biological moiety.

Therefore, exploring the immobilization of curcumin onto PEG-IONPs through a simple statistically optimized (response surface methodology) sonication mediated route is an interesting proposition. The influence of various sonication parameters like cycle, amplitude and duration on the loading of curcumin onto the polymer supported nanomaterial and the consequences of bioconjugation on the magnetometric parameters of the nanoparticles and the particle morphology have been assessed. With a premonition of modulation of free-radical scavenging potency of the conjugating partners, DPPH radical scavenging of the prepared system has also been evaluated. The study has been focused to comprehend the interfacial events of polymer-nanomaterial-biomolecule interaction which may provide new avenues to design materials for *avant-garde* applications for multiple domains.

4A.2. Experimental

4A.2.1. *Materials*

The starting materials for the preparation of the immobilization platform *i.e.,* PEG-IONPs were the same as mentioned in section 2A.2.1. Curcumin was isolated from about 20 g of sun-dried turmeric powder (obtained from *Curcuma longa*, collected from the local

area) by solvent extraction technique using toluene followed by recrystallization from ethanol. This was then subjected to vacuum drying at about 25-28 ^{0}C. About 0.242 g of dried curcumin extract was obtained. This was further subjected to purification and characterization according to previously reported method.[21] The spectroscopic data and the analytical results confirmed the sole ingredient of the extract as curcumin.

4A.2.2. *Preparation of PEG-IONPs*

PEG-IONPs were prepared according to the procedure described in section 2B.2.2.

4A.2.3. *Curcumin immobilization onto PEG-IONPs*

Stock solutions were prepared by dissolving the extracted curcumin in DMSO (1 mg/mL), adjusted to slightly acidic pH of 6.5 using ascorbic acid. For the immobilization, 0.3 mL of the curcumin solution and 25 mg of the PEG-IONPs were taken and subjected to sonication. Ultrasonication was carried out with standard sonotrode (tip-diameter of 3 mm) in UP200S (Hielscher Ultrasonics GmbH, Germany) for various time periods and at specific amplitude (as mentioned in the subsequent section) to produce a homogeneous dispersion. The mixing beaker was maintained at 4 ^{0}C in a thermostatic bath during the ultrasound irradiation.

4A.2.4. *Statistical optimization of sonication parameters*

For the evaluation of the effect of sonication, RSM was used to estimate the main effects on response *i.e.*, percentage of curcumin loaded. Three factors with three levels consisting of 32 experimental runs were used to analyze the experimental data including five replicates at the center point.[22] Time of sonication (C_1), cycles (C_2) and amplitude percent (C_3) were chosen as the experimental factors or the independent variables capable of influencing the percentage of curcumin loaded (Y). Analysis was done using coded values (-1 for C_1=2 min, C_2=0.1 and C_3=30%; 0 for C_1=5 min, C_2=0.4 and C_3=60%; 1 for C_1=8 min, C_2=0.7 and C_3=90%). Using this design, the experimental data were fitted according to the equation (4A.1) as a second order polynomial equation including individual and cross effect of each variable.

$$Y = a_0 + a_1C_1 + a_2C_1^2 + a_3C_2 + a_4C_2^2 + a_5C_3 + a_6C_3^2 + a_7C_1{*}C_2 + a_8C_1{*}C_3 + a_9C_2{*}C_3 \quad \text{....(4A.1)}$$

where a_0, a_1, a_2, a_3, a_4, a_5, a_6, a_7, a_8, a_9 are the regression coefficients. Analyses were carried out in duplicates. The data tabulated were (Table4A.1) the average of the measurements. Multiple regression analysis, response surface plots and statistical analyses were performed using Minitab 15 Statistical Software® (Minitab Inc., PA, USA). The percentage of curcumin loading was estimated according to centrifugation method.[23]

Table4A.1. *Observed and predicted values of response (percent loading of curcumin)*

Time of sonication (min)(C_1)	*Cycle (C_2)*	*Percent Amplitude (C_3)*	*Observed Response*	*Predicted Response*
-1	-1	-1	51	48.73
-1	-1	0	54	56.17
-1	-1	1	52	52.23
-1	0	-1	62	65.23
-1	0	0	76	72.29
-1	0	1	66	69.23
-1	1	-1	61	61.00
-1	1	0	70	68.95
-1	1	1	68	65.50
0	-1	-1	61	59.87
0	-1	0	65	67.14
0	-1	1	64	63.03
0	0	-1	74	77.03
0	0	1	81	80.70
0	1	-1	73	73.48
0	1	0	78	81.25
0	1	1	74	77.64
1	-1	-1	62	60.95
1	-1	0	66	68.06
1	-1	1	65	63.78
1	0	-1	78	78.78
1	0	0	86	86.14
1	0	1	83	82.12
1	1	-1	79	75.89

Table continued on the next page

1	1	0	83	83.50
1	1	1	81	79.73
0	0	0	84	84.56
0	0	0	84	84.56
0	0	0	84	84.56
0	0	0	83	84.56
0	0	0	84	84.56

4A.2.5. *Characterization tools*

XRD was traced in an X-ray diffractometer 'Miniflex', (Rigaku Corporation Japan) at room temperature (ca. 23 ^{0}C). The scanning rate used was 8.0^0 min^{-1} over the range of 2θ = 10-70^0. FTIR spectra were recorded in a Nicolet (Impact 410, Madison, WI, US) FTIR spectrophotometer by using KBr pellets. Lakeshore VSM (Model 668, Westerville, OH, US) was used to study the magnetic behavior of the samples. Size and distribution of the MNPs before and after bioconjugation were studied using JEOL, transmission electron microscope (TEM) (JEMCXII, TOKYO, Japan) at operating voltage of 100 kV.

4A.2.6. *DPPH free radical scavenging analysis*

Four different samples prepared in DMSO, namely (a) PEG-IONPs, (b) curcumin, (c) the system under investigation *i.e.*, curcumin-PEG-IONPs and (d) mere physical mixture of curcumin and PEG-IONPs (10 μL, 20 μL and 40 μL each) were analyzed for the free radical scavenging potency according to modified DPPH method (described in section 3B.2.5).[24] The free radical scavenging potency of freshly extracted curcumin was also tested against the sample stored at ambient condition for three months. Controls having only DMSO were also recorded for correction of DPPH scavenging and dilution factors. All analyses were done in triplicates.

4A.3. Results and discussion

4A.3.1. *Preparation of the PEG-IONPs*

From a broad perspective, two different approaches can be generalized for controlling nanoparticles distribution while preventing random-order orientation.[25] In the

first approach, a multidimensional morphology directing potential, such as spatially varying field or susceptibility within the material is created using an external means. This complex field re-orients the nanoparticles into pre-described, ordered assembly (external-in, directed patterning of nanoparticle dispersions, DPND) through a resulting mass flow of nanoparticles for minimizing the potential energy of the system within the externally applied field. However, in the other approach (internal-out, mesophase assembly of nanoparticles, MANP), uniform modulation in the system's environment (intrinsic parameters like pressure or temperature and extrinsic like number density or entropy) is used to tailor the particle-particle and particle-matrix interactions, resulting in a thermodynamically stable and defined mesophase. Typically, in the mesophase assembly, polymer-hard body spherical particles systems serve as ideal candidates to study phase behavior of nanomaterial-polymer interaction. In an ideal system, the inter-particle interaction is characterized by short-range repulsive forces that are operative at the contact point with no dissipative force. Interestingly, size differences existed between IONPs prepared via the modified protocol reported in section 2B.2.2 (executed in the present case) as against that reported in section 2A.2.2. It may be envisaged that sonication generated well dispersed, dense population of IONPs (Fig.4A.1a) of a narrow size range (2-5 nm). PEG chains confer steric stabilization. Systems that are sterically stabilized tend to remain well-dispersed even under conditions where the zeta potential of the surfaces is significantly reduced. Furthermore, steric stabilization is effective at both high and low solid contents.

4A.3.2. *Immobilization of curcumin onto PEG-IONPs*

Recently, the efficacy of co-administrated paclitaxel and curcumin in nanoemulsion formulation has been reported to countercheck the multi-drug resistance in tumor cells.[26] Coalescing of functionality directly at the extensive interfacial area afforded by the narrow-sized and well dispersed iron oxide nanoparticles was the next objective of the present work. Evaluation of the efficiency of sonication in conjugating curcumin onto a biocompatible polymer *i.e.,* PEG templated nanomaterial was assessed.

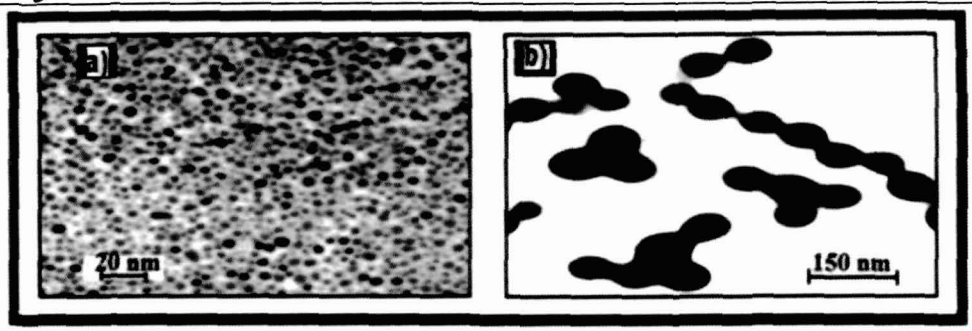

Fig.4A.1. *TEM micrograph of PEG assisted iron oxide nanoparticles (a) before and (b) after immobilization of curcumin*

The cavitation forces induced during transient collapse of cavitating bubbles are of immense significance, particularly in the domain of material science. Several chemical and physical effects of sonication have been reported in literature.[27] Sonication seems to be an attractive means for bioconjugation onto polymer supported nanomaterial, thereby shunning the use of toxic linkers such as carbodiimide, routinely employed for coupling antibodies, enyzmes etc. which has been also highlighted in the previous chapter.

The influence of sonication with three variable parameters, namely duration of sonication (min), cycle and percent amplitude on the percent loading of the curcumin was analyzed statistically using response surface methodology (RSM). The parameters of equation (4A.1), given in the experimental section were determined by multiple regression analysis. The overall second-order polynomial equation is represented as

$$Y = 84.56 + 6.61\,C_1 - 5.02C_1^2 + 7.05\,C_2 - 10.36C_2^2 + 1.83\,C_3 - 5.69\,C_3^2 + 0.66\,C_1{*}C_2 - 0.16\,C_1{*}C_3 + 0.25\,C_2{*}C_3 \quad \text{..... (4A.2)}$$

All the three chosen variables (time of sonication, cycle and percent amplitude) had both linear and quadratic effect on the percent loading of the curcumin (Fig.4A.2). The model contained three two-way interactions (time of sonication*cycle, time of sonication*percent amplitude and cycle*percent amplitude). For each of these interactions, p-value was more than 0.05 (chosen α value) (Table4A.2), which indicated that these cross-interactions did not to have a significant effect on determining the loading percent. The model yielded a R^2 value that could explain up to 95.83% of the sample variance. Maximum curcumin loading (86%) onto the PEG-IONPs was obtained under the optimized sonication parameters of 8 min, 0.4 cycle and 60% amplitude. Response surface methodology and the experimental design we applied, given the limits imposed by the nature of the experiment,

revealed themselves to be efficient in the determination of the optimal conditions of sonication for theoretically obtaining maximal bioconjugation.

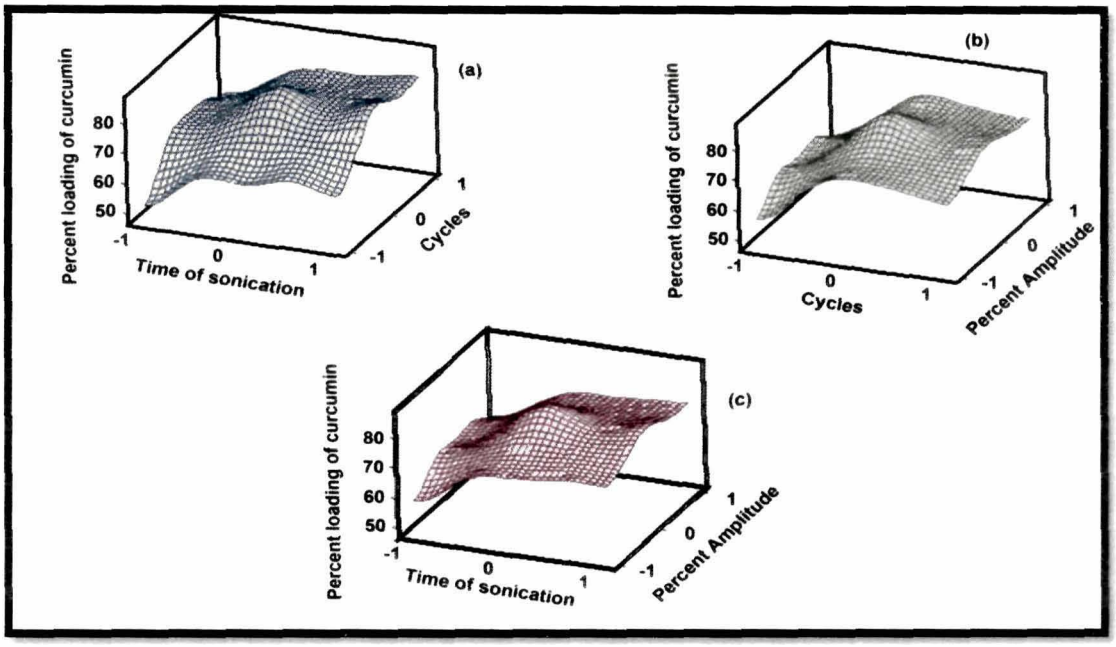

Fig.4A.2. *Response surface plots of percent drug loading vs. (a) time of sonication vs. cycle, (b) cycle vs. percent amplitude and (c) time of sonication vs. percent amplitude*

Table4A.2. *Model coefficients estimated by multiple regressions (model adequacy checking)*

Factor	*Coefficient*	*t-value*	*p-value*
Constant	84.56	89.68	0.000<0.05
C_1	6.61	10.61	0.000<0.05
C_2	7.05	11.32	0.000<0.05
C_3	1.83	2.94	0.009<0.05
C_1*C_1	-5.02	-5.04	0.000<0.05
C_2*C_2	-10.36	-10.38	0.000<0.05
C_3*C_3	-5.69	-5.70	0.000<0.05
C_1*C_2	0.66	0.87	0.392>0.05
C_1*C_3	-0.16	-0.21	0.829>0.05
C_2*C_3	0.25	0.32	0.746>0.05

As the optimum had been located, the experimental domain and the spacing of levels were adequately chosen. The choice of a second order polynomial regression model was also satisfactory, and the estimation of coefficients by multiple linear regressions was a priori much more explanatory than that obtained by any classical analysis of variance.

It is clear that the ultrasound irradiation must be adequately controlled in order to achieve the maximal dispersion with optimal interaction of the PEG-IONPs and the biomolecule. Sonication facilitates interaction by bringing the reacting moieties into closer proximity. The propagation of ultrasonic waves in a liquid medium generates massive pressure (reaching thousands of atmospheric pressure), causing a colossal stress that raze the binding energy of the inter-particles. Gas bubbles from the cavity intrude into the new inter-particle crevices and decrease the diameter of the agglomerated mass. If there is not enough energy given to the mixture, the nanoparticle- agglomerates cannot escape the resisting force thus the aid for dispersion is limited. Thus, both the timing and the amplitude are critical. On the other hand, if too much energy is given to the system, then the frequency of collision between the nanoparticles increases and as such the probability of forming larger agglomerates is enhanced. This eventually reduces the effective surface area available for bioconjugation. Hence the bioconjugation may be adversely affected by more than necessary input of energy. Therefore, optimum sonication parameters must be determined in order to obtain the maximum dispersion as well as conjugation.

4A.3.3. *TEM imaging and directed morphogenesis*

The photodegradation of curcumin has been reported both in solution and in solid form. A recent review mentions the importance of breakage of β-diketone link forming smaller phenolic compounds in the light-mediated degradation of curcumin, though the mechanism has not been traced completely.[28] It has been reported that iron and aluminum salts and nanoparticles like silver and zinc ferrite influence the photodegradation of curcumin.[13-15]. The increased photodegradation of curcumin in presence of nanoparticles and metal salts is being employed to develop methods for removing turmeric stains from cotton fabrics.[28] Assessing the degradability of curcumin conjugated to polymer templated iron oxide (ferrous ferrite) nanoparticles was interesting. Curcumin was dispersed in DMSO through sonication and observed under TEM. The photo/thermal instability of the spherical nanoparticles of unconjugated curcumin to high energy electron beam was indicated by their quick dissolution (on constant focusing of the electron beam). On the other hand the curcumin conjugated nanoparticles were distributed within a size window of 80-90 nm (Fig.4A.1b). The increase in the particle size of polymer supported MNPs is attributed to the surface encapsulation due to bioconjugation. Conjugation of curcumin

with beta-cyclodextrin, PEG- folic acid complex {CD-(C6-PEG)5-FA}[8] has been instrumental in reducing its degradation rates by statistically significant amount with respect to alterations in pH with concomitant multifold increase in its solubility. Similar improvement was also noted for curcumin's formulation with MePEG-b-PCL.[9] Furthermore, PEGylation of curcumin also improves its bioactivity as evident from the greater cytotoxicity of PEG conjugated curcumin compared to the free counterpart.[10] From this standpoint, PEGylation can also be thought of as plausible reason for greater stability of the conjugated curcumin towards external factors like intense light energy. The nanochemistry of the iron oxide-nanoparticles with high active surface area cannot be overruled. This however, needs deeper probing. Some additional interesting observations emanated during the TEM imaging, as discussed below.

The introduction of curcumin into the system sets in a whole new set of higher ordered architecture of the nanoparticles. At this juncture it is relevant to mention that the contributions of enthalpic and entropic interactions to the chemical potential, topological constraints imposed by size and geometry and the added complexity of surface interactions have a major morphology dictating influence. Intermolecular interactions and the relative impact of mixing on the internal degrees of freedom of the constituents (as in case of chain-formation), magnitude of intensive variables (temperature, pressure etc.), polydispersity of the constituents- all the factors govern the great structural richness with a possibility of forming a variety of exotic phases in a polymer nanocomposite. The TEM micrographs revealed that artistically appealing products can be generated through an intersection of polymer chemistry, nanoparticles synthesis and nanomaterial engineering, for a better elucidation of events at bio-nano interface. The arrangement of the bio-conjugated particles in triads, tetrads and higher aggregates with linear chains occurring with maximal frequency, as observed in several TEM fields marshaled in support of the above facts.

FTIR spectra (Fig.4A.3) of the curcumin solution in DMSO showed characteristic band at around 3443 cm^{-1} which is attributed to the O-H stretching vibration of curcumin while in the conjugated system in presence of PEG assisted nanoparticles, the O-H stretching vibration shifted to 3379 cm^{-1}. This result indicated there was an interaction among the components namely, PEG, curcumin and IONPs. The higher intensity of this band in conjugated system compared to the curcumin in absence of PEG assisted NPs confirmed the presence of more number of such bonds. Further shifting of the strong band

at 1655 cm^{-1} of curcumin to 1649 cm^{-1} in the conjugated system indicated the participation of the dione moiety in conjugation. Moreover, the shifting of the stretching vibrational band of S=O (of DMSO, used in the dispersion medium) from 1026 cm^{-1} to 1020 cm^{-1} in the conjugation system was an indication of interaction of oxygen of DMSO with the iron-oxide nanoparticles.[29]

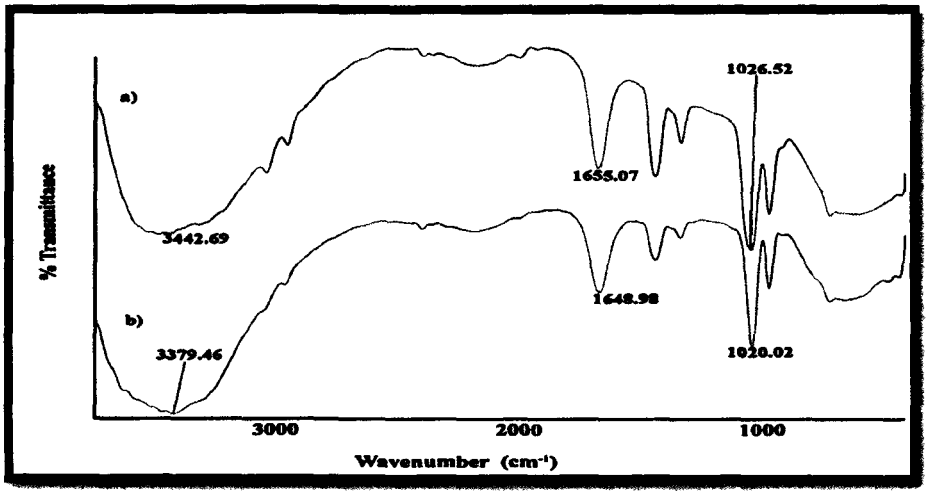

Fig.4A.3. *FTIR spectra of (a) curcumin and (b) the conjugated system, both prepared in DMSO.*

Fig.4A.4 shows the probable interactions of the differentially assembled bioconjugated polymer supported nanoparticles.

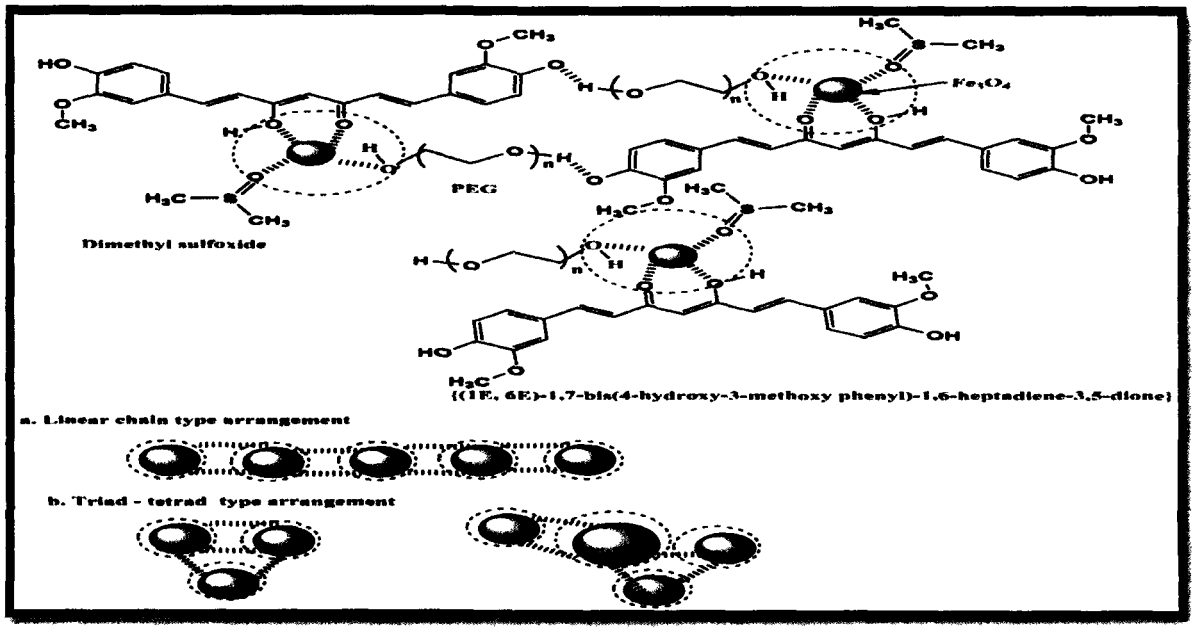

Fig.4A.4. *Probable interactions of the curcumin conjugated PEG assisted iron-oxide nanoparticles*

Self-assembly of complex structures is often discussed under two classes, namely static and dynamic. The latter is the hallmark feature of numerous biological events like cellular mitosis[30] with requisite of continual energy for maintaining quasi-equilibrium state. On the other hand, the static assembly as in the presented system generates assemblies of polypeptides, colloids or mesoparticles. Entry of an energy burden into the static state is probable without the requirement of energy expense to maintain the state. This indirectly speaks of the global or quasi-equilibrium state of the components in static self-assembly.

4A.3.4. *Magnetometric analysis*

A range of interactions are operative in the binding of magnetic particles to bioactive substances. This primarily includes the interactions between organic ligand and various chelation-interactions between the biological moiety and the metal's centers as mentioned in Chapter 2. The magnetic nature of the prepared system was demonstrated by their physical attraction towards a magnetic bead. Lakeshore VSM was used to study the magnetic behavior of the free PEG-IONPs and the curcumin-PEG-IONPs at room temperature. The magnetization value was found to be the 43.67 emu g^{-1} for the PEG-IONPs (Fig.4A.5a). However, on curcumin loading, the system registered a decrease in the magnetization value by almost 13.53% (37.76 emu g^{-1}) (Fig.4A.5b).

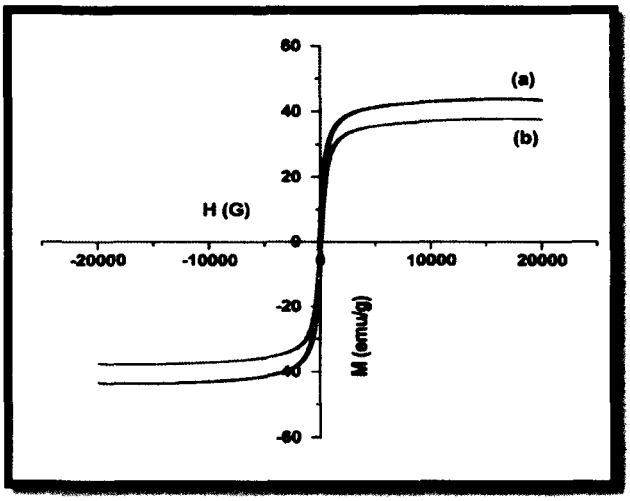

Fig.4A.5. *Hysteresis loops of PEG-IONPs (a) before and (b) after loading with curcumin*

This is an indirect indication for the probable coating/complexation of the iron oxide nanoparticles with curcumin. The retentivity showed a similar trend: μ_r = 11.865 emu g^{-1} and 8.365 emu g^{-1} for the polymer templated nanoparticles before and after curcumin

conjugation. The above results indicated that the magnetometric parameters of the polymer-supported magnetic iron oxide nanoparticles were altered in presence of curcumin; however, the system still retained its responsiveness to magnetic field.

4A.3.5. *DPPH scavenging analysis*

Utilization of diphenyl-1-picrylhydrazyl (DPPH) radical for rapid and inexpensive determination of anti-oxidant potency of various materials has been reported.[31, 32] It has also been used to quantify antioxidants in complex biological systems in recent years. The DPPH method can be used for both solid and liquid samples. It is independent of sample polarity and not specific to any particular antioxidant component, but determines the overall antioxidant capacity of the sample. The decolorization of DPPH during the scavenging process is stoichiometric with respect to number of electrons captured.

Various mechanistic approaches have been put forth to comprehend the anti-oxidant potency of curcumin (H_3CU). In this context, it was proposed[12] that curcumin + DPPH ($R^{\bullet}$) reaction is mediated through sequential proton loss electron transfer (SPLET):

$$H_3CU \rightarrow H_2CU^{-} + H^{+} \quad \text{.....(4A.3)}$$

$$H_2CU^{-} + R^{\bullet} \rightarrow H_2CU^{\bullet} + R^{-} \quad \text{.....(4A.4)}$$

$$H_2CU^{\bullet} \rightarrow HCU^{\bullet -} + H^{+} \quad \text{.....(4A.5)}$$

With the anticipation that the bioactivity of the isolated curcumin could show a dip (implying degradation) on storage under ambient conditions, the free radical scavenging potency was assessed for two batches of curcumin: one freshly isolated and dissolved in DMSO and the other, isolated three months prior to the date of analysis and dissolved in the same solvent. The freshly extracted curcumin showed 60% greater DPPH scavenging than the three month old sample. The scavenging potency of the stored curcumin in its free and conjugated state was also compared.

Fig.4A.6 depicts the free radical scavenging potency of the various systems. The scavenging potential of curcumin-iron oxide complex was found to be the highest (33.49 %) for the sample volume of 40 μL for an incubation period of 30 min. The order of DPPH scavenging capacity as evident from the graph was: curcumin-PEG-IONPs>PEG-IONPs> physical mixture of curcumin and PEG-IONPs>curcumin, for an applied volume of 40 μL as well as for 20 μL. For an applied volume of 10 μL, the order of DPPH scavenging changes between curcumin-iron oxide physical mixture (8.38 %) and iron oxide nanoparticles (7.36

%) as compared to the higher volumes applied, though not significant. The results have shown that 'nano-effect' complemented by the templating attribute of polymer can have profound influence on modulating the bioactivity of the conjugated natural compound.

Paul et al.[20] have reported the free radical scavenging property of iron oxide particles as a surface dependent property. The poly(ethylene glycol)-supported iron oxide nanoparticles prepared for the present study also exhibited free radical scavenging potency. Furthermore, the anti-oxidant potency of the nanoparticles was higher than that of the phytocompound. This finding reaffirmed the decrease in bioactivity of the stored unconjugated curcumin. Due to a large surface area to volume ratio and an ambient electrostatic field, iron oxide nanoparticles have high tendency to adsorb ionic or DPPH-like species.

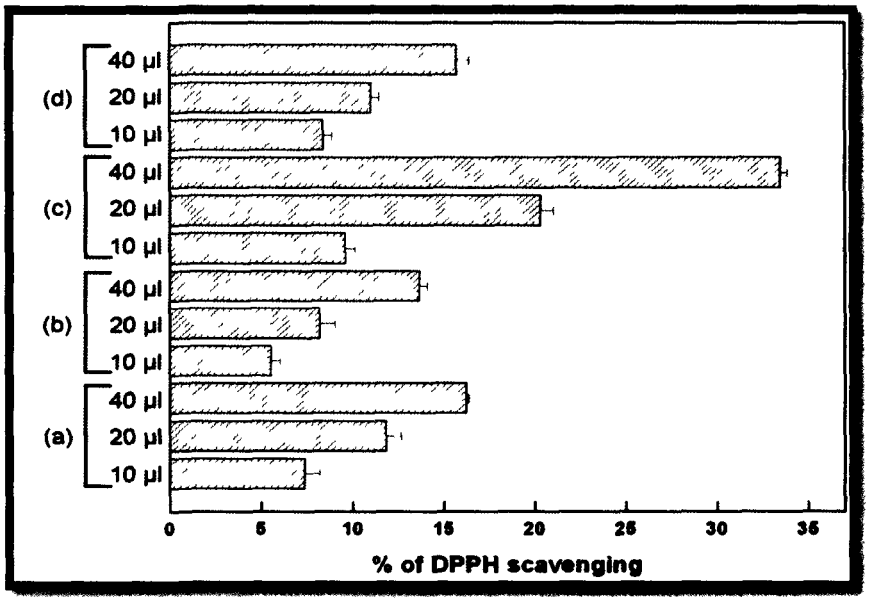

Fig.4A.6. *Graph showing the free radical scavenging potency of (a) unconjugated/free curcumin, (b) PEG supported iron-oxide nanoparticles, (c) curcumin conjugated PEG supported iron oxide nanoparticles (d) physical mixture of curcumin and PEG supported iron oxide nanoparticles*

Furthermore, as mentioned previously, iron in magnetite has both tetrahedral and octahedral co-ordinations with oxide anions. Attributed to high surface activity, Fe^{2+} may donate an electron to DPPH for its neutralization and undergoes reduction. The nanochemistry involved in this newly reported feature of metal oxide nanoparticles needs further investigation. To further validate the results, the free radical scavenging potency (if any) of the polymeric support *i.e.*, poly(ethylene glycol) alone was also tested. However,

this assumption was nullified by similar sets of experiments, repeated thrice. This was followed by investigation of the probable difference in the free radical scavenging capacity of physical mixture of curcumin (stored)-iron oxide nanoparticles and curcumin conjugated onto nanoparticles by sonication. In the former system, though the anti-oxidant potency of the partners have been separately established, the physical mixture did not show any significant additive effect on the free radical scavenging potency of the individual components. In fact, for higher concentrations of the two partners in the physical mixture, the anti-oxidant efficacy was found to be lower than the iron-oxide nanoparticles alone. The mere physical mixture had distinct phase differences with reduction in effective surface area available for scavenging the free radical. Thus, in case of the curcumin-polymer supported iron oxide hybrid system, the DPPH scavenging potency was higher as compared to their physical mixture. The possible synergism may be due to a number of concerted effects. It has already been cited that PEGylation of curcumin augments its bio-action, and stability.[8-10] Furthermore, the anti-oxidant efficiency of iron-oxide particles has been attributed as a surface dependent feature. Lowering of photo/thermal degradation rates and possible structural modulation of curcumin (that needs molecular modeling/computational probing) may also result in consequent enhancement of bio-potency, evaluated in terms of free-radical scavenging potency of the conjugated biomolecule.

Considering the prospective practical utility in the medical domain, neuronal impairment is a common feature in a myriad of maladies. Amongst others, Japanese encephalitis is a common confrontation of the pediatric population in particular, with newer geographical regions coming under its onslaught. It has been recently reported that curcumin has *in vitro* cytoprotective role and it also reduces replication of the Japanese Encephalitis Virus.[33] Survey of literature reveals that poly(ethylene glycol) (PEG) can immediately repair neuronal membranes and inhibit *rather than scavenge* free radical production following trauma.[34] High biocompatibility and non-adhesive properties that arise from steric stabilizing effects at bio-interfaces, highly dynamic motion, and extended chain conformation[35, 36] makes poly(ethylene glycol) (PEG) an ideal polymer to coat MNPs for biomedical applications. Furthermore, MNPs modified with PEG have a relatively long circulation time in the bloodstream and are non-immunogenic, non-antigenic, and resistant to protein binding.[37-39] Thus, the curcumin conjugated system reported here represents yet

another prospective application oriented bio-conjugated system that may be developed as magnetically responsive drug delivery system.

4A.4. Conclusion

In this work a simple sound wave-assisted bio-conjugation of curcumin onto polymer-assisted iron oxide nanoparticles was achieved. The presence of a biomolecule on the surface of nanoparticles can have profound consequences in diverse aspects as evident from the morphology directed modulation and alteration of magnetometric parameters. The stability and synergism in free radical scavenging potency of the phytocompound in immobilized state was another interesting feature of the reported bio-nano-polymer interface. Exploring the polymer supported bio-conjugated nanosystem for magnetically controlled release and site-specific targeting, without inducing host immune response could be the objective for the next level of study.

4B. NANOFIBROUS HYBRID OF POLYANILINE AND LYCOPENE

4B.1. Introduction

Lycopene is bequeathed with multiple bio-protective roles, primarily attributed to its unique molecular structure. Modulation of molecular pathways involved in cell proliferation, apoptosis and intercellular gap-junction communication, reduction of inflammatory response through alterations in cytokine production, excellent singlet oxygen quenching potential, regulation of cholesterol synthesis and its cellular efflux, prevention of atherosclerosis marshal in support of lycopene's varied roles and position in the biomedical research domain.[40-42] Harnessing the roles of such a wonder-biomolecule via immobilization onto nanostructured materials for advanced applications forms an interesting proposition.

It is pertinent to mention that most of the research on lycopene has been focused on tomato and tomato products. Globulous chromoplasts containing primarily β-carotene are found in the jelly part of the pericarp while voluminous sheets of lycopene can be found in the chromoplasts of the outer pericarp. Amongst others, the peels, a rich source of lycopene,[43-44] are a common waste generated during tomato processing.

Biocatalytic lysis of the cell wall is an effective and green route to release intracellular contents for the extraction of myriad of substances. To cite for evidence, capsaicinoids and carotenoids were extracted enzymatically from *Capsicum annuum* (chilli) using ethanol as the solvent.[45] Recently developed extraction protocols for lycopene have relied on the use of supercritical carbon dioxide[46] and enzyme assistance[47, 48] amongst other. The multifaceted aspects of another green chemistry tool *i.e.*, sonication in the domain of food technology[49] for processing, preservation and release of various bioactive moieties from cellular compartments including the enhanced extraction of lycopene (on coupling to microwave)[50] have received considerable attention. The advantages of ultrasonication over heating, microwave-assisted and enzyme-assisted extractions of flavonoids from *Folium eucommieae* have also been documented.[51] Sonication assisted extraction of carnoxic acid from rosemary[52] and chitin from fresh water prawn shells[53] vouch for the reduction in the extraction time and simplicity with production of less crystalline polymers for better conversion to chitosan respectively.

In the context of the above discussion, probing into the simultaneous use of ultrasonication and biocatalysis for lycopene extraction seems to be interesting. The effect of ultra-sonication on the cellulase Onozuka R-10 (isolated form *Trichoderma viride*) assisted extraction of lycopene from tomato peels has been evaluated in the present work. Furthermore, various sonication parameters have been optimized for the coupled system using RSM for the maximal extraction of lycopene. FTIR spectra, derivative plots of the UV-visible spectra and free radical scavenging potency of the extracted lycopene, were also analyzed. A plausible mode of action of the concomitant use of sonication and biocatalysis on the extraction of lycopene has also been proposed.

In the next phase of the study, the coupling of the extracted lycopene onto nanoscaled polyaniline (PAni), prepared through an interfacial polymerization route has been delved into. As noted in Chapter 1, in the family of intrinsically conducting organic nanostructured polymers, PAni has captured a unique niche due to its ease of synthesis, environmental stability and straightforward doping/de-doping chemistry.[54] Among the synthesis protocols of PAni nanofibers, interfacial polymerization merits special mention as far as suppression of secondary growth (to retain the nanofibrillar morphology of PAni) and ease of synthesis are concerned.[55] Immobilization studies of a spectrum of biomolecules onto 1-D polymer matrix have been reported for various advanced applications.[56] To cite for evidence, DNA templates have been used to fabricate PAni nanowires on thermally oxidized silicon surfaces.[57] In another study, micro RNA/PANI nanocomposites displayed a plethora of structural variations including overlapped nanowires, dots and even short rods owing to shielding of negative charges on the nucleic acid template during polymerization.[58] On the other hand, high lipase loading onto PAni nanotubes (as a fibrous network) has been obtained through covalent coupling, holding promise for the development of biosensor for triglyceride detection.[59]

As noted in subchapter 4A, ultrasonic irradiation could serve as an efficient tool to bring reactants in close proximity for optimal interaction. Sonication mediated conjugation of curcumin led to triads, tetrads and chain like organization of polymer supported iron oxide nanoparticles. It is pertinent to mention that although with a large solvent accessible area of 897.08 $Å^2$, the polar surface area of lycopene is zero (calculated online on www.chemicalize.org). To evaluate the efficacy of sonication in coupling a non-polar molecule like lycopene (without the use of any coupling agent) onto conducting polyaniline

nanofibers was an interesting proposition. The concomitant influence of sonication and the biomolecule present in the vicinity on the assembly of the PAni nanofibers, in terms of modulation in morphology and alterations in d-spacing and strain in the PAni backbone post lycopene binding has been probed into using a number of analytical tools.

Various computational approaches have been used to comprehend, in particular, the relationship of conformations of PAni bases and the electronic properties.[54] In the present context, DMol^3 program was employed for the quantum molecular calculations of lycopene interacting with PAni (via non-covalent functionalization involving π–π stacking).

Nanofibrous polymers are currently being viewed as excellent material to mimic the extracellular matrix and modulate cell behavior in tissue engineering. However, a limited literature is available on the cytocompatibility of PAni nanofibers. The bio-conjugated system in the present work was fortified with an anti-carcinogenic agent. The effect of the bio-conjugated system on the proliferation of L929 (normal cell line) and HeLa (cancerous cell line) was analyzed. Free radical scavenging potency and anti-lipid peroxidation were instrumental in attesting the system's bio-activity. Furthermore, a preliminary evaluation has also been made to check the eco-compatibility of the prepared bio-conjugated system by assessing its effect on the germination of *Cucumis sativus* seeds.

4B.2. Experimental

4B.2.1. *Materials*

Tomatoes, procured from the Tezpur University grocery were used for the extraction of lycopene using sonication and cellulase 'Onozuka R-10' (Merck). It is pertinent to mention that cellulase 'Onozuka R-10' represents a multi-component system. With extraneous activities of α-amylase, pectinase, protease, hemicellulase, it also degrades mannans, xylans, galactomannans, pectins and other polysaccharides. On the other hand, PAni nanofibers, prepared using an interfacial polymerization route were used as the immobilization platform. Aniline ($C_6H_5NH_2$) (Merck, India) was used as the precursor material for PAni. It is important to note that aniline/phenylamine/aminobenzene, a prototypical aromatic amine is used as a starting material of many industrial chemicals and polymers like polyurethane. Although it is colorless, it slowly oxidizes and resinifies in air, giving a red-brown tint to aged samples. And as such, prior to use, aniline was purified by

vacuum distillation in the presence of zinc dust (S.D. Fine-Chem Ltd, India, atomic weight 65.37 g/mol). The solvents namely, chloroform ($CHCl_3$, b.p. 61.7 ^{0}C, density 1.48 g/cm^3) and toluene ($C_6H_5CH_3$, bp 110.6 ^{0}C, density 0.87 g/cm^3) were distilled by extractive distillation and vacuum distillation method respectively prior to use. Ammonium peroxydisulphate ($(NH_4)_2S_2O_8$) (Merck, India) and hydrochloric acid (Merck, India) (0.9269mL, 1 M) were used as the oxidant and the dopant respectively.

4B.2.2. *Extraction of lycopene*

The protocols followed for the sample preparation and enzyme aided extraction were same as reported previously[47] with various modifications as described underneath. A batch of 180 g of tomato peels was homogenized for 3 min, using a domestic blender in 200 mL of 0.2 M acetate buffer (pH 4.5). The homogenized mass was distributed equally (5 g each) into tightly-closed glass containers, wrapped with aluminium foil. Samples were stored at 2–8 ^{0}C and used within 24 h.

The unaided extraction of lycopene (without the use of enzyme or/and sonication) in 1:1 v/v petroleum ether and acetone (Merck Ltd., India) mixture at (30 ± 2) ^{0}C served as control. The unaided solvent extraction was done (in duplicate) in separating funnels under dark condition. The separating funnels were shaken for 10 min and allowed to stand for 20 min. Lycopene, being lipophilic was collected in the upper organic phase. The collected petroleum ether extracts of lycopene were passed through a desiccant, anhydrous sodium sulphate (1 g). It is critical to mention that optimization of the unaided process can be instrumental in dictating the overall lycopene yield. The influence of temperature (20 ^{0}C, 30 ^{0}C, 40 ^{0}C), time of extraction (*i.e.*, the standing time in the separating funnel, 10 min, 20 min and 30 min) and petroleum ether: acetone volume ratio (0.35:0.65, 1:1, 0.65:0.35) on the unaided process were also assessed. The parameters (30 ^{0}C, 20 min and 1:1 ratio) (under which the solvent extraction protocol was executed) were found to be optimal.

As far as enzyme-mediated extraction was concerned, 20 mL of 0.2 M acetate buffer, pH 4.5 was added to the well-homogenized sample. Varied amounts (1, 3, 5, 7 w/w %) of cellulase 'Onozuka R-10' (source organism: *Trichoderma viride*, activity: 1 U/mg, Merck) (dissolved in the same buffer) with respect to the weight of the tomato peel, was added to assess the optimal enzyme concentration for maximal lycopene extraction in the absence (Set A) and presence (Set B) of ultrasonication. Post addition of the enzyme, samples of Set

B were subjected to ultrasonication with standard sonotrode (tip-diameter of 3 mm) in UP200S for various time periods and at specific amplitude (as mentioned in the subsequent section). The sterilized beakers used for the extraction were maintained at 4 ^{0}C in a thermostatic bath for the entire duration of ultrasonication. Samples of both the experimental sets were then incubated at 55 ^{0}C for various time periods (5-25 min) to optimize the time of extraction.

This was followed by filtration and solvent extraction of the filtrate and the residue (separately) under similar conditions as outlined above for the unaided process. The extracts of lycopene from the filtrate and the residue were pooled together and passed through the above mentioned desiccant. Finally the volume was adjusted up to 40 mL with petroleum ether. A parallel set of experiment was also executed to assess the effect of only ultrasonication (without any enzyme treatment). To evaluate this, ultrasonication was carried out under the same parameters as optimized for the coupled system. Furthermore, to make comparative assessment of biocatalytic extraction, experiments were also run using Celluclast-1.5 L, reported previously.[47]

4B.2.3. *Statistical optimization of sonication parameters*

For the evaluation of the effect of sonication in the coupled system, RSM was used to estimate the main effects on the response *i.e.*, the amount of extracted lycopene. Three factors with three levels consisting of 32 experimental runs were used to analyze the experimental data including five replicates at the center point.[22] Time of sonication (C_1), cycles (C_2) and percent amplitude (C_3) were chosen as the experimental factors or the independent variables capable of influencing the amount of extracted lycopene (L). Analysis was done using coded values (-1 for C_1=3 min, C_2=0.2 and C_3=20%; 0 for C_1=6 min, C_2=0.4 and C_3=40%; 1 for C_1=9 min, C_2=0.6 and C_3=60%). Using this design, the experimental data were fitted according to the equation (4B.1) as a second order polynomial equation including individual and cross effect of each variable.

$$L = a_0 + a_1C_1 + a_2C_1^2 + a_3C_2 + a_4C_2^2 + a_5C_3 + a_6C_3^2 + a_7C_1{*}C_2 + a_8C_1{*}C_3 + a_9C_2{*}C_3 \quad \text{.....(4B.1)}$$

where a_0, a_1, a_2, a_3, a_4, a_5, a_6, a_7, a_8, a_9 are the regression coefficients. Analyses were carried out in triplicates. The data tabulated were (Table 4B.1) the average of the measurements. The statistical analyses were performed using Minitab 15 Statistical Software® (Minitab Inc., PA, USA).

Table4B.1. *Observed and predicted values of response (amount of lycopene extracted in μg/g of the tomato peel used)*

Time of sonication (C_1)	*Frequency (C_2)*	*Percent amplitude (C_3)*	*Experimental value*	*Optimized response*
-1	-1	-1	421	401.0
-1	-1	0	425	413.4
-1	-1	1	433	424.3
-1	0	-1	429	443.9
-1	0	0	445	456.5
-1	0	1	449	467.6
-1	1	-1	489	489.5
-1	1	0	500	502.2
-1	1	1	521	513.5
0	-1	-1	529	537.8
0	-1	0	530	545.4
0	-1	1	540	551.6
0	0	-1	545	560.5
0	0	0	570	568.2
0	0	1	580	574.6
0	1	-1	600	585.8
0	1	0	605	593.7
0	1	1	610	600.2
1	-1	-1	570	572.8
1	-1	0	572	575.6
1	-1	1	579	577.1
1	0	-1	590	575.2
1	0	0	592	578.3
1	0	1	596	579.9
1	1	-1	574	580.3
1	1	0	569	583.5
1	1	1	566	585.3
0	0	0	570	568.2

Table continued on the next page

0	0	0	570	568.2
0	0	0	570	568.2
0	0	0	570	568.2
0	0	0	570	568.2

4B.2.4. *Lycopene estimation and characterization*

The extracted lycopene in petroleum ether was estimated by the standard spectrophotometric method[60] with characteristic absorbance noted at 445, 472 and 503 nm. UV-visible spectra of the samples were recorded in Hitachi (U-2001, Tokyo, Japan) UV-visible spectrophotometer. The absorbance at maximum wavelength (λ_{max}) of 472 nm was considered for calculation as given underneath

$$\text{Amount of lycopene (mg)} = A \times df \times V_t \times 10 \times 1/\varepsilon_{3450} \quad \text{.....(4B.2)}$$

where A, absorbance of the solution in 1cm cuvette; df, dilution factor; V_t, total volume (mL) of the sample; and ε_{3450} specific extinction coefficient for lycopene in petroleum ether.

From each of the spectrum, the following indices, indicating the ratios between molar extinction coefficients at the peak maxima, were enumerated: $\varepsilon_{445}/\varepsilon_{472}$ and $\varepsilon_{503}/\varepsilon_{472}$. In order to get a theoretical indication of the retention of structural attribute of the extracted lycopene, the first- and second-order derivative spectra were plotted. FTIR spectra for the samples were recorded in a Nicolet (Impact 410, Madison, WI) FTIR spectrometer by using KBr pellets.

4B.2.5. *Free radical scavenging analysis*

10 μM of the respective lycopene samples (extracted through various protocols as outlined previously) were analyzed (in triplicates) for the DPPH (2 mL, 100 μM, prepared in 80% methanol) scavenging post incubation for 30 min in the dark at room temperature (~28 ^{o}C) using the following equation:

$$\text{DPPH scavenging} = (A_C - A_S)*100/A_c \quad \text{.....(4B.3)}$$

where A_C and A_S are absorption of blank DPPH and DPPH incubated with the sample (lycopene) at 517 nm, respectively. Vitamin E was used as positive control.

4B.2.6. *Enzyme activity measurement*

The elucidation of the effect of sonication on the enzyme activity was crucial. The activity of the enzyme was determined prior to and post sonication in the absence of the substrate. Furthermore, the cellulase activity in the aqueous portion that was obtained post solvent extraction was assessed. Activity of cellulase was measured by using 1% (w/v) carboxymethyl cellulose (CMC) as the substrate and 0.02 M acetate buffer (pH 4.5) as the medium. Free cellulase (1 mL) was added to 4 mL of the CMC solution and incubated at 55 ^{0}C for 25 min. The amount of generated glucose was determined by the 3, 5-dinitrosalicylic acid agent (DNSA) method.[61] One unit of activity was defined as 1 μmol of glucose/min.

In order to probe into the probable structural modulation of the enzyme post sonication, an aliquot of 3 mL of the enzyme sample was transferred to a quartz cuvette and the UV-visible spectra were recorded for a wavelength range of 240–550 nm. Results were analyzed in correspondence to control samples (*i.e.*, prior to sonication).

4B.2.7. *Interfacial route to PAni nanofibers*

Ammonium peroxydisulphate ($(NH_4)_2S_2O_8$) (1.369 g, 0.02 M) and hydrochloric acid (0.9269mL, 1 M) were dissolved in doubled distilled water in a glass vial. In a separate glass vial, the distilled aniline (0.365 mL, 0.02 M, aniline/oxidant ratio of 1:1) was dissolved in the organic solvent mixture (toluene and chloroform, 1:1 v/v). The aqueous to organic phase ratio was kept at 2:1. The organic solvents were allowed to mix for 30 min prior to dissolution of aniline. The organic phase containing the dissolved aniline was carefully added to the aqueous solution of the oxidant and the dopant. The mass of PAni nanofibers formed were found to be dispersed in the inter-phasic region. The PAni nanofibers were periodically sampled with a pipette from the reaction vessel. These samples were likely to contain PAni nanofibers together with aniline oligomers, unreacted aniline and oxidant. Further polymerization was quenched by dilution with water followed by filtration to remove the byproducts and to avoid the *ex situ* formation of nanofibers. The mass of PAni nanofibers was then centrifuged and washed with double-distilled water and methanol several times until the filtrate became colorless. The product was finally dried in vacuum oven at 40 ^{0}C for 24 h.

4B.2.8. *Immobilization of lycopene*

50 mg of the PAni nanofibers and 5 mg of the extracted lycopene were dispersed in 10 mL of petroleum ether for about 6 h over a magnetic stirrer. The dispersion was then subjected to ultrasonication with standard sonotrode (tip-diameter of 3 mm) in UP200S, Hielscher Ultrasonics GmBH, Germany) for various time periods and at specific amplitude. During the entire duration of dispersion, the reaction vessel was maintained in ice-cold conditions to prevent thermal degradation of the biomolecule. Response surface methodology (RSM) (not shown) was used to optimize the various parameters of sonication, namely, time of sonication (C_1), cycles (C_2) and percent amplitude (C_3) to ensure maximal loading, the independent variable (L).

Post sonication, the dispersed mass was subjected to centrifugation at 6000 rpm for 15 min. The collected mass was repeatedly washed thrice with petroleum ether. The decanted petroleum ether was pooled together and estimated for lycopene content spectrophotometrically as mentioned in section 4.B.2.4. The amount of lycopene conjugated (L) was calculated using the relation:

Percent lycopene conjugated, LC = (OL-WL) * 100/OL ..... **(4B.4)**

where OL, amount of lycopene loaded into the original dispersion; WL, amount of lycopene dissolved out in the washing step.

The statistical analyses as performed using Minitab 15 Statistical Software® (Minitab Inc., PA, USA) revealed that the optimized parameters of 2 min, 0.6 cycle and 60 percent amplitude resulted in a maximal lycopene loading of about 60%. Prior to all the bio-assays, the unconjugated and lycopene loaded polyaniline nanofibers were surface sterilized in 70% ethyl alcohol (Changshu Yangyuan Chemical Co. Ltd.). This was followed by washing with and final dispersion in Millipore water.

4B.2.9. *Characterization of the bioconjugated PAni fibers*

The FTIR spectra of lycopene, polyaniline and the conjugated system were recorded in Nicolet FTIR Impact 410 spectrometer. The wide-angle X-ray diffractograms of the PAni prior to and post bio-conjugation were measured by a Rigaku X-ray diffractometer (Miniflex, UK) with a scanning rate of 0.05 min^{-1} over scanning angle of 2θ = 10-70^0 using CuK_α radiation. PAni in free and bio-conjugated states were casted on carbon-coated copper grids and their morphology was observed using a JEOL, JEM 2100 (Japan) transmission electron microscope (TEM) at an operating voltage of 200 KV. The I-V

(current-voltage) characteristics of pellets of the PAni and PAni-lycopene conjugated systems were recorded with a Four Probe Set Up (INDOSAW) at 298 K. The conductivity of the respective pellets was calculated using the following equations:

$$\rho_o = (V/I)2\pi S \quad \text{.....(4B.5)}$$

$$\rho = \rho_o/G(W/S) \quad \text{.....(4B.6)}$$

$$\sigma = 1/\rho \quad \text{.....(4B.7)}$$

where G (W/S) is a correction divisor which is a function of sample thickness and probe spacing; I, V, W, and S are the current (mA), voltage (mV), thickness of the pellet (cm), and probe spacing (cm), respectively.

4B.2.10. *Computational modeling and calculations*

The quantum molecular calculations for lycopene interacting with PAni via non-covalent functionalization involving π–π stacking between the benzenoid ring of PAni and the unsaturated ring of lycopene were carried out using DMol^3 program.[62] The geometry of PAni, lycopene and PAni-lycopene conjugated system was individually optimized in gas phase and the energy calculations on the optimized geometries were performed using spin restricted calculations at the Generalized Gradient Approximation (GGA)/PBE functional and DNP basis set which is equivalent to the 6-31G** Gaussian basis set.[63,64] The PAni-lycopene interaction was modeled via parallel stacking of the two units so as to increase the maximum interaction between them. From the optimized geometries, quantum molecular descriptors like the global hardness, chemical potential and electrophilicity indices (derived using the Koopmans' theorem[65]) were calculated and compared.

To evaluate the interaction of PAni with lycopene, the binding energy was calculated with the equation:

$$E_b = E_{\text{PAni-lycopene}} - E_{\text{PAni}} - E_{\text{lycopene}} \quad \text{.....(4B.8)}$$

where $E_{\text{PAni-lycopene}}$ is the total energy of PAni interacting with lycopene after full geometry optimization, E_{PAni} is the total energy of PAni and E_{lycopene} is the total energy of lycopene molecule. A negative binding energy value implies thermodynamic favorability towards the non-covalent interaction between the two conjugating partners.

The solvation studies were performed for the individual PAni, lycopene and PAni-lycopene units using the Conductor like Screening MOdel (COSMO)[66] as implemented in Dmol^3 for three different solvents namely water (dielectric constant, ε = 78.54), DMSO (ε =

46.70) and chloroform (ε = 4.806). The solvation energy calculations were performed on the geometries of the structures post optimization so as to overcome the computational costs. The difference in energies between the gas phase and solvent phase geometries yielded the Gibb's free energy of solvation.

4B.2.11. *DPPH scavenging and anti-lipid peroxidation assays*

Free radical scavenging activity of 1 mg each of lycopene, PAni and lycopene-PAni conjugates was measured by using the modified DPPH method as described by Serpen and his colleagues.[24] On the other hand, anti-lipid peroxidation potency of 1 mg each of lycopene, PAni and PAni-lycopene conjugate was evaluated (against vitamin E as the standard) on goat liver tissue homogenate as described in section 3B.2.4.

4B.2.12. *Cell viability test by MTT*

HeLa (cancerous cell line) and L929 (normal cell lines) were adjusted to 1×10^4 cells/mL and 180 µL of each were seeded into 96 well plates. Cells were allowed to attach for at least 4 h followed by the addition of different weights (0.1-0.4 mg) of the respective test samples into the wells against phosphate buffered saline (PBS) in the control wells. The cells were cultured for 72 h at 37 ^{0}C in a 5% CO_2 incubator and proliferation was estimated by MTT assay method at 595 nm.[67] All experiments were performed in triplicates.

4B.2.13. *Analysis of morphological and nuclear change*

Cancerous (HeLa) as well as normal (L929) cells lines were used to detect changes in the morphology. Approximately, 2.5×10^5 cells were plated into 24 well plates and then 0.1 to 0.4 mg of the desired samples against PBS in the control wells. Cells were incubated for 32 h after which control and treated groups were stained with 20 µg/mL of DAPI (4',6-diamidino-2-phenylindole) (Invitrogen) and observed under Olympus fluorescence microscope to analyze any change in the nuclear morphology. The cells were also observed under confocal microscope to check for any change in the structural modulation post treatment with lycopene, PAni and PAni-lycopene conjugate.

4B.2.14. *Phytocompatibility analysis*

The phytocompatibility (in terms of the effect on the seed germination rate, the seedling root length and shoot length post transferring to soil beds) of 5 mL of the respective aqueous dispersion of the test samples (lycopene, PAni and PAni-lycopene conjugate) with *Cucumis sativus* seeds was evaluated according to previously described (section 3A.2.6) protocol.

4B.3. Results and Discussion

4B.3.1. *Extraction of lycopene and statistical optimization*

Owing to its multiple roles, extraction of lycopene has received considerable impetus across different domains in recent years. In this pursuit, the concomitant use of two of the green chemistry tools- biocatalysis and ultrasonication has been explored to facilitate the extraction of lycopene from tomato peel. Conventionally, pure extractants (*e.g.*, dichloromethane), mixtures of polar or polar–non polar extractants in different ratios, ethylene acetate, benzene, ethyl ether and petroleum ether have been used for lycopene extraction.[68] The extraction of lycopene in the reported protocol was also performed in organic solvents, which have obvious hazardous effects and as such the whole process was not green per se. The prime factor responsible for this is the poor solubility of lycopene in aqueous medium (the ideal 'green' solvent). Micelle formation, microemulsions and use of cyclodextrins have been used to increase the solubility and stability of lycopene. However, it has been highlighted[68] that the half-life of lycopene in organic aqueous solutions, which was expected to increase in the presence of organic co-solvents, such as tetrahydrofuran (THF) and dimethylsulfoxide (DMSO) was less than 120 min. Although supercritical fluid extraction (SFE) (a green chemistry tool) is marked by low contaminant, non-toxic and non-flammable characteristics, high investments and high purity, prerequisite for SFE and mandatory presence of a stabilizer and a co-solvent due to its non-polar character does not draw much demand. This leaves scope to develop and use alternative greener solvents for the extraction process.

Nevertheless, extraction protocol without any treatment *i.e.*, enzymatic or ultrasonication (control) had yielded about 80 μg lycopene per gram. Lycopene content in fresh tomatoes ranges from 8.8-42 μg/g wet weight[68] while processing of the tomato products increases the total extractable lycopene. This range has been determined through experiments which primarily rely on the conventional extraction protocol using organic

solvents. On the other hand, Perkins-Veazie and colleagues[69] have reported the range to be 50-60 μg/g for organically produced tomatoes with the maximal value of 107 μg/g. Choudhari & Ananthanarayan[47] have cited the references of Gross[70] and Baysal et al.[71] They have reported the lycopene content to range between 90 and 190 μg/g fresh weight. Considering these points, the lycopene yield that has been quantified in the present work was within the expected range. It is to be taken into account that lycopene content of tomato is dictated by numerous factors.[72-74] Lycopene concentrations in fruits may depend on genetics, and consequently the choice of cultivated variety is important; the influence of major factors of environment and cultivation techniques on the lycopene content in tomato fruits must also be known. This is again dependent on other factors like storage and age of the tomatoes.

Only cellulase treatment resulted in an increment of about 225% (260 μg/g) over the untreated sample. 5% (w/w) of the biocatalyst and incubation period of 20 min were found optimal for maximal lycopene extraction from the samples of set A (*i.e.*, only enzyme treated) as opposed to previous results of 3 % and 15 min.[47] These alterations may be attributed to the difference in the batch of the tomato peel (substrate) used with different proportions of extractable lycopene, a variable parameter dictated by various factors as outlined above. Furthermore, cellulase used in this study was isolated from *T. viride* (Cellulase 'Onozuka R-10', Merck) while *T. reesei* (Celluclast-1.5 L, Novozyme, Bangalore) was the source of the biocatalyst (which registered only about 107 % increment in yield) in the previous study.[47] In the present study, the percent increment in lycopene yield using Celluclast-1.5 L, under optimized conditions (3% w/w and incubation period of 15 min) over the unaided process was only about 160% as compared to 225% using Cellulase 'Onozuka R-10'. The significant increment in the extracted lycopene could be easily inferred. At this juncture, it is appropriate to highlight the findings of another research report on the utility of this enzyme in the material science domain. This is related to change of mechanical properties and nanostructural attributes of wood cell wall, with induction of large pore-formation post enzyme treatment.[75] The cell wall degrading potential of the enzyme (primarily attributed to the cleavage of β-D-glucosidic linkages in cellulose) is often exploited in combination with macerozyme R- 10 for the isolation of protoplasts.

Sonication is endowed with the advantages of inexpensiveness, simplicity, reproducibility, and ease of operation during the extraction protocols of myriad bioactive

components. Bates et al.[76] have demonstrated the improvement in the liquid phase extraction of valuable chemical components from solid material by using preferentially immersed ultrasonic sonotrode. Keeping this in mind, the present study was restricted to horn type sonicator.

RSM has been used to analyze the influence of sonication with three variable parameters, namely duration of sonication (min), cycle and percent amplitude on the amount of extracted lycopene. The parameters of equation (1), given in the experimental section were determined by multiple regression analysis. The overall second-order polynomial equation is represented as

$$L = 568.2 + 60.9\,C_1 + 24.2\,C_2 + 7.1\,C_3 - 50.9\,C_1{*}C_1 + 1.30\,C_2{*}C_2 - 0.7\,C_3{*}C_3 - 20.3\,C_1{*}C_2 - 4.8\,C_1{*}C_3 + 0.2\,C_2{*}C_3 \quad \text{..... (4B.9)}$$

Response surface plots aid in the visualization of the predicted model equation. For quadratic models, the critical point can be characterized as maximum, minimum, or saddle. If there are three or more variables, the plot visualization is possible only if one or more variables are set to a constant value. Rotation of the respective plots in the Minitab 15 Statistical Software® helped to accentuate the ridge and valleys of the L values *i.e.*, the amount of lycopene extracted along z-axis. The 3D wireframe plots (Fig.4.B.1) indicated that the maximum amount of lycopene (> 600 µg/g) could be extracted when sonication was done for 6 min at 0.6 cycles and 60% amplitude.

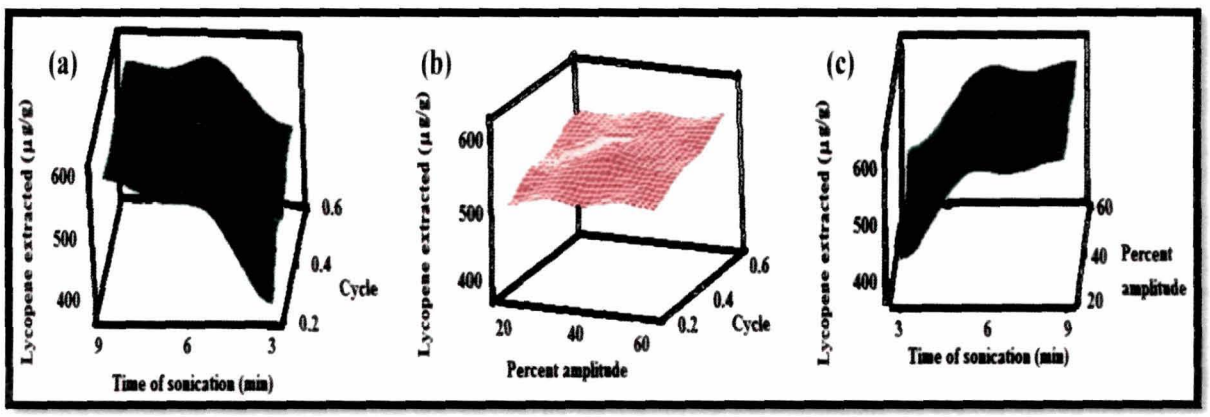

Fig.4B.1. *Response surface plots of amount of lycopene extracted vs. a) time of sonication vs. cycle, b) cycle vs. percent amplitude and c) time of sonication vs. percent amplitude*

All the three chosen variables (time of sonication, cycles and percent amplitude) exerted a linear effect on the response *i.e.*, the yield of lycopene was dictated individually by each of the chosen variables. On the other hand, the quadratic influence of time of

sonication could be visualized through the curvature in the corresponding plots. The model contained three two-way interactions (time of sonication*cycles, time of sonication*percent amplitude and cycles*percent amplitude). Barring the significant cross effect of time of sonication*cycles, p-value was more than 0.05 (chosen α value) (Table 4B.2) for the other two. The model yielded a R^2 value that could explain up to 96.42% of the sample variance.

The Ultrasonics Processor UP200S generated longitudinal mechanical vibrations by means of electric excitation (reversed piezoelectric effect) with a frequency of 24 kHz. The vibrations were amplified by the sonotrode fitted to the horn and formed as a $\lambda/2$ vibrator and transferred via its end face to the medium to be sonically irradiated. The amplitude/ultrasonic output of the sonotrode fitted (tip diameter of 3mm) in the present instrument could be adjusted steplessly between 20% and 100%. For 60% amplitude, the ultrasonic output was 126 μm. This value was found to be the best to facilitate optimal diffusion and interfacial interaction of the enzyme and the substrate.

When the variable parameters were set at values lesser than the optimal, the sonication-mediated effective facilitation of diffusion and interfacial interaction of the enzyme and the substrate could not be realized, which, vouch for the corresponding lesser yield of lycopene. Sonication at low frequencies dissipates most of the ultrasound energy through the process of cavitation.

Table4B.2. *Model coefficients estimated by multiple regressions (model adequacy checking)*

Term	*Coefficient*	*t value*	*p value*
Constant	568.2	127.9	0.000 < 0.05
C_1	60.9	19.5	0.000 < 0.05
C_2	24.2	7.8	0.000 < 0.05
C_3	7.1	2.3	0.034 < 0.05
C_1*C_1	-50.9	-10.3	0.000 < 0.05
C_2*C_2	1.3	0.3	0.795 > 0.05
C_3*C_3	-0.7	-0.1	0.889 > 0.05
C_1*C_2	-20.3	-5.3	0.000 < 0.05
C_2*C_3	-4.8	-1.2	0.226 > 0.05
C_3*C_1	0.2	0.04	0.966 > 0.05

However, at high frequencies and prolonged sonication, a significant amount of energy is dissipated through heating (at the expense of cavitational dissipation). Thus, on increasing the time of sonication, a corresponding increase in the lycopene yield was not recorded (Table4B.1). In this context, the plausibility of thermal denaturation of the enzyme due to longer duration of irradiation in the medium could not be ruled out. Interestingly, on sonicating for 9 min at 60% amplitude and 0.6 cycles (the maximal values for all the three chosen parameters), isomerization of trans-lycopene to cis-form were noticed as evident from the appearance of additional absorbance peak at around 360 nm in the UV-visible spectra.

On the other hand, 200 μg/g of lycopene could be extracted through the sonication-mediated extraction in the absence of the biocatalyst. These results were indicative of the synergistic action of the enzyme and ultrasonication under optimized conditions.

Response surface methodology and the experimental design that was applied, given the limits imposed by the nature of the experiment, revealed themselves to be efficient in the determination of the optimal conditions of sonication for theoretically obtaining maximal lycopene yield in enzyme mediated extraction. As the optimum had been located, the experimental domain and the spacing of levels were adequately chosen. The choice of a second order polynomial regression model was also satisfactory, and the estimation of coefficients by multiple linear regressions was a priori much more explanatory than that obtained by any classical analysis of variance.

Furthermore, enzyme associated parameters such as pH and temperature were optimized prior to and post sonication. Interestingly no change was registered for the optimal values. Hence, the optimization data of the enzyme associated parameters and corresponding response surface plots are not shown here. However, two parameters, *viz.*, the time of incubation and the amount of enzyme, were found to be influenced by sonication.

It was also interesting to note that 3% (w/w) of the enzyme and incubation period of 12 min were optimal for the extraction of lycopene when used under the assistance of ultrasonication. A reduction of 40% of enzyme use and decrease in time of incubation by 8 min over the corresponding parameters optimized for enzyme treatment alone (indicated earlier) were indicative of clear advantage of the coupled system. At this juncture it is critical to note that post optimization of all the parameters, concomitant use of Celluclast-

1.5 L and sonication could register only about 463% increase in the lycopene yield over the unaided process which was much lesser than the concurrent use of cellulase 'Onozuka R-10' and sonication. It was however interesting to note that the optimum concentration of the Celluclast-1.5 L remained the same i.e., 3% (w/w) while the incubation period reduced to 12 min in the coupled system. The change in the observed kinetic parameters of both the enzymes needs a greater delving. This study thereby vouched for the differential efficacy of the two studied enzymes.

4B.3.2. *Probable mechanism of action*

Comprehending the role of sonication in the enhanced extraction of lycopene (Fig. 4B.2a) is of utmost significance. Ultrasonication is based on the creation of high frequency mechanical vibrations by stimulating piezoelectric crystals with high frequency oscillating electrical currents. Ultrasonic probe attached to the crystal oscillate up and down. A typical oscillation involves a contraction on application of electrical current and an expansion on the reversal of the current. When the probe contracts, negative pressure causes the liquid to flow up with the probe while the expansion of the crystal pushes the liquid. As the liquid cannot keep pace with the oscillation of the crystal, small cavities are formed during the contraction. In general, cavitation refers to the occurrence of vapor in a fluid due to local low pressures which are generated by high local flow velocities. The size of the cavitation bubbles is a function of the rarefaction and compression cycles. The dynamics of cavity growth and collapse are dependent on the type of liquid, frequency of oscillation, presence of any nucleating agent such as dissolved species and gases in the liquid, and temperature of the liquid. The mechanism of cavitation inception *i.e.,* the beginning of cavitation, involves growth of small gas bubbles called nuclei, present in the fluid. Cavitation nuclei are often viewed as gas pockets stabilized in crevices of solid surfaces, either bounding walls or particles present in the liquid.[76] During the expansion cycle, the cavities rapidly implode and create microscopic shock waves. It is pertinent to mention that the transient cavitations end up in collapse, within a short span of time, resulting in shock waves, while stable cavitations resonate in the applied sound field, surviving the local pressure variations for a number of acoustic cycles. A large amount of energy is released during a compression cycle due to the collapse of the cavitation bubbles of size that have reached a critical point. When collapse of a cavity occurs in a solution free of solid particles, heating is

the only consequence. However, if implosion occurs near a solid surface, implosion is asymmetric. As water rushes to fill the void left by the imploding bubble (*e.g.,* at speeds near 400 m/s) shock pressures of 1-5 kPa can be generated. In our system, the role of these microjets is exploited for the enhanced extraction of lycopene. Fig.4B.2 b and c highlight this aspect. During a compression cycle, cavitation bubble (generated close to the tomato peel surface) collapses with the generation of a microjet directed towards the plant matrix. The high pressure and temperature released in this cascade breaks open the cell walls and releases the content into the medium.

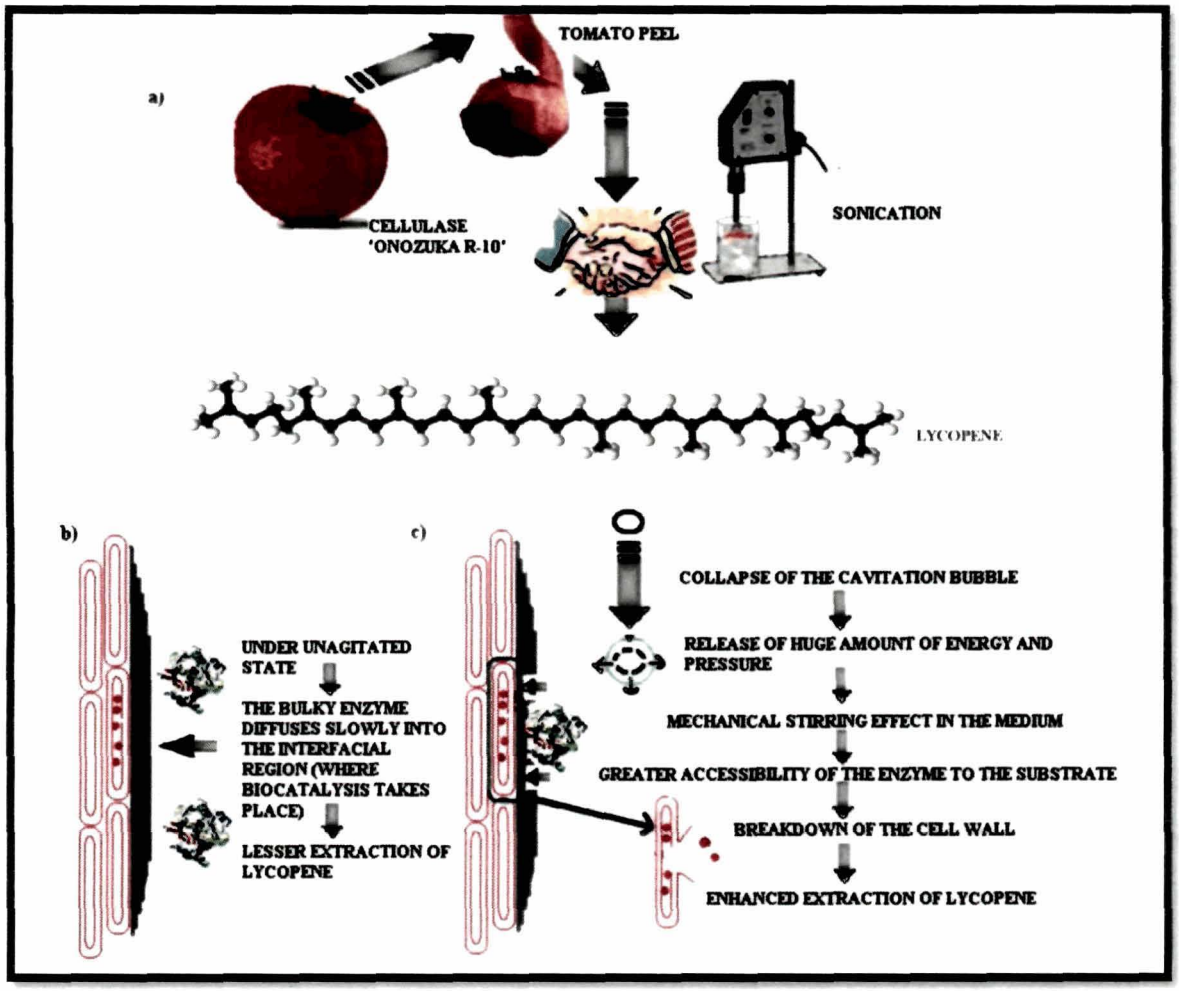

Fig.4B.2. *a) Schematic representation of the coupled action of sonication and biocatalysis in the extraction of lycopene, b) and c) Proposed mechanism of enhanced extraction of lycopene under the concomitant exploitation of ultrasonication and biocatalysis*

The diffusion rate of the biocatalysts has a prime role in dictating the overall reaction rate of their substrate hydrolysis. Sonication of enzyme solution under specific conditions could provide a far more efficient transport mechanism for "bulky" enzyme

macromolecules throughout the immediate border layer of liquid at the substrate surface. The rapid collapse of the cavitation bubbles is accompanied by generation of significant shear forces in the bulk liquid immediately surrounding the bubbles. This provides a strong stirring mechanical effect that can significantly increase mass and heat transfer to the surface of the substrate through disruption of the solid-liquid interfacial boundary layer. This immediate layer is practically immobile and then the velocities of the subsequent layers rapidly increase to the maximum constant value governed by the power of agitation of the bulk solution. The enzyme-substrate interaction occurs in this interfacial region. The agitation of this normally immobile layer of liquid through collapse of the cavitation bubbles tremendously increases the access of the chosen enzyme (cellulase) to the surface of the substrate, eventually leading to enhanced performance. As noted later, the optimized sonication parameters were suitable for enhancing the lycopene extraction without compromising with the structural integrity and bioactivity of the extracted lycopene.

4B.3.3. *UV-visible derivative spectra, FTIR spectra and DPPH scavenging potency of the extracted lycopene*

Investigating the change in the structural/molecular properties and functionality of bioactive moieties in response to the sonication assisted extraction is of paramount importance particularly for thermolabile components. In order to evaluate this, the 1st order derivative and the 2nd order derivative plots of the UV-visible absorbance of the lycopene extract of the enzyme (cellulase 'Onozuka R-10')-mediated, sonication-mediated and the optimized coupled system mediated extraction protocols were analyzed. It is pertinent to mention that derivative techniques in UV spectrophotometry are instrumental in separation methods for the analysis of drug mixtures, determination of degradation products as well as in stability studies.[77] The spectral indices of lycopene (*viz.*, $\varepsilon_{445}/\varepsilon_{472}$ and $\varepsilon_{503}/\varepsilon_{472}$) extracts in petroleum ether for the control, only enzyme treated, coupled system treated and only sonication treated samples were 0.911, 0.941, 0.951, 0.934 and 0.926, 0.952, 0.962, 0.945 respectively. Fig.4B.3 a and b show the first- and second-order derivative spectra (*i.e.*, $dA/d\lambda$ and $d^2A/d\lambda^2$ against λ) respectively for these samples. Molecular rearrangements or other structural modifications of the absorbing compound can be easily detected through higher resolution of these spectra. It is pertinent to mention that UV-visible spectra can also be instrumental in detecting *cis-trans* isomerisation. Due to

bent-geometry of *cis*-compound, a peak at around 360 nm appears. Additionally, a hypochromatic effect (decrease in intensity) is observed upon isomerization. This is because the isomerization is reversible and an equilibrium *trans-cis* mix eventually forms. Finally, a slight hypsochromatic shift (blue shift to shorter wavelengths) is also observed.[78] A careful inspection and comparison of these spectra of lycopene extracted from the various samples did not reveal any significant change in the region of 350-550 nm.

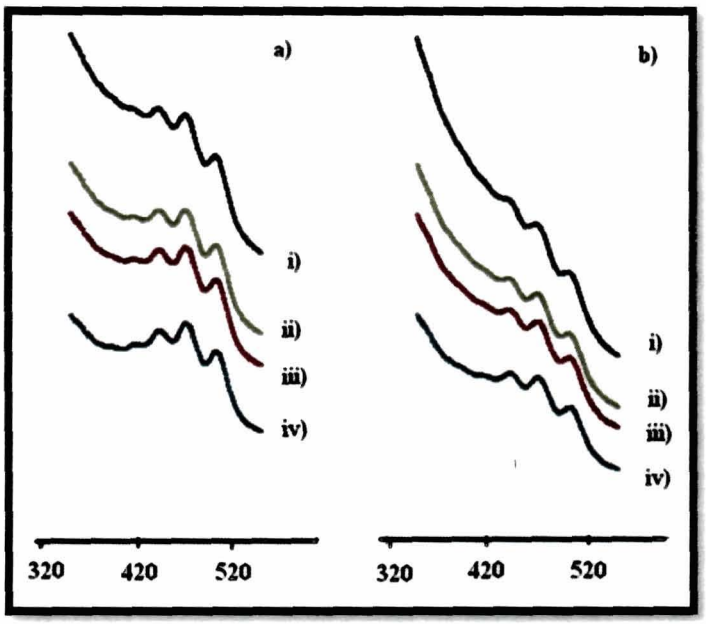

Fig.4B.3. *a) First order and b) second order derivative spectra of lycopene obtained from i) control (unaided extraction), ii) only enzyme treated, iii) coupled system treated and, iv) only sonication (under the same optimized parameters as for the coupled system) treated samples.*

It was thus assumed that the molecular and structural integrity of the bioactive molecule was retained post treatment of the samples with sonication and biocatalyst. Furthermore, FTIR spectra (Fig.4B.4) of lycopene (band at around 813 cm^{-1} corresponding to wagging vibration of ((RH)-C=C-(RH)), 1388 cm^{-1} corresponding to vibration due to symmetric deformation of $-CH_3$ and 1467 cm^{-1} due to deformation vibration of $-CH_2$) extracted via the various approaches showed no shift in the band position. It is critical to note that *cis*-isomer absorbs more strongly than *trans* isomer (*cis* is less symmetrical than *trans*). This study confirmed that there was no change in the position and type of functionality in the extracted biomolecule prior to and post sonication. However, in order to establish the purity of the extracted lycopene, techniques like HPLC analysis and NMR spectroscopy are prerequisite.

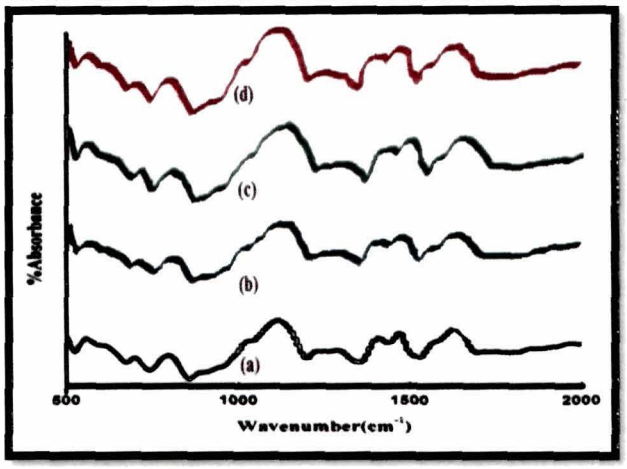

Fig.4B.4. *FTIR spectra of lycopene obtained from a) control (unaided protocol) b) only enzyme treated, c) coupled system treated and, d) only sonication (under the same optimized parameters as for the coupled system) treated samples.*

The singlet oxygen and peroxyl radical scavenging potency of lycopene is well documented. Adduct formation, electron transfer to the radical and allylic hydrogen abstraction are the three possible mechanism of action of lycopene towards reactive species.[79] In order to assess the bioactivity of the extracted lycopene, free radical scavenging (DPPH) potency of lycopene was analyzed. Free radical scavenging efficiency by 10 μM of lycopene extracted through control, enzyme treated, coupled system treated and only sonication treated was about 35%, 37.5%, 38.2% and 36.3% respectively. These results confirmed the retention of the bioactivity of the extracted biomolecule.

4B.3.4. *Cellulase 'Onozuka R-10' activity measurement*

It is pertinent to mention that ultrasonication is used for inactivating various enzymes and as such it is a common approach in food-preservation.[80] It is commonly perceived that the powerful shock waves resulting from the collapse of cavitation bubbles could damage or at least inactivate the very sensitive and overall structure of biocatalysts. The confounding effects can range from partial aggregation, partial denaturation, to ultrasonically induced self-chemical modulation involving reactions of its UV-absorbing amino acidic residues.[81] Although ultrasound in combination with mild heat treatment and/or pressure has shown potential for both enzyme and pathogen inactivation, sonication alone may not be adequate for inactivation of various spoilage and harmful enzymes present in food.[80]

Although the possible consequences of thermal denaturation (due to collapse of cavitation bubbles) could not be completely ruled out, all samples were ultrasonicated at ice bath temperature to minimize the same. UV-visible absorption spectrophotometric analyses were performed to assess the effect of ultrasonication on the enzyme structure. The absorbance of solutions in the spectral region of 240 and 550 nm remained the same which implied that the enzyme samples (prior to and post sonication) maintained their global protein structure without substantial chemical modification. According to a recent study, ultrasonicated glucose oxidase showed an altered composition with reduced α-helix and β-sheet fractions compared to the pristine enzyme.[81] However, low-temperature ultrasonic processing of the enzyme did not compromise the bioactivity. The changes (if any) induced in the structure of the enzyme moiety in response to ultrasonication merit further in-depth investigation. The enzyme activity that was retained post exposure to sonication in the absence of substrate was 95% of the activity prior to sonication. When collapse of a cavity occurs in a solution free of solid particles (substrate *i.e.,* tomato peel in the present case), heating is the only consequence, as noted previously. This may explain the 5% loss of enzyme activity. However, if implosion occurs near a solid surface, implosion is asymmetric, followed by generation of microjets. The role of these microjets directed towards the plant cells, facilitating better enzyme-substrate interaction is exploited for the enhanced extraction of lycopene. However, the activity in the filtrate was about 71% of the initial activity. This decrease may be due to probable loss of enzyme during the extraction protocol and subsequent handling. Post extraction, precise determination of the cellulase activity was difficult as the recyclability of the enzyme was not ensured. This opens up a prospective scope to immobilize the enzyme onto suitable supports like magnetic iron oxide nanoparticles.

4B.3.5. *Preparation and physico-chemico characterization of the conjugate*

Nanofibrillar morphology is intrinsic to PAni synthesized in water and changing the organic solvent does not have a major dictate over the final product in interfacial polymerization.[55] In the present report, the recipe in the organic phase consisted of a mixture of two solvents namely chloroform and toluene. The choice of solvents was made in such a way that these interact with each other via complex formation[82] together with lowering of surface tension of the organic phase compared to the aqueous phase. This in

turn increased the interfacial surface area for the polymerization reaction. The intermolecular π-association of chloroform with toluene led to decreased solubility or solvation of aniline monomer in the organic phase, thereby decreasing the induction time (of formation) of PAni nanofibers. Water has a high dielectric constant resulting in the solvation of the oxidant and dopant dissolved in it. This facilitated a better interaction of the solvated ions in the aqueous phase with the aniline monomer. The aqueous phase with a higher surface tension exerted a strong pull on the neighboring liquid (aniline) present in the organic phase having lower surface tension. In other words aniline monomer moved across the interface of the two phases due to surface tension gradient. This may be viewed as an extension of the Marangoni effect in the nanofiber formation.

4B.3.5.1. *TEM imaging*

In order to illustrate the time-dependence of growth of the nanofibers, two of the TEM images (Fig.4B.5 a and b) of the PAni nanofibers at two different stages of the reaction are shown. The polymerization for 30 min (Fig.4B.5a) resulted in the nanofibrillar morphology of the PAni fibers with average diameter of around 30-40 nm (and a few fibers with tapering appearance of 14-22 nm) with no branched network structure. Increment of polymerization time resulted in nanofibers with entangled structure with gradual agglomeration of the PAni chains. The growth in the secondary structures and formation of agglomerated mass with increasing reaction time (2 h) is exemplified by Fig.4B.5b. The PAni nanofibers synthesized with 1:1 toluene-chloroform solvents in the organic phase showed the maximal loading of lycopene than the ones synthesized using either of the single solvents, due to the small average diameter of the PAni nanofibers produced within 30 min.

Post conjugation via sonication generated PAni nanofibers with trifoliate branching (Fig.4B.5.c) (mimicking the branching pattern as in *Poncirus trifoliate* (L). Raf). The fibers and the trifoliate branches were about 45-52 nm and 23-37 nm wide respectively. Laslau et al.[83] have proposed that stacking, hydrogen bonding and charge-charge repulsion from protonation among three intrinsic morphologies *viz.,* nanofibrils, nanosheets and nanoparticles lead to the growth, agglomeration and curling behaviours of conducting polymers. This ultimately leads to the genesis of unique nanostructured morphology. This

pattern of self-assembly involving the Y-junctions (branching) may be interpreted in the framework of an extended multi-layer theory.[83]

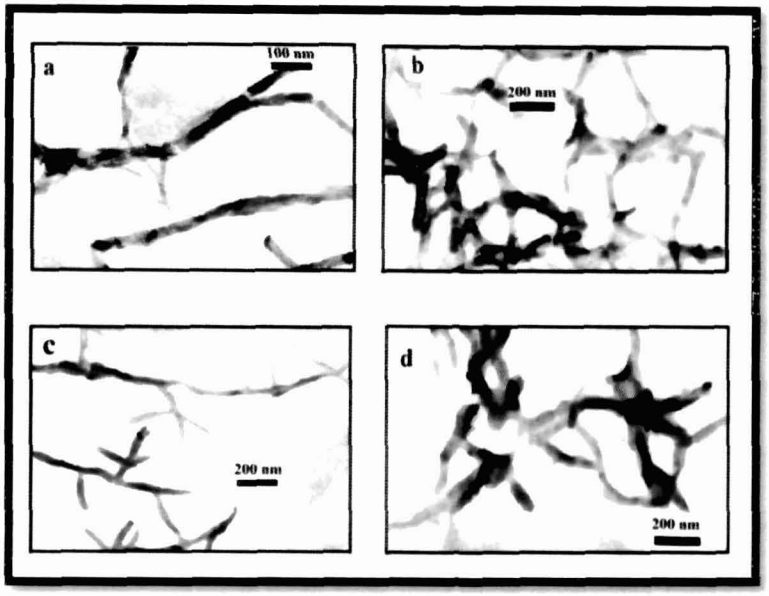

Fig.4B.5. *TEM micrograph of PAni nanofiber a) after 30 min of induction time, b) after 2 h of induction time, and post sonication of (a) under statistically optimized parameters of 2 min, 0.6 cycle and 60 % amplitude in the c) presence and d) absence of tomato-peel lycopene*

Thus, the results presented in the subsequent section correspond to the PAni nanofibers synthesized using the recipe of 1:1 toluene-choloroform in the organic phase and extracted within 30 min of reaction time. Sonication mediated immobilization of lycopene onto the PAni nanofibers under optimized parameters (optimization data not shown) of 2 min, 0.6 cycle and 60 percent amplitude resulted in a maximal loading of about 60%. It is pertinent to mention that sonication under the same optimized parameters in the absence of lycopene resulted in agglomeration (Fig.4B.5d). This was suggestive of the influence of the biomolecule in dictating the shape-size accord of the polyaniline nanofibers in presence of ultrasound. However, increased time and frequency of sonication resulted in *cis*-isomerism of lycopene. Furthermore, TEM imaging of bio-conjugated systems, prepared at higher frequency and sonication time resulted in agglomeration.

4B.3.5.2. *X-ray diffraction*

Broad reflections at around 2θ values of 19.2° and 26°, typical of HCl doped PAni[84] were recorded in the X-ray diffractogram of the PAni nanofibers. These peaks corresponding to the (100) and (110) reflections were assigned to the regular spacing

between phenyl rings of adjacent chains of PAni in parallel and perpendicular orientation, respectively. On the other hand, characteristics peaks for lycopene were observed at around 2θ = (5-30)^0 and a sharp peak at around 44^0.[85] On the other hand, the (100) reflection in the bio-conjugated PAni became narrower and showed shift in the peak position by one unit towards higher 2θ values. A single-line method employing a Voigt function has been used to analyze the origin of line broadening in the x-ray diffraction pattern.[84] The more intense reflection peak at about 26° has been de-convoluted computationally (Fig.4B.6) to calculate the *d*-spacing, domain length and strain (Table 4B.3) produced in the PAni chains.

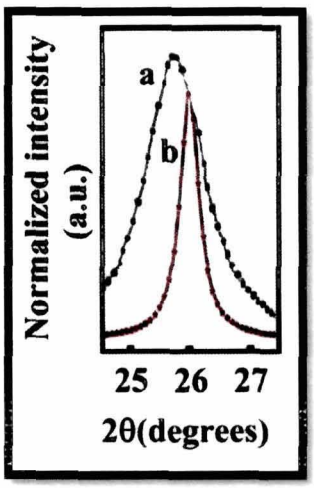

Fig.4B.6. *Deconvoluted peak at around 2θ=26^0 of PAni nanofiber a) prior to and b) post bioconjugation*

The increase in the *d* spacing from 3.49 to 3.801 Å, post lycopene loading, suggested an increase in the angle at which the chains tilted with respect to the (*a, b*) basal plane of PAni.[84]

Table4B.3. *d-spacing, crystallite size and strain of PAni nanofibers prior to and post loading with lycopene*

Sample	*d-spacing (Å)*	*Crystallite size (Å)*	*Strain (ε) (%)*
PAni nanofibers	3.49	21.699	2.9
Lycopene-PAni hybrid	3.801	209.807	1.6

The increase in the tilt angle of C_{ring}-N-C_{ring} indicated reduction in π-stacking among the PAni chains. It was interesting to observe the increase in the crystallite size from ~ 21.7 Å to 209.8 Å. Thus, the narrowing of the most intense (110) reflection in the conjugated system could be attributed to the increase in the domain length along with the decreasing strain. These results could be interpreted in terms of the decrease in the concentration of defects within the polymeric skeleton of PAni nanofibers.

4B.3.5.3.*Conductivity measurement*

The electrical conductivity of the pellets of PAni and PAni-lycopene conjugate were found to be 8.27×10^{-5} S/cm and 3.16×10^{-5} S/cm respectively. These values revealed that post lycopene immobilization, the semiconducting-behavior of the PAni nanofibers was retained although lycopene coupling resulted in decrease of the former's conductivity value. It is pertinent to mention that effective conjugation length of PAni nanofibers is strongly influenced by the conformation because the degree of the *p*-orbital overlap in the extended π-bond is dictated by the torsion angle of the backbone.[84] The decrease in conductivity value post lycopene coupling may be attributed to the decrease in the π-stacking of the PAni chains and density of defect states. These results corroborated well with the XRD results.

4B.3.5.4. *FTIR analysis*

Characteristic FTIR bands (Fig.4B.7) for the wagging vibration of ((RH)-C=C-(RH)), symmetric deformation of $-CH_3$ and deformation vibration of $-CH_2$ of lycopene were evident at 813 cm^{-1}, 1388 cm^{-1} and 1467 cm^{-1} respectively, as mentioned in section 3.B.3.3.

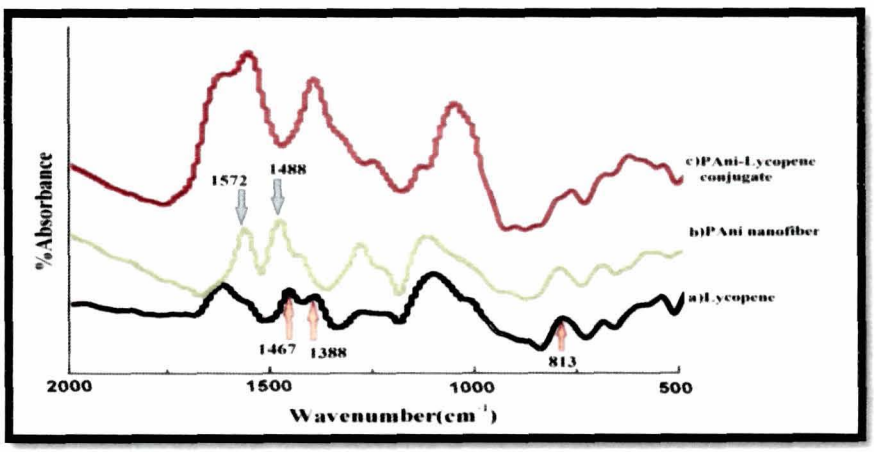

Fig.4B.7. *FT-IR spectra of a) lycopene, b) PAni nanofiber and c)PAni-lycopene conjugate*

On the other hand, the quinoid ring and the benzenoid ring of the PAni nanofibers exhibited the C=C stretching vibration at 1572 cm^{-1} and 1488 cm^{-1} respectively.[84] Considerable shifts in the corresponding band position and disappearance of few of the characteristic bands of the conjugating partners were indicative of considerable interaction in the bioconjugated state. In order to have a better insight into the interaction, tools of computational chemistry were utilized as described underneath.

4B.3.6. *Computational study*

4B.3.6.1. *Optimized geometry and energetics*

The optimized geometries of PAni, lycopene and PAni-lycopene units are shown in Fig.4B.8. The optimized structure of PAni (un-doped structure was taken for the study) assumed a twisted conformation with the central benzenoid rings moving out of the molecular plane (Fig.4B.8a). The lycopene chain comprising of two units remained mostly planar (Fig.4B.8b) maintaining the linearity of the unsaturated C=C backbone. For the computational study, the length of PAni was taken as 4.04 nm and that of lycopene was 3.78 nm. Upon interaction of PAni with lycopene (Fig.4B.8c) the optimum distance of interaction was found to be 3.83 Å. The preferred interaction via the unsaturated C=C bond of lycopene and the delocalized aromatic ring of PAni resulted in the weak binding between the two conjugating partners, with a binding energy value of – 0.393 eV. The non-planarity of PAni might weaken the maximum overlapping interaction accountable for the low binding energy value.

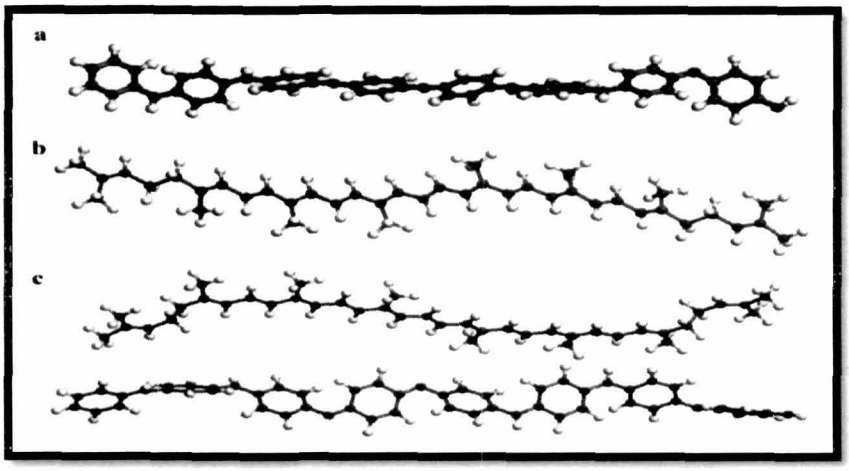

Fig.4B.8. *Optimized geometry of a) PAni nanofibers, b) lycopene and c) PAni-lycopene conjugated system*

The low value of binding energy at the optimum distance suggested the weak π-π stacking interaction coming into play between the aromatic ring of PAni and conjugated π-electron system of lycopene extended throughout the chain-length.

4B.3.6.2. *Frontier orbital analysis and quantum molecular descriptors*

The frontier orbital plots depicting the HOMO and LUMO for PAni, lycopene and PAni-lycopene complex are given in Fig.4B.9 and Fig.4B.10 respectively while the corresponding values of the HOMO–LUMO energy gap and global reactivity descriptors are provided in Table4B.4.

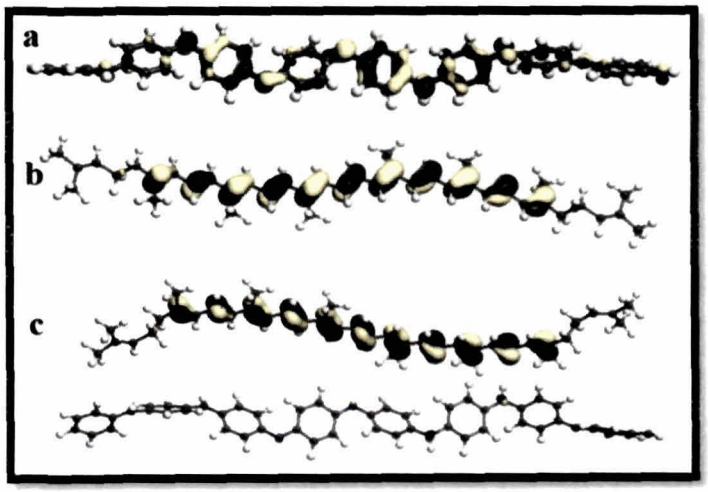

Fig.4B.9. *The frontier orbital plots depicting the HOMO for a) PAni, b) lycopene and c) PAni-lycopene conjugated system*

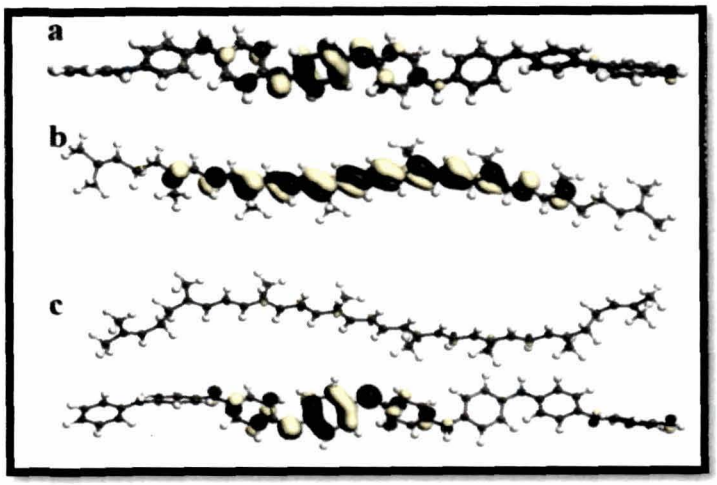

Fig.4B.10. *The frontier orbital plots depicting the LUMO for a) PAni, b) lycopene and c) PAni-lycopene conjugated system*

In PAni, the HOMO (Fig.4B.9a) was found to be delocalized throughout the aromatic ring with greater contribution from the central aromatic rings and decreasing charge towards the edges. The LUMO also had major contribution from the central aromatic ring with almost no contribution coming from the edges (Fig.4B.10a). In lycopene, the HOMO and LUMO are highly delocalized around the central C=C bonds of the unsaturated backbone with no charge distribution towards the edges (Fig.4B.9b and Fig.4B.10b). Upon interaction of PAni with lycopene the reorientation of frontier orbitals was quite interesting as observed in Fig.4B.9c and Fig.4B.10c.

Table4B.4. *Energetics of PAni, lycopene and PAni-lycopene conjugated system in gas phase*

Parameters	*PAni*	*Lycopene*	*PAni-Lycopene*
Total Energy (Ha)	-2289.9	-1557.7	-3847.6
Binding Energy (eV)	-	-	-0.39344
HOMO (eV)	-4.246	-3.942	-4.064
LUMO (eV)	-3.278	-2.997	-3.146
HOMO – LUMO gap (eV)	0.968	0.945	0.918
$\eta = (I - A)/2$ (eV)	0.484	0.4725	0.459
$\mu = -(I + A)/2$ (eV)	-3.762	-3.4695	-3.605
$\omega = \mu^2/2\eta$ (eV)	14.6205	12.738	14.1569

The HOMO-LUMO gap and η followed the order – PAni > lycopene > PAni-lycopene conjugated system. Although individual PAni and lycopene units were otherwise quite stable in gas phase, the reduced values of the above parameters were suggestive of favorable features for the conjugated system from the energetics' perspective. The chemical potential (μ) followed the order: PAni < PAni-lycopene < lycopene. Likewise, the electrophilicity index (a measure of the electrophilic power in a molecule) followed the order: PAni > PAni-lycopene > lycopene. Higher the ω value greater is the tendency to behave as an electrophile.

4B.3.6.3. *Solvation studies using COSMO*

Water happens to be the physiological solvent system. Compared to the gas phase studies, solvation studies was illustrative of an important facet of the developed system *i.e.*, the enhanced solubility of PAni-lycopene complex in aqueous media compared to organic

solvents. The dielectric solvation energy values of the PAni-lycopene system in three different solvents are given in Table4B.5.

Table4B.5. *Dielectric solvation energy values of PAni-lycopene system in different solvents*

Parameters	*Water*	*$CHCl_3$*	*DMSO*
Total Energy (Ha)	-3847.73459	-3847.71218	-3847.73342
Dielectric solvation energy (eV)	-2.433	-1.544	-2.382
HOMO (eV)	-4.224	-4.179	-4.222
LUMO (eV)	-3.448	-3.34	-3.442
HOMO – LUMO gap (eV)	0.776	0.839	0.78
$\eta = (I - A)/2$ (eV)	0.388	0.4195	0.39
$\mu = -(I + A)/2$ (eV)	-3.836	-3.759	-3.832
$\omega = \mu^2/2\eta$ (eV)	18.9625	16.8461	18.8259

Greater the negative value of the solvation energy, greater is its solubility in any given solvent. Upon conjugation of PAni with lycopene, the trend in solubility as judged from the dielectric solvation energy value followed the order: water>DMSO>$CHCl_3$. However, for the solvation studies the variation in HOMO–LUMO energy gap and global reactivity descriptors were not very dramatic and are not therefore discussed.

4B.3.7. *Action at the bio-interface*

4B.3.7.1. *Anti-lipid peroxidation and free radical scavenging potency*

In the biological milieu, lycopene acts as singlet oxygen ($^1O_2$) and peroxyl radical scavenger (LOO·).[79] Three possible reaction mechanisms[29] of lycopene with various radical species ($R^\bullet$) are shown underneath:

a. Adduct formation: Lycopene + $R^\bullet$ ⟶ R-Lycopene$^\bullet$
b. Electron transfer: Lycopene + $R^\bullet$ ⟶ Lycopene$^{\bullet+}$ + R^-
c. Allylic H abstraction: Lycopene + $R^\bullet$ ⟶ Lycopene$^\bullet$ + RH

The first mechanism is exemplified by the reaction of lycopene with lipid peroxyl radical. This involves the formation of resonance-stabilized carbon centered-peroxyl radicals where the peroxyl radical attaches to the polyene chain to form a lycopene-peroxyl radical adduct (ROO-lycopene$^\bullet$).[79] It is pertinent to mention that lycopene is the best anti-oxidant based on the electron transfer cascade[79] that involves the formation of its cation

radical, anion radical or alkyl radical. In the anti-lipid peroxidation assay, generation of lipid peroxides is followed by formation of peroxyl radicals. The assay is based on the detection of a stable product which is formed between the aldehydes (such as hexanal, malondialdehyde (MDA) and 4-hydroxynonenal generated in a decomposition stage) and thiobarbituric acid in the aqueous phase. On the other hand, PAni nanofiber has been established as a hemo-protective nanoscaled material.[86] Banerjee et al.[86] have reported that a single unit of the emeraldine salt can donate one hydrogen atom, thereby eliminating DPPH free radicals. This was evident (Fig.3.B.11) by corresponding decrease in the peak intensity at 517 nm. The results of anti-lipid peroxidation and DPPH scavenging assays are presented in Fig.4B.11a and Fig.4B.11b respectively. In the present study, the PAni nanofibers exhibited about 43% and 32% DPPH scavenging and anti-lipid peroxidation respectively (against vitamin E as the positive control in each of the assays) while the corresponding values for lycopene alone were 60% and 58% respectively.

Comparatively higher DPPH scavenging action has been reported for the formulations of lycopene with other anti-oxidants such as Vitamin C, vitamin E and ß-carotene than the individual scavenger.[79] Such combinations also displayed a higher inhibitory activity towards diene hydroperoxides produced from linoleic methyl ester with 2, 2'-azobis (2,4-dimethylvaleronitrile) (AMVN) induced oxidation.[79]

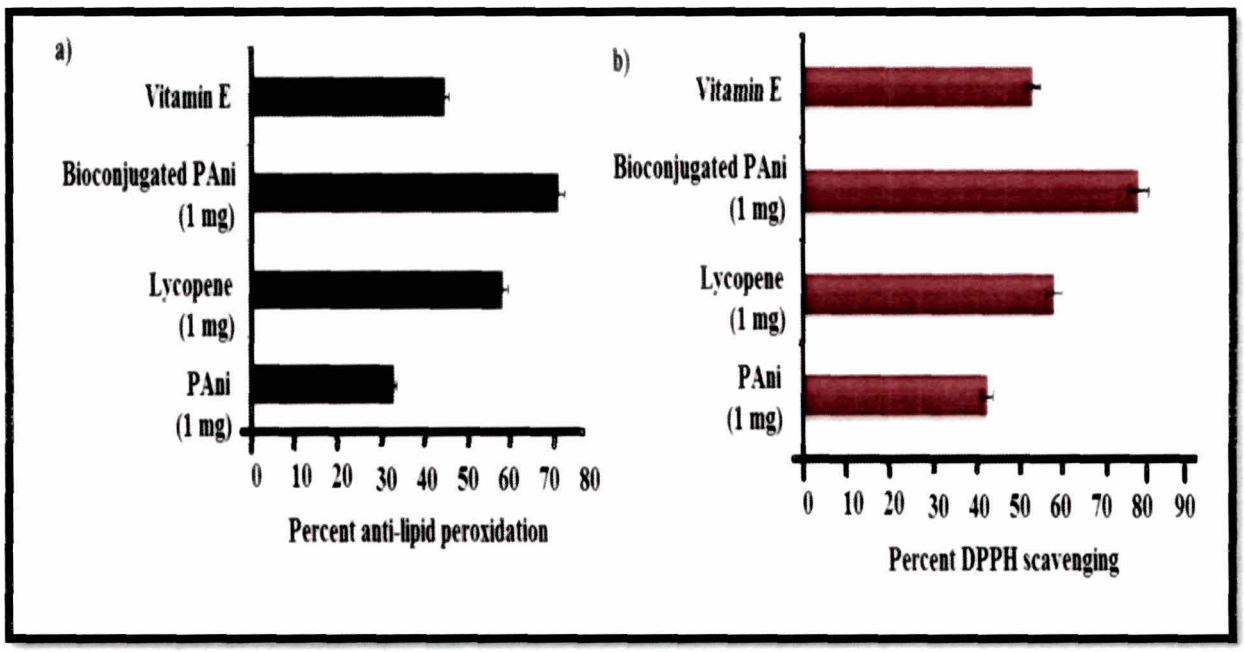

Fig.4B.11. *a) Anti-lipid peroxidation and b) DPPH scavenging assay*

Keeping in tract with these, a synergy was observed between the conjugating partners, *viz.*, PAni nanofibers and lycopene in the DPPH scavenging (~80%) as well as anti-lipid peroxidation (~70%) respectively.

4B.3.7.2. *In vitro cytocompatibility and anti-proliferative activity*

Assessing whether bio-conjugation could influence the cytocompatibility of PAni nanofibers was interesting. The applicability of PAni for tissue engineering has been reviewed by Guimard et al.[87] with an important observation that compatibility of PAni is cell-specific. Both non-covalent and covalent (involving various surface functionalization)[88] strategies have been explored for improving the cytocompatibility of PAni.

In the present investigation, it was interesting to record an augmentation in the proliferation (by about 54% on incubation with 0.4 mg of the conjugated system) of normal L929 cell line on exposure to the present reported bio-conjugated system compared to the control as evident from MTT analysis. Lycopene alone did not seem to affect the cell viability. It has been reported that lycopene at the physiological range does not significantly affect cell proliferation in an *in vitro* model as tested against seven different cell lines.[89] It seemed that the branched conjugated network somewhat had a better cushioning effect than the conjugating partners, thereby mimicking the extracellular matrix that provides a number of chemo-mechanical cues for cell-division. Here lies the plausibility of exploring the bio-conjugated system in the niche of tissue engineering. On the other hand, MTT assay attested the anti-proliferative action of the bio-conjugated system against HeLa cell line. Surprisingly, PAni alone did not seem to exhibit any cytotoxicity in HeLa cells but when conjugated with lycopene the cytotoxicity was explicitly amplified towards cancer cells (68% decrease in viable cells with 0.4 mg of the sample) with respect to the toxicity level of lycopene alone (45% decrease in viable cells). The above data thereby exemplified the potency of lycopene-PAni conjugated system as an antitumor biomaterial. The present study clearly demonstrated that there exists a differential *i.e.*, cell specific or receptor specific action of the nanomaterials at the bio-interface, affecting the proliferative potency of the cells. It is pertinent to mention that the lycopene that is converted to the biological active metabolite, apo-10′-lycopenoic acid both *in vitro* and *in vivo* transactivates the retinoic acid receptor ß (RAR ß) promoter and induce the expression of RAR ß in HeLa cells.[90, 91] RAR ß, which is regulated by retinoic acid via

RARs (retinoic acid receptors) has been suggested to be tumor suppressor gene. Here lies the scope for the biologists to understand the metabolism of lycopene in the presence of PAni nanofibers and the modulations in gene profile of cancerous cell lines.

Epiflorescence microscopic analysis (using an Olympus fluorescence microscope) revealed no alteration in the cellular morphology of the L929 cells in relation to the untreated sample (Fig.4B.12a1-a4). DAPI preferentially stains dsDNA and associate with the AT clusters in the minor groove.

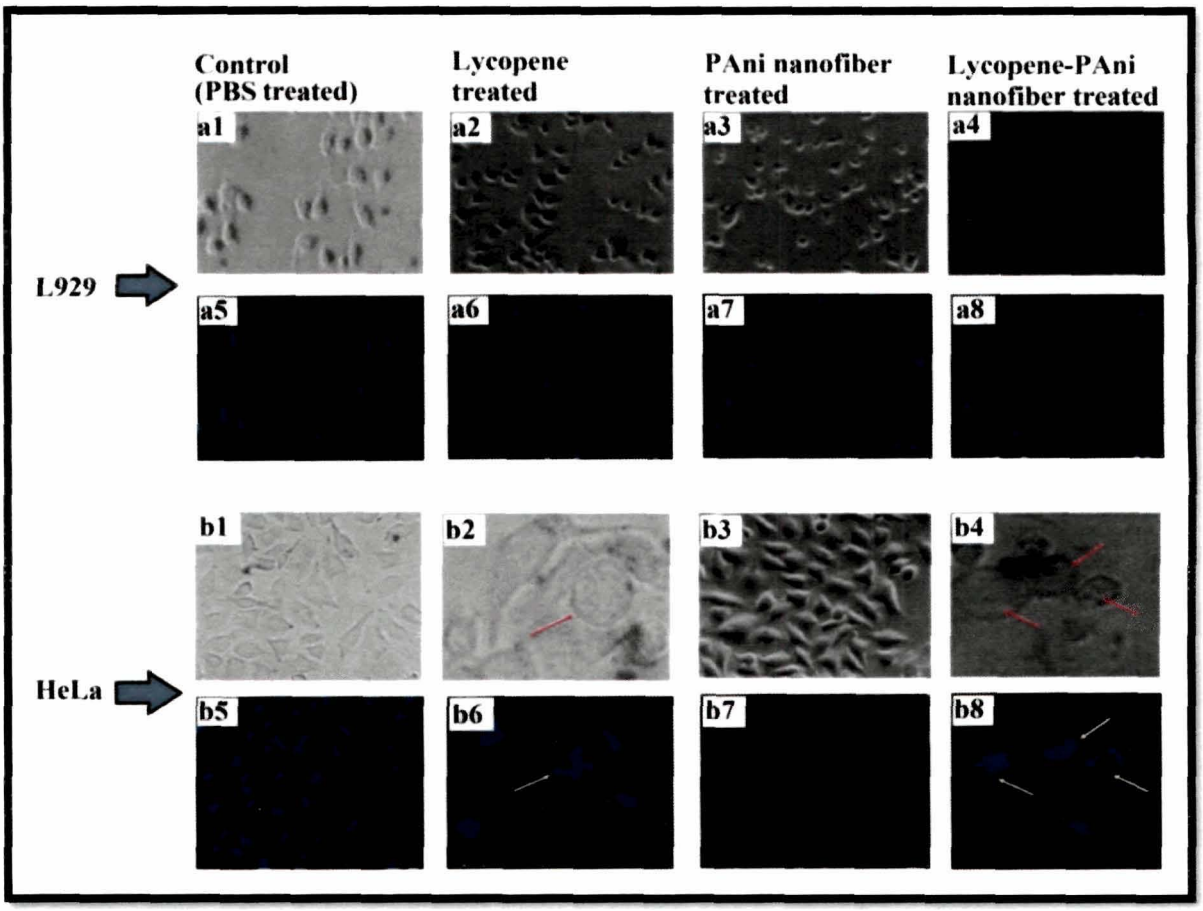

Fig.4B.12. *Epiflorescence microscopic images showing the effect of control (PBS), lycopene, PAni nanofiber and the conjugated system on normal L929 cells and HeLa cells.*

Perturbations in the nuclear morphology of the L929 cells were not evident post DAPI staining, thereby establishing the cytocompatibility of the reported system (Fig.4B.12a5-a8). PAni nanofibers showed no effect on the morphology of HeLa cells (Fig.4B.12b3). However, treatment with lycopene and the bio-conjugated system led to morphological alterations in the HeLa cells. Fig.4B.12b2 and Fig.4B.12b4 depict the rounded cellular morphology (shown by red arrows) (a characteristic of stressed cell)

while nuclear condensation and multi-nucleate/nuclear fragmentation (shown by yellow arrows) including membrane blebbing indicating apoptotic HeLa cells are exemplified by Fig.4B.12b6 and Fig.4B.12b8 respectively. Nuclear condensation due to cell stress is one of the signature events in cytotoxicity.[92]

4B.3.7.3. *Phytocompatibility assay*

The preliminary effect of the bio-conjugated system on the physiological change (if any) was evaluated on germinating seeds. The emergence of radicle or cotyledon coming out of the seed coat was documented as being germinated. The average germination rate of all the seeds in the control system and those exposed to PAni nanofibers, lycopene and bio-conjugated system was cent percent. However, there was subtle difference in the average radicle length post 5 days incubation. These were about 4 cm each for the control and the lycopene exposed seeds. Surprisingly, the corresponding values for seeds exposed to the PAni nanofibers in the free and bio-conjugated state were 4.4 and 4.8 cm respectively. All the seedlings exhibited cent percent survival 5 days post-transplantation. A striking observation was also made for the average shoot length. The seedlings emanating from control, lycopene, PAni nanofiber and the bio-conjugated system exposed seeds exhibited 5, 5, 6 and 6.2 cm of shoots respectively. At this juncture, it would be difficult to explain this observation. Unlike nanoparticles (which are more likely to penetrate the plant-cell membrane), the mass of nanofibers may act more as a suitable artificial substratum for the germinating seeds. The interaction of the PAni nanofibers with various seed coat proteins and, eventually modulating the signaling cascade of nutrient mobilization within the germinating seeds may be viewed as a plausible reason. Furthermore, the branched architecture of the bio-conjugated system may be critical in dictating the transmission of the differential chemo-mechanical cues, registering the enhanced radicle and shoot lengths. Further, a number of issues emanate out of this study. Is this augmentation and synergy a universal phenomenon, to be more precise, same for dicots and monocots? Does the anti-oxidant attribute of the nanofibers play any role? Do the seeds exposed to the test samples have better resistance to pathogenic microbes? Elucidation of these facets needs a greater delving using a multi-disciplinary integrated approach.

4B.4. Conclusion

The two of the green chemistry tools namely, sonication and biocatalysis have been successfully utilized for improving lycopene extraction from tomato peel, generated as a by-product of the food-processing industry. Multifold increment in the enzyme (cellulase 'Onozuka R-10)-mediated extraction of lycopene was recorded under statistically optimized sonication parameters over the unassisted protocol. Furthermore, use of sonication resulted in decrease in the requisite optimal enzyme concentration and incubation period. Derivative spectra of the first and the second order, FTIR analysis and free radical scavenging test vouched for the retention of the structural integrity and bioactivity of lycopene, extracted using the developed process. Consequently, the plausibility of integrating the innate attributes of this bio-medically important phytocompound *i.e.*, lycopene with PAni nanofibers has been delved into. The physico-chemical characterization and computational study revealed the morphological and molecular level modulation of the polyaniline structure post bio-conjugation. The computational study using different solvent systems highlighted the aptness of aqueous system for dissolution of the prospective drug-conjugated system with anti-lipid peroxidation and free radical scavenging potency. The establishment of biocompatibility with normal cell line complemented by anti-cancerous potency attested the system's suitability in the biomedical domain. On the other hand, the stimulatory effect of the conjugated system on seed germination calls for a greater delving into the action of nanoscaled materials in the ecosystem.

References

1. Yallapu, M.M., et al. *Colloid Surf. B* **79**, 113--125, 2010.
2. Anand, P., et al. *Biochem. Pharmacol.* **76**, 1590--1611, 2008.
3. Basile, V., et al. *Biochem. Pharmacol.* **78**, 1305--1315, 2009.
4. Rai, D., et al. *Biochem. J.* **410**, 147--155, 2008.
5. Mishra, S., et al. *Bioorg. Med. Chem.* **13**, 1477--1486, 2005.
6. Dahl, T.A., et al. *Arch. Microbiol.* **151**, 183--185, 1989.
7. Di Mario, F., et al. *Helicobacter* **12**, 238--243, 2007.
8. Bisht, S., et al. *J. Nanobiotechnol.* **5**, 3, 2007.
9. Salmaso, S., et al. *J. Drug Target* **15**, 379--390, 2007.
10. Letchford, K., et al. *J. Pharm. Sci.* **97**, 1179--1190, 2008.
11. Safavy, A., et al. *J. Med. Chem.* **50**, 6284--6288, 2007.
12. Feng, J-Y., & Liu, Z-Q. *J. Agric. Food Chem.* **57**, 11041--11046, 2009.
13. Galano, A., et al. *Chem. Phys.* **363**, 13--23, 2009.
14. Canamares, M.V., et al. *Appl. Spectrosc.* **60**, 1386--1391, 2006
15. Skrzypczak-Jankun, E., et al. *Int. J. Mol. Med.* **12**, 17--24, 2003.
16. Waranyoupalin, R., et al., *Cent. Eur. J. Chem.* **7**, 388--394, 2009.
17. Daniel, S., et al. *J. Inorgan. Biochem.* **98**, 266--275. 2004.
18. Borsari, M., et al. *Inorg. Chim. Acta* **328**, 61--68, 2002.
19. Xu, H., et al. *Biomaterials* **32**, 9758--65, 2011.
20. Paul, S., et al. *J. Magn. Magn. Mater.* **321**, 3621--3623, 2009.
21. Almeida, L. P., et al. *Food Res. Int.* **38**, 1039--1044, 2005.
22. Haaland, P.D. (ed.). *Experimental Design in Biotechnology*, Marcel Dekker Inc., New York, 1989.
23. Mulika, R., et al. *Eur. J. Pharm. Sci.* **37**, 395--404, 2009.
24. Serpen, A., et al. *J. Agric. Food Chem.* **55**, 7676--7681, 2007.
25. Vaia, R.A., & Maguire, J.F. *Chem. Mater.* **19**, 2736--2751, 2007.
26. Ganta, S., & Amiji, M. *Mol. Pharmaceut.* **6**, 92--939, 2009.
27. Raman, V., & Abbas, A. *Ultrason. Sonochem.* **15**, 55--64, 2008.
28. Priyadarsini, K.I. *J. Photoch. Photobio. C* **10**, 81--95, 2009.
29. Guin, D., et al. *Bull. Mater. Sci.* **29**, 617--621, 2006.

30. Shapiro, J.A. *Annu. Rev. Microbiol.* **52,** 81--104, 1998.

31. Koleva, I.I., et al. *Phytochem. Analysis* **13**, 8--17, 2001.

32. Deka, G., et al. *J. Macromol. Sci. A PAC* **46**, 1128--1135, 2009.

33. Dutta, K., et al. *J. Neuroimmune Pharmacol.* **4**, 328--337, 2009.

34. Chen, H., et al. *Pathobiology* **76,** 117--128, 2009.

35. Wang, S.X., et al. *Colloid Surf. B* **67,** 122--26, 2008.

36. Seigel, R.R., et al. *Anal. Chem.* **69,** 3321--3328, 1997.

37. Hu, F.X., et al. *Biomacromolecules* **7,** 809--816, 2006.

38. Gupta, A.K., & Gupta, M. *Biomaterials* **26,** 3995--4021, 2005.

39. Zhang, M.Q., et al. *Biomaterials* **19**, 953--960, 1998.

40. Ford, N.A., et al. *Nutr. Cancer* **63**, 256--63, 2011.

41. Palozza, P., et al. *J. Nutr. Biochem.* **22**, 971--8, 2011.

42. Palozza, P., et al. *Arch. Biochem. Biophys.* **504**, 26--33, 2010.

43. Sharma, S. K., & Le Maguer, M. *Ita. J. Food Sci.* **2**, 107--13, 1996.

44. Sadler, G., et al. *J. Food Sci.* **55**, 1460--1461, 1990.

45. Santamaria, R.L., et al. *J. Agric. Food Chem.* **48**, 3063--3067, 2000.

46. Egydio, J.A., et al. *J. Supercrit. Fluids* **54,** 159--164, 2010.

47. Choudhari, S. M., & Ananthanarayan, L. *Food Chem.* **102**, 77--81, 2007.

48. Zuorro, A., & Lavecchia, R. *Biotechnol. Biotechnol. Eq.* **24**, 1854--1857, 2010.

49. Chemat, F. et al. *Ultrason. Sonochem.* **18**, 813--35, 2011.

50. Liangfu, Z., & Zelong, L. *Ultrason. Sonochem.* **15**, 731--737, 2008.

51. Huang, W., et al. *Food Chem.* **114,** 1147--1154, 2009.

52. Albu, S., et al. *Ultrason. Sonochem.* **11,** 261--265, 2004.

53. Kjartansson, G.T., et al. *J. Agric. Food Chem.* **54**, 3317--3323, 2006.

54. Lee, K-H., et al. *Macromol. Theory Simul.* **18**, 287--298, 2009.

55. Huang, J., & Kaner, R.B. *J. Am. Chem. Soc.*, **126**, 851--855, 2004.

56. Lu, X., et al. *Prog. Polym. Sci.*, **36**, 671--712, 2010.

57. Ma, Y., et al. *J. Am. Chem. Soc.* **126**, 7097--101, 2004.

58. Fan, Y., et al. *J. Am. Chem. Soc.* **129**, 5437--43, 2007.

59. Dhand, C., et al. *Electrochem. Commun.* **11**, 1482--6, 2009.

60. Davis, W.B. *Anal. Chem.* **21,** 1226--1228, 1949.

61. Zhou, J. *J. Agric. Food Chem.* **58**, 6741--6746, 2010.

62. Delley, B. *J. Chem. Phys.* **92**, 508--518, 1990.

63. Perdew, J.P., et al. *Phys. Rev. Lett.* **77**, 3865--3868,1996.

64. Perdew, J.P., & Wang, Y. *Phys. Rev. B* **45**, 13244--13249, 1992.

65. Chattaraj, P.K., et al. *Chem. Rev.* **106**, 2065--2091, 2006.

66. Andzelm, J., et al. *J. Chem. Phys.* **103**, 9312--9320, 1995.

67. Mosmann, T., *J. Immunol. Methods* **65**, 55--63, 1983.

68. Rolda´n-Gutie´rrez, J. M., & de Castro, M. D. L. *Trends Anal. Chem.* **26**, 163--170, 2007.

69. Perkins-Veazie, P., et al. *J. Vegetable Sci.* **12**, 93--106, 2006.

70. Gross, J. *Pigments in fruits,* Academic Press Inc., London, 1987.

71. Baysal, T., et al. *J. Agric. Food Chem.* **48**, 5507--5511, 2000.

72. Kubota, C., et al. *HortScience* **41**, 522--525, 2006.

73. Helyes, L., et al. *Acta Aliment.* **38**, 27--34, 2009.

74. Kuti, J.O., & Konuru, H. B. *Sci. Food Agric.* **85**, 2021--2026, 2005.

75. Goswami, L., et al. *J. Mater. Sci.* **43**, 1286--1291, 2008.

76. Morch, K.A. *Phys. Fluids* **19**, 072104--7, 2007.

77. Malipatil, S.M., et al. *Int. J. Pharm. Pharm. Sci.* **3**, 13--15, 2011.

78. Tan, B., & Soderstom, D. N. *J. Chem. Educ.* **66**, 258, 1989.

79. Kong, K-W., et al. *Molecules* **15**, 959--987, 2010.

80. O'Donnell, C.P., et al. *Trends Food Sci. Technol.* **21**, 358--367, 2010.

81. Guiseppi-Elie, A., et al. *J. Mol. Catal. B: Enzym.* **58**, 118--123, 2009.

82. Tokuhirol, T., & Woo, K.W. *J. Phys. Chem.* **80**, 733--740, 1976.

83. Laslau, C., et al. *Prog. Polym. Sci.* **35**, 1403--1419, 2010.

84. Pramanik, S., et al. *J. Appl. Polym. Sci.* **126**, 830--836, 2012.

85. Shu, B., et al. *J. Food Eng.*, **76**, 664--669, 2006.

86. Banerjee, S., et al. *Nanotechnol.* **21**, 045101 (8 pp), 2010.

87. Guimard, N.K., et al. *Prog. Polym. Sci.* **32**, 876--921, 2007.

88. Guterman, E., et al. *Polym. Preprints (Am. Chem. Soc., Div. Polym. Chem.)* **43**, 766--767, 2002.

89. Burgess, L.C., et al. *Toxicol. In Vitro.* **22**, 1297--1300, 2008.

90. Hu, K-Q., et al. *J. Biol. Chem.* **281**, 19327--19338, 2006.

91. Lian, F., et al. *Carcinogenesis* **28**, 1567--1574, 2007.

92. Patra, H.K., et al. *Nanomed. Nanotech. Biol. Med.* **3**, 111--119, 2007.

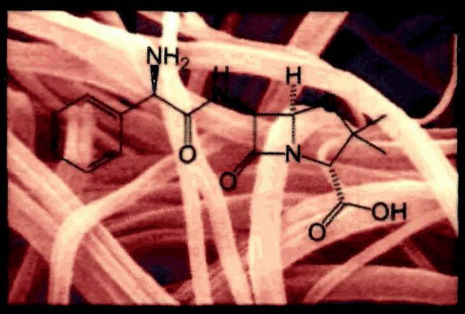

Chapter 5

Tuning the bio-physico-chemical properties of electrospun polymeric nanofibers

HIGHLIGHTS OF THE CHAPTER*

In the wide milieu of application-oriented electrospun fibers, cellulose acetate (CA) nanofibers have fetched a wide spectrum of commercial applications. In this context, the subchapter 5A is focussed on the use of Box-Behnken design technique for tuning the diameter of electrospun cellulose acetate (CA) fibers. The study pertained to three chosen process variables namely potential difference, distance between tip-to-collector and feed rate. The chosen factors exerted linear and quadratic influence on the fiber diameter. Subchapter 5B deals with the modulations in some of the bio-physico-chemical attributes of cellulose acetate (CA) nanofibers in the presence of poly(ethylene glycol), electrospun under the same optimized processing parameters (as given in subchapter 5A). The modulations in the morphology (as observed under SEM), surface area and the thermal response of the blend in comparison to pristine electrospun CA fibers, complemented by FTIR and Raman spectroscopic analyses are reported. In the perspective of transdermal drug delivery, ampicillin adsorbed eCA and eCAPEG were checked for the biocompatibility with peripheral blood mononuclear cells and antibacterial action against *Staphylococcus aureus*.

*Parts of this chapter are published in

1. Konwarh, R., & Karak, N., et al. *Carbohyd. Polym.* **92**, 1100--1106, 2013.
2. Konwarh, R., & Karak, N., et al. *Biotechnol. Adv.* **31**, 421--437, 2013.
3. Konwarh, R., & Karak, N., et al. *ACS Appl. Mater. Interfaces* (Communicated).

5A. DIAMETER-TUNING OF ELECTROSPUN CELLULOSE ACETATE FIBERS: A BOX-BEHNKEN DESIGN (BBD) STUDY

5A.1. Introduction

Electrospun cellulose acetate (CA) nanofibrous mats have carved a unique niche of their own as biomimetic tissue engineering scaffolds,[1] biomolecule-immobilization platforms,[2] bioremediation mats,[3] and energy storage materials[4] amongst others. A handful of works has focussed upon suitability of different solvent systems for electrospinning CA.[5,6] In the context of issues related to toxicity of various conventionally used organic solvents,[5] the recent reports on the use of binary mixture of water (considered as a green solvent) and acetic acid for electrospinning CA is attractive.[6] However, it is pertinent to mention that electrospinning, being a multi-parameter-dictated process, demands an inevitable optimization of the solution-property, ambient variables and the processing conditions to fine tune the shape-size unison of the electrospun fibers[7] that eventually dictates their bio-physico-chemico attributes.

Vrieze et al.[8] have studied the effect of ambient parameters including relative humidity and temperature on the diameter of the electrospun CA nanofibers. However, reports on the effect of the electrospinning process parameters like applied potential, feed rate and so on are not available. Though the influence of these parameters on the fiber diameter has often been investigated individually, elucidation of the cross-effect or interaction effects among the chosen parameters is expected to present a more convincing picture. A narrow-size window of electrospun fibers may be indispensable for a number of applications, as for example, to mimic the extracellular matrix in a better way during tissue engineering applications or to increase the drug-loading percentage, dependent on the surface area to volume ratio of the fibers.

A number of studies has focussed on optimizing the processing parameters for various electrospun materials like silk,[9], poly (D, L- lactide)[10] and titanium dioxide[11] using different statistical approaches. In this context, response surface methodology (RSM) is often viewed as an apt choice in compilation of mathematical and statistical

tools for designing experiments, constructing numerical models, assessing the effects of variables and searching for optimum combinations of variables.[12]

This work highlights the use of Box-Behnken Design (BBD) as an optimization tool to minimize the diameter of electrospun CA fibers. It is pertinent to mention that the use of BBD is often advantageous when compared to central composite design (CCD) for a quadratic response surface model with three or more factors.[11] Using the system reported by Han et al.[6] as reference for the study, the effect of modulating the process parameters like applied potential, tip-to-collector distance and feed rate on the diameter of electrospun CA fibers was studied. The objective was to assess whether such parametric modulations subjected to statistical optimization can be really useful to reduce the average diameter of the CA nanofibers or not.

5A.2. Experimental

5A.2.1. *Materials*

Cellulose acetate, CA (acetyl content 39.8 %, average M_n = 30,000 by GPC) and acetic acid (~99.5% pure) were purchased from Aldrich and ACROS respectively. Milli-Q water was used throughout the experiment.

5A.2.2. *Electrospinning and characterization*

CA dissolved in acetic acid and Milli-Q water (75:25, w/w) (abbreviated to AcW) was electrospun in ME MECC NANON 01 electrospinning machine (Canada Foundation for Innovation) under different parametric modulations of voltage, tip-to-collector distance and feed rate as outlined in subsequent sections (relative humidity , R_H = 29-32% and temperature = 23 ^{0}C). The viscosity of the AcW solution was found to be ~5500 cP as determined using Brookefield digital viscometer at room temperature (~23 ^{0}C).

The morphology of the electrospun CA fibers was observed on a scanning electron microscope (SEM, INSPECT™ S50-FEI) post gold coating in Cressington Sputter coater for about 40 seconds. The distribution of the electrospun fiber diameter was determined using image analysis processing as developed by Shin et al.[13] In brief, the analysis consisted of two phases. The first phase comprised of generation of threshold and binary images of the acquired SEM image, followed by boundary detection. It is pertinent to mention that Canny Edge detecting method was applied to separate the

boundary of each fiber at the fiber-to-fiber cross-over areas. In the second phase, skeletonization was used to define the fiber centre line. The distance from the centre to the boundary was calculated using distance transform. While a manual method for calculating the size of the beads was used in case of the beaded fibers. Fiji was used for evaluating orientation and coherency of the fibers electrospun under optimized process parameters.

5A.2.3. *Experimental design, model development and verification*

For the evaluation of the effect of varying electrospinning parameters in the generation of CA fibers, BBD technique was used to estimate the main effects on the response *i.e.*, the diameter of the electrospun nanofibers. Table5A.1 represents the design matrix for experimental factors and response.

Table5A.1. *Box Behnken Design Matrix containing 17 experimental runs*

Run Order	*Applied potential (kV)*	*Tip-to-collector distance (cm)*	*Feed rate (mL/h)*	*Response, Y (fiber diameter in nm)*
6	30	13	1	144
10	25	15	1	141
9	25	11	1	151
16	25	13	2	144
12	25	15	3	145
5	20	13	1	153
14	25	13	2	143.8
11	25	11	3	153
8	30	13	3	147
2	30	11	2	148
4	30	15	2	139
13	25	13	2	143.8
7	20	13	3	156
3	20	15	2	151
15	25	13	2	144.2
17	25	13	2	144
1	20	11	2	160

In this experiment, applied voltage (*A*), distance between the tip and the collector (*B*) and feed rate (*C*) were chosen as the experimental factors or the independent variables capable of influencing the diameter of the electrospun fibers (*Y*). The three factors with three levels consisting of 17 experimental runs were used to analyse the experimental data including multiple replicates at the centre point. This allows better estimate of the experimental error and provides extra information in the interior of the experimental region.[14] Analysis was done using coded values (-1 for *A*=20 kV, *B*=11 cm and *C*=1 mL h^{-1}; 0 for *A*= 25 kV, *B*=13 cm and *C*=2 mL h^{-1}; 1 for *A*= 30 kV, *B*=15 cm and *C*= 3 mL h^{-1}). Using this design, the experimental data were fitted according to the equation (5A.1) as a second order polynomial equation including individual and cross effect of each variable.

$$Y = a_0 + a_1A + a_2A^2 + a_3B + a_4B^2 + a_5C + a_6C^2 + a_7A*B + a_8A*C + a_9B*C \quad \text{.....(5A.1)}$$

Where, a_0, a_1, a_2, a_3, a_4, a_5, a_6, a_7, a_8, a_9 are the regression coefficients. Analyses were carried out in triplicates. The data tabulated were (Table5A.1) the average of two sets of measurements. An analysis of variance (ANOVA) of the experimental response was performed to assess the full quadratic approximation of the BBD response surface model. The statistical computations were performed using the software Design-Expert 8.0.6. The significance of each coefficient was determined from the *t-values* and *p-values.* Coefficients in the equation with t-values greater than t-values at 95% level of confidence or $p>0.05$ were considered statistically significant. The final response surface model was further refined by deleting the terms found to be associated with a level of significance greater than 5% ($p>0.05$).[15]

5A.3. Results and Discussion

As an empirical model, RSM designing technique is used to evaluate the relations existing among a group of controlled experimental factors and the observed results of one or more selected criteria. The indispensability is of a preliminary knowledge of the studied process for achieving a realistic model. The utility of RSM for elucidating the influence of few selected process parameters on the diameter of electrospun CA fibers was assessed. It is needless to mention about the intricate play of different process parameters in electrospinning.

5A.3.1. *Backdrop of the selected levels of the chosen parameters*

The response surface model developed for the electrospun CA nanofibers is presented in the subsequent sections. However, one might be intrigued about the backdrop of setting the afore-stated levels of the selected factors. This selection was based on the available resources and results from preliminary experiments (feasibility study). In the process-parameters' optimization for electrospun titanium dioxide, it has been pointed out the production of electrical arcs between the electrodes (as the static potential exceeds the resistance of the enclosed air inside the chamber) to be responsible for discontinuous withdrawal of fluid jet beyond the selected highest potential difference and lowest separation distance.[11] In the present study, three levels of the potential difference were distributed between 20 kV and 30 kV. It was difficult to observe a continuous fiber formation without sputtering of the polymer solution below the lowest selected potential difference (<20 kV). This may be attributed to the lower net effect of the applied voltage than the opposing forces on the solution droplet at the needle tip. A potential difference of 30 kV (the maximal limit of the electrospun machine used) could withdraw a continuous strand of fluid jet across the separation distance of 15 cm with continuous fiber formation. At feed rates greater than 3 mL/h, particularly at higher values of the applied potential difference resulted in beaded fibers (Fig.5A.1a). At very high feed rates (>3 mL/h), electrospinning of the fibers was intermittent. The sporadic behavior may be attributed to the short residence time of the drop and solidification of an accumulated mass of the polymer solution at the needle tip. The fibers electrospun under high potential difference (30 kV), short separation distance between tip and collector (11 cm) and high feed rate (3 mL/h) were bead-free and appeared flat and ribbon-like though the maximal number of fibers in the observed microscopic fields had considerably large diameter (Fig.5A.1b). It is pertinent to mention that Han et al.[6] have reported the controlling of the average diameters of the CA nanofibers from 160 nm to 1280 nm as a function of the composition of the mixed solvent of acetic acid and water. Considering the minimal separation distance of 10 cm as reported by them for rotatory collector, this was initially selected as the central value for the plate collector system as well in the present system. Interestingly, electrospinning with a separation distance below this value (<10 cm) at potential difference set at 30 kV, highly polydispersed fibers (size spectrum: 153-1185 nm) with mixed morphology including branched architecture (like dendritic branching) (Fig.5A.1c) could be observed. Spindle-shaped beads as large as about 9 microns were

also noted. Henceforth, the selected levels for the tip-to-collector level ranged from 11 cm to 15 cm. These observations were indicative of the existence of certain optimal process parametric values. Under these optimal settings, the residence time for drop formation at the needle tip along with increased 'time-of-flight' for the charged ejected jet are supposed to augment the solvent evaporation and consequently enhance the sol-gel conversion into solid phase.

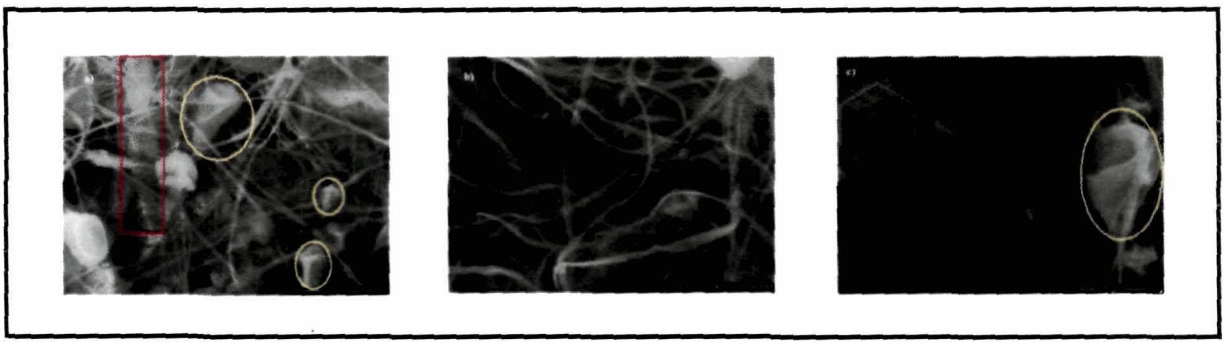

Fig.5A.1. *SEM micrographs of few feasibility experiments (details in the text) - the yellow (circular), red (rectangular) and green (hexagonal) boundaries are meant to indicate the beads, flattened structure (probably due to solvent-impact) and branched structures respectively*

5A.3.2. *Response surface model*

As noted previously, the CA fibers were electrospun at each design point of the three chosen variables (potential difference, tip-to-collector distance and feed rate) and three levels of the BBD. The diameter of the fibers generated from each experiment was measured and documented as response variable. The column Y in Table5A.1 represents the average of two sets of experiments.

Initially, sequential model sum of squares (Type I) was used to select the highest order polynomial where the additional terms are significant and the model is not aliased. The sequential p-value<0.0001 suggested a quadratic model although the model summary statistics was suggestive to focus on the model, maximizing adjusted R-squared (0.97393) and the predicted R-squared (0.8584). In order to evaluate the quadratic response surface model, the experimental data was then subjected to an analysis of variance (ANOVA) using partial or Type III sum of squares (SS) that calculates the SS for a term post correction for all other terms in the model. The ANOVA results (Table5A.2) showed that the model was statistically significant with linear and quadratic terms. Values of "Prob>F" less than 0.0500 indicated the significant model terms. In this case A, B, C, A^2, B^2, C^2 were found to be significant model terms. If there

are many insignificant model terms (not counting those required to support hierarchy), model reduction is often used to improve the model. A backward elimination method was applied and the statistically insignificant terms ($p>0.05$) were deleted from the full quadratic model to obtain a refined response surface model. It was interesting to note that only the linear and quadratic terms for the three electrospinning variables found place in the refined model. The model F-value of 149.72 implied the model to be statistically significant. There was only a 0.01% chance that a "model F-value" this large could occur due to noise.

Table5A.2. *ANOVA for Response Surface Reduced Quadratic Model*

Source	*Sum of squares (SS)*	*Degrees of Freedom (DF)*	*F-value*	*p-value prob>F*
Model (Significant)	504.15	6	149.72	<0.0001
A	220.50	1	392.91	<0.0001
B	162.00	1	288.67	<0.0001
C	18.00	1	32.07	0.0002
A^2	68.04	1	121.25	<0.0001
B^2	9.73	1	17.33	0.0019
C^2	17.18	1	30.61	0.0002

The pred R-squared of 0.9565 was in reasonable agreement with the adj R-squared of 0.9824 in the refined model. The experimental fiber diameter versus the model predicted diameter is shown in Fig.5A.2.

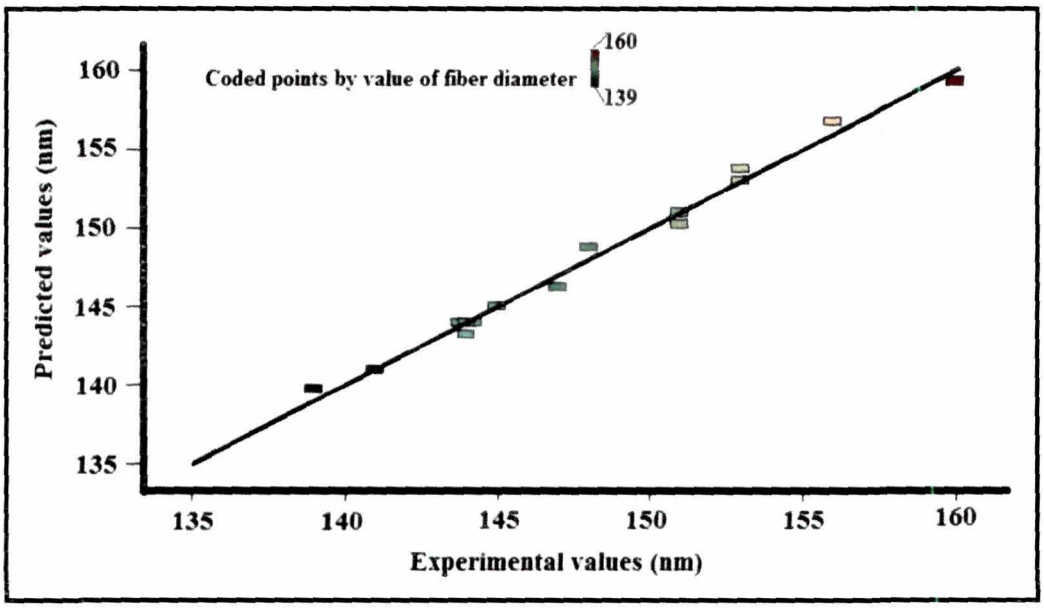

Fig.5A.2. *Plot of model-predicted versus observed response (fiber diameter)*

Computation of the linear correlation coefficient suggested a reasonable agreement between the experimental and model values over the entire factor space under consideration. The 'adequate precision' measures the signal to noise ratio. A ratio greater than 4 is desirable. In this case, a value of 40.565 indicated an adequate signal and therefore the model could be used to navigate the design space. The refined response surface model comprising of terms which are statistically significant at $p<0.05$ is represented in the following equation:

$$Diameter = 143.96 - 5.25 *A - 4.5*B + 1.5* C + 4.02* (A)^2 + 1.52*(B)^2 + 2.02*(C)^2 \quad \textbf{...(5A.2)}$$

5A.3.3. *Perturbation plot*

A Perturbation plot is like "one factor at a time" experimentation. However, these plots help to compare the effect of all the factors at a particular point in the design space. The response is plotted by changing only one factor over its range while holding all the other factors constant. By default, Design-Expert sets the reference point at the midpoint (coded 0) of all the factors. The value of each variable was changed between +1 and -1 levels, keeping the other two corresponding variables constant to assess the respective effect on the fiber diameter. A steep slope or curvature in a factor shows that the response is sensitive to that factor. A relatively flat line shows insensitivity to change in that particular factor. The plots (Fig.5A.3) revealed that the fiber diameter was sensitive to change in each of the three chosen variables- the applied potential difference, tip-to-collector separation distance and feed rate. For reference, the influence of change in voltage (Fig.5A.3a i-v), separation distance (Fig.5A.3b vi-x) and feed rate (Fig.5A.3c xi-xv) are shown by keeping the other two corresponding parameters at their central values.

Fibers electrospun under a separation distance of 13 cm and feed rate of 2 mL/h showed a progressive decrease in fiber diameter with increase in applied potential. Greater the separation distance, smaller was the fiber diameter (at potential difference of 25 kV and 2 mL/h feed rate). Under a potential difference of 25 kV and 13 cm separation distance, a feed rate of 2 mL/h was found to be optimal for minimal fiber diameter.

The plausible explanation of the observed trends is put forward with a greater insight into the influence of the chosen variables on the fiber diameter through the response surface plots in the subsequent section.

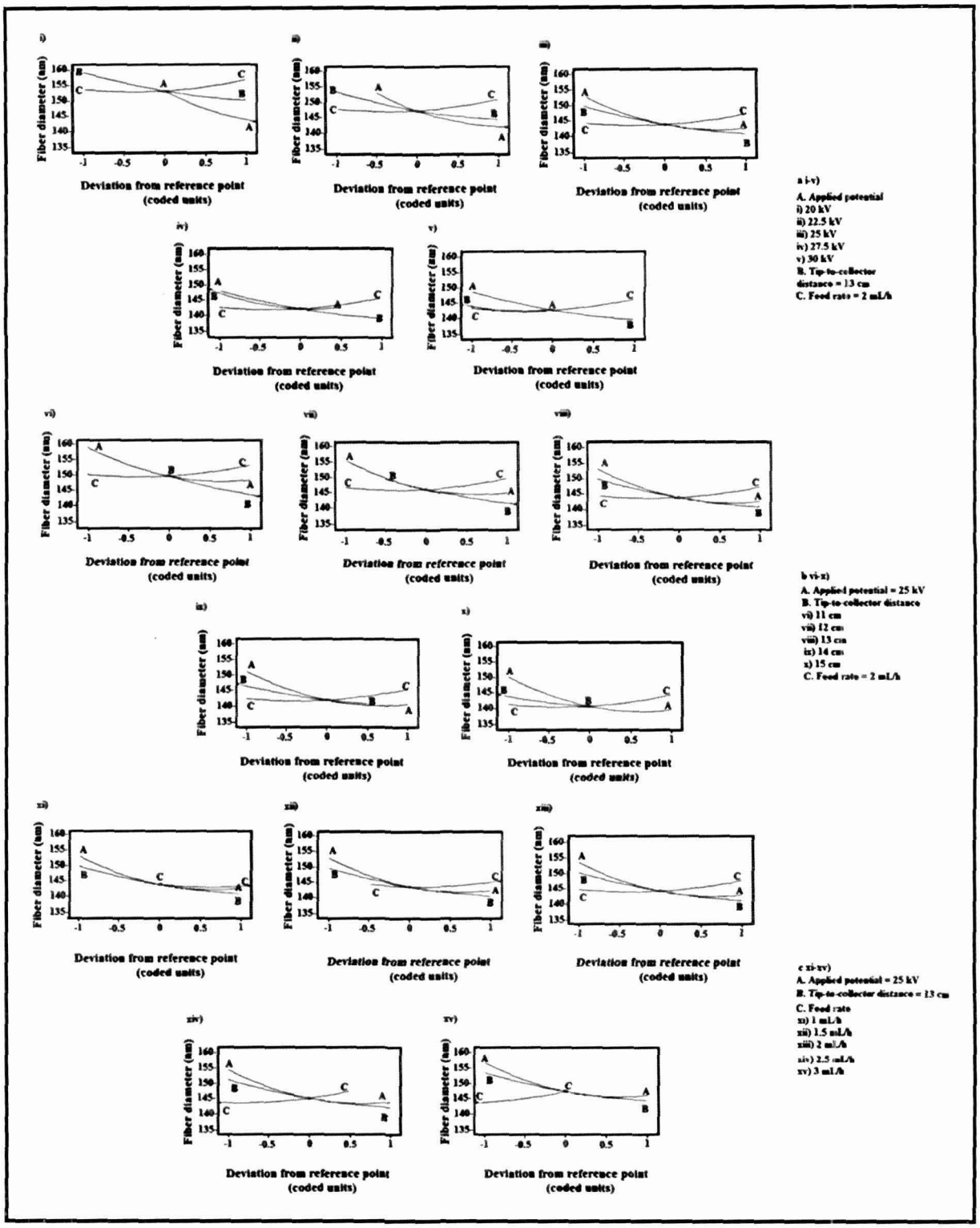

Fig.5A.3. *Perturbation plots showing the effect of modulation in a i-v) applied potential, b vi-x) tip-to-collector distance and c xi-xv) feed rate (with the other two corresponding parameters remaining constant in each case) on the fiber diameter*

5A.3.4. *Response Surface Plots*

The three dimensional surface plots of the response variable, CA fiber diameter (nm) versus two-variables-at-a-time (keeping the third variable constant at the central value, 0) are depicted in Fig.5A.4.

A number of interesting observations emanate from these plots. Considering, Fig.5A.4a, fibers were minimal diameter were produced for the combination of highest potential difference (30 kV) with the maximal separation between the tip and the collector (15 cm) (the feed rate considered is 2 mL/h).

On the other hand, decreasing the voltage to the minimum (20 kV) and feeding the polymer solution at the maximum rate of 3 mL/h led to the generation of fibers with the highest diameter (~160 nm) (tip-to-collector distance = 13 cm) (Fig.5A.4b).

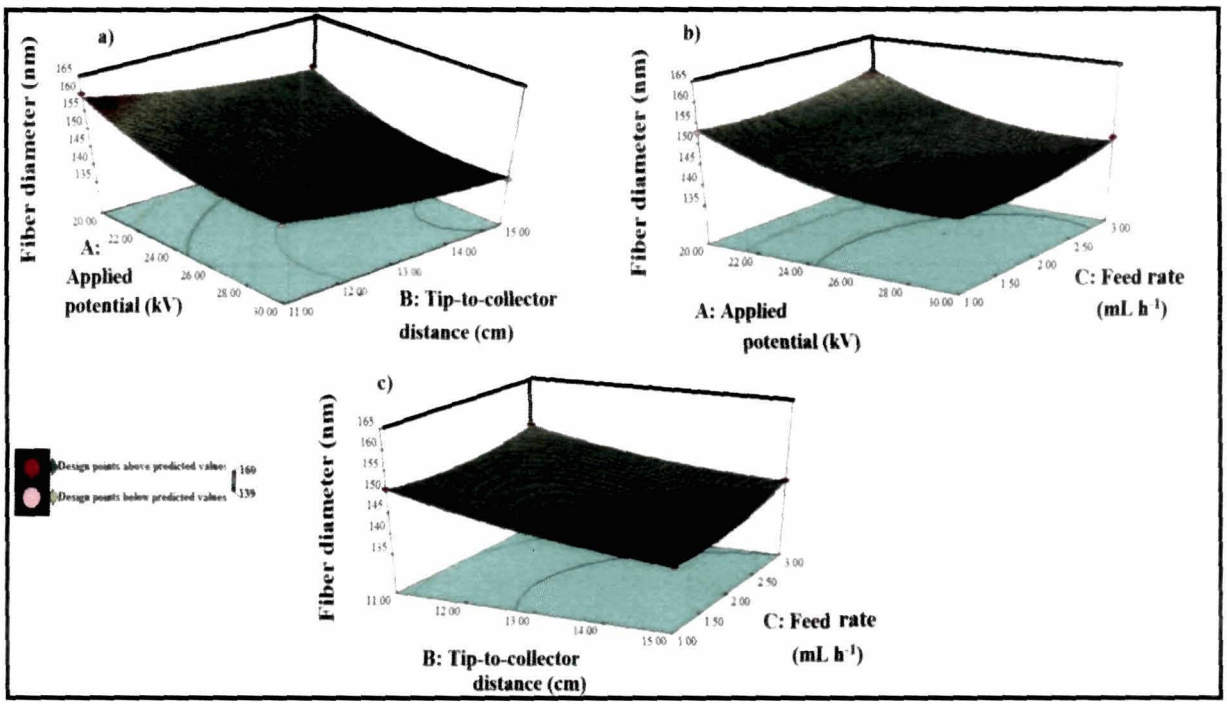

Fig.5A.4. *Response Surface plots of fiber diameter versus a) applied potential versus separation distance, b) applied potential versus feed rate and c) separation distance versus feed rate*

Altering the central value, 0 of the third variable to +1 and -1 levels in the software yielded other interesting plots. A few generalized inferences were drawn from such plots regarding the electrospun cellulose acetate fibers: a) the fiber diameter decreased over all the levels under consideration in response to corresponding increment of the potential difference b) irrespective of the potential difference, increasing the separation distance leads to decrease in fiber diameter, and c) the fiber diameter was minimal for the central value of feed rate *i.e.*, 2 mL/h under all levels of

applied potential difference. The SEM micrograph of the electrospun fibers generated under the optimal conditions is shown in Fig.5A.5.

The average diameter of the fibers was calculated to be around 139 nm. A mean coherency co-efficient of 0.5192 was calculated using the software Fiji. A coherency coefficient close to 1, represented as a slender ellipse, indicates a strongly coherent orientation of the local fibers in the direction of the ellipse long axis. A coherency co-efficient close to zero, represented as a circle, denotes no preferential orientation of the fibers.

Ramakrishna et al.[16] have presented the effects of various electrospinning parameters on fiber-diameter and their shape-size accord of different polymeric materials. The experimental observations of differential fiber diameter of electrospun CA in response to parametric modulations are vouched by a number of comprehensive reports on electrospinning as discussed underneath.

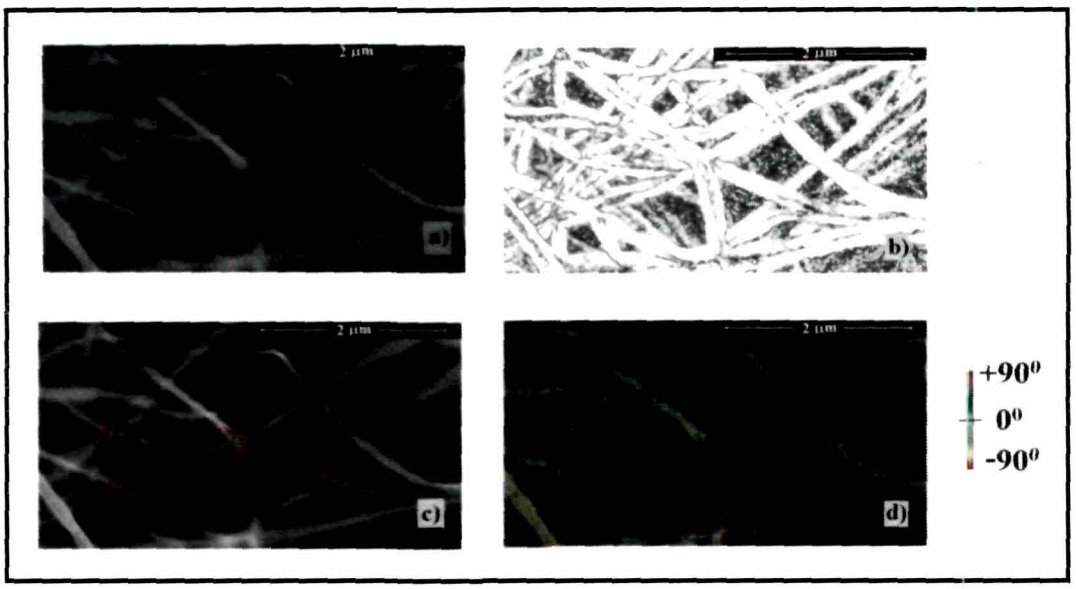

Fig.5A.5. *a) SEM micrograph (20,000 X) of the fibers electrospun under optimized process parameters, b) coherency map, c) SEM micrograph (for calculation of coherency co-efficient and d) HSB colour-coded map*

Solution property to a large extent dictates the effect of varying the distance between the tip and the collector (profoundly affecting the flight-time and the field strength) on the fiber morphology. Interestingly, a couple of contrary reports exist as far as the separation distance and fiber diameter is concerned. Often the formation of beads has been reported for too short separation between the tip and the collector due to increased field strength[17] resulting in the increased instability of the jet. An increased

separation has been associated with decreased fiber diameter in terms of longer flight time for the solution to be stretched prior to deposition on the collector.[18] On the contrary, Lee et al.[19] reported the increase in fiber diameter corresponding to increase in separation distance in terms of decrease in field strength. However, Zhao et al.[18] reported that fibers are not deposited if the separation distance is too high. Thus it appears that the stretching and acceleration of the jet (consequently the morphology and diameter of the electrospun fibers) are profoundly affected by the supplied voltage and the resultant electric field. Various studies have shown that higher voltage leads to greater stretching of the solution owing to greater columbic forces in the jet, consequently reducing the fiber-diameter.[17,19] It is important to note that the viscosity of 17 wt% CA solution was only about 5,500 cP. It was interesting to note that at higher voltage, secondary jets were also generated. When a solution of lower viscosity is used, a higher voltage may favour the formation of secondary jets during electrospinning. This has the effect of reducing the fiber diameter.[20] However, the formation of beads cannot be completely overlooked on application of very high voltage, which is often co-related with decreased flight-time of the polymer solution (due to greater stretching) and its recession into the needle-tip. The consideration of feed rate is very important at this juncture. In an interesting observation, Krishnappa et al.[21] reported that increasing voltage will increase the beads density, which at an even higher voltage, the beads will join to form a thicker diameter fiber. This may also partially explain the observation of Fig.5A.1.

Thus, it is confirmed that the different electrospinning parameters work to varied extents in influencing the fiber diameter.

5A.4. Conclusion

The present work attested the successful development of a response surface model based on BBD technique to predict the diameter of electrospun cellulose acetate fibers. The chosen factors exerted linear and quadratic influence on the fiber diameter. RSM and the experimental design that was applied, given the limits imposed by the nature of the experiment, revealed themselves to be efficient in the determination of the optimal values of the three chosen variables for theoretically obtaining electrospun CA fibers with minimal diameter. The choice of a second order polynomial regression model was also satisfactory. The model can be used for devising strategies to fine tune

the application-dependent shape-size accord of electrospun cellulose acetate fibers. However, it is pertinent to mention that an important limitation of the study was in terms of limited number of variables chosen. This work may be extended to understand the concomitant roles of the environmental factors and the solution properties.

5B. PHYSICO-CHEMICAL MODULATIONS OF ELECTROSPUN CELLULOSE ACETATE FIBERS BY POLY(ETHYLENE GLYCOL) AND PROSPECTIVE BIOMEDICAL APPLICATION

5B.1. Introduction

Delving into the modulations in physical properties (including viscoelastic behaviour, mechanical properties and water permeation), consequently affecting the (cast) film forming characteristics (in various pharmaceutical controlled release film coatings) of cellulose acetate post addition of plasticizers like poly(ethylene glycol) has remained focal points of research over the years.[22-24] On the other hand, as far as electrospun CA is concerned, a handful of recent reports are focused on electrospinning CA with an additional polymer, *e.g.*, epoxy or polyurethane (for modulation of surface chemistry and roughness),[25] and chitosan (for tuning the mechanical stiffness for cell-culture application)[1] amongst others. Furthermore, the recent demonstration of commendable ability to regulate their interior temperature with the altered ambient temperature has given a whole new perspective to electrospun CA/PEG fibers in the realm of thermoadaptable fabrics.[4]

In the previous subchapter, the application of Box-Behnken Design technique based response surface model was demonstrated for the prediction of diameter of electrospun CA fibers. An applied voltage of 30 kV, tip-to-collector distance of 15 cm and feed rate of 2 mL/h were the optimal electrospinning (in acetic acid/water solvent system, 75:25 w/w) process parameters for obtaining the CA fibers with minimal diameter of 139 nm. The focus of the present work was to scrutinize the plausible modulations in some of the material properties of CA fibers when electrospun (under the same optimized parameters) in presence of poly(ethylene glycol). The morphological modulations, the alterations in thermal attributes, surface area and surface functionalities of the CA fibers when electrospun in presence of PEG have been documented. Needless to say that PEGylation is a common strategy to improve stability and bio-acceptance of myriad of biomolecules including enzymes and various drug moieties respectively, which has been highlighted in the various preceding chapters of the thesis. Herein, ampicillin adsorbed pristine and hybrid CA mats were assessed for their compatibility with peripheral blood mononuclear cells (that plays critical role in

wound healing) and antibacterial potency against *Staphylococcus aureus* for prospective transdermal drug delivery.

5B.2. Experimental

5B.2.1. *Materials*

The starting materials for electrospun cellulose acetate (eCA) fibers were the same as descripted in section 5A.2.1. On the other hand, for the preparation of electrospun cellulose acetate-poly(ethylene glycol) (eCAPEG) fibers, PEG4000 (Aldrich) was used along with CA.

5B.2.2. *Electrospinning and characterization*

CA, dissolved in acetic acid and Millipore water (75:25, w/w) was electrospun (eCA) in ME MECC NANON 01 electrospinning machine (Canada Foundation for Innovation) under the optimized process parameters (as given in the previous subchapter) of 30 kV (voltage), 15 cm (tip-to-collector distance) and 2 mL/h (feed rate) (relative humidity , R_H = 29-32% and temperature = 23 ^oC). On the other hand, the effect of PEG on the various physico-chemical attributes of CA was assessed by electrospinning the latter in presence of 5 wt% of the former (eCAPEG) under the same conditions as outlined above.

The morphology of eCAPEG fibers was observed on a scanning electron microscope (SEM, INSPECT™ S50-FEI) post gold coating in Cressington Sputter coater for about 40 seconds. The distribution of the electrospun fiber diameter was determined using image analysis processing as described in the previous subchapter.

Multiple point Brunauer-Emmett-Teller (BET) nitrogen adsorption method was applied to determine the specific surface area of the eCA and eCAPEG mats using NOVA 2000 and Autosorb-1-C Instruments (Quantachrome, Osaka, Japan), after pre-treating the samples overnight under vacuum. For calculation of BET specific surface area, relative pressures in the range of 0.05-0.2 were used.

FTIR spectra were recorded in Nicolet 6700-FTIR, Thermo Scientific, USA. On the other hand, Renishaw 2000 Raman Microscope was used to obtained the RAMAN spectra (spectral range: 100-3200 cm^{-1}) of the samples. The experimental conditions

were: 785 nm laser, 100% power (300 mW), 10 sec exposition time, 5 accumulations and 20X objective.

TGA Q500 (TA Instruments-Q2000 series, USA) was used to obtain the TG curves of PEG, CA powder, eCA and eCAPEG mats. The experimental conditions were: platinum pans; nitrogen atmosphere at a flow rate of 60 mL/min; heating rate of 10 ^{o}C/min in the temperature range of (10-600) ^{o}C. Differential scanning calorimetry (DSC) with three cycles was performed by differential scanning calorimeter from TA Instruments-Q2000 series (USA) in the temperature range between -30°C and 280°C with heating and cooling rates of 10 and 5°C/min, respectively.

5B.2.3. *Action at the biointerface*

eCA and eCAPEG mats were cut into small discs and incubated in Ampicillin (HIMEDIA) solution (50 μg/mL) at room temperature with continuous shaking for 6 h and allowed to dry. Inoculum of *Staphylococcus aureus* (MTCC 737) was spread on to Luria Broth Agar (HIMEDIA) plates. Taking ampicillin adsorbed filter paper (Amp-FP) as the positive control, the disc diffusion method was executed for Amp-eCA and Amp-eCAPEG discs as the test materials against eCA and eCAPEG discs as the negative control to check the antibacterial activity. The plates were incubated at 37 ^{o}C for 12 h.

On the other hand, peripheral blood mononuclear cells play pivotal role in wound healing. In this context, the ampicillin loaded discs were checked for cytocompatibility with PBMCs isolated from goat blood. These experiments were conducted in accordance to the guidelines set by Tezpur University Ethical Committee. In brief, the PBMCs were separated by sedimentation through Histopaque (Sigma), a high density medium (1.077g/mL). Goat blood was collected in sodium citrate (Merck) and diluted in 1:1 ratio with Phosphate Buffer Saline, PBS (pH7.4) (HIMEDIA). The blood was then layered with a Pasteur pipette on Histopaque in 3:2 ratios in a wide transparent centrifuge tube. The cells at the interface were collected after centrifugation at 400 g for 15 minutes and transferred to serum free DMEM (Sigma) medium. The diluted cell suspension was washed twice in 20 mL serum free media at 70 g for 10 minutes. The final aliquot of goat blood lymphocytes was re-suspended in 2 mL of serum free medium. The PBMCs were cultured for 2 h in DMEM medium supplemented with 10% foetal calf serum (Himedia) and antibiotic penicillin-streptomycin-neomycin solution (Sigma) and incubated in a humidified 95% O_2/5% CO_2 atmosphere at 37 ^{o}C. The eCA, eCAPEG, Amp-eCA and Amp-eCAPEG discs were added to the wells containing

confluent cells (10^7cells/mL) and incubated for 24 h. Wells containing cells, incubated without the discs served as control. The Trypan blue exclusion assay was performed to assess the viability of the cells. Trypan blue dye is excluded by the viable cells thereby enabling the visual distinction between unstained viable cells and blue-stained nonviable cells. The cells were stained with 0.4% Trypan Blue (Sigma) solution in PBS (pH7.4) and observed on haemocytometer post incubation for 3 min. 40X magnification in Leica Fluorescence microscope was used to visualize the cells.

.

5B.3. Result and Discussion

5B.3.1. *Physico-chemical characterizations*

As reported in the previous subchapter, the pristine CA fibers electrospun under the optimized parameters of 30 kV (voltage), 15 cm (tip-to-collector distance) and 2 mL/h (feed rate) were around 139 nm. However, there seemed to be a morphological transition from ribbon like distribution (of the pristine fibers, as noted in the previous subchapter) to comparatively straighter and sturdier appearance in the presence of PEG (as observed under SEM, Fig.5B.1). A striking feature of the PEGylated fibers was their line or grooved surface texture. The fibers appeared to be arranged in parallel-stacks, ranging from 730-890 nm.

Fig.5B.1. *SEM image of eCAPEG mat, pseudo coloured in Fiji.*

Fibers with rough surface provide more topological cues and as such more conducive to cell adhesion.[26] In this context, it has been recently shown that parallel line surface texture of electrospun cellulose acetate butyrate fibers (using a solvent mixture of acetone and *N,N′*-dimethylacetamide) assisted in the growth of Schwann cells.[27] An intricate interplay of solvent volatility, evaporation rate and viscosity of the residual solution after the solvent evaporation has been envisaged for formation of voids,

elongation and solidification resulting in line or grooved surface texture.[27] Nevertheless, the PEGylated CA fibers, generated through the present protocol can find immense scope for nerve cell culture and may be viewed as one of the prospective future research-niches.

Fig.5B.2 shows the FTIR spectra for CA powder, pristine eCA mat and eCAPEG mats. The various band assignments[28] are presented in Table5B.1.

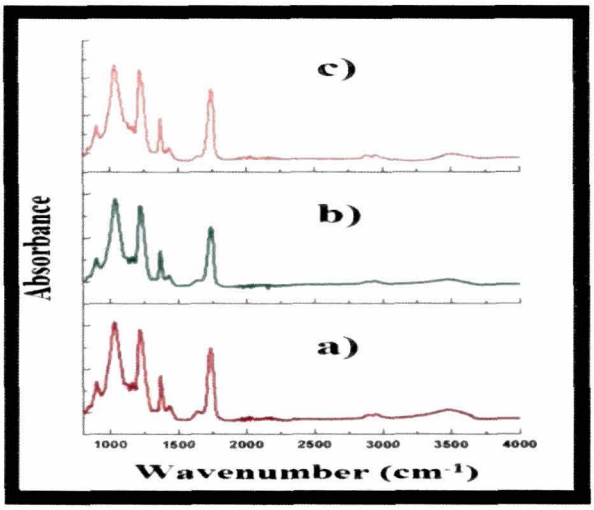

Fig.5B.2. *FTIR spectra of a) CA powder, b) pristine eCA mat and c) eCAPEG mats.*

Table5B.1. *Assignments of FTIR bands of CA powder, eCA mat and eCAPEG mat*

Band position			Assignment
CA powder	eCA mat	eCAPEG mat	
899	899	899	ß-glycosidic linkages between the sugar units
1030	1030	1030	C-O symmetric stretching of primary alcohol
1030	1030	1030	C-O-C anti-symmetric bridge stretching
1154	1154	1161	C-O stretching of acetyl group
1213(s)	1219(s)	1213(s)	C-O stretching of acetyl group
1370	1370	1370	C-H deformation (CH_3 or OH in plane bending)
1435	1435	1435	CH_2 bending or OH in plane bending
1638	1638	1638	H-O-H bending of absorbed water
1736 (s)	1736(s)	1736(s)	C=O stretching of ester
			H-O-H bending of absorbed water
2875, 2948	2888, 2948	2888, 2948	CH stretching of acetyl or carboxylic acid
3477	3478	3479	OH stretching

However, it is pertinent to mention that the low intensity of band located between 3200 and 3600 cm^{-1}, corresponding to the overlapping vibration bands in the OH stretching region, and of the peak at 1636 cm^{-1} (bending of adsorbed water), corroborated the presence of low amounts of water.

Recently, FT Raman spectroscopy has been used as a novel technique to characterize CA and determining the contents of acetyl groups.[29] In this context, Raman spectral analysis (region of 1800-300 cm^{-1}) (Fig. 5B.2) was illustrative of a number of interesting modulations of eCA mat in presence of PEG.

A characteristic Raman peak at around 1,740 cm^{-1}, ascribable to stretching vibrations of C=O bonds in acetyl groups.[30-32] was evident for both the electrospun mats (CA with and without PEG). Schenzel et al.[33] noted that the presence of a band at around 1464 cm^{-1} (representing the characteristic bending vibrations of CH_2-groups) with and without a band at 1,481 cm^{-1} is typical of cellulose I and cellulose II respectively. It was interesting to note the prominence of the band at about 1460 cm^{-1} over 1481 cm^{-1} band for both the samples. (However, the intensity of the band at 1481 cm^{-1} was slightly more for eCAPEG). The plausible similarity in structures of cellulose acetate and cellulose II has been proposed[29] in the context of similarity of the bands within their respective Raman spectra. To comment on the observation of this report, a plausible interpretation may be the retention of the structure of the starting material *i.e.,* cellulose acetate (bearing resemblance to cellulose II) post electrospinning with and without PEG. Both the samples showed an intense band at around 1437 cm^{-1}, which is assignable to the deformation vibrations of CH_3– groups.[34] A less intense band at around 1444 cm^{-1} was evident for eCAPEG mat, attributed to δ(CH) deformations of PEG4000. Quite a prominent band at 1380 cm^{-1} due to various deformation ($\delta(CH_2)$, δ (HCC), δ (HCO) and δ (COH)) vibrations of cellulose backbone was noticeable in both the spectra. It is of pertinence to mention about the signal at 1364 cm^{-1}, much more prominent in the spectra of eCA mat compared to its counterpart. This signal is ascribed to CH_3-groups within the acetyl groups.[35]

Zhang et al.[29] reported the progressive increase in the intensity of the band in correspondence to growing DS_{Ac} (degrees of substitution ascribed to acetyl groups). Multiple bands existed in the region between 1,200–1,030 cm^{-1}. These are assigned to stretching vibrations of C–O groups in pyranose compounds or deformation vibrations of COH groups in cellulose.[30] The signal of eCA at 1151 cm^{-1} (ascribed to asymmetric

vibrations of CC and CO bonds in cellulose *i.e.*, ring breathing)[36] shifted to 1148 cm^{-1} for eCAPEG with slightly greater intensity of the latter.

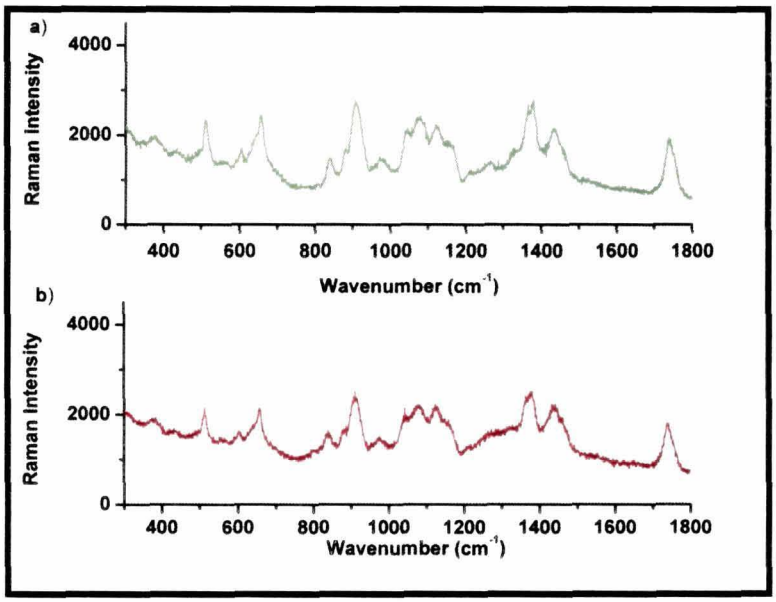

Fig.5B.3. *Raman spectra of a) eCA and b) eCAPEG mat*

However, the band at 1080 cm^{-1} (symmetric ring breathing vibrations of COC groups)[29] and 1120 cm^{-1} of eCA remains almost constant at 1079 $cm^{-1}$and 1,123 cm^{-1} respectively for eCAPEG . Moreover, the band at 909 cm^{-1} of eCA shifted to higher wave number of 912 cm^{-1} in the eCAPEG mat. For both the samples, vibrations of the bonds within the CH_3CO groups, predominantly the deformation vibrations of C=O bonds in ester groups (COO- groups)[34] accounted for signals at around 604 (for eCA, 602 for eCAPEG) and 656 cm^{-1} and with a shoulder at around 644 cm^{-1} (for eCA, 646 for eCAPEG). On the other hand, the vibrations at around 351, 379, 443, 464 and 510 cm^{-1} observed in the Raman spectra of eCA showed significant decrease in the intensity and minor shift to higher wave number in eCAPEG. These peaks are ascribable to δ(COC), δ(CCO), δ(CO), δ(CCC), respectively.[36]

The subsequent section focuses on the modulations of the thermal properties. Fig.5B.4 shows the non-isothermal TGA measurements of cellulose acetate powder, poly(ethylene glycol) and eCA and eCAPEG. 95% weight loss of CA and PEG occurred at 285 ^{0}C and 379.5 ^{0}C respectively. On the other hand, electrospinning seemed to modulate the thermal behaviour of CA with and without PEG. This may be bracketed together with a greater ordered structure of the CA chains achieved on electrospinning. 95% weight loss for eCA occurred only after heating the sample to 309 ^{0}C. eCAPEG registered the equivalent weight loss at 326.2 ^{0}C.

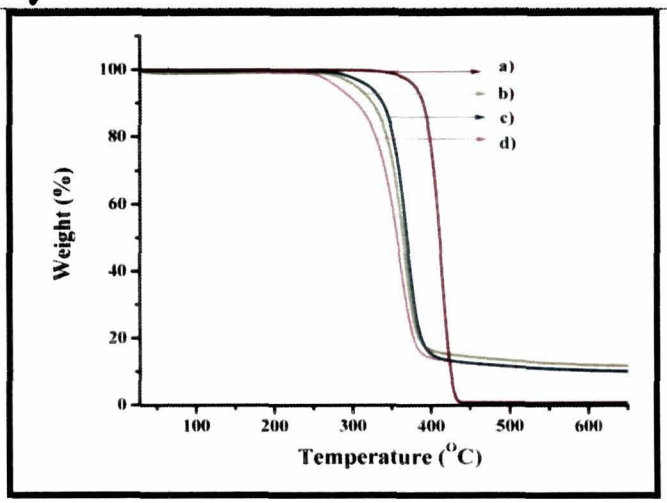

Fig.5B.4. *Non-isothermal TG plots of a)PEG4000, b) eCA mat, c) eCAPEG, and d) CA powder*

The DSC plots are shown in Fig.5B.5. PEG (Fig.5B.5a) shows a single peak at melting point in the first heating cycle at 62.5 °C. While in second and third cycles two peaks are observed at 59 and 62 °C. These cycles are reproducible and indicate the material's behaviour. The difference between first and subsequent cycles is due to the thermal history of material which is cleared after the first melting. eCA mats (Fig.5B.5b) showed a peak at around 75.3 °C which disappeared in the next cycles. This peak could be due to moisture or some volatiles in the sample. T_g and T_m in the first cycle were 195.3 and 225.7 °C, respectively. But in the next cycles they reduced to 190.6 and 221.6 °C respectively. Melting enthalpy also reduced from 5.3 J/g to 1.1 J/g and 0.5 J/g respectively. This change can be due to changes in the crystalline structure of the material during the cooling cycle in context of the process conditions. In the cooling cycle only one exothermic peak was observed at 207 °C in all cycles.

In presence of PEG (Fig.5B.5c), a broad peak appeared around 75 °C in the first cycle (same as eCA and probably due to residues of solvent and other volatiles). In presence of PEG, the T_g of the fiber reduced to 191 °C. PEG having a lower T_g reduced the glass transition temperature of the blend. In the first cycle, single melting point was observed at 227 ^{0}C. The presence of only one sharp melting point attested the homogeneity of the fiber blend. At the end of first cycle, both polymers melted completely and resulted in two different phases on cooling. This may explain the presence of two melting points (one for PEG and the other for CA) in the subsequent cycles.

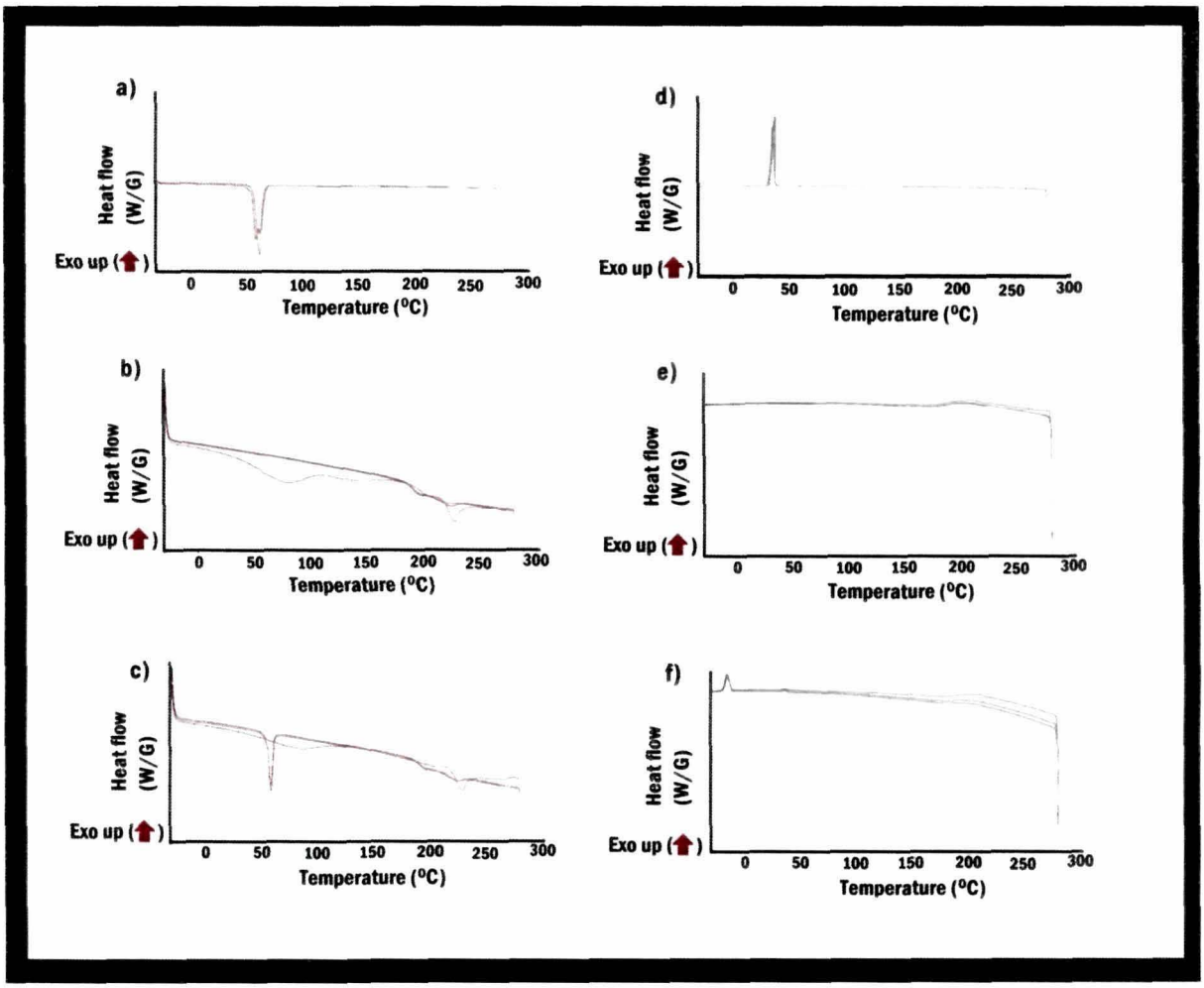

Fig.5B.5. *DSC plots showing three heating and cooling cycles of PEG (a and d), eCA mat (b and e) and eCAPEG mat (c and f)*

It is pertinent to mention that phase change materials like PEG impart desirable thermal storage and release properties to fabrics. However, investigation of tactile comfort (determined by total value) perceived by human beings is another prerequisite.[37] In this context, it would be interesting to probe into the plausible application of the developed eCAPEG mat, occurring as grooved fibrous mesh (mentioned in the previous discussion), as thermal storage material, capable of regulating the interior temperature in response to altered ambient conditions.

It has been reported that parallel line surface structures can increase the surface area of cellulose acetate butyrate by 30%.[27] However, the blended fibrous mats with grooved architecture in the present case had lesser surface area than the pristine fibrous mats. Multipoint BET surface areas for eCA and eCAPEG mats were 274.54 m^2/g and 236.67 m^2/g respectively.

Moving ahead, the activity of antibiotic loaded eCA and eCAPEG mats is dealt with in the following section.

5B.3.2. *Action at the bio-interface*

Recently, Heunis & Dick[38] have pointed out that use of antibiotic loaded nanofibers can serve as an apt strategy for treatment of skin infections. In this context, electrospun PLLA loaded with rifampin, doxorubicin hydrochloride and paclitaxel[39], PEVA loaded with tetracycline hydrochloride[40] and PLGA/PEG-b-PLLA electrospun fibers loaded with mefoxin[41] merit special mention. In this work, the loaded antibiotic (via physical adsorption) was ampicillin. Ampicillin is a competitive inhibitor of transpeptidase, an enzyme critical in the synthesis of bacterial cell wall[42] and it has received FDA approval for its mechanism of action. The test organism chosen was *Staphylococcus aureus.* It is pertinent to mention that despite being harmless in most individuals, *S. aureus* is responsible for various infections of the skin and other organ. Such infections are common in individuals with frequent skin injury, particularly if the skin is dry and highly prevalent in atopic dermatitis patients.[43]

A number of interesting observations emanated from the disc diffusion assay (Fig.5B.6).

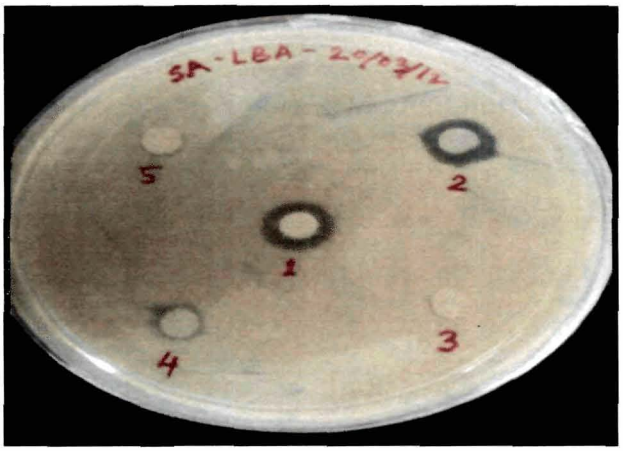

Fig.5B.6. *A representative Petri dish depicting the disc diffusion assay to check the antibacterial action of 1) Amp-FP, 2) Amp-eCA, 3) eCA, 4) Amp-eCAPEG, and 5) eCAPEG*

Amp-FP (central disc) served as positive control in the test for evaluating the antibacterial efficacy of Amp-eCA and Amp-eCAPEG discs. However, the zone of inhibition for sample 2 was almost 14% larger than that of Amp-FP. The cellulosic fibers of filter paper are distributed in the microscale regime while for sample 2 the CA fibers lie in the domain of nanoscale. This could be attributed to the higher surface area

available for drug loading in the latter and possibly this resulted in greater zone of inhibition. With respect to Amp-eCAPEG, it is worthy to mention that the fibers as seen under SEM appeared in bundle assemblage, thereby comparatively reducing the active surface area (also attested by BET analysis) available for drug loading and hence smaller zone of inhibition was anticipated. In these lines, the zone of inhibition of Amp-eCA was almost 29.5% larger in comparison to that of Amp-eCAPEG.

Poly(ethylene glycol) (PEG) is often used as stabilizing as well as cross-linking agent for different bioactive moieties like proteins, enzymes, antibodies (mentioned in different sections of this thesis). The presence of number of functional groups on both PEG and cellulose acetate backbones facilitated the immobilization of ampicillin. Compared to Amp-FP, the zone of inhibition of Amp-eCAPEG was much smaller (which might be attributed to differential amount of loading and nature of interaction of ampicillin with cellulosic fibers of the filter paper and blended fibers of CA and PEG in eCAPEG respectively, thereby affecting the diffusion. In this context, the following objectives may be set in the next level of study:

1. Studying the diffusion pattern of the immobilized ampicillin, both at *in vitro* and *in vivo* levels.
2. Investigating the structural change (if any) of the antibiotic post diffusion using different analytical and spectroscopic tools.
3. Delving into the interaction of ampicillin with eCA and eCAPEG using different computational tools.
4. Modulating the percentage of either of the polymers and studying the differential drug loading and release profile.
5. Furthermore, it would be interesting to study ampicillin immobilization onto the eCA and eCAPEG mats using other techniques like co-electrospinning etc.
6. Probing into the toxicity and compatibility of the mats using different cell lines *e.g.*, keratinocytes, to evaluate the assistance in wound healing.

In this context, as a preliminary study, the compatibility of the mats was assessed using peripheral blood mononuclear cells. It is pertinent to mention that skin injury by a burn or cut triggers the activation of the wound healing process as well as the immune system. Inflammation, cell proliferation and migration, angiogenesis, and extracellular matrix production by the infiltrated inflammatory cells and dermal cells play a key role in the healing process.[44] Peripheral blood has been used as a source of lymphocytes and wound fibroblasts[45] to study the repair phase of the wound. Therefore, as attested

by Fig.5B.7 (Trypan blue assay, clicked in bright field), the discs were found to be compatible with the primary culture of goat peripheral blood mononuclear cells (PBMCs).

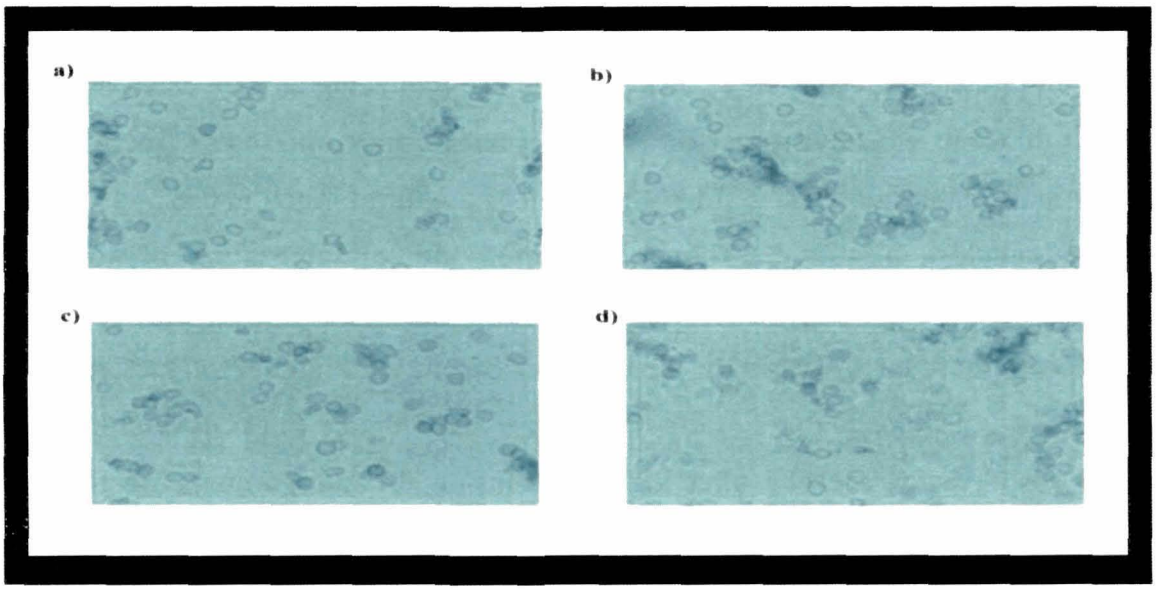

Fig.5B.7. *Trypan blue assay showing the compatibility of goat blood PBMCs when incubated with a) eCA, b) eCAPEG, c) Amp-eCA and d) Amp-eCAPEG mats*

However, establishment of the biocompatibility demands deeper delving and *in vivo* assessments.

5B.4. Conclusion

Electrospinning CA in presence of a common plasticizer, PEG, resulted in modulations of a myriad of properties as attested by various microscopic, spectroscopic and analytical techniques. Exploring the grooved architecture of the eCAPEG for cell culturing can be an interesting proposition. Future studies may be directed in understanding the mechanical properties in the context of different weight percentages of CA and PEG. On the other hand, activity of ampicillin adsorbed onto eCA and eCAPEG mats (compatible with PBMCs) was manifested via the differential antibacterial potency. The various possible scopes of investigation for the reported immobilization platform *i.e.*, eCAPEG, as mentioned in the preceding section would complement our understanding in the context of transdermal drug delivery studies.

References

1. Rubenstein, D.A., et al. *J. Biomater. Sci.* **21**, 1713--1736, 2010.
2. Chen, P-C., et al. *Cellulose,* **18,** 1563--1571, 2011.
3. Xiao, S., et al. *ACS Appl. Mater. Inter.* **1**, 2848--2855, 2009.
4. Chen, C., et al. *Appl. Energ.* **88,** 3133--3139, 2011.
5. Haas, D., et al. *J. Mat. Sci.* **45,** 1299--1306, 2010.
6. Han, S.O., *Mater. Lett.* **62**, 759--762, 2008.
7. Doshi, J., & Reneker, D.H. *J. Electrostat.* **35**, 151--160, 1995.
8. Vrieze, S.D., et al. *J. Mat. Sci.* **44**, 1357--1362, 2009.
9. Amiraliyan, N., et al. *Fiber Polym.* **10,** 167--176, 2009.
10. Gu, S-Y., & Ren, J. *Macromol. Mater. Eng.* **290**, 1097--1105, 2005.
11. Ray, S., & Lalman, J.A. *Chem. Eng. J, 169,* 116--125, 2011.
12. Meyer, R.H., & Montogomery, D.C. *Response Surface Methodology: Process and Product Optimization Using Designed Experiment,* 2nd ed. John Wiley and Sons, New York, 2002.
13. Shin, E.H., et al. *Macromol. Res.* **16**, 314--319, 2008.
14. Haaland, P.D. (ed.). *Experimental Design in Biotechnology*, Marcel Dekker Inc., New York, 1989.
15. Box, G.E.P., & Draper, N.R. *Empirical Model Building and Response Surfaces*, John Wiley and Sons, New York, 1987.
16. Ramakrishna, S., Fujihara, K., Teo, W-E., Lim, T-C., & Ma, Z. *An Introduction to Electrospinning and Nanofibers*, World Scientific Publishing Co. Pvt. Ltd. Singapore, 2005.
17. Megelski, S., et al. *Macromolecules* **35,** 8456--8466, 2002.
18. Zhao, S. L., *et al. J. Appl. Pol. Sci.* **91**, 242--246, 2004.
19. Lee, J.S., et al. *J. Appl. Pol. Sci.* **93**, 1638--1646, 2004.
20. Demir, M. M., et al. *Polymer* **43**, 3303--3309, 2002.
21. Krishnappa, R. V. N., *J. Mat. Sci.* **38**, 2357--2365, 2003.
22. Rowe, R.C., et al. *Int. J. Pharmaceut.* **22**, 57--62, 1984.
23. Sakellariou, P., et al. *Int. J. Pharmaceut.* **31**, 55--64, 1986.
24. Guo, J.H. *Drug Dev. Ind. Pharm.* **19**, 1541--1555, 1993.
25. Liao, H., et al. *Polym Composite* **32**, 837--845, 2011.
26. Stevens, M.M., & George, J.H. *Science* **310**, 1135--1138, 2005.

27. Huang, C., et al. *Soft Matter* **7**, 10812--10817, 2011.

28. Barud, H.S., et al. *Thermochim. Acta* **471**, 61--69, 2008.

29. Zhang, K., et al. *Cellulose* **18**, 995--1003, 2011.

30. Guo, Y., & Wu, P. *Carbohyd. Polym.* **74**, 509--513, 2008.

31. VanderHart, D.L., et al. *Macromolecules* **29**, 730--739, 1996.

32. Yu, Z., et al. *Food Chem.* **87**, 447--481, 2004.

33. Schenzel, K., et al. *Cellulose* **12**, 223--231, 2005.

34. Socrates, G. *Infrared and Raman Characteristic Group Frequencies*, 3rd ed. Wiley, England, 2001.

35. Colthup, N.B., Daly, L.H., & Wiberley, S.E. *Introduction to IR and Raman Spectroscopy*, 3rd ed., Academic Press, London, 1990.

36. Schenzel, K., & Fischer, S. *Cellulose* **8**, 49--57, 2001.

37. Wang, N., et al. *Macromol. Rapid Commun.* **31**, 1622--1627, 2010.

38. Heunis, T. D. J., & Dicks, L.M. T., *J. Biomed. Biotechnol.* 510682 (10 pp), 2010.

39. Zeng, J., et al. *J. Control. Release* **92**, 227--231, 2003.

40. Kenawy E.-R., *J. Control. Release* **81**, 57--64, 2002.

41. Kim, K., et al *J. Control. Release* **98**, 47--56, 2004.

42. Katzung, B.G. *Basic and Clinical Pharmacology*, 10th ed., McGraw Hill Medical, New York, 2007.

43. http://dermnetnz.org/bacterial/staphylococci.html, accessed on January 2, 2012.

44. Yang, L., et al. *Lab. Invest.* **82**, 1183--1192, 2002.

45. Abe, R., et al. *J. Immunol.* **166**, 7556--7562, 2001.

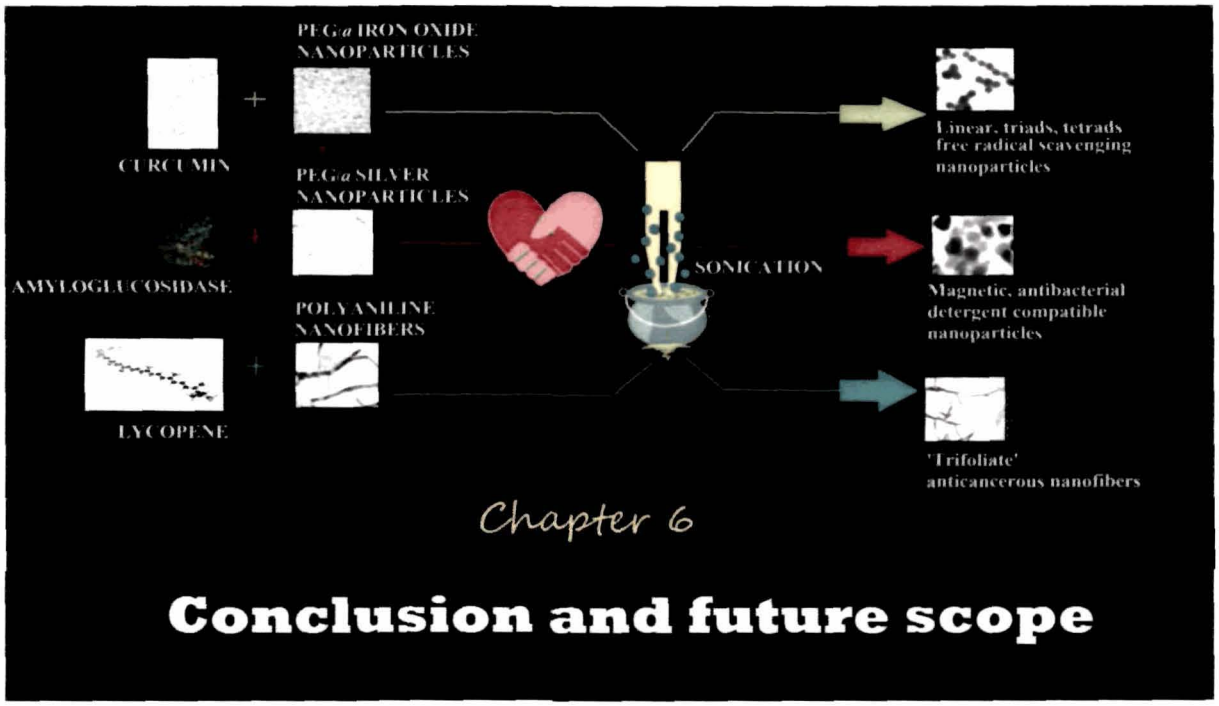

Chapter 6

Conclusion and future scope

HIGHLIGHTS OF THE CHAPTER

In this chapter, an effort has been made to re-scrutinise and critically analyse the preparation and applications of the biomolecule immobilized hybrid systems, reported in the thesis. The major achievements, the limitations and most importantly the future prospects of the reported works are highlighted.

The increasing number of reports and patents of the recent years stand testimony to the ever widening portal of the art of biomolecule immobilization. The present thesis is devoted to the development of bioconjugated polymer supported nanomaterials for prospective applications in industrial and biomedical domains. The works compiled in the thesis unmask a couple of interesting observations, achievements and prospects for future works.

Immobilization of enzymes, amongst others is a common strategy for augmenting their activity, stability and reuse in various industrial domains. The studies pertaining to enzyme immobilization (presented in this report) vouched for this. Keratinase was successfully immobilized onto PEG-IONPs for prospective clean depilatory or hair-shaving application in leather industry. Sonication was an apt tool to immobilize porcine pancreatic lipase and amyloglucosidase for applications in detergent and food industry onto magnetically recyclable and antimicrobial PEG-green Ag-IONPs, displaying exotic morphology. The documented increase in the activity, thermostability, storage stability and recyclability of these immobilized enzymes on their respective immobilization platforms are few of the desirable features that endow the developed systems with prospective credentials for industrial applications.

Although, bioresources like aqueous extracts of orange peel and *Mesua ferrea* L. leaf can be good choice for preparing polymer supported nanomaterial, it is pertinent to mention that the nanomaterials prepared through green routes may not be green *per se* as far as their action at the bio-interface (be it with the prokaryotes or the eukaryotes) is concerned. The bio-nano interfacial action is a reflection of the shape-size-concentration accord. Prior to commercialization of the nanomaterials, an indispensable requisite is the compilation of a toxicity profile.

It was also interesting to note that statistical tools like response surface methodology (RSM) can be instrumental in optimizing both the preparative protocol of polymer supported nanomaterials as well as maximizing the biomolecule loading. Furthermore, such tools can be instrumental in various biochemical engineering process optimizations as well. To cite for evidence, RSM was effectively used to optimize the parameters of the green chemistry tool of sonication used in conjunction with a biocatalyst (cellulase) to augment the laboratory scale isolation of tomato peel lycopene. The same tool of sonication was employed to develop anticancerous lycopene

coupled 'trifoliate' polyaniline nanofibers as multifunctional biomaterial. On the other hand, artistically appealing assemblage of free radical scavenging curcumin loaded PEG-IONPs were prepared for prospective drug delivery.

Electrospinning has conferred a whole new perspective to application oriented utility of varipous polymeric nanofibers. In this context, statistical optimization of few selected process parameters was instrumental in electrospinning cellulose acetate nanofibers with minimal diameter. However, when electrospun in the presence of a common plasticizer *i.e.,* PEG, a plethora of bio-physico-chemical properties (including antimicrobial activity on ampicillin loading) of electrospun CA fibers were modulated.

Thus, the major accomplishments may be summed as follows

- Keratinase immobilized onto PEG-IONPs for prospective application in leather industry.
- Lipase immobilized onto PEG-Ag-IONPs for application in detergent industry.
- Amyloglucosidase immobilized onto PEG-Ag-IONPs for application in detergent and food industry.
- Bioresource based preparation of biopolymer-templated silver nanoparticles.
- Artistically appealing assemblage of free radical scavenging curcumin loaded PEG-IONPs for prospective drug delivery.
- Augmented laboratory scale isolation of tomato peel lycopene by the coupled tools of sonication and biocatalysis
- Establishment of anticancerous lycopene coupled 'trifoliate' polyaniline nanofibers as multifunctional biomaterial.
- Statistical optimization of few selected process parameters for minimal diameter of electrospun cellulose acetate nanofibers
- Ampicillin adsorbed electrospun CA-PEG nanofibers for prospective transdermal drug delivery.

The different biomolecule immobilization studies, reported in the thesis forward the various polymer assisted nanomaterials as *avant garde* immobilization platforms. Immobilization onto polymer supported nanomaterials can have profound consequences in the context of modulations of bio-physico-chemical properties of both the immobilization platform and the immobilized biomolecules for application oriented utilities. These studies have not only paved the way for a number of prospective

industrial and biomedical applications but also opened the window to a couple of pertinent issues to be delved into, as discussed underneath.

From the perspective of material chemistry, it would be interesting to observe the real-time genesis of the exotic nanostructures post biomolecule immobilization and modulations of various parameters to arrest the growth at particular stage. On the other hand, use of advanced analytical and computational tools would complement our understanding on the possible structural modulations of the biomolecules post immobilization. The suitability of other green tools like microwave irradiation and biocatalysis for the immobilization of various other prospective biomolecules on a wider spectrum of polymer supported nanomaterials could be another long-term objective.

A life-cycle assessment would complement the actual potential of the developed systems for applications via the analysis of the environmental impacts associated with all the stages of the prepared nanomaterial's life (prior to and post biomolecule immobilization) from cradle-to-grave. Compilation of an inventory of relevant energy, material inputs, environmental release etc. is critical prior to commercialization of the reported systems. This is particularly important in the present context as the preliminary eco-toxicity studies reported in the different chapters stand in support of the tremendous impact of nanomaterials on the growth and development of plants (*Cucumis sativus* taken as the test species). A critical issue to address is the plausible transfer of the nanomaterials to various food webs and partitioning across different trophic levels.

Considering the issues of nanotoxicity of the prepared systems, a deeper delving is prerequisite both at the *in vitro* and *in vivo* levels. For example, it is mandatory to understand the immune response to the various nanoscale drug formulations. Depending on the intended use, standardized blood compatibility tests like haemolysis, complement activation, thrombogenicity etc. need to be validated. Furthermore, the genotoxicity assessment has to be dealt with elaborate analytical tools. Transdermal delivery system (as in the case of electrospun fibers) need further *in vivo* assessment. The differential interaction of the nanoparticles (say silver) with Gram positive and Gram negative bacteria or that of the lycopene-polyaniline nanofiber hybrid's with HeLa and normal cell lines need a deeper insight at molecular level. It would also be

interesting to assess the aptness of quantitative structure-activity relationship (QSAR) method to predict the cytotoxicity of the various nanomaterials like metal oxides to complement (*not substitute*) the various experimental evaluations (which are generally expensive and time consuming).

Nevertheless, the compiled works hold prospects for myriad of applications as well as testify a plethora of '*happenings*' at the polymer-nano-bio interface.

LIST OF PUBLICATIONS/SEMINARS/CONFERENCES

PUBLICATIONS - INCLUDED IN THE Ph.D. THESIS

1. **Konwarh, R.,** Karak, N., & Misra, M. Electrospun cellulose acetate nanofibers: the present status and gamut of biotechnological applications. *Biotechnol. Adv.* **31,** 421--437, 2013 (IF: 9.646)
2. **Konwarh, R.,** Misra, M., Mohanty, A.K., & Karak, N. Size-tuning of electrospun cellulose acetate fibers under optimized process parameters: a Box-Behnken design (BBD) study. *Carbohyd. Polym.* **92,** 1100--1106, 2013. (IF: 3.628)
3. **Konwarh, R.,** Pramanik, S., Devi, K. S. P., Saikia, N., Boruah, R., Maiti, T. K., Deka, R. C., & Karak N. Lycopene coupled 'trifoliate' polyaniline nanofibers as multi-functional biomaterial. *J. Mat. Chem.* **22,** 15062--15070, 2012. (IF: 5.968)
4. **Konwarh, R.,** Pramanik, S., Kalita, D., Mahanta, C.L., & Karak, N. Ultrasonication – A complementary 'green chemistry' tool to biocatalysis: A laboratory-scale study of lycopene extraction. *Ultrason. Sonochem.* **19,** 292--299, 2012. (IF: 3.567)
5. **Konwarh, R.,** Gogoi, B., Philip, R., Laskar, M. A., & Karak, N. Biomimetic preparation of polymer- supported free radical scavenging, cytocompatible and antimicrobial "green" silver nanoparticles using aqueous extract of *Citrus sinensis* peel. *Colloid Surf. B* **84,** 338--345, 2011. (IF: 3.456)
6. **Konwarh, R.,** Karak, N., Sawian, C.E., Baruah, S., & Mandal, M. Effect of sonication and aging on the templating attribute of starch for "green" silver nanoparticles and their interactions at bio-interface. *Carbohyd. Polym.* **83,** 1245--1252, 2011. (IF: 3.628)
7. **Konwarh, R.,** Saikia, J.P., Karak, N., & Konwar, B K. 'Poly(ethylene glycol)-magnetic nanoparticles-curcumin' trio: directed morphogenesis and synergistic free radical scavenging. *Colloid Surf. B* **81,** 578--586, 2010. (IF: 3.456)
8. **Konwarh, R.,** Kalita, D., Mahanta, C.L., Mandal, M., & Karak, N. Magnetically recyclable, antimicrobial, and catalytically enhanced polymer-assisted "green" nanosystem-immobilized *Aspergillus niger* amyloglucosidase. *Appl. Microbiol. Biotechnol.* **87,** 1983--1992, 2010. (IF: 3.425)
9. **Konwarh, R.,** Karak, N., Rai, S.K., & Mukherjee, A.K. Polymer-assisted iron oxide magnetic nanoparticle immobilized keratinase. *Nanotechnol.* **20,** 225107, 2009. (IF: 3.979)
10. **Konwarh, R.,** Gogoi, B., Barua, N., Misra, M., Buragohain, A.K., & Karak, N. Poly(ethylene glycol): modulator of a spectrum of bio-physico-chemical properties of

antimicrobial, biocompatible electrospun cellulose acetate nanofibrous mat. *ACS Appl. Mater Interfaces (Communicated)*

11. **Konwarh, R.,** Shail, M., Medhi, T., Mandal, M., & Karak, N. Sonication assisted assemblage of exotic polymer supported nanostructured bio-hybrid system and prospective application. *Ultrason. Sonochem. (Communicated)*
12. **Konwarh, R.,** & Karak, N. Biomolecule adsorbed polymer supported exotic nanostructures and action at bio-interface: harnessing the green chemistry tool of sonication. *Adv. Colloid Interface Sci. (Communicated)*

OTHER PUBLICATIONS

1. Pramanik, S., **Konwarh, R.**, Deka, R.C., Aidew, L., Barua, N., Buragohain, A.K., Mohanta, D., & Karak, N. Microwave-assisted poly(glycidyl methacrylate)-functionalized multiwall carbon nanotubes with a 'tendrillar' nanofibrous polyaniline wrapping and their interaction at bio-interface. *Carbon* **55**, 34--43, 2013 (IF: 5.378)
2. Barua, S., **Konwarh, R.**, Bhattacharya, S.S., Das, P., Devi, K.S.P., Maiti, T.K., Mandal, M., & Karak, N. Non-hazardous anticancerous and antibacterial colloidal 'green' silver nanoparticles. *Colloid Surf. B* **105,** 37--42, 2013 (IF: 3.456)
3. Pramanik, S., **Konwarh, R.**, Sagar, K., Konwar, B.K., & Karak, N. Bio-degradable vegetable oil based hyperbranched poly(ester amide) as an advanced surface coating material. *Prog. Org. Coat.* **76,** 689--697, 2013 (IF:1.977)
4. Saikia, J.P., **Konwarh, R.,** Konwar, B.K., & Karak, N. Isolation and immobilization of aroid polyphenol on magnetic nanoparticles: enhancement of potency on surface immobilization. *Colloid Surf. B* **102,** 450--456, 2013. (IF: 3.456)
5. Singh, S.P., **Konwarh, R.,** Konwar, B.K., & Karak, N. Molecular docking studies on analogues of quercetin with D-alanine–D-alanine ligase of *Helicobacter pylori. Med. Chem. Res.* **22,** 2139--2150, 2013 (IF: 1.271)
6. Barua, S., **Konwarh, R.**, Mandal, M., Gopalakrishnan, R., Kumar, D., & Karak, N. Biomimetically prepared antibacterial, free radical scavenging poly(ethylene glycol) supported silver nanoparticles as *Aedes albopictus* larvicidal agent. *Adv. Sci. Eng. Med.* **5**, 201--208, 2013. (IF: Not Assigned)
7. Karak, N., **Konwarh, R.,** & Voit, B. Catalytically active vegetable-oil based thermoplastic hyperbranched polyurethane/silver nanocomposite. *Macromol. Mater. Eng* **295,** 159--169, 2010. (IF: 1.986)
8. Rai, S.K., **Konwarh, R.,** Mukherjee, A. K. Purification, characterization and biotechnological application of an alkaline α-keratinase produced by *Bacillus subtilis* RM-01 in solid-state fermentation using chicken-feather as substrate. *Biochem. Eng. J.* **45,** 218--225, 2009. (IF: 2.645)

CONFERENCES/ SEMINARS

1. **Konwarh, R.**, & Karak, N. *Biohybrids of polymeric nanomaterials/ nanocomposites: from clean hair-shaving technology to multifunctional biomaterial,* in National Conference on Advanced Materials and Applications (2013), National Institute of Technology, Tiruchirapalli, Tamil Nadu, India.
2. **Konwarh, R.**, & Karak, N. *Polymer supported nanomaterials as immobilization platform for microbial biocatalysts: prospective application from leather industry to detergent industry,* in National Seminar cum Workshop on Recent Advances in Microbial Biotechnology and Molecular Evolution (2013), Tezpur University, Assam, India
3. **Konwarh, R.,** Mohanty, A.K., Misra, M., & Karak, N. *Electrospun cellulose acetate mats for automotive applications*, in Ontario Biocar Initiative, 8th Biannual Research Meeting (2011), University of Windsor, Windsor, Ontario, Canada.
4. Barua, S., **Konwarh, R.,** Mandal, M., & Karak, N. *Greener approach to prepare polymer stabilized biocidal silver nanoparticles*, National Workshop on Recent Trends on Nanoscience and Technology(2011), Bahona College, Jorhat, Assam, India.
5. **Konwarh, R.,** Pramanik, S., Boruah, R., & Karak, N. *Tailoring the photoluminescent attributes of nanoscaled polyaniline*, in National Workshop on Nuclear and Atomic Techniques Based Pure and Applied Sciences (NATPAS 2011), Tezpur University, Assam, India.
6. **Konwarh, R.,** Pramanik, S., Boruah, R., & Karak, N. *Bioconjugation of Polyaniline nanofibers for avant garde applications*, in National Conference on Smart Nanostructures (2011), Tezpur University, Assam, India.
7. Saikia, J.P., **Konwarh, R.,** Konwar, B.K., Borah, N.N., & Karak, N. *Immobilization of polyphenolic compound from Colocasia esculenta onto polymer supported magnetic nanoparticles and their efficacy as antioxidant and antimicrobial agent,* in National Seminar on Medicinal Plant and Microbe Diversity and their pharmaceuticals (2010), Tezpur University, Assam, India.
8. **Konwarh, R.** *Avant-garde materials at the intersection of polymeric nanocomposite, green technology and bioconjugation,* in Young Scientist Colloquium (2010), Materials Research Society of India (MRSI), Kolkata Chapter, BESU, Shibpur, West Bengal, India.
9. Karak, N., Mahapatra, S.S., Dutta, S., Deka, H., Konwar, U., Das, G., & **Konwarh, R.** *Polymer nanocomposites - multifaceted advanced materials for today's society*, in National Seminar on Photonics and Quantum Structures (2009), Tezpur University, Assam, India.